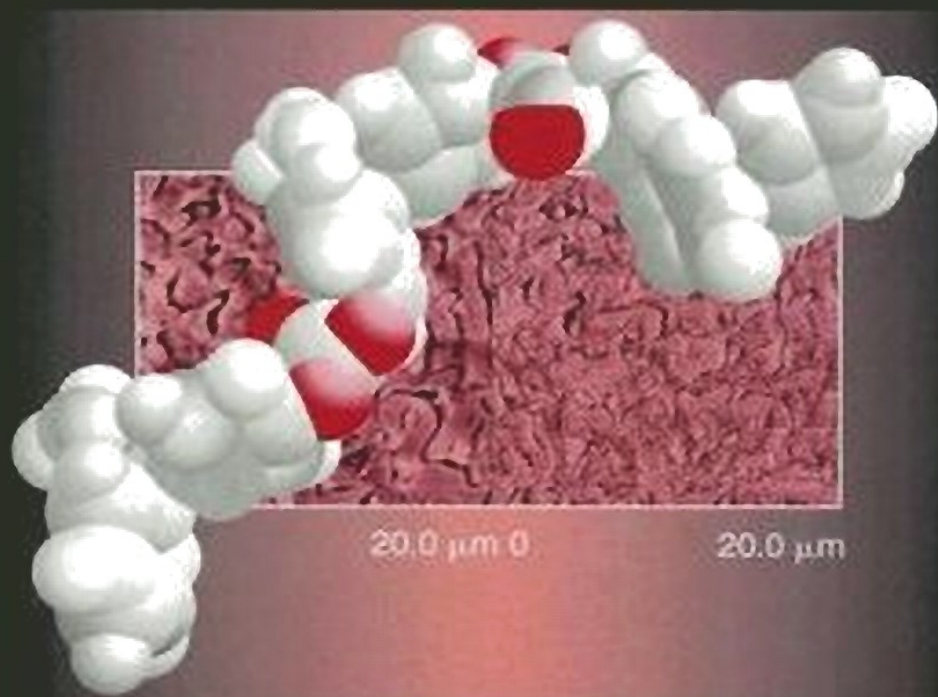


ACS SYMPOSIUM SERIES 898

Advances in Polycarbonates



EDITED BY

Daniel J. Brunelle and Michael R. Korn

Advances in Polycarbonates

ACS SYMPOSIUM SERIES **898**

Advances in Polycarbonates

Daniel J. Brunelle, Editor
GE Global Research

Michael R. Korn, Editor
Texas State University—San Marcos

Sponsored by the
ACS Division of Polymer Chemistry, Inc



American Chemical Society, Washington, DC



Advances in polycarbonates

Library of Congress Cataloging-in-Publication Data

Advances in polycarbonates / Daniel J. Brunelle, editor, Michael R. Korn, editor.

p. cm.—(ACS symposium series ; 898)

Includes bibliographical references and index.

ISBN 0-8412-3887-1 (alk. paper)

1. Polycarbonates—Congresses.

I. Brunelle, Daniel J. II. Korn, Michael R., 1961- III. American Chemical Society. Division of Polymer Chemistry, Inc. IV. American Chemical Society. Meeting (225th : 2003 : New Orleans, La.) V. Series.

TP1180.P57.A38 2005
668.4'23—dc22

2004062718

The paper used in this publication meets the minimum requirements of American National Standard for Information Sciences—Permanence of Paper for Printed Library Materials, ANSI Z39.48-1984.

Copyright © 2005 American Chemical Society

Distributed by Oxford University Press

All Rights Reserved. Reprographic copying beyond that permitted by Sections 107 or 108 of the U.S. Copyright Act is allowed for internal use only, provided that a per-chapter fee of \$30.00 plus \$0.75 per page is paid to the Copyright Clearance Center, Inc., 222 Rosewood Drive, Danvers, MA 01923, USA. Reproduction or reproduction for sale of pages in this book is permitted only under license from ACS. Direct these and other permission requests to ACS Copyright Office, Publications Division, 1155 16th Street, N.W., Washington, DC 20036.

The citation of trade names and/or names of manufacturers in this publication is not to be construed as an endorsement or as approval by ACS of the commercial products or services referenced herein; nor should the mere reference herein to any drawing, specification, chemical process, or other data be regarded as a license or as a conveyance of any right or permission to the holder, reader, or any other person or corporation, to manufacture, reproduce, use, or sell any patented invention or copyrighted work that may in any way be related thereto. Registered names, trademarks, etc., used in this publication, even without specific indication thereof, are not to be considered unprotected by law.

PRINTED IN THE UNITED STATES OF AMERICA

American Chemical Society
Library
1155 16th St., N.W.
Washington, D.C. 20036

Foreword

The ACS Symposium Series was first published in 1974 to provide a mechanism for publishing symposia quickly in book form. The purpose of the series is to publish timely, comprehensive books developed from ACS sponsored symposia based on current scientific research. Occasionally, books are developed from symposia sponsored by other organizations when the topic is of keen interest to the chemistry audience.

Before agreeing to publish a book, the proposed table of contents is reviewed for appropriate and comprehensive coverage and for interest to the audience. Some papers may be excluded to better focus the book; others may be added to provide comprehensiveness. When appropriate, overview or introductory chapters are added. Drafts of chapters are peer-reviewed prior to final acceptance or rejection, and manuscripts are prepared in camera-ready format.

As a rule, only original research papers and original review papers are included in the volumes. Verbatim reproductions of previously published papers are not accepted.

ACS Books Department

Table of Contents

Preface <i>Daniel J. Brunelle and Michael R. Korn</i>	xi-xii
1 Advances in Polycarbonates: An Overview <i>Daniel J. Brunelle</i>	1-5
<i>Synthesis of Poly(bisphenol A carbonate)</i>	
2 Evolution of Polycarbonate Process Technologies <i>Daniel J. Brunelle, Paul M. Smigelski, Jr., and Eugene P. Boden</i>	8-21
3 Monomers for Polycarbonate Manufacture: Synthesis of BPA and DPC <i>E. J. Pressman, B. F. Johnson, and S. J. Shafer</i>	22-38
4 End-Functionalized Poly(bisphenol A carbonate) Oligomers Part I: Synthesis and Examples <i>Michael R. Korn</i>	39-57
5 End-Functionalized Poly(bisphenol A carbonate) Oligomers Part II: Characterization via UV-vis, FTIR, GPC, NMR, and DSC <i>Michael R. Korn</i>	58-69
6 End-Functionalized Poly(bisphenol A carbonate) Oligomers Part III: Characterization via HPLC and Mass Spectrometry <i>Michael R. Korn</i>	70-85
7 Solid-State Polymerization of Poly(bisphenol A carbonate) Facilitated by Supercritical Carbon Dioxide <i>Douglas J. Kiserow, Chunmei Shi, George W. Roberts, Stephen M. Gross, and Joseph M. DeSimone</i>	86-94
<i>Poly(bisphenol A carbonate) Copolymers</i>	
8 Copolycarbonate of Bisphenol and 4,4'-Dihydroxydiphenyl <i>Alexander Karbach, Doris Drechsler, Claus-Ludolf Schultz, Ute Wollborn, Melanie Moethrath, Michael Erkelenz, James Y. J. Chung, and James P. Mason</i>	96-111
9 Mechanical and Morphological Properties of the Copolycarbonate of Bisphenol A and 4,4'-Dihydroxydiphenyl <i>Alexander Karbach, Doris Drechsler, Claus-Ludolf Schultz, Ute Wollborn, Melanie Moethrath, Michael Erkelenz, James Y. J. Chung, and James P. Mason</i>	112-121
10 Ductile Polycarbonates Containing Bisaryl Units: Theory and Modeling <i>John T. Bendler and David A. Boyles</i>	122-132

11 Synthesis of 1,1-Dichloro-2,2-bis[4-(4'-Hydroxyphenyl)phenyl]ethene and Its Incorporation into Homo- and Heteropolycarbonates
David A. Boyles, Tsvetanka S. Filipova, John T. Bendler, Maria J. Schroeder, Rachel Waltmer, Guy Longbrake, and Josiah Reams 133-146

Poly(bisphenol A carbonate) Blends and Composites

12 Composites of Polycarbonate with Multiwalled Carbon Nanotubes Produced by Melt Mixing
Petra Pötschke, Arup R. Bhattacharyya, Andreas Janke, and Harald Goering 148-163

13 Melt-Mixed Blends of Carbon Nanotube-Filled Polycarbonate with Polyethylene
Petra Pötschke, Arup R. Bhattacharyya, Mahmoud Abdel-Goad, Andreas Janke, and Harald Goering 164-177

Modeling of Poly(bisphenol A carbonate)

14 Advanced Solution Characterization of Polycarbonate Materials across the Molecular Weight Distribution
Arno Hagenars, Bernard Wolf, and Christian Bailly 180-199

15 Ring-Opening and Branching in Polycarbonates: A Density Functional-Monte Carlo Study
R. O. Jones, J. Akola, and P. Ballone 200-213

Aliphatic Polycarbonates

16 Synthesis and Physical Properties of Tetramethylcyclobutanediol Polycarbonates
A. Ersin Acar and Daniel J. Brunelle 216-228

17 Synthesis of Novel Aliphatic Poly(ester-carbonates) Containing Pendent Olefin and Epoxide Functional Groups
Brian D. Mullen, Robson F. Storey, and Chau N. Tang 229-243

18 Ammonolysis of Polycarbonates with (Supercritical) Ammonia: An alternative for Chemical Recycling
Werner Mormann and David Spitzer 244-261

Indexes

Author Index 265

Subject Index 267-281

Color Figure Inserts C11-C17

Preface

It has been 50 years since the aromatic polycarbonates of bisphenol A were independently discovered by Daniel Fox at GE and Herman Schnell at Bayer A G. Since the first commercialization of these polycarbonates in 1960, the market has grown to more than two-million tons per year, produced by more than a dozen companies. Polycarbonate's versatility as an engineering material results from many important properties: optical-quality transparency, high glass transition temperature, and exceptional impact strength at room temperature and below. Polycarbonates have been used in a very large variety of applications, ranging from optical recording media (such as CDs and DVDs), sporting equipment, unbreakable glazing materials, and automotive exteriors and interiors.

Its commercial success notwithstanding, polycarbonate has continued to be an item of research interest both academically and industrially. The number of patents and publications on polycarbonate continues to increase yearly, with about 5 800 patents and 3100 publications appearing since 2000. The nature of research on polycarbonates has varied with time. In the early years, development of processes for efficient manufacturing was important, as were specific compositions that might lead to enhanced properties (high heat, hydrolysis resistance, and flame retardance). During the decade of the 1980s much of the research work was involved in blending or stabilization of polycarbonates. As more manufacturers entered the market in the 1990s, again a significant amount of work on optimization of both melt (non-phosgene) and interfacial processes appeared. Very recently, new copolymer work, with attempts to improve or maintain several properties at the same time, has been reported.

Analytical and theoretical work on polycarbonate has also continued unabated. Modelers have continually strived to understand the nature of polycarbonate's unusually high-impact resistance and to design alternative polycarbonates that should theoretically provide both high-heat and high-impact strength. Other research has been targeted at

obtaining specific improvements in properties, such as very-low-temperature impact resistance, using silicone–polycarbonate block copolymers, or low birefringence in optical materials by use of new monomers.

New and revived research trends in polymer, organic, and materials chemistry during the past decade, has also been applied to polycarbonate including biodegradable aliphatic polyester carbonates, cycloaliphatic polycarbonates, dendrimers and hyperbranched polycarbonates, liquid crystalline polycarbonates, supercritical CO₂ chemistry, recycling, chirality, and nanocomposites (clay and nanotubes).

This volume is based on a symposium on *Advances in Polycarbonate*, which was held at the American Chemical Society (ACS) meeting in March 2003. Topics covered in that symposium, as well as in this volume, include theory and modeling, synthesis of new polycarbonates, development of enhanced properties in polycarbonates (such as conductivity, weatherability, higher heat, or better low-temperature ductility), recycling, and development of new methods for production of aliphatic polycarbonates using CO₂ insertion chemistry. A variety of researchers from industry, government, and academics have provided a diverse array of research results.

With BPA-polycarbonate now essentially a commodity resin, it is anticipated that further growth in the field will result from discovery of new monomers or new processes for its manufacture, or from the design of polycarbonates for totally new applications. This book provides the reader with the opportunity to learn the latest activities from academics and industry in polycarbonate research. It should be useful to a variety of specialists, from modelers and theorists to synthetic chemists and product development specialists.

We thank the supporters of the Polycarbonate symposium: the Petroleum Research Fund, the ACS Division of Polymer Chemistry, Inc., GE Global Research, Bayer Corporation, and Dow Chemical.

Daniel J. Brunelle
GE Global Research
Building K–1, Room 5A26
1 Research Circle
Niskayuna, NY 12309

Michael R. Korn
Department of Chemistry and Biochemistry
Texas State University–San Marcos
601 University Drive
San Marcos, TX 78666–4616

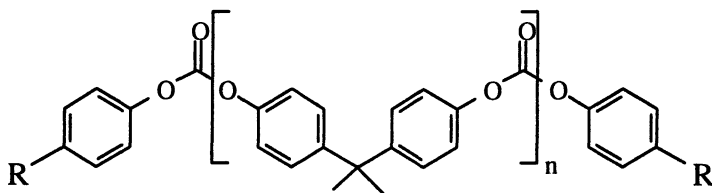
Chapter 1

Advances in Polycarbonates: An Overview

Daniel J. Brunelle

GE Global Research, 1 Research Circle, Niskayuna, NY 12309

Polycarbonates (1) are an interesting and commercially successful class of polymers. Known for useful properties such as high heat capability, optical clarity, and incredible toughness, polycarbonates continue to generate academic interest as well as finding new avenues for commercial utilization. Although aromatic polycarbonates were first reported in the literature just over 100 years ago, the number of patents and publications continues to climb each year. The field of polycarbonate research is very diverse, with novel work covering the entire range of theoretical calculations, synthesis, physical measurements and analysis, as well as new additives, blends and applications. This volume is based on a symposium, "Advances in Polycarbonates," held at the National ACS Meeting in New Orleans, in March, 2003. It collects chapters from a variety of authors describing recent work or reviews on an assortment of polycarbonate topics.



BPA-Polycarbonate

The polycarbonate from bisphenol A (BPA) was first prepared in 1953 by chemists Daniel Fox at GE (1) and Herman Schnell at Bayer, AG, (2) while working independently at their respective companies. The glassy material was immediately recognized to have unique characteristics, including clarity, a relatively high softening temperature (glass transition temperature, $T_g \sim 155^\circ\text{C}$),

and remarkable impact toughness. Within a decade, both companies had built production facilities, and were selling BPA polycarbonate. Most of the early work on polycarbonate was targeted at developing efficient processes for its manufacture, and in scoping of other monomers similar to BPA to see if additional benefits could be gained. Despite a significant amount of research, only the polycarbonate from BPA proved commercially successful for more than 2 decades.

During the 1970's and 1980's, BPA polycarbonate became a major item of commerce, and research was carried out on the full range of its properties, including optical characteristics, electrical properties, chemical and hydrolytic stability, flame retardant behavior, processing and rheology, thermal oxidative stability, the full range of mechanical properties, etc. Because of its ability to be modified and tailored to specific applications, the polycarbonate market is very broad, with over 500 different formulations being sold. Many types of additives, fillers, and blends were reported as well, and many of these (for example blends with poly (butylene terephthalate) or with ABS) became commercial successes in their own right.

In the late 1980's, and into the mid-1990's, a great deal of effort on polycarbonate was centered on optimization and control of manufacturing processes, as the market for this material grew from hundreds of millions to *billions* of kilograms. One of the principal developments was implementation of melt processes for its manufacture, which avoided use of solvent or phosgene. Other areas of intensive research during that time (some of which continue today) were the preparation of oligomeric cyclics and their conversion by ring-opening polymerization into very high molecular weight polycarbonates, (3) and solid-state polymerization (SSP) (4) as a means to increase molecular weight beyond that achievable via conventional processes. In Chapter 7, Kiserow, *et al.* discuss use of supercritical CO₂ to enhance the SSP process. A description of the processes used for preparation of polycarbonate is presented in Chapter One, along with experimental techniques for several laboratory methods. As melt polycarbonate techniques were examined anew, leading to commercialization of a solvent- and phosgene-free process for making BPA polycarbonate, the importance of monomer quality became very apparent. Pressman, *et al.* in Chapter 3 review the chemistry of the two major components of the melt reaction, BPA and diphenyl carbonate.

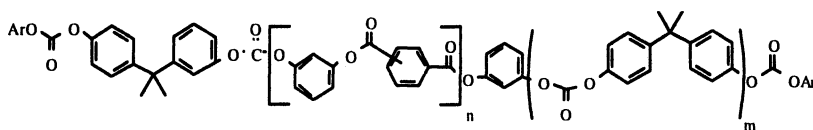
Over the past ten years, another renaissance in polycarbonate chemistry has been occurring, with several activities. New monomers which can enhance ductility even further, lead to higher T_g polymers, or improved solvent resistance are being incorporated into polycarbonates. Karbach, *et al.*, of Bayer present details on the enhanced properties of 4,4'-biphenol/BPA copolycarbonates in chapters 8 and 9. Work on copolymers, both random and block has progressed, affording far greater than incremental improvements in properties. GE has recently introduced Lexan[®] EXL, a block polycarbonate-

dimethylsiloxane copolymer, which has greatly improved low temperature ductility and resistance to hydrolysis. (5) Polycarbonates can be easily end-functionalized, by either melt or interfacial processes, and a summary of recent work on end-functionalized oligomers is presented in chapters 4-6.

Research on the use of catalysis to use CO or CO₂ for the formation of polycarbonates has been very successful, especially in the area of aliphatic polycarbonates. (6, 7) Although the vast majority of polycarbonates produced today are BPA-based, many of these new materials are reaching commercial acceptance as value-added polymers. In Chapter 16, Acar and Brunelle report their work on aliphatic polycarbonates based on tetramethylcyclobutanediol. Mullen, *et al.* in Chapter 17 report their recent work on functionalization of aliphatic polycarbonates with pendent olefin or epoxide groups.

Polycarbonate has long been used as an unbreakable window glass-replacement material. Specialty laminated glazing materials are capable of withstanding gunfire, even point-blank shotgun blasts, and are used for security installations and military canopies. With the advent of the digital recording industry, it became apparent that BPA polycarbonate was the polymer of choice for compact discs, opening a major new market. Use of polycarbonate for storage of digital data has continued to grow, with many developments in use of new monomers in polycarbonates, as the storage density increases from CD's to DVD's and beyond. (8) Because of its high refractive index, clarity, UV absorption characteristics, and toughness, polycarbonate is ideal for eyewear, including the ophthalmic market for corrective lenses, sunglasses, and safety eyewear.

Very recently, weatherable polycarbonate compositions, which can retain both mechanical and esthetic properties after long-term outdoor aging have been developed and commercialized. Lexan[®] SLX, a block polycarbonate-resorcinol polyarylate was designed for weatherable applications, utilizing a UV-light induced photo-Fries rearrangement to form a polymeric UV-absorbant coating, in a self-protecting system. (9)



Lexan[®] SLX

Since its invention, BPA polycarbonate has been an object of theoretical interest, in attempts to understand the source of its exceptional ductility. Direct evidence of molecular motion can be seen in a large low temperature (-100°C) loss peak measured by dynamic mechanical analysis. Understanding these molecular motions, and how they might absorb and disperse the energy of an impact has been the object of study of several groups. A variety of molecular

motions, including spinning, cis-trans isomerization about the carbonate bond, have been identified and studied. By understanding the source of the dramatic ductility of BPA polycarbonate, it is hoped that such properties can be incorporated into other polymers.

With increased computational capability, modelling work has reached the point of predictive ability for designing new monomers. Bendler and Boyles have presented work suggesting that the cross-sectional area and aspect ratio of monomers used for polycarbonates may be a key factor controlling high ductility. Their computational and experimental work is presented in Chapters 10 and 11. Jones, *et al.* have used density functional/Monte Carlo calculations to study the mechanism of transesterification in ring opening of cyclic oligomers, and the effects of various catalysts on that reaction. That work was extended to study the effects of catalyst structure on degree of branching in polycarbonates prepared at high temperatures in the melt, presented in Chapter 15. Hagenars, *et al.* has extended the characterization techniques for studying polycarbonate, and reports on use of molecular weight fractionation methods in chapter 14.

Because polycarbonate is very tough, and easily molded, new applications are always being sought. Polycarbonate highly filled with carbon black can be made slightly conductive, conducive to powder-coating and other operations. Pötschke, *et al.* have found that multi-walled carbon nanotubes can be dispersed in polycarbonate, leading to highly conductive, filled polymers at loadings of less than 2% nanotubes. Her work in that area, and on the study of nanotube-filled polycarbonate/polyethylene blends appears in Chapters 12 and 13.

Polycarbonate is an unusual polymer in that it has a wide variety of applications in several families of formulations. Clear, transparent grades are popular for optical or glass-replacements. Opaque or highly colored grades are common for business machines, sporting goods, etc. Many filled or reinforced grades are also used for high modulus applications. Because of the multiple market applications, recycle of polycarbonate has been little exploited. In Chapter 18, Mormann and Spitzer report on a technique for chemical recycling of polycarbonate, using ammonia.

In summary, although polycarbonate should be considered a mature area of research, because of the breadth of applications available to such a unique material, research continues unabated in both industry and academics. With new techniques for controlling chemical structure and morphology of the polymer, and with the number of potential additives growing with the onset of the nanotechnology era, it appears that polycarbonate will remain an item of interest for some time to come.

References

1. Fox, D.W. U.S. Pat. 3,144,432 assigned to the General Electric Company. **1964**.
2. Schnell, H. *Angew. Chem.* **1956**, 68, p. 633. Schnell, H. *Ind. Eng. Chem.* **1959**, 51, p. 157.
3. Brunelle, D. J., Shannon, T. G., *Macromolecules*, **1991**, 24, 3033-3044.
4. Schulz, J. M., Fakirov, S. *Solid State Behavior of Linear Polyester and Polyamides*, Prentice Hall 1990.
5. Davis, G. C., Wisnudel, M. B., Dris, I., US Patent 6,492,481, to General Electric, **2001**.
6. Beckman, E. J., *Polym. Prep.*, **2003**, 44(1), 734.
7. Moore, D. R., Allen, S. D., Goates, G. W., *Polym. Prep.*, **2003**, 44(1), 735.
8. Davis, G.C., Davis, I., Wisnudel, M. B., Boven, G., Johannes, J., van Ginneken, C., Goewey, C., US Patent 6,395,364, to General Electric, **2002**.
9. Suriano, J. A., Siclovan, T. M., Pickett, J. E., Brunelle, D. J., O'Neil, G. A., Zhou, H., *Polym. Prep.*, **2003**, 44(1), 748.

Synthesis of Poly(bisphenol A carbonate)

Chapter 2

Evolution of Polycarbonate Process Technologies

Daniel J. Brunelle, Paul M. Smigelski, Jr., and Eugene P. Boden

GE Global Research, 1 Research Circle, Niskayuna, NY 12309

Two very different processes are used for the production of bisphenol A polycarbonate, melt transesterification and interfacial phosgenation. Each process has its own advantages and disadvantages, but both are commercially feasible. Although both processes form the same polycarbonate backbone, several important differences between the two product polymers can be seen. In addition, ring-opening polymerization of cyclic oligomers and solid state polymerization techniques have recently been investigated, although not yet commercialized.

Introduction

In 1898, Einhorn reported the first aromatic polycarbonates via reaction of hydroquinone or resorcinol with phosgene in pyridine.(1) A few years later, Bischoff, *et al.* prepared the same materials via transesterification of the diols with diphenyl carbonate.(2) The hydroquinone polymer was brittle, crystalline, insoluble in most solvents, and melted at $> 280^{\circ}\text{C}$. The polymer from resorcinol was glassy and brittle, although it crystallized from solution, and melted at about $190\text{-}200^{\circ}\text{C}$. Due to difficulties of processing and characterization, neither was developed further. However, it is interesting to note that both of the processes commercially utilized for polycarbonate production today had been identified in that early work. Almost 50 years passed before aromatic polycarbonates were investigated again. In 1953, independent discoveries of Bisphenol A (BPA) polycarbonate by Schnell (Bayer AG) and Fox (GE) established that these

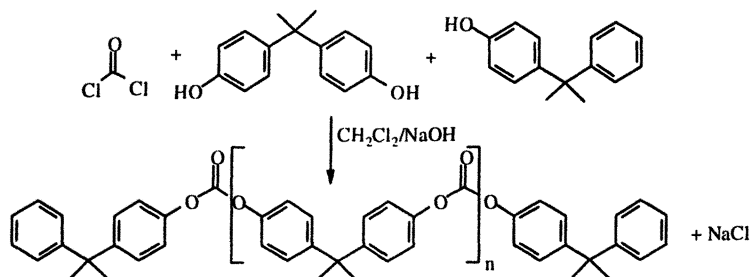
materials afforded extremely tough polymers.(3,4,5,6) Again, two processes were demonstrated, a melt transesterification technique by Fox, and a solution process using phosgene by Schnell. Since that time, polycarbonate has grown into a major business, with commercial production of over 2 million tons/year from more than a dozen producers. The broad utility of polycarbonate stems from a combination of important properties: high glass transition temperature, optical clarity, and high impact resistance. This chapter will highlight the characteristics of the two principal processes used for commercial production of polycarbonate, as well as some of the alternative schemes such as use of bischloroformates, solid state polymerization and ring opening of cyclic oligomers. Specific experimental examples of various processes from the literature are also included.

Solvent based synthesis

One of the earliest techniques for the synthesis of polycarbonate involved the direct coupling of bisphenols with phosgene in pyridine solvent.(5) In this system, pyridine functioned as a solvent, a hydrogen chloride acceptor and possibly a catalyst by formation of a phosgene-pyridine complex.(7) Due to difficulties with separation and purification of the polymer from the pyridine and its hydrochloride, and with recycle of pyridine, this procedure was not commercially attractive. Bayer and GE both pursued the melt process as early as 1953, but both companies abandoned the process due to the inferior product quality resulting from long reaction times needed at high temperatures.

The most common commercial route to polycarbonate became the amine-catalyzed, interfacial process that was commercialized by Bayer in 1958 and G.E. in 1960.(8) This process is still the dominant method for the production of polycarbonate worldwide, due to the ready access to phosgene, and to the fact that NaCl can be recycled via chlor-alkali processes. The interfacial process is a complex process, involving 4 phases (CH_2Cl_2 , aq. NaOH, solid BPA, and phosgene gas), with careful control of mixing, exotherm and pH being necessary. In addition, the equilibria of BPA and NaOH with mono- or disodium salts of BPA can become important,(9) as do $\text{CO}_2/\text{NaHCO}_3/\text{Na}_2\text{CO}_3$ equilibria. In the interfacial synthesis, phosgene is added to a stirred slurry of aq NaOH, catalytic amine/ CH_2Cl_2 and BPA, in the presence of a mono-functional phenol, such as phenol, p-t-butylphenol or p-cumylphenol to control the molecular weight of the polymer. Caustic is added to generate phenoxide and/or quench HCl formed during phosgenation, and is normally metered via a pump and pH controller, resulting in a brine solution at the end of reaction. Reaction pH must be carefully controlled throughout the reaction, since high pH can lead to hydrolysis of phosgene, intermediate chloroformates, or of the polymer itself, whereas low pH leads to very slow reaction rates and residual chloroformates.

Changes in pH can also change the effectiveness of the tertiary amine catalysts, since the pK_a of protonated amine is about 10, near the pK_a of bisphenol A. Under these conditions, the reaction yields the kinetic product, which may include low levels of cyclics or oligomeric bis-capped polycarbonate oligomers. Polymer polydispersivities (M_w/M_n) typically range from 2.2 to 2.8. The general interfacial synthesis is shown in Scheme 1.



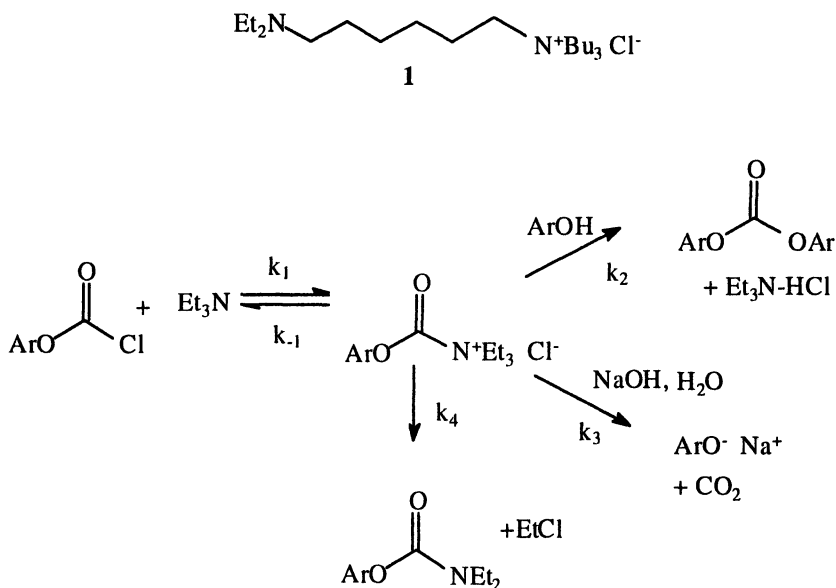
Scheme 1: General synthesis of BPA-PC by the interfacial process.

The polycarbonate product in CH₂Cl₂ is typically purified by separating the aqueous brine, then washing with aq. HCl (to remove tertiary amine catalyst), and water, followed by isolation of the polymer. Removal of the methylene chloride by a variety of techniques, including steam crumbing, solvent anti-solvent precipitation, or devolatilization is facile.

Several variations of interfacial reactions exist. Triethylamine and other tertiary amines are convenient catalysts for polycarbonate formation, since they can function either as bases or as nucleophiles, forming activated acyl ammonium salts (Scheme 2).⁽¹⁰⁾ In absence of amine catalysts, high molecular weight polycarbonate will not form, even at high pH, although some oligomerization and formation of chloroformates will occur. Activation of a chloroformate as an acyl ammonium salt can lead to enhanced reaction rates of both condensation and hydrolysis. Because triethylamine catalyzes hydrolysis, interfacial reactions normally utilize 10-20% excess phosgene. Toward the end of reaction, as the amount of unreacted phenol groups diminishes, reaction with water becomes more likely, and most hydrolysis is seen during the final stages of reaction. Acyl ammonium salts, bearing a positive charge are attacked by water at the organic/water interface much more readily than are chloroformates.

Use of phase transfer catalysts (PTC) greatly diminishes hydrolysis reactions, since a different mechanism is operative, with no acyl ammonium salts being formed (Scheme 3). The PTC operates by solubilizing normally insoluble sodium phenoxides, and generally does not solubilize hydroxide. For that reason, by using PTC, phosgene utilization can be greatly improved with only 1-2% excess phosgene being necessary for complete reaction.⁽¹¹⁾ If elimination of hydrolysis reactions is required, care must be taken with selection

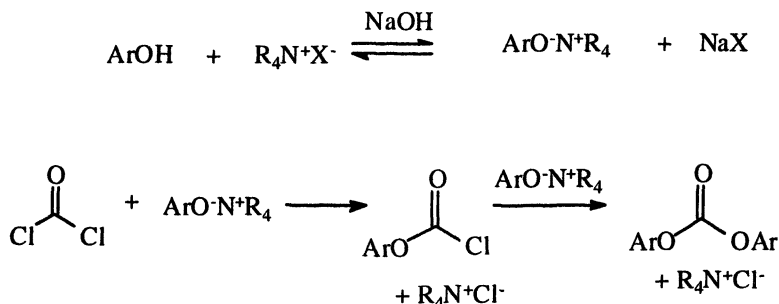
and purity of the phase transfer catalyst, since commercial catalysts often contain significant levels of tertiary amines as impurities. Furthermore, PTC agents (such as benzyl triethylammonium chloride) which can react via S_N2 reactions to form tertiary amines should be avoided. On the other hand, if a PTC is used exclusively as the catalyst, some small amount of chloroformate end group might remain on the polymer, even through workup. The residual chloroformate can be reacted either by increasing reaction pH for a period of time, or by adding a very small amount of tertiary amine catalyst at the very end of the polymerization reaction. Alternative techniques to achieve the same goals are to use a binary catalyst mixture, consisting of both a PTC and a greatly reduced amount ($\sim 1/100$ the normal level) of tertiary amine,⁽¹²⁾ or to use a bifunctional catalyst, such as tributylammonium-6-(N,N-diethyl)hexane bromide (1), which contains both a PTC functionality as well as a tertiary amine.⁽¹³⁾



Scheme 2. Activation of chloroformate via acyl ammonium salt toward condensation (k_2), hydrolysis (k_3) or decomposition to dialkylurethane (k_4).

Specific amine catalysts which are more nucleophilic than triethylamine have been used for the preparation of polycarbonates of hindered bisphenols. For example, preparation of the polycarbonates of 3,5,3',5'-tetramethyl or tetrabromobisphenol normally require 10-20% catalyst, large excesses of phosgene, and high pH using triethylamine as the catalyst. However, these polymers can be conveniently prepared using only 1% amine if a less hindered

tertiary amine, such as dimethylbutyl amine is used.(14) Studies on the rates of reaction of various amines with chloroformates, and of the subsequent reactions of the acyl ammonium salts formed via condensation have been reported.(15) Reaction of diethylmethylamine with phenyl chloroformate is about 4000 times faster than reaction of triethylamine. It is apparent that reduced steric hindrance, rather than increased basicity of the amine affords the increased reaction rates. 4-Dialkylaminopyridines are alternative nucleophilic catalysts, but are much more expensive, and may have toxicity issues.(16)



Scheme 3. Formation of soluble phenoxide and reactions with PTC.

Preformed bischloroformates have also been used in interfacial reactions, and are particularly effective for preparation of polymer with low levels of diaryl carbonates (formed from reaction of chain stopper with phosgene), and for preparation of alternating polycarbonates. Oligomeric bischloroformates can be prepared by phosgenation in the absence of catalyst.(17) By controlling reaction pH and temperature, monomeric bischloroformates can be prepared in reasonably high yield (70-90%).(18) When use of pure bischloroformates is combined with PTC, strictly alternating copolycarbonates can be prepared from equimolar quantities of bisphenol and bischloroformate.(19) However, if amine catalysts are used with bischloroformates, more random polymers form, due to hydrolysis reactions, forming free phenols from the chloroformate hydrolysis.

Finally, it is possible to carry out strictly anhydrous reactions, most conveniently using equimolar amounts of bischloroformates and bisphenols. These reactions require the use of two equivalents of tertiary amine to absorb the HCl generated. Care must be taken in these reactions to control the temperature, since the acylammonium salts which form are susceptible to further reaction, leading to a dialkylurethane and alkyl chloride (see Scheme 2). The kinetics of urethane formation via such a mechanism has been studied.(20) Some amine catalysts form urethanes less readily than does triethylamine, and hindered tertiary amines (such as diisopropylethylamine) which do not form acyl ammonium salts, will not lead to urethane formation.

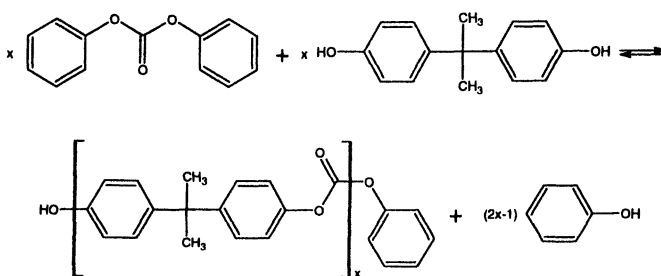
The range of techniques for interfacial synthesis have made it possible to prepare a large range of polycarbonate materials. Although use of phosgene may not be convenient on a laboratory scale, large scale use (and recovery of NaCl via chlor-alkali process) is routine in the chemical industry. Convenient laboratory alternatives to phosgene are diphosgene, triphosgene, and use of commercially available bischloroformates.

Melt phase synthesis

Like the solvent process, the melt process for preparation of polycarbonate traces back 100 years, when Bischoff, et al. prepared the polycarbonate of hydroquinone via transesterification with diphenyl carbonate.(2) Mid-century, Fox at GE used a similar process to prepare the polycarbonate of Bisphenol A.(4) However, at that time, the effects of catalyst, thermal oxidation, formation of Fries rearrangement products and high color were not recognized, and so this process was supplanted by the solvent process. Several decades later, when the technology for processing the high viscosity resin, suitable catalysts, and high purity monomers became available, interest in the melt process revived. In the melt process, BPA is reacted with diphenyl carbonate using a basic catalyst, leading to transesterification, with cleavage of phenol, which is removed via distillation. Use of high purity monomers and very low catalyst levels (10^{-3} - 10^{-4} mole %) proved to be extremely important. Diphenyl carbonate can be prepared either directly, from phosgene and phenol, or by a multistep transesterification process from dimethyl carbonate. Since dimethyl carbonate can be made directly by carbonylation of CO, the melt process can provide a phosgene-free synthesis of polycarbonate. GE was the first to commercialize this solventless synthesis of polycarbonate. The process for preparation of diphenyl carbonate is described in some detail in Chapter 3 of this volume. Significant progress has been made toward a one-step process for direct carbonylation of phenol, however the economics of the synthesis have so far prevented implementation. Likewise, a significant body of work on direct formation of polycarbonate via direct carbonylation has been carried out. Very recently, some success has been achieved at preparation of moderately high Mw polycarbonate by direct carbonylation.(21)

The preparation of BPA polycarbonate from the melt follows the general reaction shown in Scheme 4. A slight stoichiometric excess of diphenyl carbonate is employed principally for molecular weight control, and also to compensate for any loss due to devolatilization from the reactor. The primary means of controlling the molecular weight is by extent of reaction, with higher molecular weight being achieved as phenol or diphenyl carbonate is removed. Because the equilibrium between diphenyl carbonate and BPA approaches unity, removal of phenol from the system is necessary to drive the reaction. Although

the distillation of phenol is trivial in the initial stages of the reaction, in the final stages of the polymerization the reaction becomes mass transfer limited owing to the viscosity of the melt. The increased difficulty of removing phenol from the melt significantly reduces the effective reaction rate. This is partially overcome by increased temperature, vacuum and surface renewal. The reaction is terminated by returning the reactor to ambient pressure when the desired melt viscosity is reached. The result is a polymer endcapped with 60-90% phenyl carbonate moieties, the remaining endgroups being BPA-hydroxyl functionalities. The addition of mono-functional phenolics for increased endcap and molecular weight control have been employed successfully although they are not routinely used.



Scheme 4. General synthesis of BPA-PC by the melt process.

Since reaction on diphenyl carbonate is essentially energetically equivalent to reaction on a carbonate in the polymer chain, unlike the interfacial process, the melt process yields the *thermodynamically* controlled molecular weight distribution. Thus, any oligomeric species or cyclics are present at their equilibrium levels, which can often be lower than those obtained from kinetically-controlled processes. Because the polymer is generated in its equilibrium state, it suffers little or no alteration of molecular weight or distribution upon thermal processing.

The polymer produced in this manner is substantially free of solvent or other impurities, and is directly isolated via extrusion. This simplifies the manufacturing process by removal of the polymer isolation and purification operations. The phenol distillate generated during the reaction is purified prior to reuse in the synthesis of diphenyl carbonate. The finished polymer can be compounded directly following the last reaction stage.

Following are general characteristics of the melt and interfacial schemes for preparation of polycarbonates. Each has its own advantages. The interfacial process is particularly well-suited for preparation of polycarbonates with sensitive substrates, and the melt process for manufacture of excellent quality low to medium molecular weight resins.

Table 1. Comparison of Interfacial and Melt Processes

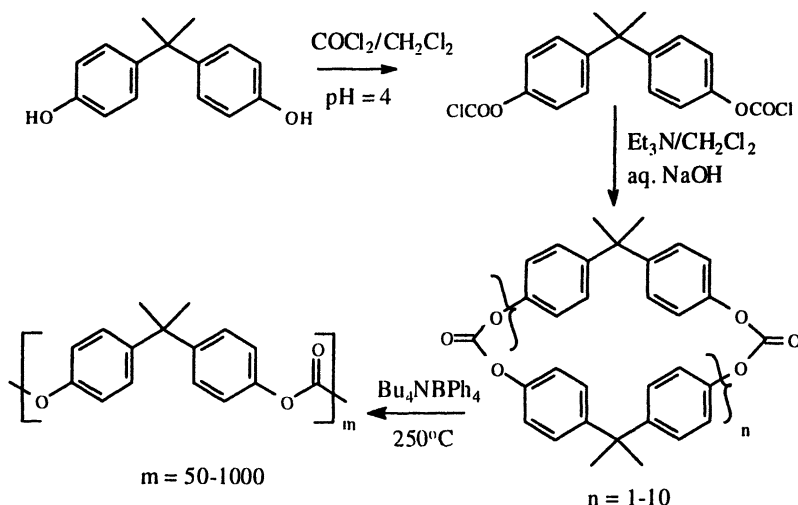
Interfacial Process	Melt Process
Kinetically controlled reaction	Thermodynamic control
Mw control via chainstopper	Mw control via extent of reaction
Amine catalysis in solvent	Base catalysis of condensation
Low temperature (~40°C)	High temperature (~300°C)
Washing and isolation necessary	Direct isolation via extrusion
High Mw can be easily achieved	Low Mw easy to achieve (Optical)
Good color, near 100% endcapping	Good color, 60-90% endcapping
Few by-products or side reactions	Side reactions may occur at high T
Requires phosgene and solvent	Requires DPC and basic catalyst
Brine recycle controls Cl usage	May or may not require phosgene

Polycarbonate from Cyclic Oligomers

Preparation of polycarbonate via a ring-opening polymerization (ROP) of cyclic oligomers is an appealing concept, since very low Mw oligomers lead to very high Mw polycarbonate in fast reactions, without formation or removal of any by-products being necessary. The ROP reaction is thermodynamically driven, and leads to a polymer with characteristics similar to those obtained via the melt process, but with much higher molecular weight. The cyclic tetramer of BPA was prepared about 40 years ago, but was not studied extensively, since the preparation was low yielding (~25%), required significant purification steps, and afforded a discrete cyclic with a mp of 375°C.(22) In 1991, the preparation of *mixtures* of oligomeric cyclics in high yields was reported.(23) The cyclic mixture, which contained less than 0.01% linears, melted at 190-200°C, which allowed extensive studies of melt polymerization. The cyclic route to polycarbonate has aspects of the interfacial, kinetically-controlled reaction, as well as the melt, thermodynamically-controlled polymerization (Scheme 5).

Slow addition (30 min) of a 1.0 M solution of BPA-bischloroformate to an efficiently stirred mixture of CH₂Cl₂, triethylamine, and aqueous NaOH, using pH control but no chain stopper provided a remarkably selective formation of oligomeric cyclic carbonates, with almost total exclusion of linear oligomers. Importantly, the preparation gave very high yields (~90%; remainder is high Mw polymer), and very high selectivity toward oligomeric cyclics, rather than linears, which made purification unnecessary. The reaction can have excellent productivity, forming cyclics with up to 1.0M monomer concentration in 30 minute reaction times. The cyclics have an average Mw of ~1200, and are formed along with high Mw polymer in about 90/10 ratio. Most of the cyclic oligomer (>90%) have DP of <10. The cyclics melt at ~200°C, and have a melt viscosity about 10⁵ lower than typical polycarbonates (~100 poise at 200°C).

Because of this low viscosity, a variety of mixing, molding, and fabrication techniques which are not suitable for high molecular weight polymers can be utilized.



Scheme 5. Conversion of BPA to its bischloroformate, to cyclic oligomers, and ROP to high molecular weight polycarbonate.

Polymerization of the oligomeric cyclic carbonates can be carried out in the melt, above $\sim 200^\circ\text{C}$, or in solution at ambient temperature.(24) The polymerization reaction on the almost strain-free rings has near zero enthalpy (-1.2kJ/mol) and is driven by entropy, leading to very high molecular weight polycarbonate. For example, use of 0.10 mole% $n\text{-Bu}_4\text{NBPh}_4$ (relative to BPA monomer units) leads to polycarbonate with $M_w = 280\text{K}$ and $M_w/M_n = 2.2$. Only about 0.25% cyclic oligomers remain in the product polymer (the same equilibrium amount seen in conventionally prepared melt polycarbonates). The polymerization is living-like, with typical initiation and propagation steps, and forms polymer with active chain ends. However, because ring-chain and chain-chain reaction rates are similar, polydispersivities approach 2.0.

The cyclic oligomer approach has been utilized to prepare a large variety of cyclic types, and is amenable to the incorporation of diverse functionality into the polymer, including imide, urethane, etherketone, ethersulfone, thio, etc.(25) The procedure has also been used to prepare copolymers for example with silicones or with other cyclic esters such as pivalolactone. Processing techniques such as pultrusion or reaction injection molding have been utilized to prepare glass- or carbon-reinforced composites with very high fiber loadings. The cyclic oligomer technique for polycarbonate has not been commercialized.

Solid State Polymerization

Solid state polymerization (SSP) is a widely practiced polymerization technique to obtain high molecular weight crystalline polymers such as poly(ethylene terephthalate).⁽²⁶⁾ This technique consists of heating a crystalline prepolymer under vacuum or in a stream of an inert gas. As polymerization proceeds, reaction by-products are swept away. Typically, the reaction temperature of the SSP process needs to be above the polymer T_g in order to have enough chain mobility for the chain extension reaction to take place, but below the polymer T_m, in order to prevent coalescence or melting of the prepolymer particles.

In the last few years SSP has been receiving increased attention for the synthesis of bisphenol-A polycarbonate (PC). Indeed, the very high reaction temperature needed to have a reasonable melt viscosity in PC melt synthesis may give rise to degradation reactions and yellowing of the final polymer. The temperature for the SSP process is lower compared to that of the melt polycondensation and thus less degradation or side reactions such as the Fries rearrangement occur during the synthesis by SSP.

PC has a very slow crystallization rate and several days of annealing at 200°C are necessary in order to induce the crystallization.⁽²⁷⁾ In the literature several procedures are reported to promote PC crystallization: solvent induced crystallization,⁽²⁸⁾ addition of nucleating agents,⁽²⁹⁾ treatment with supercritical CO₂ ⁽³⁰⁾ and the addition of plasticizers.⁽²⁷⁾ The melting temperature of the oligomers crystallized using those techniques is typically below 230°C. If such crystalline PC oligomers are subjected to SSP conditions below their melting point, an increase in molecular weight can be achieved. SSP conditions must typically be carried out for many hours before suitable commercially useful molecular weights are reached, but because of the lower temperatures utilized, good quality polymers can be obtained. During SSP, the melting point of the crystalline PC often increases, due to annealing, and a temperature ramp to ~240°C can be used in order to accelerate the polymerization. Extrusion of the polycarbonate under standard conditions returns the material to the amorphous state. Despite the simplicity of the SSP procedure and the advances in SSP of polycarbonate oligomers over the past decade, this technique has not yet been commercialized.

Conclusions

The melt and the interfacial processes for the production of bisphenol-A based polycarbonate each have their own characteristics. Whereas the interfacial process provides a low-temperature and convenient process, which is amenable to diverse chemistries, the melt process provides a

thermodynamically-equilibrated product without the use of solvents. Each process provides significant attributes, and each is suited toward particular applications. Many other techniques for preparation of a variety of polycarbonates also exist, and some may have meaningful commercial utility. Generally, either the interfacial or melt processes are used for very large scale preparation of BPA polycarbonate, whereas other techniques are commonly used for specialty materials.

Experimental

General. Following are several procedures for the preparation of polycarbonates taken from the literature. (*Caution!! Phosgene is highly toxic, and should be used only in a secure system with appropriate sensing and containment devices, and by trained personnel.*) Molecular weights were generally determined using SEC chromatography on Polymer Laboratories Mixed Bed C columns, using chloroform as the mobile phase, and using polystyrene calibration standards. A correlation with M_w determined by light scattering can be found in the literature.(31)

Synthesis of BPA polycarbonate. A. Melt Process: Melt transesterification reactions were carried out in a 1-Liter, glass batch-reactor equipped with a solid nickel helical agitator. The reactor bottom had a breakaway glass nipple for removal of the final melt. To remove any basic species from the glass, the reactor was soaked in 3N HCl for at least 12 hours followed by a soak in 18 Mohm deionized water for at least 12 hours. The reactor was then dried in an oven overnight and stored covered until use. Alternatively, quartz reactors could be used. The temperature of the reactor was maintained using a fluidized sand bath with a PID controller and measured near the reactor and sand bath interface. The pressure over the reactor was controlled by a nitrogen bleed into the vacuum pump downstream of the distillate collection flasks and measured at higher pressures (760 mmHg - 40 mmHg) with a mercury barometer and at lower pressures (40 mmHg - 1 mmHg) with an Edwards pirani gauge.

A one-liter glass reactor was charged with solid bisphenol-A (150g 0.6570 mol) and solid diphenyl carbonate (152g, 0.7096 mol). The reactor was then assembled, sealed and the atmosphere was exchanged with nitrogen three times. The reactor was brought to near atmospheric pressure and submerged into a fluidized bed that was at 180°C while a nitrogen blanket was applied. After five minutes agitation was begun at 250 rpm. After an additional ten minutes a clear homogenous melt was attained. The catalyst solutions were injected sequentially, first the alkyl ammonium catalyst (2.50×10^{-4} mol/mol BPA) and then the alkali metal hydroxide catalyst (1.0×10^{-6} mol/mol BPA). After the

final catalyst was added, timing began and the temperature was increased to 210°C in five minutes. The temperature and vacuum were increased to maintain efficient removal of the phenol reaction product. Once a viscous colorless melt was achieved the finishing stage was employed. In the final stage, full vacuum was applied and after 30 minutes, the reactor was removed from the fluidized bed and the melt was extruded into liquid nitrogen to quench the reaction. Mw=39.2K, Mn=18K.

Synthesis of BPA polycarbonate. B. Interfacial PTC Process.-(10) A 500-mL, 5-necked flask was fitted with an efficient condenser vented to a caustic scrubber, a mechanical stirrer, a pH probe, a dip-tube for addition of phosgene, and a port for addition of 50% NaOH. The flask was charged with 100 mmol of bisphenol A (22.83 g), 4.0 mmol of phenol (0.376 g), 637 μ L of a 40% solution of tetrabutylammonium hydroxide (1.0 mmol), 200 mL of CH₂Cl₂, and 100 mL of water. With efficient interfacial mixing, phosgene was admitted into the reaction at a rate of 0.75 g/min for 13.5 min (102 mmol), while the pH of the reaction mixture was maintained at 10.5-11 by dropwise addition of 50% sodium hydroxide solution. For convenience, a pH controller can be set up to provide base automatically, using a peristaltic pump. Upon completion of the reaction, the presence of chloroformates in the reaction mixture could be detected using commercial phosgene detection paper. Reaction of residual chloroformates could be carried out either by stirring at pH 11 for 50-60 min, or by addition of a small amount of triethylamine (~0.13 mmol) and stirring for 15 minutes at pH 11. To workup the reaction, the pH of the mixture was dropped to pH 8 by addition of HCl, then the brine phase was separated, and the organic phase was washed twice with HCl and 3 times with deionized water. The polycarbonate obtained had Mw = 41.5K and Mw/Mn = 2.6 by GPC analysis relative to polystyrene standards.

Synthesis of BPA polycarbonate. C. Interfacial BCF Process.-(15) A 1-L, jacketed and baffled reactor fitted with a mechanical stirrer, a pH probe, a thermocouple, and two condensers cooled to -18°C and fitted with addition tubes for phosgene and for caustic solution was charged with 500 mL of CH₂Cl₂, 100 mL water, and 0.5 mol (114 g) of BPA. Phosgene was admitted for 20 min at 3.7g/min, while stirring and maintaining the pH at 9.5. After completion, the reactor was sparged with nitrogen for 5 min to remove unreacted phosgene. HPLC analysis indicated a mixture of oligomeric mono- and bischloroformates with an average degree of polymerization of 2.4, and with a bischloroformate/monochloroformate ratio of ~3.

A 500 mL Morton flask was charged with 100 mL of the organic phase from the reaction above and 140 mL of water. A solution of phenol (485 mg, 5.15 mmol) and triethylamine (84 mg; 0.83 mmol) was added over 5 min while the reaction

was stirred and maintained at pH 12 by the addition of 50% NaOH solution. After 20 min, linear polycarbonate with $M_w = 34K$ was detected by GPC analysis.

Synthesis of 3,5,3',5'-tetramethyl-BPA polycarbonate. C. **Interfacial Process using unhindered amine.**-(13) A 1-liter, 5-necked Morton flask equipped with a mechanical stirrer, pH electrode, caustic addition port, phosgene dip tube, and chilled brine condenser vented to a caustic scrubber was charged with 56.8 g of 2,2-bis-(3,5-dimethyl-4-hydroxyphenyl)propane (TMBPA; 200 mmol), 816 mg of 2,4,6-mesitol (6 mmol), 300 mL of CH_2Cl_2 , 100mL of water, and 1 g of a 75% solution of methyltributylammonium chloride solution in water. Phosgene (22 g) was introduced at 1.25 g/min at a pH between 13.5 and 14. Following phosgene addition, the mixture tested positive for chloroformates with phosgene test paper. N,N-dimethylbutylamine (0.05 mL; 0.4 mmol) was added and the reaction mixture stirred at ambient temperature for 10 minutes, at which point no chloroformates were detected. The resulting polycarbonate had a $M_w = 53K$.

Solid State Polymerization.-(32) Oligomeric polycarbonate pellets prepared via transesterification of BPA with diphenyl carbonate, and having $M_w = 9.5K$ were crystallized using pure isopropanol vapor at a temperature of 150°C in a pressure vessel for one hour. The crystallized pellet, which had $M_w = 16.2K$ were then heated in a stream of nitrogen under the following sets of conditions: 1) 200°C for 0.5 h, followed by 230°C for 1 h, leading to $M_w = 53.4K$; 2) 200°C for .5 h, then 230°C for 1.5 h, then 240°C for 1 h, leading to $M_w = 63.7K$; 3) 200°C for .5 h, then 230°C for 1.5 h, then 240°C for 2 h, leading to $M_w = 70K$.

Acknowledgement. The authors would like to thank their colleagues at the General Electric Company for their extensive discussions into the process chemistry of polycarbonates

References

1. Einhorn, A., *Liebigs Ann. Chem.* **1898**, 300, 135.
2. Bischoff, C. A. and Hedenstroem, A. v., *Berichte* **1902**, 35, 3431.
3. Schnell, H. *Angew. Chem.* **1956**, 68, p. 633. Schnell, H. *Ind. Eng. Chem.* **1959**, 51, p. 157.
4. Fox, D.W. U.S. Pat. 3,144,432 assigned to the General Electric Company. **1964**
5. Christopher, W. F. and Fox, D. W. *Polycarbonates*. Reinhold Publishing Corporation, New York, **1962**, pp. 16-18.
6. Schnell, H.; Bottenbruch, L. and Krimm, H. U.S Pat. 3,028,365 assigned to Farbenfabriken Bayer AG. **1962**.

7. King, J.A. *Jour. Amer. Chem. Soc.*, **1988**, *110*, 5764-5767.,
8. King, J.A. "Synthesis of Polycarbonates", chapter 2 in *Handbook of Polycarbonate Science and Technology*, Legrand, D.G.; Bendler, J.T., Eds., Marcel Dekker, Inc., New York **2000**.
9. Kosky, P.G.; Silva, J.M.; Guggenheim, E.A. *Ind. Eng. Chem. Res.* **1991**, *30*, 462-467.
10. Schnell, H. *The Chemistry and Physics of Polycarbonates*, Wiley-Interscience, New York, 1964.
11. Boden, E. P., Phelps, P. D., Ramsey, D. L., Sybert, P. D., Flowers, L. I., Odle, R. R. U. S. Patent 5,391,692 1995.
12. Boden, E. P., Flowers, L. I., Odle, R. R., Phelps, P. D., Ramsey, D. L., Sybert, P. D., U. S. Patent 5,519,105 1996.
13. Brunelle, D. J., Phelps, P. D., Boden, E. P., Nelson, M. E., Flowers, L. I., Sybert, P. D., Capelle, E. H. A. US Patent 5,821,322 1998.
14. Phelps, P. D., Shanklin, E. W., Brunelle, D. J. U. S. Patent 6,576,739 2003
15. Aquino, E. C., Brittain, W. J., Brunelle, D. J., *J. Polym. Sci. A: Polym. Chem.*, **1994**, *32*, 741.
16. Munjal, S., Cummings, C. J., Kao, C-I. U.S. Patent 5,212,281, 1993.
17. Silva, J. M., Fyvie, T. J. U. S. Patent 5,034,505 1991.
18. Brunelle, D. J., Shannon, T. G., and Bonauto, D. K., *Polymer International*, **1995**, *37*, 179.
19. For example, see: Vitalini, D., Mineo, Placido, Di Bella, S., Fragala, I., Maravigna, P., Scamporrino, E., *Macromolecules*, **1996**, *29*, 4478-4485.
20. Kosky, P. G., and Boden, E. P., *J. Polym. Sci.*, **1990**, *28*, 1507.
21. Okuyama, K-i., Sugiyama, J-i., Nagahata, R., Asai, M., Ueda, M., and Takeuchi, K., *Macromolecules*, **2003**, *36*, 6953-6955.
22. Schnell, H., Bottenbruch, L., *Macromol. Chem.*, **1962**, *57*, 1.
23. Brunelle, D. J., Shannon, T. G., *Macromolecules*, **1991**, *24*, 3033-3044.
24. Evans, T. L., Berman, C. B., Carpenter, J. C., Choi, D. Y. Williams, D. A., *Polym. Prep.* **1989**, *32(2)* 573.
25. Brunelle, D. J., Shannon, T. G. *Makromol. Chem., Macromol. Symp.* **1991**, *42/43*, 155-166.
26. Schulz, J. M., Fakirov, S. *Solid State Behavior of Linear Polyester and Polyamides*, Prentice Hall 1990.
27. Von Falkai, B., Rellesman, W., *Makromol. Chem.*, **1964**, *75*, 112.
28. Turska, E., Janezek, H. *Polymer*, **1979**, *20*, 855.
29. Legras, R., Mercier, J. P., Nield, E. *Nature*, **1983**, *304*, 432.
30. Gross, M. S., Roberts, G. W., Kiserow, D. J., DeSimone, J. M. *Macromolecules*, **2000**, *33*, 40.
31. Brunelle, D. J., "Polycarbonates" in *Kirk-Othmer Encyc. Of Chem. Tech., 4th Ed, Vol. 19*, John Wiley and Sons, 1996, p. 589.
32. Hait, S. B., Day, J., U.S. Patent 6,255,435 2001.

Chapter 3

Monomers for Polycarbonate Manufacture: Synthesis of BPA and DPC

E. J. Pressman, B. F. Johnson, and S. J. Shafer

GE Global Research, 1 Research Circle, Niskayuna, NY 12309

The melt or LX process, involving the solventless transesterification of diphenyl carbonate (DPC) with bisphenol A (BPA), is the preeminent commercial non-phosgene route to bisphenol A polycarbonate. Polycarbonate purity and manufacturing cost are highly dependent on the synthetic methods used to prepare the constituent monomers. This report surveys progress in the synthesis of BPA and DPC.

Introduction

Bisphenol-A (BPA) polycarbonate was first manufactured in separate semi-facilities by Bayer AG and General Electric in 1958.(1) Each company subsequently commercialized "interfacial" processes (Figure 1), variations of which became the predominant mode of polycarbonate manufacture for the succeeding forty years. The generalized interfacial process involves reaction of phosgene with BPA in a two-phase system (aqueous caustic and methylene chloride) containing amine catalyst and a monohydroxyphenolic chain stopper.(2)

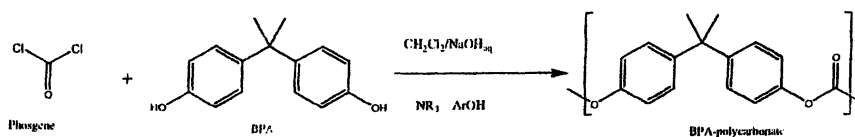


Figure 1. Interfacial process to manufacture BPA polycarbonate

GE and Bayer remain the volume leaders in polycarbonate manufacture. Total worldwide production exceeds 4 billion lbs/year(3) with markets ranging from architectural to automotive, digital recording, electrical, electronic, and safety.(2) Over the past thirty years, pursuit of process simplification and cost reduction have prompted efforts directed towards the development of alternative, non-phosgene routes for polycarbonate manufacture. The melt process, involving the solventless transesterification of diphenyl carbonate (DPC) with BPA, has been of particular interest (Figure 2).(2) This report describes progress in the synthesis of DPC and BPA, the key monomers required by the melt polycarbonate process.

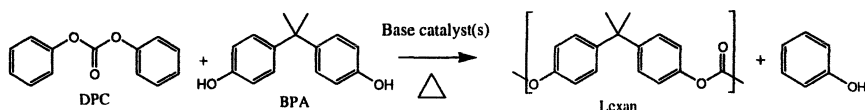


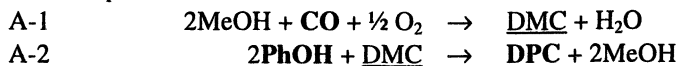
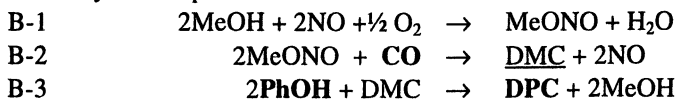
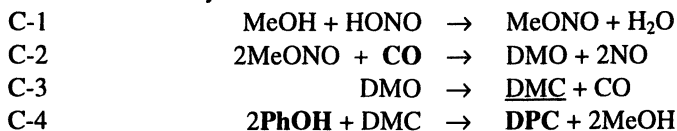
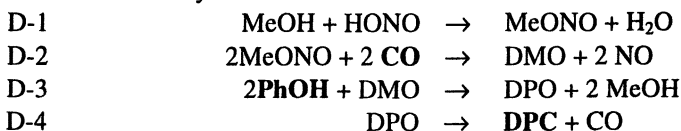
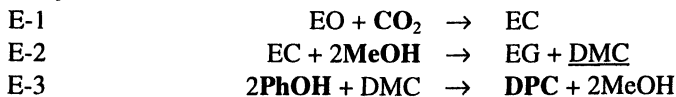
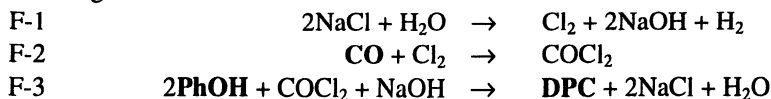
Figure 2. Melt process to manufacture polycarbonate

DPC synthesis

The general methods of DPC synthesis are shown in Figure 3, and will be described further in subsequent sections. The primary commercial value of DPC is as a comonomer for BPA polycarbonate. Phosgene and DMC (dimethyl carbonate) processes have been commercialized, and all of the remainder have been through some level of scale up or semi-works. Four of the methods (DMC, methyl nitrite, DMO decarbonylation, and cyclic carbonate processes) involve thermodynamically unfavorable transesterification of dimethyl carbonate (DMC) with phenol as the final step, and a fourth method (the DPO decarbonylation process) involves a similar transesterification of dimethyl oxalate in an intermediate step. All but the phosgene process are phosgene-free, and most are solvent-free. The DMC and one step processes involve oxidative carbonylation of methanol and phenol respectively, possess the fewest reaction steps, and appear to have the simplest recycles.

Process chemistry for DPC has been the object of intense industrial research, as summarized in Table 1. Transesterification of DMC to DPC (A-2, B-3 and C-4) and 1-step processes (G-1) have received the most attention; the latter in particular since 1998, with GE, Bayer, Mitsubishi and Teijin showing the highest level of activity. The oxalate process is nearly the sole domain of Ube. Bayer and Mitsubishi have been active in development of phosgene

Figure 3. Processes to make DPC

A DMC process**B Methyl nitrite process****C DMO decarbonylation****D DPO decarbonylation****E Cyclic carbonate transesterification****F Phosgene****G 1-step DPC**

DMO = Dimethyl oxalate

DPO = Diphenyloxalate

EO = Ethylene oxide

EC = Ethylene carbonate

EG = Ethylene glycol

processes. Asahi, GE, Mitsubishi and a host of other companies (Misc.) have been active in the DMC transesterification process.

Table 1: IP covering processes to make DPC

Process Type->	A-2, B-3, C-4	D	F	G	Misc.	Purification	Total
Asahi	1/11	/	/	/5	/	1/1	2/17
Bayer	/8	/	4/15	8/21	/3	/4	12/51
Dow	/2	/	/10	/	/	/	/12
GE	4/13	/	/2	45/61	2/6	/3	51/85
Idemitsu	/9	/	/	/3	/2	/	/14
Mitsubishi	6/18	/	13/26	2/16	1/3	2/4	24/67
Teijin	/7	1/1	/1	16/16	1/2	/	18/27
Ube	/2	25/32	1/1	/1	/	/	26/36
Other	4/31	/1	1/7	10/12	/7	/	15/58
SUM	15/101	26/34	19/62	81/135	4/23	3/12	148/367

1998→2002 / total patents

DMC process

DPC is prepared commercially by the DMC process, involving initial liquid phase, copper catalyzed oxidative carbonylation of methanol.(4, 5) Subsequent transesterification of DMC with two moles of phenol yields DPC.(6, 7) GE Plastics licenses the DMC technology from EniChem for practice in its polycarbonate plants in Cartagena, Spain and Chiba, Japan.

Additional DMC synthetic methods

DMC is a key intermediate for three DPC processes, A-C (Figure 3). Unlike DPC, DMC has significant uses beyond the manufacture of polycarbonate, including applications as an organic solvent and as an octane booster/anti-knock additive for gasoline. Prior to 1980, phosgenation of methanol was the most important method of DMC manufacture(8). Subsequently, non-phosgene routes to DMC became the focus of industrial research, as indicated in Table 2. By far, the aforementioned oxidative carbonylation of methanol has received the most attention, followed by the transesterification of cyclic carbonate and methylnitrite carbonylation.

Table 2: IP covering process to make DMC

Process Type →	A-1	B-2	C-3	E-2	Misc.	Purification	Total
Asahi	/5	/	/	3/15	1/2	/	4/22
Bayer	/6	/11	/	/7	/3	/2	0/29
Chiyoda	3/11	/	/	/3	1/4	/	4/18
Daicel	2/52	/	/1	/3	1/4	1/5	4/65
Enichem	/19	/	/1	/1	/2	/	0/23
Exxonmobil	1/1	/	/	8/10	/1	/	9/12
GE	9/12	/	/	/	3/3	/	12/15
JGC	/14	/	/	/	/	/	0/14
Mitsubishi	/12	/	/	6/15	1/9	/1	7/37
Other	14/49	1/2	/3	9/32	14/43	4/8	42/137
Texaco	/7	/	/	/3	/2	/	0/12
Ube	/1	2/32	3/11	/	/	1/3	6/47
SUM	29/189	3/45	3/16	26/89	21/73	6/19	88/431

patents issued 1998→2002 / total patents

Methyl nitrite process

The methyl nitrite process (B1, B2) represents a variation of the direct oxidative carbonylation processes (A1). Methanol is first oxidized to methyl nitrite with NO and O₂ under mild conditions (40 psia, 40 °C) in the absence of catalyst (B1); the methyl nitrite is separated from the coproduct water. In a separate step the methyl nitrite is catalytically carbonylated, in the absence of oxygen, to form DMC (B2). The reaction is typically carried out in the gas phase over a heterogeneous catalyst bed. Side products include dimethyl oxalate, methyl formate, and formaldehyde dimethylacetal.(9)

DMO and DPO decarbonylation processes

Two processes related to the methyl nitrite process are DMO (C) and DPO decarbonylation. (D). These decarbonylation routes are less significant than previously described methods, since they each require an additional process step over that of methyl nitrite carbonylation and two steps over methanol carbonylation. Carbonylation of methyl nitrite can be directed to DMC or to DMO, depending on the choice of catalyst. (10) Decarbonylation can be accomplished by several catalysts including Me₄NCl, alkali carbonates, alkali halides or alkali phosphates at 220 °C.(11, 12)

Cyclic carbonate process

The cyclic carbonate process represents the sole commercially viable

carbonate forming process that starts from CO₂ instead of CO. The unfavorable energetics of converting CO₂ to an organic carbonate is offset by the favorable energetics of opening an epoxide precursor to form a 5-membered cyclic carbonate. It is also the only process that has a stoichiometric, non-gaseous, organic coproduct, a vicinal diol, typically ethylene glycol or propylene glycol. Conversion of ethylene oxide and carbon dioxide to a cyclic carbonate (E-1) has been the subject of intensive industrial development beginning in the 1950's(13). Transesterification of the cyclic carbonates, such as ethylene carbonate (EC), to form DMC and coproduct ethylene glycol (EG) (E-2) catalyzed by 8 classes of catalysts has been experimentally examined(14). The authors conclude that base catalysis is more effective than acid catalysis. Several integrated processes have been described that cover both reactions E-1 and E-2.(15-17)

Phosgene process

Initially described in the 1940's(18), the phosgene process is an obvious route for the preparation of DPC, since it amounts to a "monomeric version" of the interfacial polycarbonate process, using phenol as the substrate instead of BPA.

One step process

The direct oxidative carbonylation of phenol (the one step process) is a simple and energetically favorable alternative non-phosgene route to DPC. Catalytic oxidative carbonylation of phenol, however, as opposed to the analogous process for aliphatic alcohols, is complicated by the increased acidity of phenol as well as its oxidative instability.(19-21) The stoichiometric carbonylation of para-substituted phenols was discovered by Chalk in the mid 1970's. A group VIII B element in oxidized (non-metallic) form selected from Ru, Rh, Pd, Os, or Ir was required, although palladium salts were by far the most effective.(22, 23) While work over the last 20 years has substantially lessened the impact of issues such as low Pd turnover number(24) and inefficient catalyst recycle(25-27), as well as co-catalyst utilization/consumption (28-32) and process complexity (33, 34) (35), those issues still remain to some extent. Consequently, one step DPC technology is not currently practiced commercially.

BPA synthesis

p,p-Bisphenol A (BPA) was chosen as the initial diol source in polycarbonate manufacture in large part due to its availability as a component in epoxy resins(36). The worldwide capacity for BPA has expanded significantly with

the growth of the polycarbonate and epoxy industries. In 1963, the estimated U.S. capacity of BPA was 75 million pounds, with ~70% of that capacity used for epoxy resins, and only 5-10% used for polycarbonate production(37). Ten years later, U.S. production of BPA had soared to 330-340 million pounds, with an estimated 50% directed towards epoxy resins and 25-30% aimed at polycarbonate production(38). The current estimate of U.S. BPA capacity is 2 billion pounds, with approximately 63% used for polycarbonate production and 27 % for epoxy resins(39). Other applications for BPA are in polysulfone resins(40), polyetherimide resins(41), and aromatic polyester resins(42). The vast majority of polycarbonate resin manufactured today still utilizes BPA as the diol source, and all reported syntheses of BPA involve the acid catalyzed condensation of two moles of phenol with one mole of acetone (Figure 4).

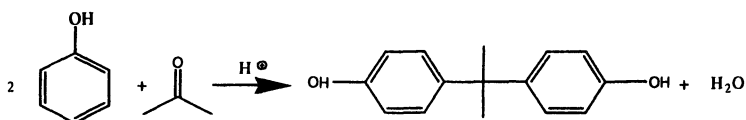


Figure 4: BPA synthesis from phenol and acetone

Most of the world supply of phenol and acetone is produced by a process involving the acid catalyzed decomposition of cumene hydroperoxide(43). In contrast to the apparent simplicity of the above figure, the BPA manufacturing process is greatly complicated by reactions which reduce phenol and acetone selectivities. Increased material expenditures, as well as increased purification-associated investment are required to generate highly pure BPA necessary for polycarbonate manufacture by the melt process. Particularly critical is the absence of acidic impurities, which would neutralize basic polymerization catalysts, and non-volatile monohydroxyphenolic byproducts, which would function as polymerization chain stoppers. The impurity levels in BPA streams prior to purification are largely determined by the reaction process, including factors such as the mode of acid catalysis (homogeneous HCl or heterogeneous acidic ion exchange resin), extent of by-product recycle, and the presence, level, and nature of reaction promoters (generally thiol).

Mechanism

Nucleophilic attack by phenol on protonated acetone may occur at the o- or p- positions, leading to a mixture of (desired) para- and (undesired) ortho-hydroxyphenylalkanols. Subsequent dehydration to a mixture of p- and o-isopropenylphenols is followed by rapid acid-catalyzed p-alkylation (sterically preferred over o-alkylation) of another mole of phenol by each of the isomeric isopropenylphenols. This leads to the desired p,p-BPA isomer and the undesired o,p-BPA isomer, the latter being the principal reaction byproduct.(44)

Catalysis

Initial reports in the 1940's described the use of hydrochloric or sulfuric acid as homogeneous acid catalysts in BPA synthesis(45). The ability to distill hydrochloric acid (HCl) away from the product mixture and avoid phenol sulfonation made its use more favorable. Several years later, Perkins et al demonstrated the value of thiol promoters, which greatly enhanced reaction rate and selectivity.(46) Thiol promotion was subsequently shown to be a rate and selectivity promoter for a wide variety of acid catalysts, as will be described below.

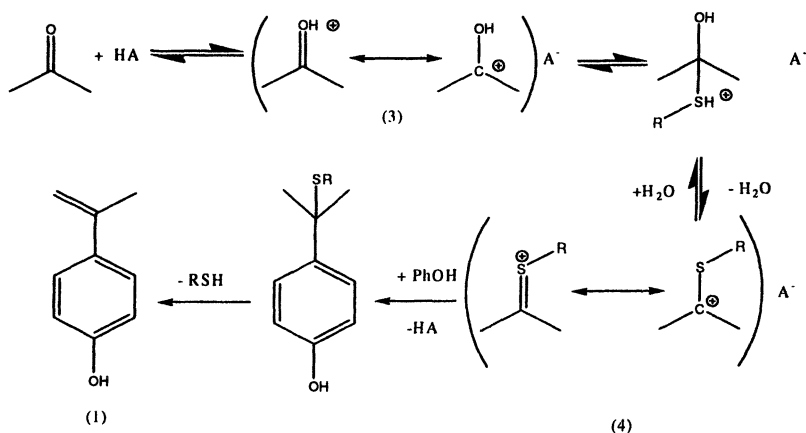
Over the last thirty years, the advantages of heterogeneous acid catalysis in BPA synthesis have become apparent. These heterogeneous catalysts, generally based on sulfonated styrene-divinylbenzene resins,(47) offer advantages over homogeneous (e.g. HCl) catalysis in that they are non-corrosive, easily separated from the reaction mixture, and conducive to continuous reaction operation.(48) Typically, a phenol-acetone stream is continuously eluted through the fixed bed (heterogeneous) catalyst. A high phenol/acetone mole ratio is generally employed, primarily to minimize byproducts derived from acetone self-condensation. Early studies with these heterogeneous acid catalysts indicated the rate of reaction was too slow for commercial viability. However, the addition of thiol promoters, shown earlier to enhance reaction rate and selectivity in the homogeneous acid catalyzed reaction, were shown to be effective at aiding the heterogeneous acid catalyzed reaction as well. Subsequently, the type of thiol and its means of introduction into the process stream became the subject of intensive study in heterogeneous acid catalyzed systems.

The thiol may be homogeneous (added to the phenol-acetone reactor feed and present in the product-containing reactor effluent), and in this case is referred to as a "bulk" promoter. In this case, the thiol promoter must be removed from the product mixture and recycled to reaction. Examples of bulk promoters include simple alkanethiols or mercaptoalkanoic acids. The combination of heterogeneous acid catalyst and bulk promoter is referred to as the "bulk promoter system".

Alternatively, the thiol may be heterogeneous, i.e. attached to the heterogeneous acid catalyst, and consequently absent from the product-containing reactor effluent. In this case, it is referred to as an "attached" promoter, and the heterogeneous acid catalyst with attached thiol promoter is referred to as the "attached promoter system". Methods for promoter attachment generally involve sacrificing some of the acid sites using functionalized thiols as the chemical means of attachment. The earliest attached promoter systems utilized covalently bound mercaptoethanol (as sulfonate ester)(48) or ionically attached aminoethanethiol (as ammonium sulfonate salt)(49, 50), with the latter type showing greater activity and reproducibility.

The precise role of thiol in BPA synthesis is not completely understood. It has been postulated that in the case of crosslinked sulfonated polystyrene catalysts, the thiol increases the tendency of the resin to swell in the presence of phenol, thus making the sulfonic acid sites more accessible to the reactants(51). However, this model does not explain the general acid catalyzed acceleration observed in homogeneous acid catalysis in the presence of thiols (46, 52). A more likely mechanism for the participation of thiols in the acid catalyzed BPA process is depicted in Figure 5.

Figure 5: Thiol promoted phenol-acetone condensation



The formation of sulfur stabilized ion (4) and, to some extent, the uptake of water by the heterogeneous acid catalyst (particularly in the case of sulfonated cross-linked polystyrene) results in a more stable intermediate relative to protonated acetone (3), thereby increasing its concentration and consequently increasing the overall reaction rate. In addition, the presence of a bulky R group (e.g. an alkyl group in the case of a bulk thiol promoter, the functionalized heterogeneous acid catalyst in the case of an attached thiol promoter) favors the depicted para- attack of phenol on steric grounds, yielding higher selectivity towards formation of p-isopropenylphenol (1) and ultimately for p,p-BPA. This would also explain the greater selectivity generally observed in attached vs. bulk promoted thiol systems(49), as well as the improved selectivity observed with increasing chain length of attached (ionically bound) aminoalkanethiol promoters (53).

Cation Exchange Resins(54)

Two types of strongly acidic (sulfonic acid) cation exchange resins are

available commercially. The initially developed *gelular* resin has no defined pore structure, and requires a swelling solvent (e.g. water) to be effective as an acid catalyst. The second, more recently developed *macroreticular* resin, has a well-defined pore structure and does not require a swelling solvent to be an effective acid catalyst. In both cases, the resins are sulfonated styrene-divinylbenzene copolymers, with *macroreticular* resins generally containing higher divinylbenzene levels, hence are more highly cross-linked(55).

The bulk of the literature suggests that despite the fact that gelular resins are recommended for aqueous environments, (which a typical BPA reaction mixture is not), gelular resins are the choice for BPA synthesis(56). The swelling characteristics of gelular resins are dependent on the liquid media they are immersed in. Presumably, the combination of phenol, acetone, BPA, byproducts, and the generated water of reaction are sufficient to provide the proper swelling for effective catalysis and high reaction rate. On a commercial scale process, the rate of reaction is a key parameter, and the diffusion of the reactants into and the products out of the polymer matrix likely affect this rate. The rate of this diffusion will likely be affected by the backbone structure of the resin in the reaction environment. In the case of gelular resins, the amount of cross-linking agent (divinylbenzene) will affect both the mechanical properties of the resin and its swelling characteristics. In general, high cross-linking level increases bead mechanical strength and allows for operation at higher space velocities, yielding higher BPA production rates. Conversely, as cross-linking increases, resin swell characteristics are diminished, as are diffusion rates of reactants and products through the polymer matrix, leading to lower reaction rates. Consequently, the choice of sulfonated polystyrene resin is a complicated one, with numerous factors working at cross purposes with each other.

Cation Exchange Resin Deactivation in BPA Synthesis

Under sustained operation, both bulk and attached promoter catalyst systems derived from cross-linked sulfonated polystyrene resins may undergo diminished BPA production. This generally takes the form of either of two forms of catalyst deactivation. The first is a "fouling" process, which is likely related to the formation of by-products which are retained by the resin, thereby inhibiting access to active sites and impeding the progress of the desired reaction. Frequently, a reduced acid milliequivalency is evident, even following treatment with strong aqueous acid solutions. The precise nature of this fouling and its root cause has not been described. Factors which influence the rate and extent of this type of deactivation likely include feed acetone level, level of effluent recycle and impurity purge, as well as cross-link level of the resin. This type of deactivation occurs in both bulk and attached promoter systems, and methods that limit the fouling or clean the fouled resin have been described(57-59).

The second type of deactivation is observed in attached promoter systems, and is further characterized by a diminished thiol milliequivalency, which is attributed to promoter leaching, promoter fouling (or occlusion) or promoter modification. Inactive ionically bound attached promoter catalyst systems are frequently regenerable by treatment with thiol or thioalkanoic compounds(60), or stripping of the modified (inactive) thiol promoter from the sulfonic acid resin by aqueous acid wash and redeposition of virgin aminoalkanethiol promoter(61). In strict terms, this does not qualify as a true regeneration, since it amounts to discarding the inactive promoter once stripped from the resin. It does serve, however, to recycle the costly cross-linked sulfonated polystyrene. Certain types of inactivated ionically bound attached promoter systems, most notably those deactivated by promoter modification due to high levels of hydroxyacetone in the feed, may be largely reactivated by a process involving treatment of the resin with anhydrous phenol at elevated temperatures.(62)

Stoichiometry and side reactions

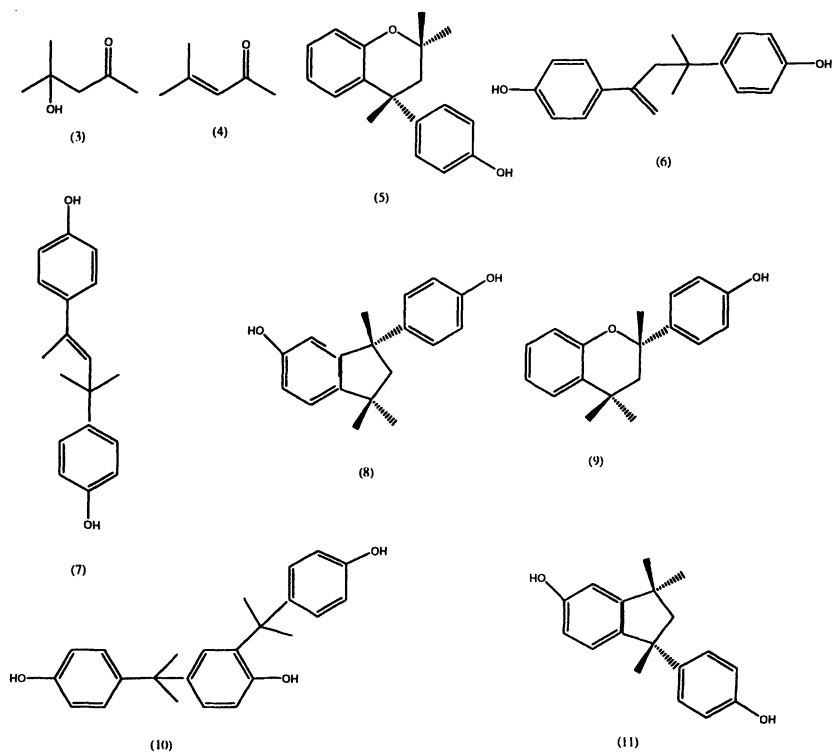
The stoichiometry of the BPA reaction requires two moles of phenol and one mole of acetone to generate 1 mole of BPA. Commercial processes, however, are generally run with phenol/acetone mole ratios of between 6/1 and 16/1. The primary reason to run with this large phenol excess is to avoid side product formation derived from acetone and/or isopropenylphenol dimerization. The main side products (other than the o,p-BPA isomer) appear to form via three basic pathways: 1) acetone self-condensation, 2) dimerization of active isopropenylphenols, and 3) over-alkylation of the desired product and/or its isomer (p,p-BPA and o,p-BPA). The structures of the main side products formed via these pathways are shown in Figure 6.

Clearly, limiting the concentration of acetone and correspondingly the concentration of isomeric isopropenylphenols will reduce by-product formation. Limiting the concentration of the main products (p,p-BPA and the o,p-BPA isomer) are the only effective means of reducing levels of trimer (10).

Isolation/Purification

The optimum mode of isolation of BPA is driven largely by the need to utilize a large molar excess of phenol vs. acetone in reaction in order to minimize byproduct formation. The product of reaction is thus a phenol solution of BPA, byproducts, and water of reaction. A simple method of isolation is afforded by the formation of a crystalline 1:1 molar BPA:phenol adduct, which has limited solubility in phenol.(63) Consequently, depending on the concentration and temperature, a significant quantity of p,p-BPA can be isolated from a reaction solution as the adduct, essentially uncontaminated by the o,p-BPA isomer or other byproducts. The adduct can be broken by either dilution with solvent(64) or application of heat. In the latter case, phenol is removed by distillation, leaving behind pure p,p-BPA.(65)

Figure 6: BPA reaction byproducts



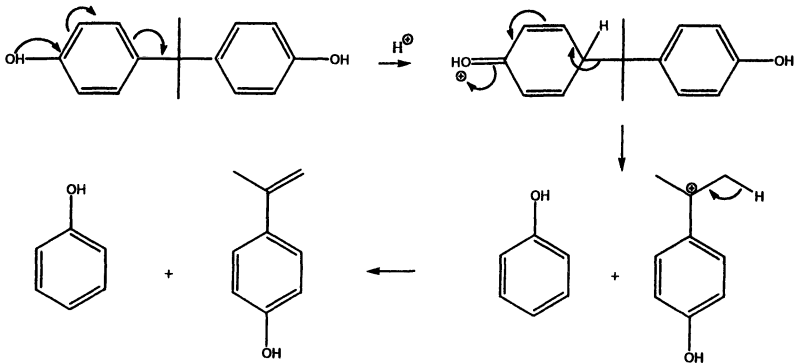
Alternatively, total distillation can be employed, removing phenol first followed by eventual distillation of p,p-BPA (boiling point 220(o)C at 4 mm Hg). This is a difficult process due to the high boiling point and extreme vacuum conditions necessary for the recovery. In addition, the thermal stability of p,p-BPA under these conditions is somewhat suspect.(66) Solvent crystallization, using methylene chloride, toluene or xylene may be employed, however this requires initial removal of excess phenol. Yet another purification method reported involves melt crystallization through the use of a falling film dynamic crystallizer(67). The purity requirements of p,p-BPA for polycarbonate use may require multiple purification steps, combining many of the discussed techniques in a process that is most efficient for the desired purity requirement(68).

Isomerization

Solutions of BPA in phenol under strongly acidic (e.g. condensation reaction)

conditions are subject to isomerization via acid catalyzed reversion to phenol and p-isopropenylphenol. A mechanism is proposed in Figure 7.

Figure 7: Acid catalyzed BPA isomerization



Phenol is then alkylated in the o- or p- position by protonated p-isopropenylphenol leading to an equilibrium mixture of p,p'-BPA and o,p'-BPA, with traces of the o,o'-BPA isomer. In addition, reactions involving the isopropenylphenols may occur, as they are reversibly formed under these conditions, leading to the formation of byproducts (6-10; Figure 6). In the case of trimer (10), reversion back to BPA and isopropenylphenol is also possible. The fate of the other byproducts is not as clear. Para alkylation of p-ipp is kinetically favored, but upon long exposure or at high temperatures, the equilibrium distribution will result)

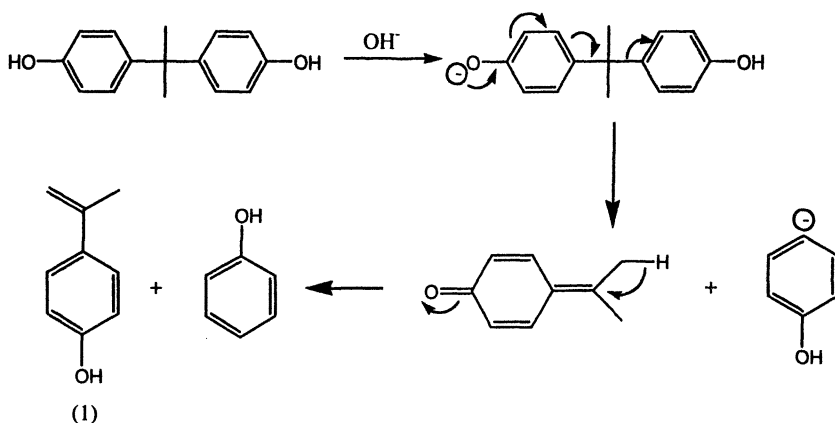
The acid catalyzed isomerization of BPA is a two-edged sword, decreasing the production of (desired) p,p'-BPA isomer under the kinetically controlled reaction environment, and converting o,p'-BPA rich feed to the desired p,p'-BPA isomer. The latter is particularly useful in increasing p,p'-BPA yield in the total process via operation on mother liquor or further processed streams from either solvent or adduct crystallization. A secondary technique, e.g. BPA:phenol adduct formation or distillation (as described above) is then required for isolation of the newly formed p,p'-BPA from the resultant enriched mixture.

Recovery/Purge

The chemical stream leaving the plant, generally a distillation residue following distillative removal of all components with boiling points lower than that of p,p'-BPA, will contain, in addition to high boiling impurities, some level of unrecoverable BPA, in the form of an organic tar for which further processing by distillation is not economically practical. In most cases, this stream will be

subjected to a "cracking" process, aimed at dealkylation of the various components in the mixture in order to recover as much phenol as possible. A number of cracking methods have been described, including both liquid and gas phase processes.(69) The catalysts include zeolites(70), acids, bases and salts.(71-73) In the case of acid catalyzed cracking, the dealkylation mechanism is believed to proceed as depicted in Figure 7, where phenol is recovered and isopropenylphenols undergo dimerization and other acid catalyzed reactions to generate a new byproduct mixture. In base catalyzed tar cracking, p-isopropenylphenol can also be recovered and cleanly converted into p,p-BPA according to Figure 8, making this a more attractive tar cracking alternative.(74)

Figure 8: Base catalyzed cracking



Conclusions

Numerous DPC syntheses have been reported, with key steps including oxidative carbonylation of alkanols or phenol, transesterification of alkyl carbonates with phenol, and phenol addition to phosgene. Synthetic methods for BPA consist almost entirely of selective acid-catalyzed condensation of phenol with acetone, using a variety of homogeneous and heterogeneous catalyst systems. Additional research to optimize and improve current manufacturing processes for these monomers will no doubt continue. Current and future focus, however, appears to be directed towards alternative and potentially simpler approaches in polycarbonate synthesis, including the direct carbonylation of BPA, and the replacement of DPC with more reactive carbonates in the melt process.

REFERENCES

- (1) Clagett, D.C.; Shafer, S.J. *Polymer Engineering and Science*, **1985**, *25*, 457.
- (2) LeGrand, D.G.; Bendler, J.T. *Handbook of polycarbonate science and technology*. 2000, New York: Plastics engineering (Marcel Dekker, Inc.).
- (3) Ring, K.-L.; Toki, G., *CEH Marketing Research Report-Polycarbonate Resins*, in *Chemical Economics Handbook*. October 2001, SRI International. p. 580.1100H.
- (4) Illuminati, G.; Romano, U.; Tesei, R. U.S. Patent 4,182,726, 1980.
- (5) Romano, U.; Tesei, R.; Cipriani, G.; Micucci, L. Ger. Offen. Patent 2,743,690, 1978.
- (6) Illuminati, G.; Romano, U.; Tesei, R. Rom. Patent 71,663, 1980.
- (7) Hallgren, J.E. Ger. Offen. Patent 3,308,921, 1983.
- (8) Babad, H.; Zeiler, A.G. *Chem. Rev.*, **1973**, *73*, 75.
- (9) Nishihira, K.; Tanaka, S.; Kodama, K.; Kaneko, T.; Kawashita, T.; Nishida, Y.; Matsuzaki, T.; Abe, K. U.S. Patent 5,380,906, 1995.
- (10) Shiomi, Y.; Matsuzaki, T.; Masunaga, K. EP Patent 0,108,359, 1987.
- (11) Harada, K.; Sugise, R.; Kashiwagi, K.; Nishio, M.; Doi, T. Jpn. Kokai Tokkyo Koho Patent 10,330,324, 1998.
- (12) Harada, K.; Suginose, Y.; Kashihagi, K.; Nishio, M.; Doi, T. Jpn. Kokai Tokkyo Koho Patent 10,330,323, 1998.
- (13) Peppel, W.J. *Industrial & Engineering Chemistry*, **1958**, *50*, 767-770.
- (14) Knifton, J.F.; Duranleau, R.G. *J. Mol. Catal.*, **1991**, *67*, 389-399.
- (15) Schlosberg, R.H.; Buchanan, J.S.; Santiesteban, J.G.; Jiang, Z.; Weber, W.A. U.S. Pat. Appl. Publ. Patent 2,003,023,109, 2003.
- (16) Buchanan, J.S.; Jiang, Z.; Santiesteban, J.G.; Weber, W.A. PCT Int. Appl. Patent 0,300,641, 2003.
- (17) Matsushita, T.; Takamatsu, K. Jpn. Kokai Tokkyo Koho Patent 2,003,081,893, 2003.
- (18) Tryon, S.; Benedict, W.S. U.S. Patent 2,362,865, 1944.
- (19) Hallgren, J.E. *J. Organometallic Chem.*, **1979**, *175*, 135.
- (20) Hallgren, J.E. *J. Organometallic Chem.*, **1981**, *204*, 135.
- (21) Hallgren, J.E.; Lucas, G.M.; Matthews, R.O. *Journal of Organometallic Chemistry*, **1981**, *204*, 135-8.
- (22) Chalk, A.J. U.S. Patent 4,096,169, 1978.
- (23) Chalk, A.J. U.S. Patent 4,187,242, 1980.
- (24) Takagi, M.; Miyagi, H.; Ohgomori, Y.; Iwane, H. U.S. Patent 5,498,789, 1996.
- (25) Bonitatebus, P.J.; Ofori, J.Y. U.S. Pat. Appl. Publ. Patent 2,003,032,547, 2003.

- (26) Ofori, J.Y.; Bonitatebus, P.J. U.S. Pat. Appl. Publ. Patent 2,003,027,709, 2003.
- (27) Grade, M.M.; Ofori, J.Y.; Pressman, E.J. U.S. Patent 6,410,774, 2002.
- (28) Takagi, M.; Kujira, K.; Yoneyama, T.; Okago, Y. Jpn. Kokai Tokkyo Koho Patent 0,9278,716, 1997.
- (29) Spivack, J.L.; Cawse, J.N.; Whisenhunt, D.W., Jr.; Johnson, B.F.; Soloveichik, G.L. PCT Int. Appl. Patent 0,066,530, 2000.
- (30) Takagi, M.; Miyagi, H.; Yoneyama, T.; Ohgomori, Y. *Journal of Molecular Catalysis A: Chemical*, **1998**, 129, L1-L3.
- (31) Pressman, E.J.; Soloveichik, G.L.; Johnson, B.F.; Shalyaev, K.V. U.S. Patent 6,172,254, 2001.
- (32) Shalyaev, K.V.; Soloveichik, G.L.; Johnson, B.F.; Whisenhunt, D.W., Jr. PCT Int. Appl. Patent 0,155,079, 2001.
- (33) Buysch, H.-J.; Hesse, C.; Rechner, J. Eur. Pat. Appl. Patent 749,955, 1996.
- (34) Buysch, H.-J.; Hesse, C.; Rechner, J.; Schomaecker, R.; Wagner, P.; Kaufmann, D.P.D.C. Ger. Offen. Patent 4,403,075, 1995.
- (35) Ofori, J.Y.; Pressman, E.J.; Shalyaev, K.V.; Williams, E.D.; Battista, R.A. U.S. Patent 6,384,262, 2002.
- (36) *Personal Communication*, Daniel W. Fox to Sheldon J. Shafer.
- (37) In *Chemical & Engineering News*; June 3, 1963, p. 35.
- (38) In *Chemistry & Engineering News*; July 16, 1973, p. 5.
- (39) In *Chemistry & Engineering News*; May 5, 2003, p. 40.
- (40) Parodi, F., *Polysulfones*, in *Comprehensive Polymer Science*. 1989. p. 561.
- (41) Sillion, B., *Polyetherimides*, in *Comprehensive Polymer Science*. 1989. p. 499.
- (42) Dean, B.D.; Matzner, M.; Tibbitt, J.M., *Polyarylates*, in *Comprehensive Polymer Science*. 1989. p. 317.
- (43) Fortuin, J.P.; Waterman, H.I. *Chemical Engineering Science*, **1953**, 2, 182-92.
- (44) Pressman, E.J.; Wetzel, J.R. U.S. Patent 5,990,362, 1999.
- (45) Perkins, R. U.S. Patent 2,191,831, 1940.
- (46) Perkins, R.; Bryner, F. U.S. Patent 235,242, 1944.
- (47) D'Alelio, G.F. U.S. Patent 2,366,007, 1944.
- (48) Apel, F.; Farevaag, F.; Bender, H.L. U.S. Patent 3,049,569, 1962.
- (49) McNutt, B.W.; Gammill, B.B. U.S. Patent 3,394,089, 1968.
- (50) McNutt, B.W.; Gammill, B.B. GB Patent 1,183,564, 1970.
- (51) Reinicker, R.A.; Gates, B.C. *AIChE Journal*, **1974**, 20, 933-40.
- (52) Janson, J.E. U.S. Patent 2,468,982, 1949.
- (53) Willey, P.R. Eur. Pat. Appl. Patent 144,735, 1985.
- (54) Faler, G.R.; Loucks, G.R. U.S. Patent 4,424,283, 1984.
- (55) Dorfner, K. *Ion Exchangers-Properties and Applications*. 1977: Ann Arbor Science Publishers Inc.

- (56) Jerabek, K.; Hankova, L.; Prokop, Z.; Lundquist, E.G. *Applied Catalysis, A: General*, **2002**, 232, 181-188.
- (57) June, R.L.; Allan, E.D.; Blackburn, R.L.; Buechele, J.L. PCT Int. Appl. Patent 9,722,573, 1997.
- (58) Melby, E.G. U.S. Patent 4,051,079, 1977.
- (59) Peemans, R.F.A.J.; Kruglov, A.; Shaffer, S.J.; Mbeledogu, C.O.; Nance, D.H.; Baro, K.A.; Georgiev, E.M.; Schalmann, E.H.; Kissinger, G.M. PCT Int. Appl. Patent 0,285,828, 2002.
- (60) Jpn. Kokai Tokkyo Koho Patent 57,075,146, 1982.
- (61) Yamamoto, S.; Asaoka, S.; Kukitome, A. Jpn. Kokai Tokkyo Koho Patent 08,323,210, 1996.
- (62) Pressman, E., J.; Shafer, S.J. U.S. Patent 5,428,075, 1995.
- (63) Stoesser, W.; Sommerfield, E. U.S. Patent 2,623,908, 1952.
- (64) Li, M.K. U.S. Patent 4,156,098, 1979.
- (65) Schuster, L. Brit. Patent 1,377,227, 1974.
- (66) Kolt, J.; Kiedik, M.; Rzodeczko, A.; Bek, T.; Czyz, J.; Zajac, E.; Mroz, J.; Bobinska, K. Pol. Patent 135,982, 1987.
- (67) Kissinger, G.; Wynn, N. U.S. Patent 5,243,093, 1993.
- (68) Pressman, E.J.; Shafer, S.J.; Wetzal, J.R.; Oyevaar, M.H. U.S. Patent 5,723,689, 1998.
- (69) Yao, B.; Bassus, L.; Lamartine, R.; Gaurvit, J.-Y.; Lanteri, P.; Longera, R. *Bull. Soc. Chim. Fr.*, **1996**, 133, 477-480.
- (70) Flock, J.W. U.S. Patent 4,351,966, 1982.
- (71) Kiedik, M.; Grzywa, E.; Kolt, J.; Terelak, K.; Czyz, J.; Niezgoda, A. U.S. Patent 4,131,749; 1978.
- (72) Carnahan, J.C. U.S. Patent 4,227,628, 1981.
- (73) Shindo, A.; Sakashita, K.; Yasui, M.; Asaoka, S. Jpn. Kokai Tokkyo Koho Patent 05,331,088, 1993.
- (74) Kato, N.; Takase, T.; Morimoto, Y.; Yuasa, T.; Hattori, M. U.S. Patent 4,242,528, 1980.

Chapter 4

End-Functionalized Poly(bisphenol A carbonate) Oligomers Part I: Synthesis and Examples

Michael R. Korn

Department of Chemistry and Biochemistry, Texas State University,
San Marcos, TX 78666

Various examples for end-functionalized PC oligomers are presented and their synthetic methods described. The two major synthetic routes involve the solution process (interfacial or homogeneous) and a transesterification process (with the use of a solvent or solvent-free in the melt or by solid state polymerization); a third route employs the reaction of bisphenol A with carbon monoxide.

Introduction

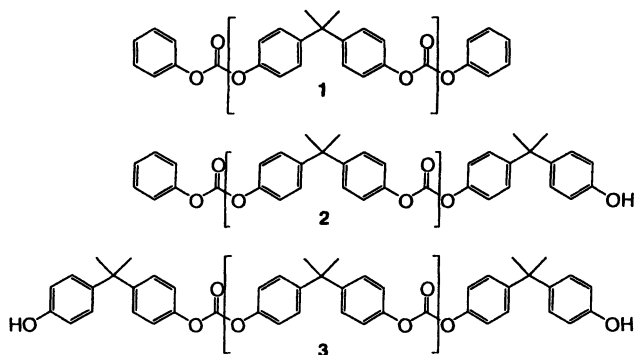
Endgroups in polymers play an important role as they not only affect overall physical properties, but also allow for chemical modifications and chain extension and often are suitable probes for analysis. Because the ratio of endgroup(s) to repeating units increases with decreasing degree of polymerization (DP) the influence of endgroups is particularly prominent in *oligomers*, i.e. polymers with molecular weights (MWs) ≤ 10 kg/mol. The cut-off value of 10 kg/mol in MW is somewhat subjective, as MW values are reported as M_n or M_w , depending on which analytical tool was employed, e.g. GPC (calibrated with PS or PC), ^1H NMR, HPLC, mass spectrometry (ESI, APCI, MALDI) or vapor pressure osmometry (VPO). A comparison of the results obtained by those various analytical tools will be discussed in the next two chapters (Part II&III).

Besides the term oligomer, the term *telechelic* is used in the literature. A telechelic is defined as an oligomer or polymer with (at least) one endgroup that

Note: Chapters 4–6 are dedicated to the Creator and Savior of this world, the Lord Jesus Christ and to my grandfather, Dr. Friedrich L. Korn, who in the 1950s and 1960s helped in transferring PC from the laboratory to full-scale production.

allows for chain extension, *e.g.* to give high(er) MW polymers, block copolymers, or polymer networks (1-3).

Considering poly(bisphenolA)carbonate (PC) and other condensation compounds, the strict definition of a telechelic, *i.e.* the necessity of an endgroup to allow for chain extension cannot be fully maintained as illustrated by compounds 1-3.



Structures 1-3 are possible products derived from the various processes described in this chapter. Following the above definition for a telechelic, only 2 and 3 would qualify as telechelics, as only they possess hydroxyl endgroups, allowing for chain extension. Chain extension can equally well occur in all three compounds 1-3 via transesterification of any of the carbonate repeating units along the polymer backbone, and therefore all three oligomers can chain extend and thus qualify as telechelics. To account for this fact, we therefore will use the more general term *end-functionalized oligomers* in this chapter rather than telechelics.

Polymers that are end-functionalized but are not true oligomers are omitted in this chapter, *e.g.* an allylphenyl terminated PC (useful for silylation reactions) with a MW of 40 kg/mol (4). Also excluded are any end-functionalized PC oligomers, which are based on other than Bisphenol A (BPA) repeating units along their polymer backbone, *e.g.* hyperbranched PC oligomers based on the BPA related compound 1,1,1-tris(4'-hydroxyphenyl)ethane (5) terminated by phenolic, carbonylimidazolide, and *tert.*-butyldimethylsilyl groups.

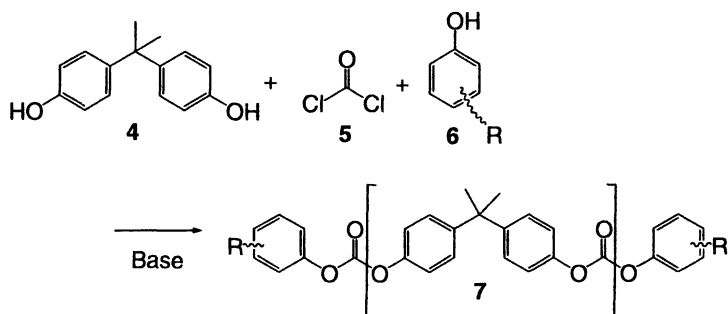
Synthesis of End-functionalized PC Oligomers

Several synthetic methods exist for the synthesis of end-functionalized PC oligomers:

A. Solution Process

Reacting BPA **4** and phosgene **5** in either an interfacial (A1) or a homogeneous (solution) process (A2) will result in PC terminated by BPA endgroups (compound **3**). To place a different group at the end, the polymerization can be conducted in the presence of a substituted mono-phenol **6** or a hydrolyzable precursor, both of which act as terminators to the PC chain (Scheme 1); prominent terminators are phenol and *tert.*-butylphenol.

Scheme 1. Synthesis of End-functionalized PC **7** via a Solvent Process.



B. Transesterification Process

Several variations have been reported which operate via a transesterification process; three are mentioned here:

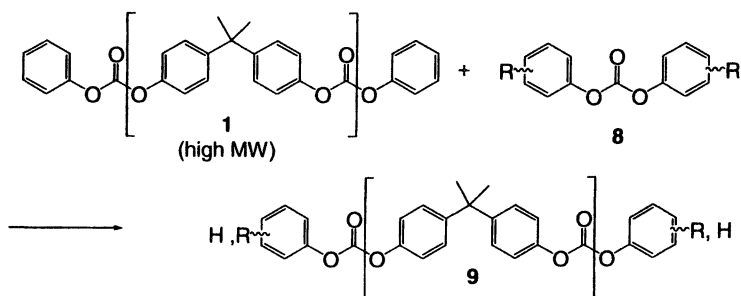
B1. The most important one is condensing BPA and DPC with an appropriate catalyst and distilling off phenol (melt process). Depending on the stoichiometry of BPA and DPC and the progress of the reaction (i.e. amount of phenol distilled off), compounds **1-3** of various molecular weights can be obtained.

Thermodynamically much less favored is the reaction of BPA with dimethylcarbonate (DMC) (removing methanol) to yield oligomers with methylcarbonate endgroups (**6**). Using DMC with bisphenol A diacetate instead of BPA (removing methylacetate) oligomers with mixed acetate and methylcarbonate endgroups are produced (**7**).

B2. In a depolymerization process, high MW PC is reacted with phenols or arylcarbonates to give oligomers with potentially mixed endgroups; the endgroups in the resulting oligomers stem from the endgroups of the depolymerized PC and the added phenols/arylcyanates. The ratio of endgroups stemming from added phenol/arylcyanate to native PC endgroups increases with decreasing MW of the starting PC and increasing amount of phenol/arylcyanate. The MW of the final oligomers is governed by the MW of the starting PC and the amount of phenol/arylcyanate and of the catalyst utilized for transesterification.

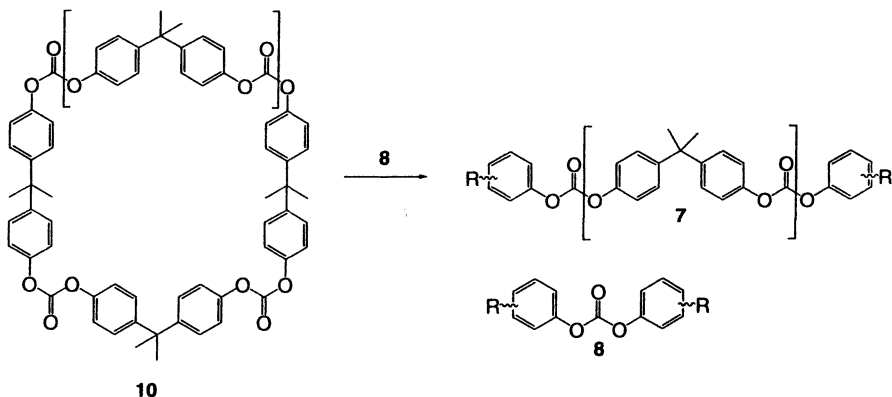
Using BPA, phenol or DPC, compounds **1**, **2** or **3** or mixtures thereof are obtained. If substituted phenols **6** or substituted arylcarbonates **8** are used, PC oligomers **9** with different endgroups are obtained (Scheme 2). This process can proceed in solution or solvent-free at high temperatures in the melt.

Scheme 2. Synthesis of End-functionalized PC via Depolymerization with Arylcarbonates.



B3. A third method employs ring-opening polymerization (ROP) of oligomeric cyclic BPA carbonates e.g. **10** with a suitable catalyst, and ROP of cyclic BPA carbonates in the presence of phenols, bisphenols or diarylcarbonates (**8-10**); the later (and catalyst residues) determine the type of endgroups present (*c.f.* Scheme 3). ROP can proceed in the melt or in solution (*11*).

Scheme 3. Synthesis of End-functionalized PC via ROP/Transesterification with Arylcarbonate **8**.



It needs to be noted that whatever method is used to produce linear oligomers, cyclic oligomers are almost always formed as well. An excellent

paper on the selective synthesis of linear vs. cyclic oligomers was published by Brunelle *et al.* (12-13), a brief summary of which is included in chapter 2.

C. Oxidative Carbonylation

To avoid the need of phosgene and phosgene based precursors as the source of the carbonyl moiety in PC, carbon monoxide (CO) is reacted with BPA in the presence of oxygen and a catalytic redox system (14-15). Depending on the catalytic system oligomers **2**, and/or **3** are formed or oligomers with undesirable *o*-phenylene carbonate and salicylic acid-type endgroups. Conducting oxidative carbonylation with the addition of phenol produces oligomers **1-3** (and byproducts), primarily through the *in situ* generation of DPC and its subsequent transesterification with BPA (16-17). A more detailed description of the oxidative carbonyl process for the synthesis of small molecules is given in chapter 3.

D. Polymeranalogous Reactions

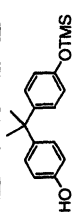
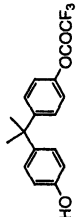
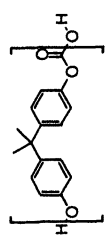
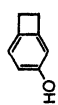
An example for a polymeranalogous reaction (modification of an existing polymer) was given by Hathaway and Pyles for high (!) MW PC (18). In their patent, OH terminated PC (MW 40 k) was reacted in solution with trimellitic anhydride acid chloride to give the anhydride terminated PC (as analyzed by NMR and FTIR). Korn *et al.* brominated methylcinnamate terminated PC oligomers (19).

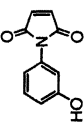
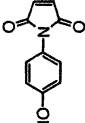
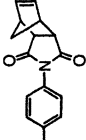

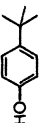

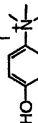
Examples for End-functionalized PC Oligomers

Table 1 contains some literature examples for end-functionalized PC oligomers prepared via the solution process (A1, A2). The structure of the respective substituted phenol for endgroup modification, the synthetic method chosen, the type of oligomer obtained, the MW(s) of the resulting oligomer(s) (given as a MW range) and the analytical methods reported for their characterization are included.

The first three entries (Table 1.a-c) yield BPA terminated PC oligomers **3**. All three processes employ protecting group chemistry to some extent. Whereas in 1.a.b oligomers of various MWs are isolated, 1.c describes the synthesis and isolation of individual oligomers (dimer through decamer). Entries 1.d-h yield oligomers **12-15** that were explored for subsequent crosslinking reactions to yield PC networks. A short summary of other PC oligomers with crosslinkable endgroups not listed in Table 1 is found in ref. 23 and 25. Oligomers **16** (entry 1.i) were synthesized to serve as a reference to **15**. Degee *et al.* report the synthesis of oligomers **17** with N,N-dimethylamino endgroups (entry 1.j) and the corresponding quaternized ionic polymer (entry 1.k) with the goal to produce physical networks, respectively.

Table 1. End-functionalized PC Oligomers by Solution Processes A1 and A2

Entry	Phenol	Process	Final Oligomer	M_n g/mol	Analysis	Ref.
a		A2	3, 11	2.3-20.6k	GPC, $^1\text{H-NMR}$ UV-vis	(20)
b		A2	3	2.3-16.0k	GPC, UV-vis, $^{19}\text{F-NMR}$	(20)
c		A2	3	Dimer (482) – decamer (2,768)	HPLC, FTIR, $^1\text{H-NMR}$, MS	(13)
d		A1	12	0.5-11.8k	GPC, HPLC, DSC	(21)

e		A1, A2	13	3-12.5k	GPC, ¹ H-NMR DSC	(22)
f		A2	similar to 13	5.8k	GPC, ¹ H-NMR DSC	(22)
g		A2	14	6.8k	GPC, ¹ H-NMR DSC	(22)
h		A1	15	2-10k	GPC, ¹ H-NMR UV-vis, [η], DSC	(23)
i		A1	16	3-10k	GPC, ¹ H-NMR IV, DSC	(23)
j		A1	17	2.5-21k	GPC, ¹ H-NMR	(24)
k		A1	17'	25k	¹ H-NMR	(24)

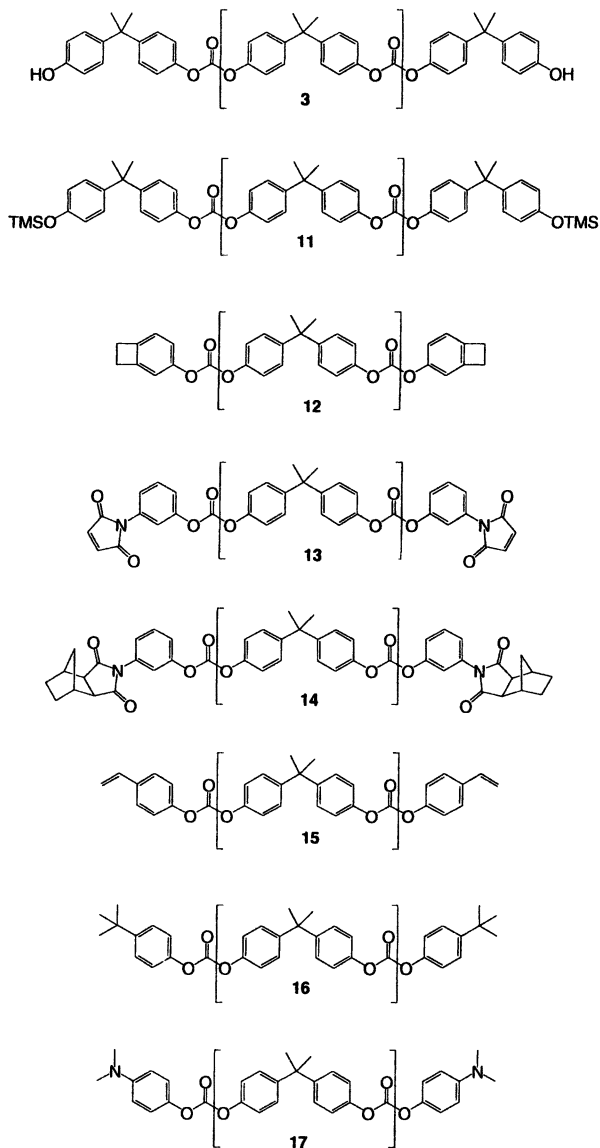
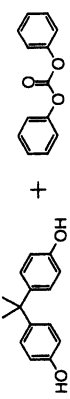
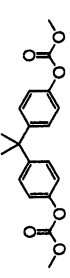
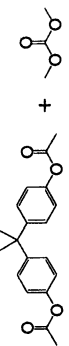


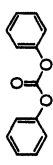
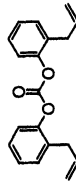
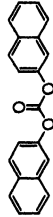
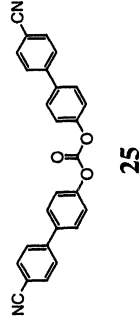
Table 2 contains end-functionalized PC oligomers synthesized via transesterification reactions; it lists the respective reagents/arylcarbonates, the type of process, the type of oligomer, the MW(s) of the resulting oligomer(s) and methods for their analysis (if more than one MW was produced, MW is given as a MW range or specified for individual experiments).

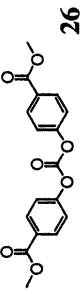
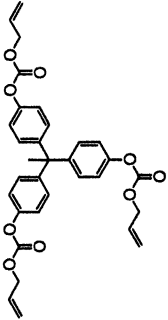
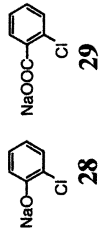
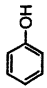
**Table 2. End-functionalized PC Oligomers via Transesterification Reactions
B1-B3**

<i>Entry</i>	<i>Reagents</i>	<i>Process</i>	<i>Final Oligomer</i>	<i>MW g/mol</i>	<i>Analysis</i>	<i>Ref.</i>
a		B1	1-3	$M_w = 2.5k$	GPC	(26)
b		B1	18	$M_n = 6.5k$	GPC, NMR, IR	(6)
c		B1	19	$M_n = 600$	GPC, NMR, MS, VPO	(7)

Continued on next page.

Table 2. Continued.

Entry	Arylcarbonates	Process	Final Oligomer	MW g/mol	Analysis	Ref.
d		B2 (solvent)	1	$M_n=1.6-4.5k$	GPC, DSC	(27)
e		B2 (solvent)	20	$M_n=2.3k$	GPC, DSC, 1H NMR	(27)
f		B2 (solvent)	21	$M_n=2k$	GPC, MALDI, DSC	(27)
g		B2 (solvent)	22a	$M_n=1.7k$	GPC, HPLC, DSC	(27)
			22b	$M_n=2.4k$	GPC, 1H NMR, HPLC, MALDI, ESI, APCI	(27)

h		26	B2 (solvent)	23	$M_n = 1.5\text{k}$	GPC	(19)
i		27	B2 (solvent)	24a 24b 24c	$M_n = 3.2\text{k}$ $M_n = 3.1\text{k}$ $M_n = 3.0\text{k}$	GPC	(19)
j		28 29	B2 (melt)	a)	$M_n = 9.4 - 19.4\text{k}$	GPC, IR, melt η	(28)
k			B2	1-3	$\eta_{rel} = 1.03$	η_{rel}	(29)

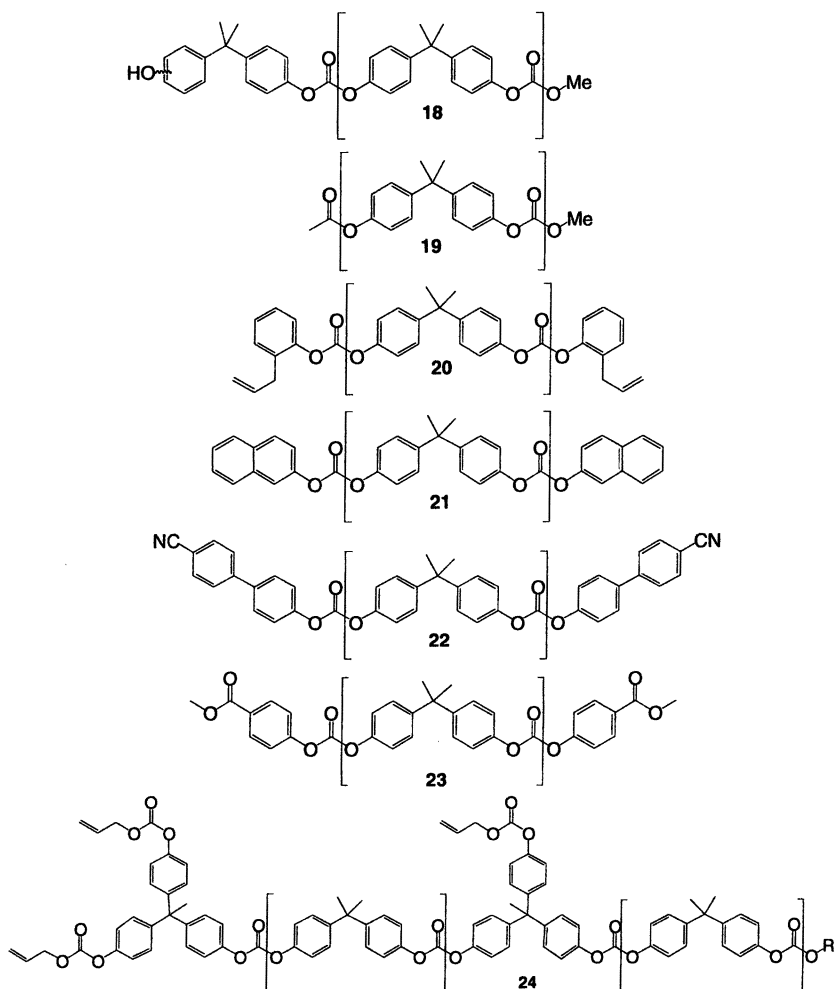
Continued on next page.

Table 2. Continued.

B3: MW build-up via ROP

Entry	Reagents	Process	Final Oligomer	MW g/mol	Analysis	Ref.
l	BPA Carbonate tetramer 10 + BPA	B3 (melt)	3	$M_w = 6k$	GPC, MALDI	(10)
m	BPA Carbonate oligomers 10 + BPA	B3 (melt)	3	$M_n = 1.3 k$	GPC, NMR, IR	(8)

a): product similar to oligomers **1-3** in which the OH groups are replaced by ONa groups.



Entry **2.a** exemplifies the typical melt process for PC oligomers; starting from BPA and DPC, the resulting endgroups are BPA and phenoxy residues (oligomers **1-3**). The catalyst employed was aq. LiOH. The synthesized oligomers were then further employed for solid state polymerization (transesterification) using supercritical CO₂ as a carrier to remove phenol; chapter 7 further details this process. Entries **2.b.c** were obtained by employing the less reactive methylcarbonate functional group. Haba *et al.* (6) employ various catalysts, of which Ti(O*i*Pr)₄ produces a PC oligomer **18** (58% yield) with less than 3% OH groups. Deshpande *et al.* (7) employ a Ti(OPh)₄ catalyst and produce oligomers **19** with low degrees of polymerization (DP = 2-4) and

various ratios of acetate vs. methycarbonate endgroups. Entries **2.d-i** were obtained by depolymerizing high MW PC in solution (THF) with KOtBu as catalyst. Figure 1 illustrates the decrease in MW with increasing amount of arylcarbonate as exemplified for DPC (entry **2.d**).

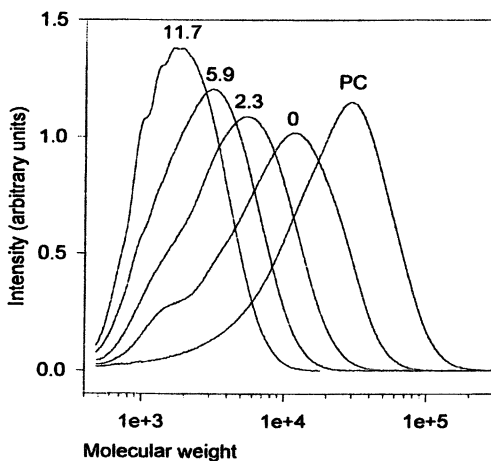


Figure 1. GPC chromatograms of oligomers 1 by depolymerizing high MW PC in THF with 0.5 mol % KOtBu (0 equivalents), 2.3, 5.9 and 11.7 equivalents of DPC (Reproduced from reference 27. Copyright 1998 American Chemical Society.)

Oligomers **20** (entry **2.e**) allow further functionalization of the double bond. **21** and **22** were primarily chosen for analytical purposes, as the naphthyl and cyanobiphenyl group absorb to higher wavelengths than PC.

Due to the difference in reactivity (basicity) of phenoxy vs. alkoxy groups, arylcarbonates bearing additional aliphatic esters (diarylcarbonate **26**) or aliphatic carbonate groups (triarylcarbonate **27**) exclusively transesterify via the phenoxy moiety and thus lead to oligomers **23** and **24** (entries **2h.i**) in which the aliphatic ester/carbonate groups remain unaffected (non-transesterified) and become endgroups. This allows the incorporation of a multitude of organic residues via esters as endgroups.

When using the trifunctional 1,1,1-tris(4'-allyloxycarbonyloxyphenyl)ethane **27** (entry **2.i**) end-functionalized hyperbranched oligomers **24** are anticipated (the structure given above depicts one of many possible structures with R = endgroup of the starting PC). To illustrate the effect of a trifunctional vs. a difunctional arylcarbonate on the MW and MW distribution (MWD), PC ($M_n = 12,700$ g/mol (corrected); PDI = 2.5) was transesterified with 10 equivalents of **26** to give **23** and with 1, 5, and 10 equivalents of **27** to give **24a**,

24b and **24c**, respectively. The calculated M_n values for **23** are 950 g/mol and for **24a-c** 4,700, 1,350 and 970 g/mol, respectively. The resulting GPC chromatograms were recorded for all experiments as well as for the starting PC and for **27**. An overlap of all six GPC chromatograms is shown in Figure 2.

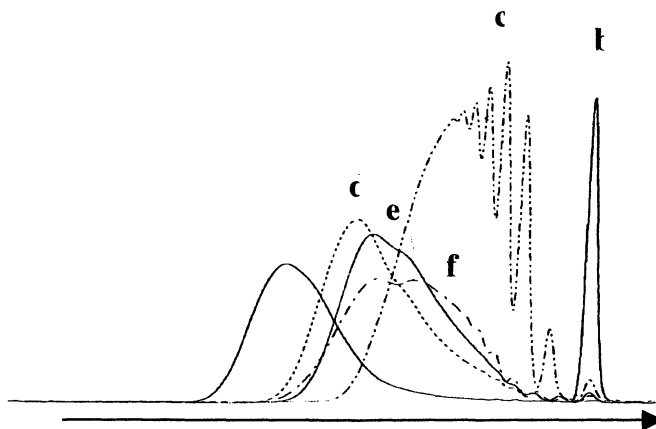


Figure 2. GPC chromatograms: (a) PC, $M_n = 12,700$ g/mol, PDI = 2.5; (b) **27**; (c) **23**, $M_n = 1,500$ g/mol, PDI = 1.6; (d) **24a** (1 equiv. of **27**), $M_n = 3,200$ g/mol, PDI = 2.3; (e) **24b** (5 equiv. of **27**), $M_n = 3,100$ g/mol, PDI = 2.3; (f) **24c** (10 equiv. of **27**), $M_n = 3,000$ g/mol, PDI = 2.0.

In all cases oligomers **24a-c** are significantly different from their linear analogues as observed for their MW and MWD. Even when using 10 equivalents of **27**, which should give a theoretical M_n similar to that of **23**, MW for **24c** is about twice as high as for the linear analogue **23**. The shape of the GPC chromatogram also becomes multimodal as expected for a mixture of hyperbranched (and linear) oligomers of various composition.

Entry **2.j** describes the depolymerization of PC with 1 - 0.1 wt % of sodium salts of phenols **28** and benzoic acids **29** in the melt for about 10 min at 242-274 °C. As a result, PC oligomers partially terminated by phenoxide residues are obtained. Reacting PC with **29** results in the release of CO₂ leading to the formation of ester bonds in the oligomers; in addition, branching and the formation of ether and salicylate groups were observed (via HPLC and NMR of hydrolyzed PC oligomers).

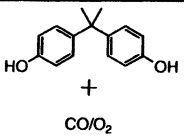
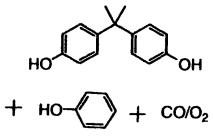
Similarly, high MW PC ($\eta_{rel} = 1.3$) was depolymerized by phenol (which also served as a solvent for PC) (**Tab. 2.k**) to give a PC with a reduced viscosity

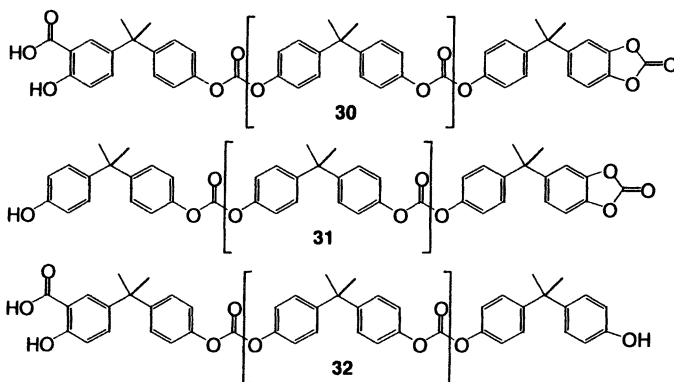
of $\eta_{rel} = 1.03$. The product contained low molecular weight oligomers, phenol, BPA (14%) and DPC (14%) as well.

ROP of a single cyclic BPA carbonate, the tetramer **10**, with 5 mol% BPA at 275°C for 15 min produced a PC with $M_w = 44,400$ g/mol (95% yield). Repeated fractionation of this high MW PC gave the oligomeric fraction **3** (entry 2.l). ROP of a mixture of PC cyclic oligomers with BPA in a 3.5 : 1.0 molar ratio with Bu_4NBPh_4 as catalyst at 255 °C for 20 min directly produced oligomers **3** (entry 2.m).

Table 3 contains end-functionalized PC oligomers synthesized via oxidative carbonylation reactions. It lists the respective reagents, type of oligomer, the MW(s) of the resulting oligomer(s) and methods for their analysis.

Table 3. End-functionalized PC Oligomers via Oxidative Carbonylation

Entry	Reagents	Final Oligomer	MW g/mol	Analysis	Ref.
a		3 , 30, 31, 32	$M_n = 1.9k$	GPC, NMR, IR, MALDI	(14, 15)
b		1-3	$M_n < 1k$	HPLC, FTIR, GC-MS	(16)



A very effective catalytic system to produce almost exclusively hydroxyl terminated PC oligomers **3** (80% yield) Tab. **3.a**) employs a mixture of PdCl₂, Ce(OAc)₃, bis(Ph₃PAnylidene)NBr, hydroquinone, molecular sieves, thus eliminating the cyclic *o*-carbonate endgroup (in **30** and **31**) and minimizing terminal salicylic acid groups (as in **30** and **32**). A mixture of oligomers **1-3** is obtained with different redox systems and the addition of phenol (Tab. **3.b**); the article (Ref. 16) also discusses the influence of solvents, bases, co-catalyst, molecular sieves, and molar ratio of BPA vs. phenol.

Experimental

Synthesis of 26. 3.04 g (0.02 mol) of 4-hydroxy-methylbenzoate was dissolved in 20 mL of dry THF; 3.10 mL (0.022 mol) of freshly distilled (fromCaH₂) NEt₃ was added and the solution stirred with a magnetic stir bar while cooling on an ice bath. 1.01 g (0.034 mol) of triphosgene in 5 mL of dry THF was then added over a period of 10 min. upon which immediate precipitation of a white solid occurred. After 2h the reaction mixture was precipitated into water, the solids filtered and dried. The solids were then extracted with 70 mL of hot ethylacetate, filtered hot, the filtrate reheated and allowed to cool down in a refrigerator to yield crystals. Isolation of the crystals (1st and 2nd crop) yielded 68% of **26**.

Synthesis of 27. To a magnetically stirred solution (cooled on an ice bath) of 3.07 g (0.01 mol) of 1,1,1-tris(4'-hydroxyphenyl)ethane, cat. DMAP, 30 mL of dry THF and 5.6 mL (0.04 mol) of freshly distilled (fromCaH₂) NEt₃ was added 4.5 mL (0.04 mol) of allyl chloroformate in 3 mL of dry THF. The reaction was allowed to warm to room temperature and was worked up after 30 h.

Oligomers 24. 508 mg (0.04 mmol) PC (from DOW; *tert*.Butylphenol terminated; D.P. = 49, M_n = 12,700 g/mol by ¹H NMR) and 224 mg (0.4 mmol), or 113 mg (0.2 mmol), or 22.5 mg (0.04 mmol) of **27** were dissolved in 10 mL of dry THF over 30 min. Then 930 uL of a solution of 3.0 mg sublimed KO^tBu in 2.5 mL of dry THF was added and the reaction run for 60 min. Afterwards the solution was precipitated from MeOH, the solids filtered, washed and dried.

Acknowledgement

Compounds and oligomers **1, 18-27** (Table **2e-i**) were synthesized during a post-doctoral appointment at UNC, Chapel Hill, NC with Prof. M. Gagné.

References

1. Percec, V.; Pugh, C.; Nuyken, O.; Pask, S. D. *Macromonomers, Oligomers and Telechelic Polymers in Comprehensive Polymer Science*, Allen, G., and Bevington, J. C., Eds.; Pergamon Press: 1989; Vol. 6, Chap. 9.
2. *Telechelic polymers: synthesis and application*, Goethals, E. J. (ed.); CRC Press: 1989.
3. Nuyken, O. *Angew. Makromol. Chem.* **1994**, *223*, 29-46.
4. Kim, S. H.; Woo, H.-G.; Kim, S.-H.; Kim, J.-S.; Kang, H.-G.; Kim, W.-G. *Macromolecules* **1999**, *32*, 6363-6366.
5. Bolton, D. H.; Wooley, K. L. *Macromolecules* **1997**, *30*, 1890-1896.
6. Haba, O.; Itakura, I.; Ueda, M. *Polym. Sci. Part A: Polym. Chem.* **1999**, *37*, 2087.
7. Deshpande, M. M.; Jadhav, A. S.; Gunari, A. A.; Sehra, J. C.; Sivaram, S. *J. Polym. Sci. Part A: Polym. Chem.* **1995**, *33*, 701-705.
8. Evans, T. L.; Carpenter, J. C. *Makromol. Chem., Makromol. Symp.* **1991**, *42/43*, 177-184.
9. Evans, T. L.; Berman, C. B.; Carpenter, J. C.; Choi, D. Y.; Williams, D. A. *Polym. Prep.* **1989**, *30(2)*, 573-574.
10. Nagahata, R.; Sugiyama, J.; Goyal, M.; Asai, M.; Ueda, M.; Takeushi, K. *Polymer Journal* **2000**, *32*, 854-858.
11. Korn, M.; Mills, W.; Gagne, M. R. for reactions in solution: unpublished data.
12. Brunelle, D. J.; Boden, E. P.; Shannon, T. G. *J. Am. Chem. Soc.* **1990**, *112*, 2399-2402.
13. Brunelle, D. J.; Shannon, T. G. *Macromolecules* **1991**, *24*, 3035-3044.
14. Goyal, M.; Nagahata, R.; Sugiyama, J.; Asai, M.; Ueda, M.; Takeushi, K. *Polymer* **1999**, *40*, 3237.
15. Goyal, M.; Nagahata, R.; Sugiyama, J.; Asai, M.; Ueda, M.; Takeushi, K. *Polymer* **2000**, *41*, 2289-2293.
16. Kim, W. B.; Park, K. H.; Lee, J. S. *J. Mol. Catal. A* **2002**, *184*, 39-49.
17. For a comparison of transesterification reactions of BPA with DPC, dimethylcarbonate and the oxidative carbonylation see: Kim, W. B.; Lee, J. S. *J. Appl. Polym. Sci.* **2002**, *86*, 937-947.
18. Hathaway, S. J.; Pyles, R. A. US 4,732,934.
19. Korn, M. R.; Gagné, M. R. unpublished data.
20. Riffle, J. S.; Shchori, E.; Banthia, A. K.; Freelin, R. G.; Ward, T. C.; McGrath, J. E. *J. Polym. Sci.: Polym. Chem. Ed.* **1982**, *20*, 2289-2301.
21. Marks, M. J.; Sekinger, J. K. *Macromolecules* **1994**, *27*, 4106-4113.
22. Marks, M. J.; Scott, D. C.; Guilbeaux, B. R.; Bales, S. E. *J. Polym. Sci.: Polym. Chem. Ed.* **1997**, *35*, 385-390.
23. Knauss, D. M.; McGrath, J. E. *Polymer* **2002**, *43*, 6407-6414.
24. Degee, P.; Jerome, R.; Teyssie, Ph. *Polymer* **1994**, *35*, 371-376.

25. Knauss, D. M.; Yoon, T.-H.; McGrath, J. E. *Polymer* **2002**, *43*, 6415-6420.
26. Gross, S. M.; Flowers, D.; Roberts, G.; Kiserow, D.; DeSimone, J. M. *Macromolecules* **1999**, *32*, 3167-3169.
27. Korn, M. R.; Gagné, M. R. *Macromolecules* **1998**, *31*, 4023-4026.
28. Bailly, C.; Daumerie, M.; Legras, R.; Mercier, J. P. *J. Polym. Sci. Polym. Phys. Ed.* **1985**, *23*, 493-507.
29. Kauth, H.; Kühling, S.; Alewelt, W.; Freitag, D. US 5,373,082 (**1994**).

Chapter 5

End-Functionalized Poly(bisphenol A carbonate) Oligomers Part II: Characterization via UV-vis, FTIR, GPC, NMR, and DSC

Michael R. Korn

**Department of Chemistry and Biochemistry, Texas State University,
San Marcos, TX 78666**

The analysis of several end-functionalized PC oligomers by analytical methods, which determine averaged physical properties (end groups, molecular weight and thermal properties) will be discussed and compared for selected examples. Analytical methods described include UV-vis, FTIR, GPC, NMR, and DSC.

Introduction

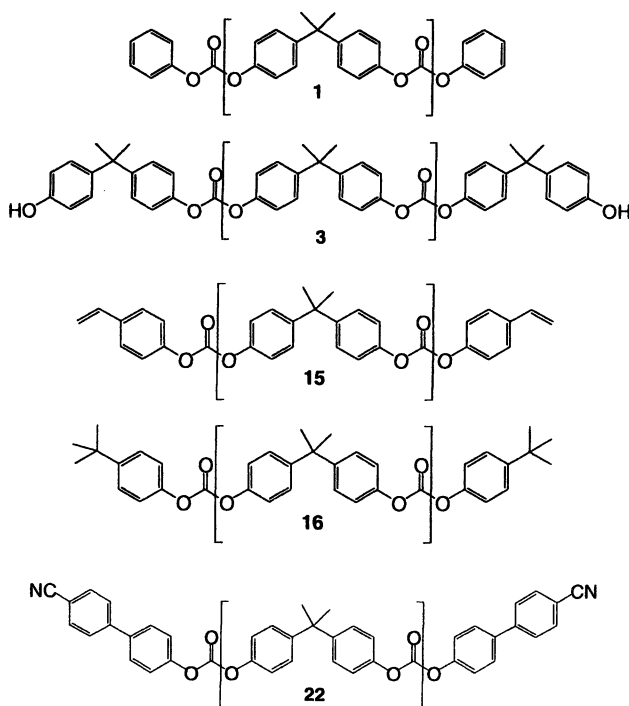
This and the following section describe the results obtained from characterizing end-functionalized PC oligomers by various analytical methods. Several end-functionalized PC oligomers were introduced in the previous chapter, and for consistency sake, the numbers assigned there will be used here and in the next chapter.

The various analytical methods discussed in this and the next chapter can be grouped into two general classes: those which integrate over all existing species and determine an average property (UV-vis, FTIR, GPC, NMR, DSC) and methods which are able to resolve and detect individual species (HPLC, MS, ESI, APCI, MALDI). This chapter focuses on the first type of analytical methods including spectroscopic, chromatographic and thermal methods. The preceding chapter deals with the analytical methods that detect individual species (HPLC and mass spectrometric methods). The analytical data reported in this chapter are taken from the literature and from so far unpublished data (oligomers 20-22 and in particular 22b).

Ultraviolet-Visible (UV-vis) Spectroscopy

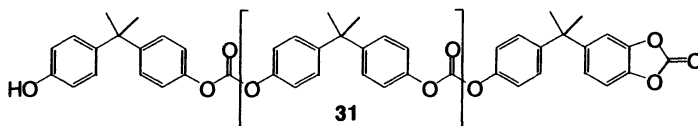
UV-vis spectroscopy was used by *McGrath et al.*(1) to determine the presence and amount of free phenolic end groups in oligomers **3** and there from the MW of the oligomers. *Mork and Priddy* extended UV-vis analysis to high MW PC (2) by comparing the UV spectra of **3** vs. the phenyl-capped oligomers **1**. Due to a shift towards higher wavelengths in the UV spectrum for OH terminated vs. capped PC oligomers, the relative ratios of the intensities of 288nm/266nm were measured and related to the average amount of free OH groups. *Mork and Priddy* also coupled UV-vis spectrometry with GPC and HPLC for analysis and calibration purposes.

Brunelle et al. employed UV-vis spectra recorded at 254 and 288 nm to distinguish between linear oligomers **3** and BPA cyclics due to the significant differences in the 254/288 nm ratio (3-4). *Knauss et al.* employed UV-vis analysis to confirm the absence of phenolic end groups in **15** and **16** (5). Due to its strong absorbance up to 350 nm, *Korn and Gagné* used the 4-cyano-biphenyl moiety as an UV-vis active end group (oligomers **22**) (6).



Fourier-Transformed Infrared (FTIR) Spectroscopy

Besides the confirmation of carbonate groups in oligomers of which the carbonyl group shows absorption at 1774 cm^{-1} , FTIR is suitable to detect the (undesirable) *o*-carbonate end group formed in some oligomers in the oxidative carbonylation reaction, e.g. in oligomer **31**, as this end group shows a sharp absorbance at 1836 cm^{-1} (7). FTIR was also employed to confirm the presence of terminal OH groups in linear oligomers **3** (3-4).



Gel Permeation Chromatography (GPC)

When using the most common GPC calibration standard, PS, one must remember that PS has a different hydrodynamic behavior than PC. To avoid those differences, GPC instruments are calibrated sometimes with high MW PC. Alternatively, universal calibration (8) can be used, and the actual data based on PS standards recalculated for PC (9). The significance of uncorrected (PS based) and corrected (PC based) MWs is illustrated in Figure 1 for oligomers **1** of various MWs (**1a-f**); **1g** is commercial PC.

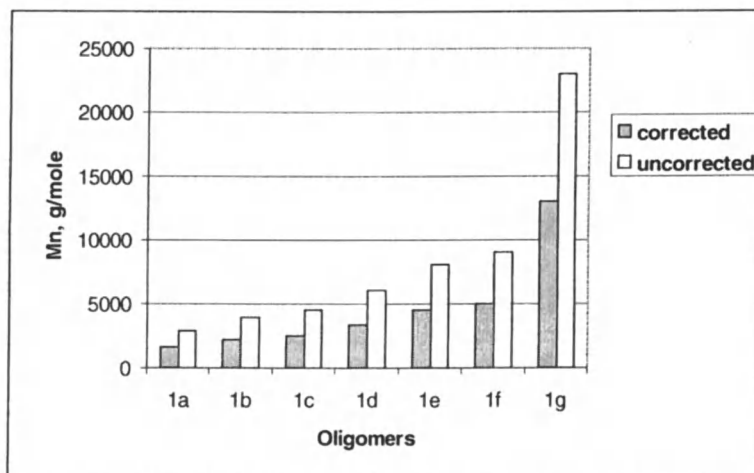
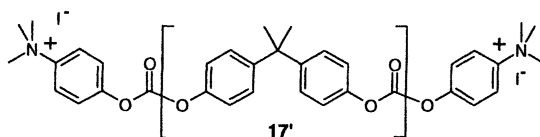


Figure 1. Corrected and uncorrected M_n values (from GPC) for oligomers **1**.

It is obvious that uncorrected vs. corrected values differ by almost 50%. This is in good agreement with the results reported by *Nagahata et al.* for MW of oligomers **3**. Analysis by GPC (PS standard) resulted in an (uncorrected for PC) M_n of 5,500 g/mol (PDI = 1.1), contrasted by MALDI-TOF analysis, which gave the more accurate M_n of 3,560 g/mol (PDI = 1.03) (10).

End groups may distort universal calibration methods, especially in the lower MW range, if end groups are “non-PC like” or when interacting with the column material (e.g. oligomer **17'**) (11).



Besides MW determination, GPC can be used for the detection of end groups. To discriminate between OH terminated oligomers **3** and fully capped oligomers **1**, *Mork* and *Priddy* employed GPC analysis coupled with UV spectroscopy (2). Based on UV-vis spectroscopy, the OH terminated oligomers show absorbance at 288 nm while the capped barely do. In their analysis, GPC traces were recorded at two different wavelengths, 264 nm and 288 nm. Depending on the whether OH end groups were present, the GPC trace at 288 nm would give a measurable response. Overlaying those two GPC traces showed two effects: a. they were basically identical in shape and covered almost the same elution volume (MW range), which means that the OH end group is present in oligomers of all MWs; b. the GPC trace for higher wavelengths is off-set towards higher retention times (lower MWs), because the contribution of the end groups becomes increasingly prominent in lower MW oligomers. This shift in retention times was reported earlier by *Warner, Howell* and *Priddy* (12), who performed an excellent study of UV active residues and their difference in GPC-UV-vis when used as end groups (shift observed) vs. as comonomers (no shift observed).

Applying the above concept, oligomers **22** were analyzed by GPC-UV-vis. The cyano-biphenylcarbonate end group is highly UV active with a strong absorbance beyond 280 nm and is thus able to serve as a probe to confirm end group functionalization. Figure 2 shows a contour plot of the starting material (Fig. 2a): high MW PC and diarylcarbonate **25**, and of the resulting oligomers **22a** (Fig. 2b). PC does not absorb beyond 280 nm whereas **25** does.

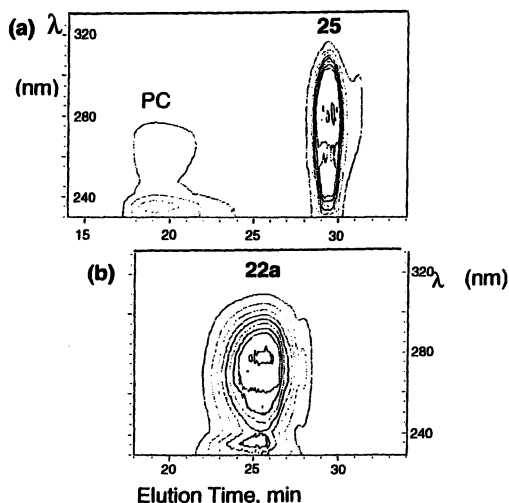
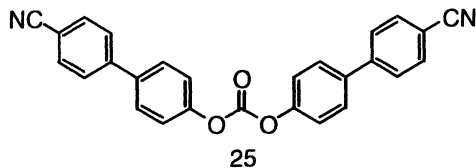


Figure 2. GPC-UV/vis analysis: (a) PC and 25; (b) 22a after precipitation (Adapted from reference 6. Copyright 1998 American Chemical Society.)

If the arylcarbonate depolymerizes PC and forms oligomers, which bear the strong UV active end groups, the final product should elude later (lower MW) and should absorb at wavelengths beyond 280 nm over the entire MWD. The contour plot for 22a (Fig.2.b) shows exactly that; a. the average elution time for the oligomer has significantly increased from 20 min to 25 min consistent with the low MW nature of 22a; b. the range of absorbance in the resulting oligomers is extended beyond 280 nm, and c. absorbance beyond 280 nm extends over the entire GPC peak (*i.e.* over the entire MW).

In another experiment, GPC traces for the similar oligomer 22b were recorded for refractive index (RI), and UV-vis at 254 nm and 300 nm. An overlay of the normalized chromatograms is displayed in Figure 3, with the experimental MWs listed in Table 1. As can be seen, the chromatogram recorded at 300 nm (Fig.3c) nicely overlaps with the 254 nm trace (Fig. 3b); it is also slightly shifted towards higher elution times (lower MWs) as discussed above.

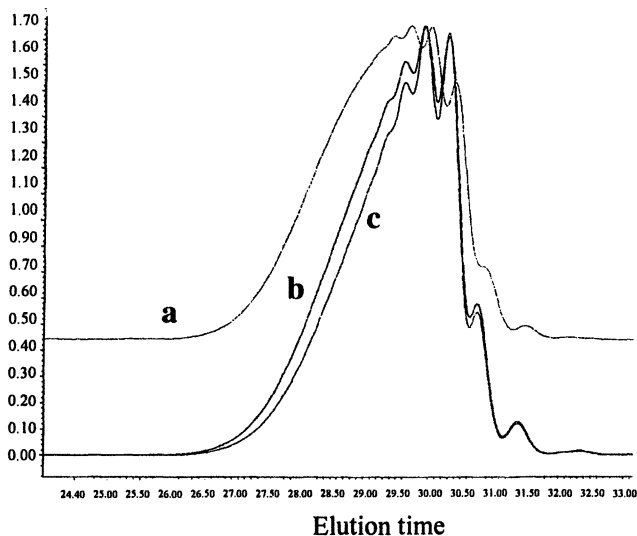


Figure 3. Normalized GPC chromatogram of 22b detected by (a) RI, (b) 254nm and (c) 300 nm.

Table 1. MW for 22b obtained by GPC^a

Analytical Tool	MW	M_n	M_w	PDI
	<i>Max. peak</i>			
	<i>g/mol</i>	<i>g/mol</i>	<i>g/mol</i>	
GPC-RI	2,164	1,995	2,646	1.32
GPC-UV 254 nm ^b	1,545	1,642	2,241	1.36

a: all GPC data are corrected for PC; b: calibration curve recorded at 254 nm

Nuclear Magnetic Resonance Spectroscopy (NMR)

Distinct resonances in the ¹H NMR spectrum from end groups can be used to determine the average number MW (M_n) of oligomers by comparing their relative amount to either the aromatic (two doublets, 8H) or the isopropylidene (singlet, 6H) resonances of the BPA repeating units. Assuming 100% end functionalization, M_n can be calculated by multiplying the resulting ratio with 254 g/mol (BPA repeating unit) and adding the molar mass of the two end

groups and one carbonate group. If end functionalization is less than 100% or if BPA cyclics are present, the calculated M_n is higher than the actual MW. An example for end group analysis by ^1H NMR is given in Figure 4 for oligomers **22b**.

The four doublets belonging to the hydrogens of the two cyanobiphenyl end groups ($\delta = 7.35\text{--}7.8$ ppm) can clearly be seen downfield from the BPA aromatic resonances ($\delta = 7.1\text{--}7.3$ ppm) (Fig.4a) as well as the BPA's isopropylidene singlet(s) at $\delta = 1.67$ ppm (Fig.4b). The integration ratios from Fig.4.a give 20 % H for the cyanobiphenyl end groups (16H for both ends) and 80% H for BPA repeating units (64H total) resulting in 64H/8H per BPA repeating unit = 8 BPA repeating units; thus a MW of $8 \times 254 + 416$ (endgroups + CO_3) = 2448 g/mol. The ratio of cyanobiphenyl end group Hs to isopropylidene Hs is 25 to 75 (16H to 48H; 48H/6H per BPA repeating unit = 8 BPA units).

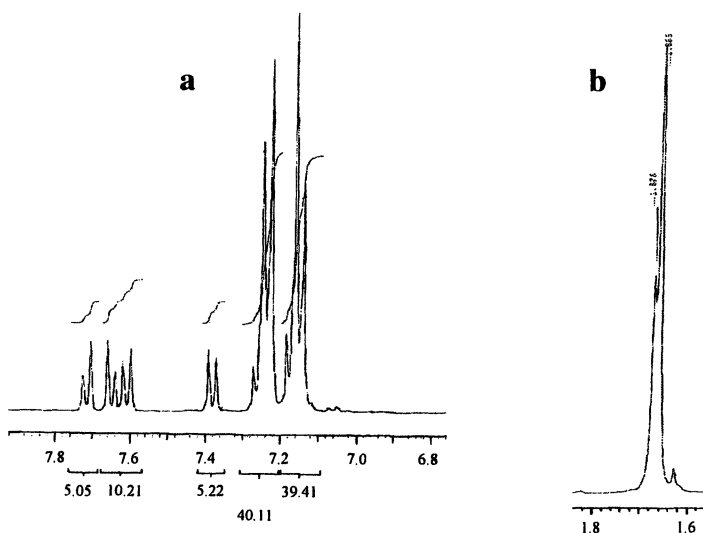
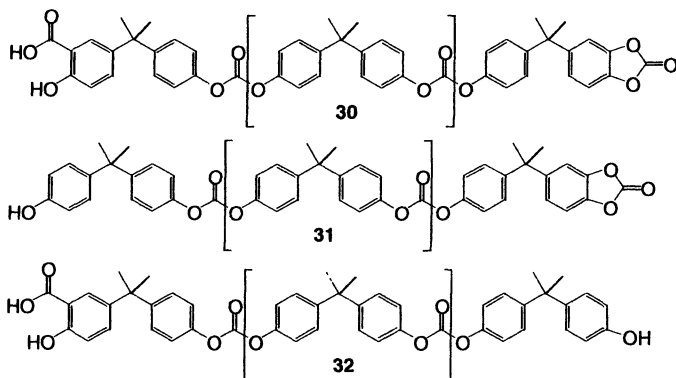


Figure 4. ^1H NMR spectrum (400 MHz, CDCl_3) of **22b**; (a) aromatic region; (b) aliphatic region.

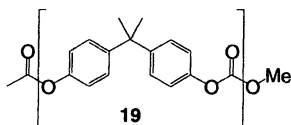
A closer look at the above spectrum reveals additional minor resonances in both regions which most likely stem from the BPA unit next to the end group as those peaks are shifted downfield (for the particular oligomer **22b**); e.g. in the isopropylidene region two major resonances are visible: the major one at 1.665 ppm and a minor one at 1.676 ppm, compared to the original high MW PC which only shows a single isopropylidene peak.

NMR spectroscopy may also reveal additional types of end groups such as 'non-functionalized' or mixed end groups (e.g. *tert.*-butylphenol based end-groups stemming from native high MW PC which show resonance at $\delta = 1.31$ ppm), and HPLC or mass spectrometry will give a more complete picture of the actual type of oligomeric species present in a given sample.

Goyal *et al.* (7) determined OH and salicylic acid end groups in oligomers 30-32 via ^1H NMR resonances at 5.33 and 10.45 ppm, respectively, with both resonances being exchangeable with D_2O .



If more than one type of end groups is present, NMR can determine the *relative* ratio of those end groups, e.g. as reported for oligomers 19 (13). Based on NMR data though, it cannot be determined what the structure of individual oligomers is: e.g. for oligomers 19, NMR data of a mixture of two types of oligomers, one bearing solely acetate end groups and one bearing solely methyl carbonate groups are indistinguishable from oligomers that have variable amounts of either end group present at the same oligomer. An accurate picture of the structure of the individual oligomers can be obtained through mass spectrometric analyses as outlined in the next chapter.



^{19}F NMR was used by McGrath *et al.* (1) to elucidate the mechanism of using trifluoroacetic acid and trifluoroacetic anhydride as protecting groups for the synthesis of 3.

^{13}C NMR can be used as well to confirm the presence/absence of end groups as well as to confirm the presence of the carbonate linkage with a resonance at around 152 ppm (14). A solid-state ^{13}C CP/MAS NMR spectrum

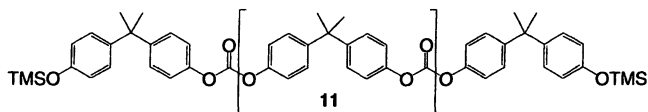
of BPA oligomers (MW = 1,000 g/mol) utilized for grating unto silica were reported in ref. 14.

MWs determined by $^1\text{H-NMR}$ analysis are often compared with GPC data and on occasion with other analytical methods. Table 2 lists a few examples for oligomers for which the reported average M_n was obtained by $^1\text{H NMR}$ spectroscopy as well as by GPC analysis (all GPC data were corrected for PC by the author if not reported as such) (15).

Table 2. MW data from $^1\text{H NMR}$ and GPC analysis^a

<i>Oligomers</i>	M_n <i>$^1\text{H NMR}$</i> <i>kg/mol</i>	M_n <i>GPC</i> <i>kg/mol</i>	<i>PDI</i> <i>(from</i> <i>GPC)</i>	<i>Other methods</i>
11	2.4			
3 (via 11)				UV analysis 2.3 k
15a	7.6	4.0	6.1	$[\eta] = 0.43$
15b	7.0	4.9	4.5	$[\eta] = 0.37$
16	7.9	4.0	4.9	$[\eta] = 0.43$
17	6.7	7.0	1.8	n/a
22b	2.4	2.0	1.3	See next chapter

a: all GPC data are corrected for PC



Whereas oligomers **3/11**, **17**, and **22b** are in good agreement, M_n values from $^1\text{H NMR}$ for oligomers **15a**, **15b**, and **16** deviate from the corresponding GPC values by 40-100%. Two reasons might account for this: a. polydispersity (PDI) is very high for all three samples; if this is caused by low MW oligomers M_n would be shifted to lower numbers in the GPC; b. the reaction conditions reported for making those oligomers (16) suggest the formation of cyclics, which contribute only to BPA resonances in the $^1\text{H NMR}$ spectrum and thus would give too high of an apparent MW. The presence of (non-functionalized) OH terminated oligomers was ruled out by $^1\text{H NMR}$ and UV-vis spectroscopy.

Differential Scanning Calometry (DSC)

Thermal properties of PC oligomers are affected by their MW and by type of end groups. Using DSC, glass transition temperatures (T_g) and, if present, melting points of PC oligomers can be determined. T_g of selected oligomers of different MWs are plotted in Figure 5 (17). M_n s were taken from GPC analysis; values for **1**, **20**, **21**, **22a** (Chapter 4, Tab. 2d-g) and **12** (Chapter 4, Tab. 1d) are based on GPC data calibrated with PC or corrected for PC; M_n values for **15** and **16** (Chapter 4, Tab. 1h.i) were reported for PS standards and have been corrected for Figure 5 using universal calibration (15). To show the significance between corrected and uncorrected GPC data, M_n values for **1** are given for both, corrected and uncorrected (designated **1'**: filled squares in Fig. 5) data.

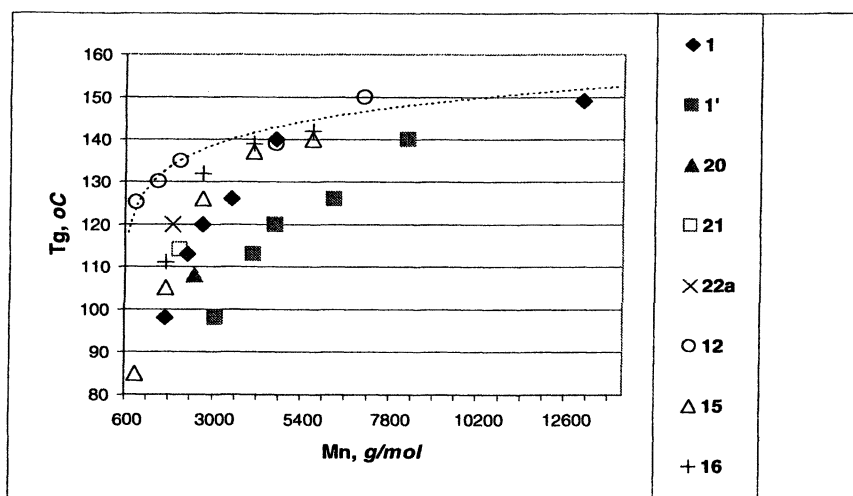
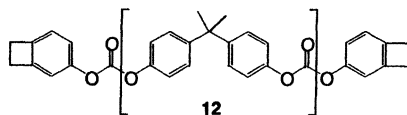
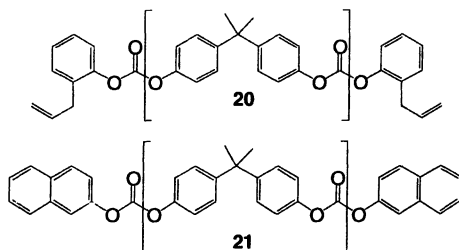


Figure 5. T_g vs. M_n for selected PC oligomers.





The graph shows that a. T_g increases with increasing MW until it levels off at M_n of about 10-11k g/mol towards the value for high MW PC ($T_g = 150\text{ }^\circ\text{C}$); b. T_g values for uncorrected M_n appear about $20\text{ }^\circ\text{C}$ higher than for the corrected MWs (**1'** vs. **1**); c. oligomers with comparable MW but different end groups show differences in T_g of up to $30\text{ }^\circ\text{C}$; this difference is the more pronounced the lower the MW of the oligomer is, as the impact of the end group increases with decreasing MW.

Experimental

GPC analysis of **22b** was performed in THF on a Waters 600 system with RI and dual wavelength detector; separation was afforded with Styragel HR5e and two Styragel HR4e columns. ^1H NMR spectra of **22b** were recorded at 400 MHz (Varian) in CDCl_3 .

Acknowledgement

All compounds **1** and **20-22** were synthesized during a post-doctoral appointment at UNC, Chapel Hill, NC with Prof. M. Gagné.

References

1. Riffle, J. S.; Shchori, E.; Banthia, A. K.; Freelin, R. G.; Ward, T. C.; McGrath, J. E. *J. Polym. Sci.: Polym. Chem. Ed.* **1982**, *20*, 2289-2301.
2. Mork, C. O.; Priddy, D. B. *J. Appl. Polym. Sci.* **1992**, *45*, 435-442.
3. Brunelle, D. J.; Boden, E. P.; Shannon, T. G. *J. Am. Chem. Soc.* **1990**, *112*, 2399-2402.
4. Brunelle, D. J.; Shannon, T. G. *Macromolecules* **1991**, *24*, 3035-3044.
5. Knauss, D. M.; McGrath, J. E. *Polymer* **2002**, *43*, 6407-6414.
6. Korn, M. R.; Gagné, M. R. *Macromolecules* **1998**, *31*, 4023-4026.

7. Goyal, M.; Nagahata, R.; Sugiyama, J.; Asai, M.; Ueda, M.; Takeushi, K. *Polymer* **2000**, *41*, 2289-2293.
8. See e.g. *Fundamentals of Polymer Science*, Painter, P. C., and Coleman, M. M., Eds.; Technomic Publishing Company: Lancaster, PA, 1994.
9. Values for K and α for various solvents can be found e.g. in: *Polymer Handbook*, Brandrup, J., and Immergut, E. H., Eds.; Wiley -Interscience: New York, $K_{PS} = 0.013$; $K_{PC} = 0.039$; $\alpha_{PS} = 0.71$; $\alpha_{PC} = 0.70$ (for THF).
10. Nagahata, R.; Sugiyama, J.; Goyal, M.; Asai, M.; Ueda, M.; Takeushi, K. *Polymer Journal* **2000**, *32*, 854-858.
11. Degee, P.; Jerome, R.; Teyssie, Ph. *Polymer* **1994**, *35*, 371-376.
12. Warner, S.; Howell, B. A.; Priddy, D. B. *Polym. Prepr.* **1989**, *30(2)*, 211-212.
13. Deshpande, M. M.; Jadhav, A. S.; Gunari, A. A.; Sehra, J. C.; Sivaram, S. *J. Polym. Sci. Part A: Polym. Chem.* **1995**, *33*, 701-705.
14. See e.g. Xie, X.-Q.; Ranade, S. V.; DiBenedetto, A. T. *Polymer* **1999**, *40*, 6297-6306.
15. Uncorrected GPC data (for PC) in the original paper were recalculated by the author using ref. 9.
16. Experimental data from ref. 5 report the use of triethylamine in a 0.1 molar solution, which according to ref. 3 & 4 strongly favors the formation of BPA cyclics.
17. Values were taken from the respective publications.

Chapter 6

End-Functionalized Poly(bisphenol A carbonate) Oligomers Part III: Characterization via HPLC and Mass Spectrometry

Michael R. Korn

Department of Chemistry and Biochemistry, Texas State University,
San Marcos, TX 78666

The analysis of several end-functionalized PC oligomers by HPLC and various mass spectrometrical methods, including ESI, APCI, and MALDI will be discussed and their results - exemplified for cyanobiphenyl-terminated PC oligomers - compared.

Introduction

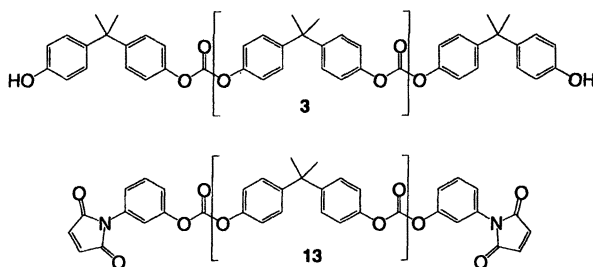
This section describes the results obtained from characterizing end-functionalized PC oligomers by analytical methods that identify *individual* species in contrast to analytical methods that determine overall averaged properties (see previous chapter). Several end-functionalized PC oligomers and chemical structures were introduced in part I and II (chapters 4 & 5), and for consistency sake, the numbers assigned there will be used here as well. The analytical data reported in this chapter are taken from the literature but also include some so far unpublished data (oligomers **20-22**, and in particular **22b**). Oligomers **22b** were analyzed by all four methods, HPLC, ESI, APCI, and MALDI as well as by GPC and NMR and thus allow a comparison of those results.

High Performance Liquid Chromatography (HPLC)

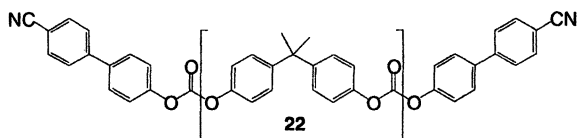
HPLC separates molecules by size and polarity, and thus is a very useful tool in shedding light on the molecular composition of an oligomeric sample. As HPLC does not only separate by size but also by polarity, an unambiguous assignment of the individual (envelope of) peaks is not always straight forward and can be facilitated by using individual authentic molecules.

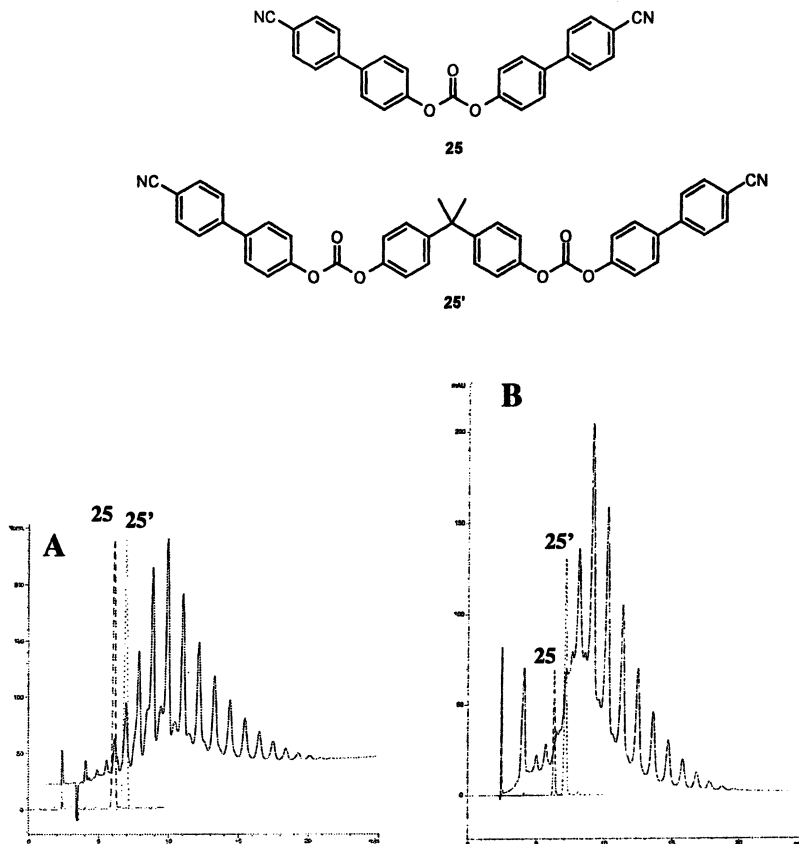
When coupled with a UV detector, oligomers with different end groups can be discriminated by certain ratios obtained from the intensities of HPLC traces recorded at different wavelengths. It must be noted though, that intensities not only depend on the amount of oligomers present but also on their individual extinction coefficient, and therefore quantitative conclusions can be made only after calibration.

Applying the above principle, *Mork and Priddy* used HPLC traces recorded at 264 nm and 288 nm to determine the average amount of oligomers terminated by OH vs. phenyl groups (1). *Brunelle et al.* distinguished linear OH terminated oligomers from cyclics by synthesizing authentic linear and cyclic oligomers and recording their HPLC traces at 254 nm and 285 nm. It could be demonstrated that the ratio 254/288 was less than 2.5 for linear oligomers **3** and about 50 for cyclics (2,3). *Marks and Sekinger* also applied HPLC for the analysis of oligomers **13** for purity purposes and to calculate M_n (4).



The analysis of **22a** and **22b** by HPLC at a wavelength of 300 nm is shown in Figure 1. A cyano-terminated silica gel column was used for separation with the compounds being eluted from THF/hexanes (30/70v/v) with a 0.5%/min. gradient in THF to 45/55v/v THF/hexanes. The starting diarylcarbonate **25** and the first member of the oligomeric envelope **25'** were eluted also to facilitate peak assignments.





*Figure 1. HPLC chromatogram at 300 nm on a cyano-modified column for **22a** (A) and **22b** (B); traces for **25** and **25'** are included (Fig. 1A is adapted from reference 9. Copyright 1998 American Chemical Society.)*

In both chromatograms, peaks are not fully resolved and both show two distinct envelopes, of which the more pronounced envelope belongs to the oligomeric series **22** ($MW = n \cdot 254$ (BPA repeating unit) + 416 (endgroups + $CO_3 = 25$)). Following peak assignment based on **25** and **25'**, the maximum peak for sample **22a** is the tetramer ($n=4$; $MW = 1432$ g/mol), and for oligomers **22b** the trimer ($n=3$; $MW = 1178$ g/mol).

Oligomers **22b** were also eluted on an amino-bonded column from CH_2Cl_2 /hexanes, which gave a slightly different chromatogram (see Fig. 4 below).

Mass Spectrometry

Mass spectrometry (MS) of polymers/oligomers has advanced greatly over the past decade and allows for the identification of individual oligomers. Especially matrix-assisted laser desorption/ionization (MALDI) coupled with a time-of-flight (TOF) analyzer and electrospray ionization (ESI) with various analyzers have become prominent over field ionization/desorption (FI/FD) mass spectrometry. The working range for FD-MS cuts off at about 10k Da (5), whereas MALDI can detect masses of up to 1 Mio. Da.

Sometimes, HPLC or gas chromatography (GC) is coupled with MS to pre-separate oligomers and simplify the resulting spectrum; thus, *Kim et al.* (6) used GC-MS in conjunction with HPLC to identify and distinguish among oligomers 1-3.

Brunelle et al. (3) employed FD-MS and thus confirmed dimer, trimer and tetramer of **3**.

For the analysis of cyanobiphenyl-terminated oligomers **22b** three techniques will be compared: (ESI), atmospheric pressure chemical ionization (APCI), and (MALDI). In all cases, only molecules that will volatilize and be converted into charged molecules can be detected. In the ideal case, the energy applied to volatilize the molecule would not induce fragmentation unless desired for further experiments (*e.g.* for MS²). All sets of oligomers contain multiples n ($n = 0, 1, 2, \dots$) of the BPA repeating unit and thus are designated as monomer ($n = 1$; equals structure **25'**), dimer ($n = 2$), trimer ($n = 3$), *etc.* The BPA carbonate repeating unit has an exact mass of 254.09 amu, and two cyanobiphenyl endgroups plus one carbonate group has an exact mass of 416.12 amu. Thus, the exact masses for oligomers **22** are $416.1 + n \cdot 254.1$, namely 670.2 (monomer), 924.3 (dimer), 1178.4 (trimer), 1422.5 (tetramer) *etc.* Sets of peaks belonging to the same oligomeric envelope should be 254.09 amu apart from each other (provided they are singly charged).

Electrospray-Ionization (ESI)

Figure 2 shows the ESI spectrum for **22b**. The sample was electrosprayed in the presence of sodium cations (MW = 23 g/mol) from a methanol/CH₂Cl₂ solution and analyzed by an ion trap. Peak assignments and calculated (exact) masses are listed in Table 1.

The major peak occurs at $m/z = 1201.5$ and belongs to the set of peaks present as 693.6, 947.5, 1201.5, 1455.5, 1710.5, 1964.5. Subtracting the value for the sodium cation (23 amu), this set represents the values for oligomers **22**, with its maximum peak at 1201.5 being the trimer.

The second set of peaks at $m/z = 1080.3, 1334.2, 1588.2, 1842.3$ matches with oligomers of structure **33** (+ Na^+). **33** can stem from the interaction of the catalyst (potassium *tert.*-butoxide) when depolymerizing PC with **25** to obtain oligomers **22**.

A third set that can be identified matches BPA cyclics + Na^+ at $m/z = n \cdot 254 + 23$. Many other small peaks are visible also.

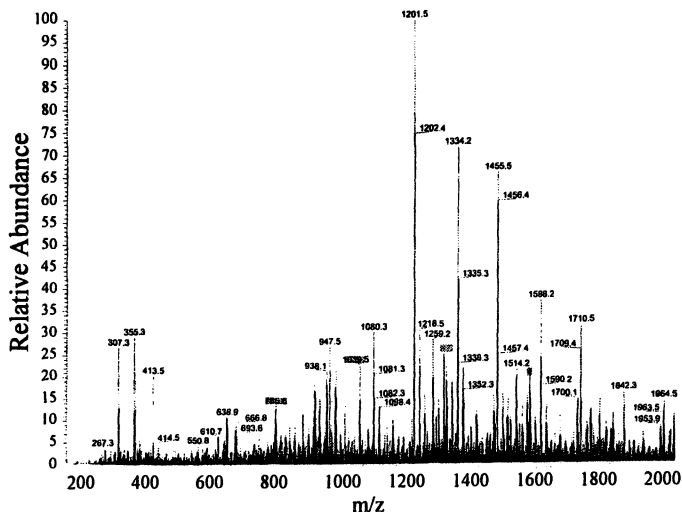
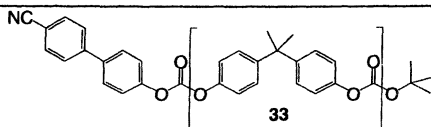


Figure 2. ESI spectrum for **22b**.

Table 1. Calculated and observed MW for **22b**, **33**, and cyclics by ESI

	Monomer	Dimer	Trimer	Tetramer	Pentamer	Hexamer
22	670.2	924.3	1,178.4	1,432.5	1,686.6	1,940.7
22+Na⁺	693.2	947.3	1,201.4	1,455.5	1,709.6	1,963.7
Observed	693.6	947.5	1,201.5	1,455.5	1,710.5	1,964.5
33	549.2	803.3	1,057.4	1,311.5	1,565.6	1,819.7
33+Na⁺	572.2	826.3	1,080.4	1,334.5	1,588.6	1,842.7
Observed	-	-	1,080.3	1,334.2	1,588.2	1,842.3
cyclics	n/a	508.2	762.3	1,016.4	1,270.5	1,524.5
cyclics+Na⁺	n/a	531.2	785.3	1,039.4	1,293.4	1,547.5
Observed	n/a	-	785.6	1039.5	Yes	yes



Atmospheric Pressure Chemical Ionization (APCI)

The same oligomers **22b** were subjected to APCI analysis. This method is energetically much harsher in its conditions as the temperature of the nozzle operates at about 400 °C. Figure 3 shows the corresponding spectrum and Table 2 lists observed and assigned peaks (as mono-protonated species).

Five different sets of peaks are visible and are assigned to the following structures:

- 1). oligomers **22** (major peaks);
- 2). fragmented oligomers **34** (second prominent set of peaks);
- 3). **cyclics**;
- 4). fragmented oligomers **35**; and
- 5). fragmented oligomers **36**.

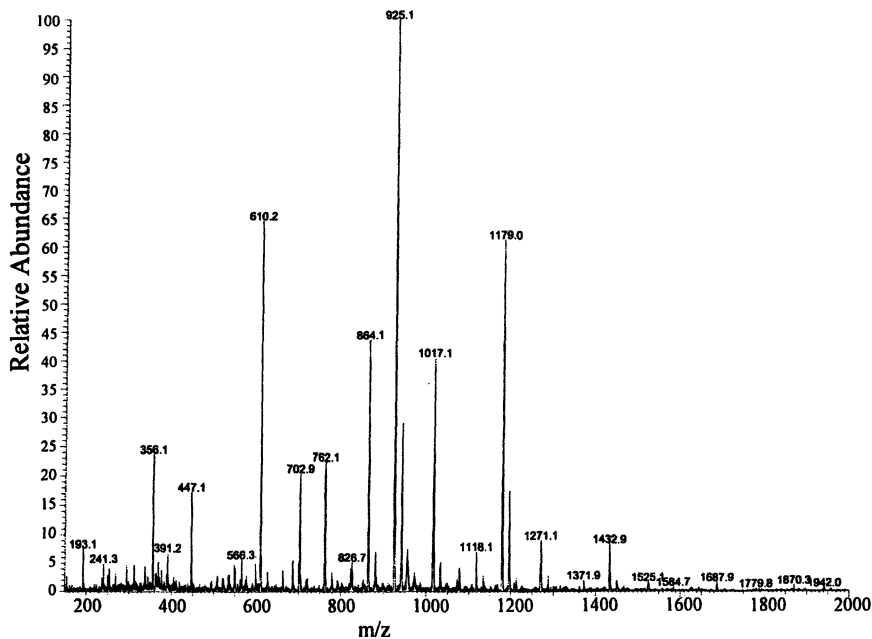
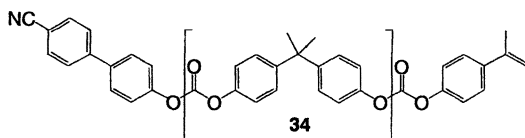


Figure 3. APCI spectrum of oligomers **22b**



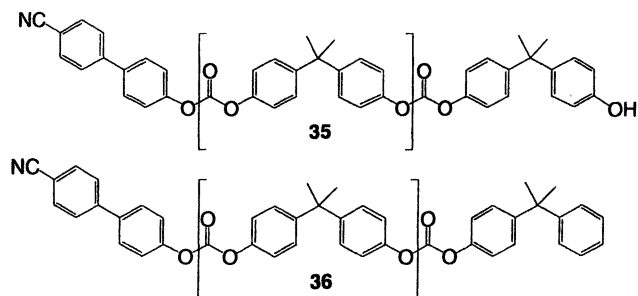


Table 2. Calculated MW of oligomers 22, 34, cyclics, 35, and 36 and observed values by APCI (all mono-protonated)

	<i>Resid.</i>	<i>0-mer</i>	<i>1-mer</i>	<i>2-mer</i>	<i>3-mer</i>	<i>4-mer</i>	<i>5-mer</i>	<i>6-mer</i>
22+H⁺			671.2	925.3	1,179.4	1,433.5	1,687.6	1,941.7
Obsv.			-	925.1	1,179.0	1,432.9	1,687.9	1,942.0
34+H⁺		356.1 ^a	610.2	864.3	1,118.4			
Obsv.		356.1	610.2	864.1	1,118.1			
Cyc+H⁺			n/a	509.2	763.3	1,017.4	1,271.5	1,525.5
Obsv.			n/a	-	762.0	1,017.1	1,271.1	1,525.1
35+H⁺	196.1 ^b	450.2 ^c	704.3					
Obsv.	193.1	447.1	702.9					
36+H⁺			688.3	942.4	1,196.4			
Obsv.			-	942.1	1,196.1			

a: **34** with n=0; b: residue is 4-hydroxy-4'-cyanobiphenyl; c: **35** with n = 0.

In both cases, ESI and APCI, oligomers **22** represent the major constituents, though the trimer is predominant in ESI whereas the dimer is in APCI. Cyclics are detected by both methods. Oligomers **33** which contain the thermally labile *tert.*-butoxy group are visible in the soft ionization method (ESI) but not observed by APCI. Also, several fragmented oligomers **34**, **35** and **36** are visible.

The fifth set of peaks observed in Figure 3 at $m/z = 942.1$ and 1196.1 is 17 amu higher than the peak observed for the corresponding dimer and trimer of **22**. Support for **36** being the correct assignment is based on MALDI analysis (see below).

LC/APCI-MS

Oligomers **22b** were subjected to HPLC separation coupled with APCI. Using a different column and different eluents than reported above (HPLC section), **22b** was eluted on an aminopropyl bonded column from dichloromethane/hexanes (10/90 v/v) linearly increasing to 80% CH₂Cl₂ over 23 min. A UV detector (254 nm) was employed for HPLC detection. Figure 4 shows the obtained chromatogram and detected masses by APCI.

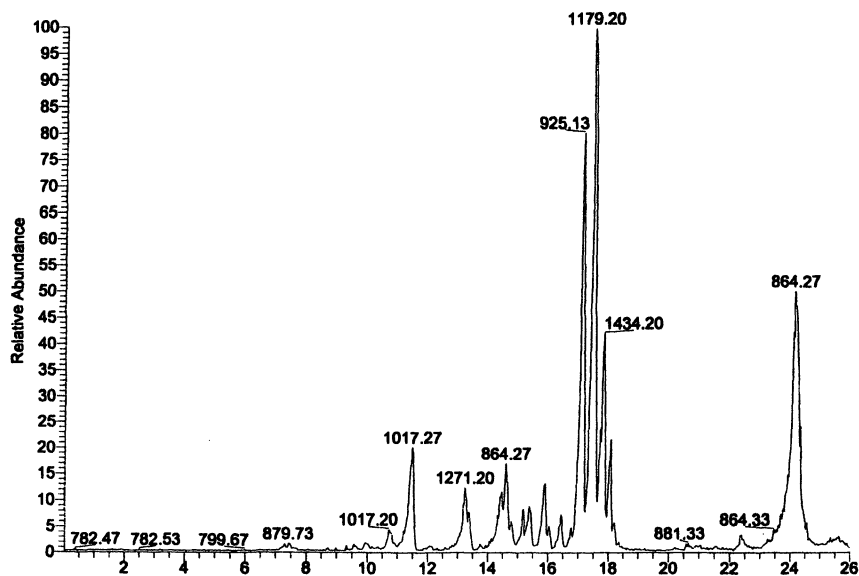


Figure 4. Chromatogram of **22b** at 254 nm (eluted on an aminopropyl modified column) with peaks characterized by APCI (x-axis is elution time, min)

The chromatogram shows a set of prominent peaks between 17 and 19 min corresponding to oligomers **22**. The trimer of **22** being the most prominent one, as seen also in the HPLC chromatogram performed on a cyano-silica column (Fig. 1). In addition, the 17-19 min. region shows the presence of another compound or set of compounds. At earlier elution times, two peaks appear at 1017.3 and 1271.2 amu which were correlated to cyclics. Because cyclics lack the cyano end group their interactions with the column is reduced and earlier elution times are expected.

Compounds eluted between 16.95 min and 18.21 min were selectively analyzed by APCI and gave the chromatogram below (Figure 5). Four distinct

sets of oligomers could be identified, and their observed values are listed in Table 3.

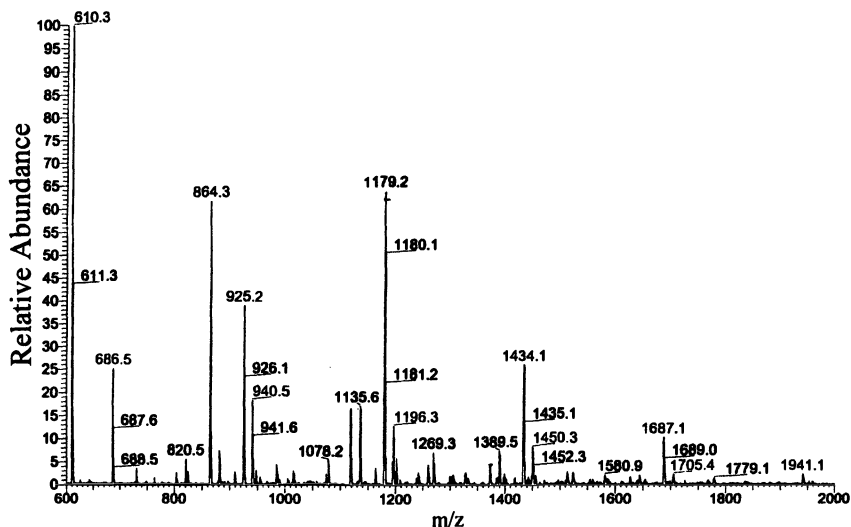


Figure 5. Fractionated LC/APCI of **22b**.

Similar to the previous APCI analysis of the entire sample (no HPLC fractionation, see Fig. 3) the fractionated sample here shows peaks consistent with oligomers **22**, **34** and **36**, but no peaks for cyclics are present (as those elude in an earlier fraction) and no peaks for fragments **35**. Rather, oligomers consistent with a structure such as **37/38** are observed, which can be explained by the loss of CO₂ (44 amu) from **22** resulting in the formation of an ether bond (the ether bond could be anywhere in the place of a former carbonate linkage). The occurrence of ether bonds as well as products from disproportionation reactions were also observed by MALDI-MS for PC when pyrolyzed (7,8).

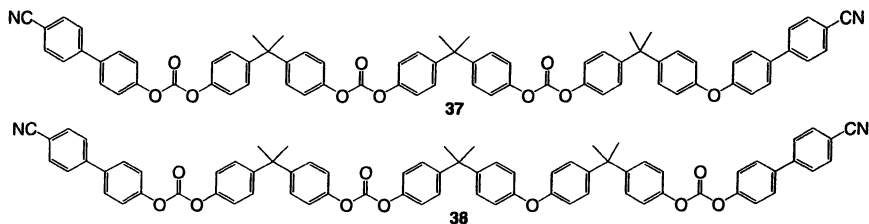


Table 3. Calculated MW of oligomers 22, 34, 36, 37/38 and observed values by LC/APCI

	<i>1-mer</i>	<i>2-mer</i>	<i>3-mer</i>	<i>4-mer</i>	<i>5-mer</i>	<i>6-mer</i>
22+H⁺	671.2	925.3	1,179.4	1,433.5	1,687.6	1,941.7
Obsv.	-	925.2	1179.0	1434.1	1,687.1	1,941.1
34+H⁺	610.2	864.3	1,118.4	1,372.5		
Obsv.	610.3	864.3	Yes	yes		
36+H⁺	688.3	942.4	1,196.4	1,450.5	1,704.6	
Obsv.	686.5	940.5	1,196.3	1,450.3	1,705.4	
37/38+H⁺		881.3	1,135.4	1,389.5		
Obsv.		-	1,135.6	1,389.5		

Matrix-assisted Laser Desorption/Ionization (MALDI)-MS

Analysis of **22b** by MALDI-TOF from an indole acrylic acid matrix shows the spectrum shown in Figure 6.

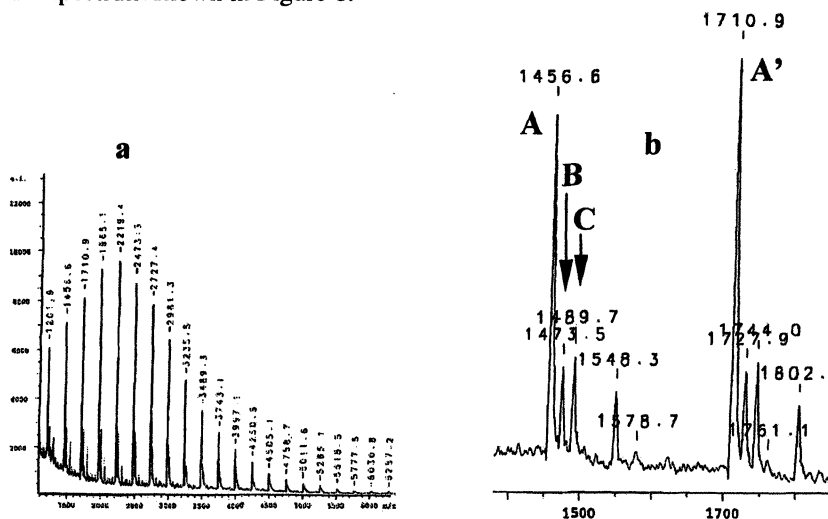


Figure 6. MALDI TOF spectrum of 22b, (a) *m/z* range from 1,000 - 7000; (b) 1,350-1,900 *m/z*.

The major envelope in the spectrum is consistent with oligomers **22** (+Na⁺) including the trimer through the 23-mer, with the highest peak observed for the

heptamer at 2,219.4 amu (calc. 2,217.7 amu). In addition, three more sets of minor peaks can be observed, of which one is consistent with cyclics+Na⁺ (peaks 1548, 1802 in Fig. 6b).

The other two sets are 16 amu apart from each other (peaks B and C in Fig. 6b) of which one is 17 amu higher in mass (peak B) than the peak for the corresponding oligomer **22** (peak A). To clarify peak assignments, MALDI-TOF spectra for related oligomers **1** (phenyl-terminated), **20** (2-Allylphenyl-terminated) and **21** (2-naphthyl terminated) were examined also, as shown in Figure 7.

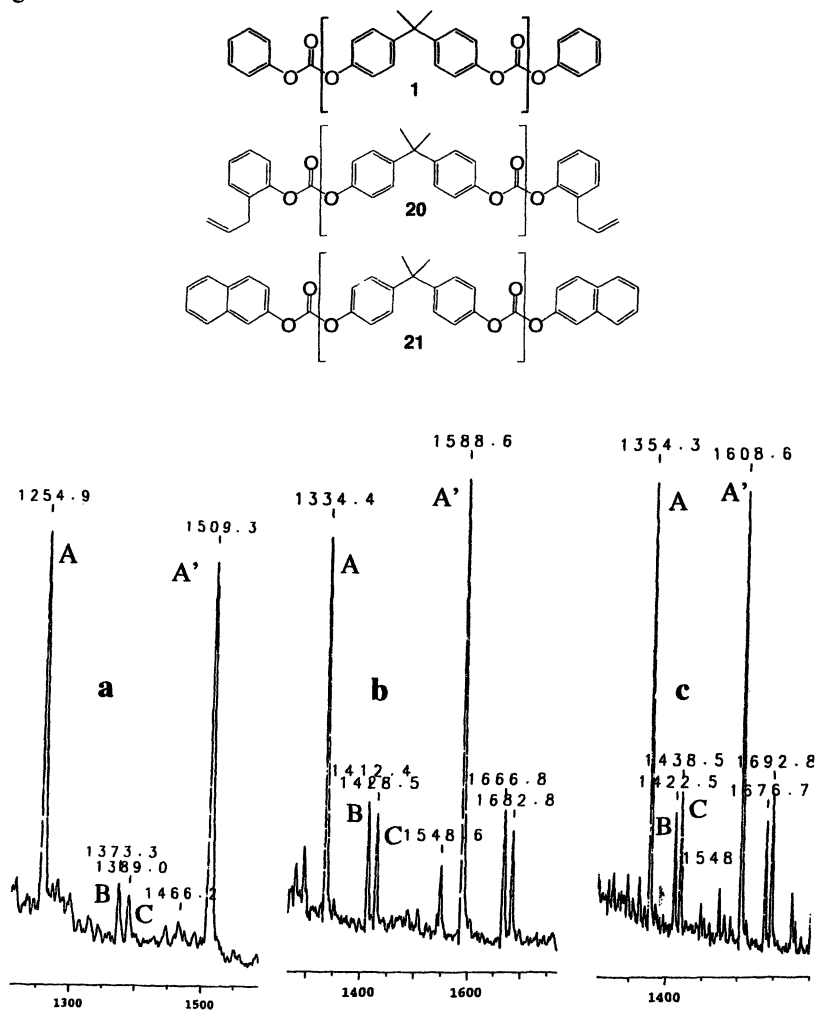


Figure 7. MALDI-TOF spectrum (selected mass range) for a. **1**; b. **20**; c. **21**

All four MALDI-TOF spectra (Fig. 6 & 7) show an identical pattern with the major set of peaks being the bis-end-functionalized oligomers (letters A and A' in Fig. 6 & 7) and a set of two smaller peaks (letters B and C in Fig. 6 & 7) 16 amu apart from each other, respectively. The position of those two smaller peaks in regards to the main oligomers is different for each set of oligomers, and only for **22b** happens to be 17 amu higher in mass than the corresponding oligomer (thus potentially being a water adduct will be ruled out). To fully confirm the proposed structures, complementary analysis, such as NMR analysis, is required. ^1H NMR analysis of **20** gave $M_n = 2,200$ g/mol (9).

To further investigate whether those set of peaks represent the same chemical motif, the mass difference between the next main peak (A') and the peak towards lower masses (C) was computed in Table 4. From this value, the mass for a single end group (EG) (Scheme 1) is subtracted resulting in a constant value of 43 amu for all four oligomers.

Scheme 1. Exact masses for end groups in **1**, **20**, **21** and **22b**.

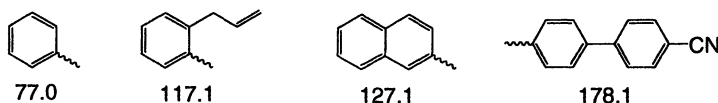
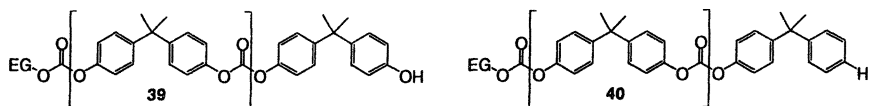


Table 4. Observed masses for peaks A, A', B and C for oligomers **1**, **20**, **21**, **22b**; theoretical values for the sodiated main peaks A, A' are given in parentheses

Oligomers	A	B	C	A'	A'-C	A'-C-EG
	<i>tetramer</i>			<i>pentamer</i>		
1+Na⁺	1,254.9 (1,253.4)	1,373.3	1,389.0	1,509.3 (1,507.5)	120.3	43.3
20+Na⁺	1,334.4 (1,333.5)	1,412.4	1,428.5	1,588.6 (1,587.6)	160.1	43.0
21+Na⁺	1,354.3 (1,353.4)	1,422.5	1,438.5	1,608.6 (1,607.5)	170.1	43.0
22b+Na⁺	1,456.6 (1,455.5)	1,473.5	1,489.7	1,710.9 (1,709.6)	221.2	43.1

Based on the above numbers, the following assignments are made: loss of CO_2 accounts for 44 amu, wherefore peak C is assigned as the main oligomer minus one end group minus one carbonyloxy group resulting in structures **39** (EG = end group as displayed in scheme 1; for EG = 4-cyanobiphenyl, **39** becomes **35**). Peak B is consistent with the further loss of oxygen (16 amu) to give oligomers **40** (for EG = 4-cyanobiphenyl, **40** becomes **36**).



Based upon those explanations, Table 5 then summarizes and assigns the major peaks in the MALDI-TOF spectrum of **22b** (Figure 6) up to the nonamer and Scheme 2 summarizes the fragmentation pattern obtained from MS data for **22b** via ESI, APCI and MALDI measurements.

Scheme 2. Breakdown of **22**.

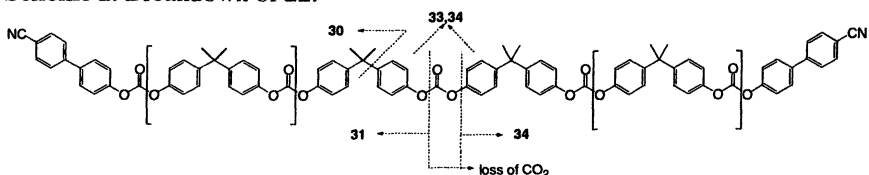
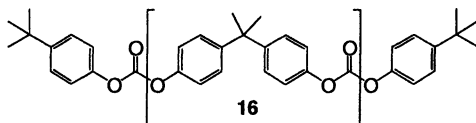


Table 5. Calculated and observed MWs of oligomers **22**, **35**, **36** and cyclics based on MALDI (Fig. 6)

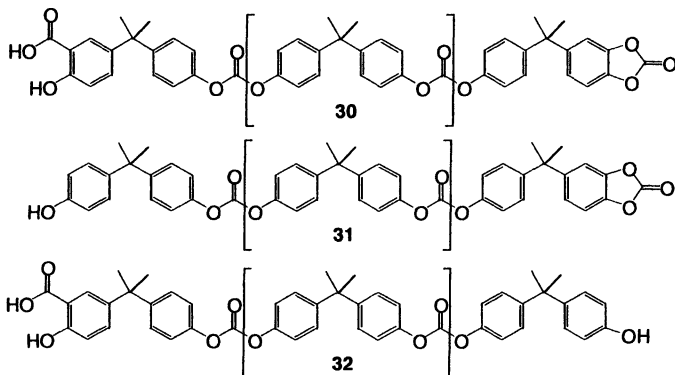
	3-mer	4-mer	5-mer	6-mer	7-mer	8-mer	9-mer
22	1,178.4	1,432.5	1,686.6	1,940.7	2,194.8	2,448.8	2,702.9
22+Na⁺	1,201.4	1,455.5	1,709.6	1,963.7	2,217.7	2,271.8	2,725.9
Obsvd	1,201.9	1,456.6	1,710.9	1,965.1	2,219.4	2,473.3	2,727.4
36	1,195.4	1,449.5	1,703.6	1,957.7	2,211.8	2,465.9	2,720.0
36+Na⁺	1,218.4	1,472.5	1,726.6	1,980.7	2,234.8	2,488.9	2,743.0
Obsvd	1,219.0	1473.5	1727.9	1982.0	yes	2490.2	2743.9
35	1,211.4	1,465.5	1,719.6	1,973.7	2,227.8	2,481.9	2,736.0
35 + Na⁺	1,234.5	1,488.5	1,742.6	1,996.7	2,250.8	2,504.9	2,759.0
Obsvd	1,235.3	1489.7	1744.0	1998.0	2252.2	2506.7	2760.5
cyclics			1,270.5	1,524.5	1,778.6	2,032.7	2,286.8
cyc.+Na⁺			1,293.4	1,547.5	1,801.6	2,055.7	2,309.8
Obsvd			1294.3	1548.3	1802.9	2056.8	2310.9

Nagahata *et al.* (10) used MALDI-TOF for the analysis of oligomers **3** (BPA terminated PC). Whereas their high MW PC ($M_n = 3.1$ k, PDI = 1.9; uncorrected MW by GPC) did not yield a good MALDI-TOF spectrum, fractionated oligomers **3** ($M_n = 3.6$ k, PDI = 1.03 by MALDI-TOF) did.

Vitalini *et al.* (11) characterized commercial PC (*tert.*-butylphenoxy end groups) and PC oligomers therefrom (via depolymerization with BPA) by MALDI-TOF. Their analysis clearly showed the presence of four envelopes representing PC cyclics, oligomers **3**, **16** and oligomers with one BPA and one *tert.*-butylphenoxy end group.



MALDI-TOF analysis undoubtedly confirmed the presence or absence of oligomers **3**, **30-32** obtained via oxidative carbonylation of BPA as reported by Goyal *et al.* (12,13).



Interestingly, they found that oligomers **3** cationize by Na^+ cations, whereas oligomers **30** and **32** were not cationized by the present sodium cation but rather by the Bu_4N^+ or Bu_4P^+ cation stemming from residual catalyst.

Comparison of Molecular Weights Obtained by Various Analytical Tools for Oligomers **22b**

Oligomers **22b** were analyzed by several analytical tools as described in this and the previous chapter. Comparing the results of the various analytical tools, the combined results from ^1H NMR, GPC, HPLC and MALDI seem to be the most descriptive for the analysis of end-functionalized PC oligomers **22**. Table 6 summarizes the obtained results. This is not to say that a different set of analytical tools might work better (*e.g.* ESI and APCI) for oligomers with

different end groups. MALDI seems to correlate best with ^1H NMR and GPC-RI data – not only for **22b** but also for several other oligomers as mentioned above.

Table 6. Comparison of MW for 22b by various analytical tools

<i>Analytical Tool</i>	<i>Max. peak g/mol</i>	<i>M_n g/mol</i>	<i>M_w g/mol</i>
^1H -NMR	-	2,380	-
GPC-RI ^a	2,164	1,995	2,646
GPC-UV 254 nm ^a	1,545	1,642	2,241
HPLC (cyano) 300 nm	1,178		
ESI	1,432		
APCI	1,432		
LC/APCI	1,179		
MALDI	2,195		

a: All GPC data are corrected for PC

Experimental

For a general procedure for the synthesis of diarylcarbonates (e.g. **25**) and oligomers **20-22**, and for the synthesis of **25'** see *ref.9*.

ESI and APCI mass spectra were obtained on a Finnigan LCQ ion trap mass spectrometer. ESI analysis was performed from a MeOH/CH₂Cl₂ (40/60) solution of the oligomer and a 0.656 mM NaCl. The spray voltage was 4.5 kV, the capillary voltage 3V and temperature 200 °C, the tube lens voltage at 30V, sheath gas N₂ at 40 and aux. gas N₂ at 5.

MALDI-TOF analysis was obtained on a Bruker Proflex III instrument in linear mode operated with a 337 nm N₂ laser; 20kV primary acceleration, 18.80 kV secondary acceleration; lens setting = 7.50 kV; no delay. Approximately 1.7 mg of sample was dissolved in 1mL of THF and mixed (50/50 v/v) with indole acrylic acid (saturated in THF) before analysis; mass range included 0-12 k Da; 200 shots; the obtained data were smoothed (Golay Savitzky 9); the instrument was calibrated externally (two points).

High Performance Liquid Chromatographic (HPLC) separations in conjunction with APCI were done using a Thermo Separation Products P4000 HPLC Pump and a Thermo Separation Products AS3000 Autosampler. A *LiChrosorb* aminopropyl bonded column (4.6 x 150 mm, dp = 5 μm) was used for the analysis. The mobile phase was a mixture of hexane and dichloromethane at a flow rate of 1.0 mL/min. A linear gradient starting with 10% dichloromethane at 0 minutes and increasing to 80% dichloromethane at 23 minutes was found to give the best separation. After 23 minutes the percent

dichloromethane was decreased back to 10% over a three-minute period. The APCI source parameters were: vaporizer temperature, 425°C; corona discharge current, 5 μ A; sheath gas, N₂ at 75; auxiliary gas, N₂ at 15; capillary temperature, 150°C; capillary voltage, 4 V; tube lens voltage, 30 V.

Acknowledgement

Compounds **1**, **20**, **21**, **22**, **25** and **25'** were synthesized during a post-doctoral appointment at UNC, Chapel Hill, NC with Prof. M. Gagné. MALDI-TOF spectra were recorded by N. Srinivasan NCSU, Raleigh, NC. ESI, APCI, and HPLC-APCI MS spectra were obtained by S. Sassman in Prof. W. Rudzinski's lab, Texas State University-San Marcos, TX, both of which I would like to thank for their helpful discussion of the data. GPC analysis of **22b** was performed in THF on a Waters 600 system with RI and dual wavelength detector; separation was afforded with Styragel HR5e and two Styragel HR4e columns. The ¹H NMR spectrum of **22b** was recorded at 400 MHz (Varian) in CDCl₃.

References

1. Mork, C. O.; Priddy, D. B. *J. Appl. Polym. Sci.* **1992**, *45*, 435-442.
2. Brunelle, D. J.; Boden, E. P.; Shannon, T. G. *J. Am. Chem. Soc.* **1990**, *112*, 2399-2402.
3. Brunelle, D. J.; Shannon, T. G. *Macromolecules* **1991**, *24*, 3035-3044.
4. Marks, M. J.; Sekinger, J. K. *Macromolecules* **1994**, *27*, 4106-4113.
5. Lattimer, R. P.; Schulten, H.-R. *Anal. Chem.* **1989**, *61*, 1201A-1215A.
6. Kim, W. B.; Park, K. H.; Lee, J. S. *J. Mol. Catal. A* **2002**, *184*, 39-49.
7. Puglisi, C.; Samperi, F.; Carroccio, S.; Montaudo, G. *Macromolecules* **1999**, *32*, 8821-8828.
8. Carroccio, S.; Puglisi, C.; Montaudo, G. *Macromolecules* **2002**, *35*, 4297-4305.
9. Korn, M. R.; Gagné, M. R. *Macromolecules* **1998**, *31*, 4023-4026.
10. Nagahata, R.; Sugiyama, J.; Goyal, M.; Asai, M.; Ueda, M.; Takeushi, K. *Polymer Journal* **2000**, *32*, 854-858.
11. Vitalini, D.; Mineo, P.; Iudicelli, V.; Scamporrino, E.; Troina, G. *Macromolecules* **2000**, *33*, 7300-7309.
12. Goyal, M.; Nagahata, R.; Sugiyama, J.; Asai, M.; Ueda, M.; Takeushi, K. *Polymer* **1999**, *40*, 3237.
13. Goyal, M.; Nagahata, R.; Sugiyama, J.; Asai, M.; Ueda, M.; Takeushi, K. *Polymer* **2000**, *41*, 2289-2293.

Chapter 7

Solid-State Polymerization of Poly(bisphenol A carbonate) Facilitated by Supercritical Carbon Dioxide

Douglas J. Kiserow¹⁻³, Chunmei Shi¹, George W. Roberts^{1,*},
Stephen M. Gross^{2,4}, and Joseph M. DeSimone^{1,2}

¹Department of Chemical Engineering, North Carolina State University,
Raleigh, NC 27695-7905

²Department of Chemistry, University of North Carolina at Chapel Hill,
Chapel Hill, NC 27599-3290

³Chemical Science Division, U.S. Army Research Office, P.O. Box 12211,
Research Triangle Park, NC 27709-2211

⁴Current address: Department of Chemistry, Creighton University,
Omaha, NE 68178

During the solid state polymerization (SSP) of poly(bisphenol A carbonate), both the forward reaction rate constant and the phenol diffusion coefficient inside the polymer particle were significantly higher when SSP was carried out in supercritical carbon dioxide (scCO₂) compared to in atmospheric N₂. These enhancements depended on the reaction conditions, and can be understood in terms of the CO₂ concentrations in the polymer. Polymer with a M_w as high as 78100 has been synthesized by SSP with scCO₂ as the sweep fluid.

Introduction

Aromatic polycarbonates are an important class of thermoplastics and have many commercial applications primarily due to their unusual toughness and optical clarity (1). A number of synthetic routes for poly(bisphenol A carbonate) have been described in the literature. Interfacial phosgenation of bisphenol A is the predominant method to produce polycarbonate industrially. However, melt phase polymerization is generating significant interest as a solvent-free and potentially phosgene-free alternative for polycarbonate synthesis, thereby alleviating the detrimental environmental impacts associated with the interfacial polycondensation. Due to the highly reversible nature of melt transesterification, the small-molecule condensate (phenol) must be efficiently removed to drive the polymer to high molecular weight. However, the high viscosity encountered in the melt phase makes condensate removal very difficult. As a result, the molecular weight obtained during melt polycondensation is limited. Additionally, side reactions are promoted at the high temperatures that must be used, which may lead to color body formation and poor optical quality.

Recent research has demonstrated that high molecular weight poly(bisphenol A carbonate) can be synthesized through solid state polymerization (SSP) (2,3). Low molecular weight prepolymer first was synthesized by melt polymerization of bisphenol A and diphenyl carbonate, and rendered crystalline either thermally (2) or with the aid of a nucleating agent or a plasticizer [e.g. supercritical carbon dioxide (3)] to prevent particle sticking during SSP. The semicrystalline prepolymer was subsequently heated to a temperature between the glass transition temperature (T_g) and the melting temperature (T_m) to allow the end groups to be mobile enough for chain extension reactions. Solid state polymerization is typically carried out under vacuum or with a continuous flow of an inert fluid (sweep fluid) to facilitate phenol removal. Previous research has shown that using $scCO_2$ as the sweep fluid for solid state polymerization resulted in a faster-rate of molecular weight increase compared to using N_2 as the sweep fluid (3). With this approach, lower polymerization temperatures can be used to synthesize certain molecular weight polycarbonate, which may improve polymer quality.

This research focuses on the reaction kinetics of the SSP of poly(bisphenol A carbonate) using $scCO_2$ as the sweep fluid (4). Reaction rate constants and phenol diffusivities in the polymer were determined and compared with the results obtained for SSP with N_2 as the sweep gas. The diffusion kinetics and the equilibrium solubility of $scCO_2$ in the polymer were measured using a high pressure microbalance under SSP conditions to better understand the rate enhancing effects of $scCO_2$.

Experimental

Prepolymer Synthesis

The prepolymer was synthesized by the melt polymerization of bisphenol A and diphenyl carbonate with $\text{LiOH}\cdot\text{H}_2\text{O}$ as the catalyst. For the study of the intrinsic reaction kinetics, the prepolymer melt was allowed to cool slowly overnight, ground to powder, and separated into different size ranges by sieving. The prepolymer powder had a crystallinity of 24% as synthesized. To investigate phenol diffusion, the prepolymer melt with no crystallinity was poured into a hot metal syringe. The prepolymer dripped from the hot syringe under its own weight into cold water to form transparent beads with an average diameter of 2 mm. The amorphous beads were then exposed to scCO_2 at 40 °C and 103 bar for 1 hour and at 70 °C and 138 bar for 4 hours to obtain a crystallinity of 22%.

Solid State Polymerization

For SSP in scCO_2 , a supercritical fluid extractor with a built-in temperature control was used as the reactor (I.D: 1/4") (4). Carbon dioxide was pressurized in a dual-barrel Isco pump and flowed through the reactor with a constant downward flow. The reaction pressure was controlled by an automated back pressure regulator. Control experiments with N_2 as the sweep gas were carried out according to the procedure described elsewhere (5).

Instrumentation and Analysis

Solid state polymerization was allowed to run for a specific period of time depending on the experiment. The resulting polymer molecular weight was determined using a Waters 150-CV GPC using a THF mobile phase and polystyrene standards. Universal calibration was carried out to convert the number average molecular weight, M_n , relative to polystyrene to the absolute number average molecular weight of polycarbonate, $M_{n,PC}$. The resulting relationship was: $M_{n,PC}=0.714M_n$. A Seiko Haake DSC 220 was used to determine the T_g , T_m , and crystallinity of the polymer in a N_2 atmosphere at a heating rate of 10 °C/min.

Carbon dioxide sorption into the polymer was measured with a microbalance with a resolution of 0.01 mg (Rubotherm) electromagnetically coupled to a high pressure vessel.

Because the transreaction during SSP involves the reaction between two dissimilar end groups, the end group stoichiometry affects both the obtainable molecular weight of the polymer and the reaction kinetics. In this research, the ratio of the end groups in the prepolymer was determined via ^1H (for hydroxyl end group) and ^{13}C NMR (for phenyl end group). Nuclear magnetic resonance spectra were obtained on a Bruker 400 MHz NMR spectrometer by dissolving the low-crystallinity prepolymer in deuterated chloroform as a 5 wt% solution. Bruker XwinNMR software was used for data manipulation and peak integration.

Results and Discussion

To study the intrinsic reaction kinetics, the experimental conditions (prepolymer particle size and sweep fluid flow rate) were adjusted to eliminate any influence of phenol transport on reaction kinetics. For example, to determine the particle size required to eliminate any intra-particle diffusion limitation, solid state polymerization was carried out at 120 °C and 345 bar with three different particle sizes. As can be seen from Figure 1, in the range of particle sizes studied, there is no effect of particle size on molecular weight evolution, indicating phenol diffusion inside the particle is not limiting the reaction rate. Therefore, a particle size of 75~125 μm was used in subsequent experiments.

For intrinsic reaction kinetics, the rate of SSP follows second order kinetics with respect to hydroxyl and phenyl end group concentrations, assuming that no side reactions occur, i.e., that the hydroxyl and phenyl end groups are consumed in a 1:1 ratio. Forward reaction rate constants were calculated by fitting the kinetic model to the experimental data of $M_{n,PC}$ evolution versus SSP time.

The forward reaction rate constants are plotted using an Arrhenius relationship in Figure 2. As can be seen from this figure, the reaction rates in the polymer during SSP in scCO_2 were significantly higher than in atmospheric N_2 . It was also observed that the rate-enhancing effect of CO_2 depends strongly on the SSP temperature and pressure. At a fixed pressure, the effect of CO_2 on the rate constant decreased with increasing temperature. There exists an optimal CO_2 pressure, near 207 bar, where CO_2 has a maximum effect on the reaction rate. Similar results were obtained for phenol diffusivity during SSP.

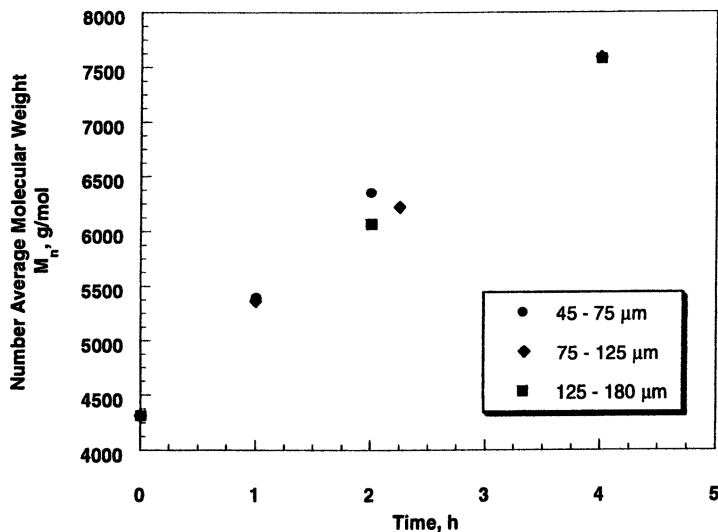


Figure 1. Effect of particle size on molecular weight evolution during SSP of BPA-PC at 120 °C and 345 bar (CO_2 flow rate = 20 mL/min). (Reproduced from reference 4. Copyright 2001 American Chemical Society.)

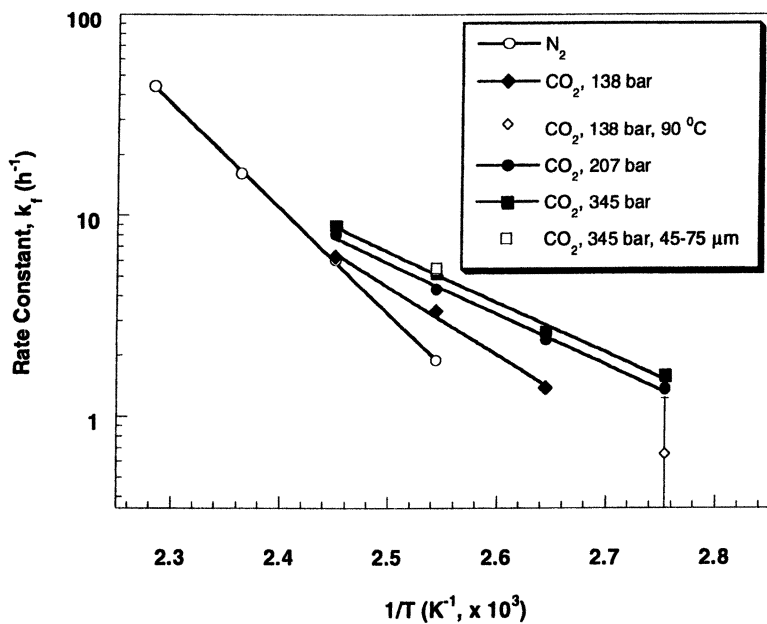


Figure 2. Arrhenius plot for the forward reaction rate constant during SSP of poly(bisphenol A carbonate) with N_2 and scCO_2 as the sweep fluid (Reproduced from reference 4. Copyright 2001 American Chemical Society)

To determine the phenol diffusivity during the reaction, large prepolymer beads were used for SSP. High sweep fluid flow rates were chosen to eliminate any effect of external phenol transport. When using the large polymer beads, phenol diffusion inside the polymer particle was the rate-limiting step for the overall reaction. Therefore, the intrinsic chemical reaction can be assumed to reach local equilibrium instantaneously. A mathematical model was developed to fit the experimental data for average $M_{n,PC}$ versus time, with phenol diffusivity as the only fitting parameter (6). Phenol diffusivities were determined at different SSP temperatures and CO_2 pressures by non-linear regression (7).

As can be seen from Table 1, at 150 °C the diffusion coefficient of phenol was almost 200% higher when using $scCO_2$ as the sweep fluid compared to using N_2 , whereas at 165 °C, the increase is only about 50%.

Table I. Phenol Diffusivity ($D_a \times 10^8 \text{ cm}^2/\text{s}$) in the Polymer during Solid State Polymerization with N_2 and $scCO_2$ as the Sweep Fluids

Sweep fluid	Temperature (°C)	
	150	165
N_2	5.63	20.8
CO_2 , 138 bar	7.13	20.7
CO_2 , 207 bar	14.5	33.8
CO_2 , 345 bar	17.4	30.3

The changes in reaction rate constant and phenol diffusivity with temperature and CO_2 pressure are similar and may be correlated with CO_2 solubility in the polymer. Different CO_2 solubilities may, in turn, result in different degrees of polymer plasticization or T_g depression during SSP. Preliminary measurements of CO_2 sorption in polycarbonate at 138 bar indicated that CO_2 achieved equilibrium solubility within 2 hours, and that the equilibrium CO_2 concentration decreased significantly as the temperature increased (Figure 3). An increase in CO_2 solubility with increasing pressure in amorphous polycarbonate has been reported previously (8). However, at very high pressures, there is little additional increase in CO_2 solubility in the polymer (9) and the static pressure tends to increase polymer T_g (10).

By synthesizing the prepolymer using appropriate monomer ratios, poly(bishpenol A carbonate) with a very high molecular weight can be produced via solid state polymerization in $scCO_2$. For example, by using initial molar ratios of 1.00 and 1.08 for diphenyl carbonate (DPC) and bisphenol A (BPA),

respectively in the melt polymerization, and carrying out SSP at 207 bar with ramped heating up to 230 °C, polymers have been synthesized with weight average molecular weight (M_w relative to polystyrene) as high as 78100 for 10 hours of SSP time. The reaction conditions and molecular weight results are summarized in Table 2.

As is shown in Table 2, when the monomer ratio DPC/BPA is 1.08, a higher molecular weight was achieved after SSP than when the monomer ratio is 1.00. End group analyses by ^1H and ^{13}C indicated that the end group ratio for each prepolymer was 1.00 within experimental error. The relationships between the initial monomer ratio, the melt polymerization conditions, and the ratio of end groups in the prepolymer are not clearly defined at this point. However, it is highly likely that during prepolymer synthesis, the loss of the more volatile DPC was better compensated by the use of excess DPC in the monomer feed, which eventually yielded a polymer of higher molecular weight after SSP.

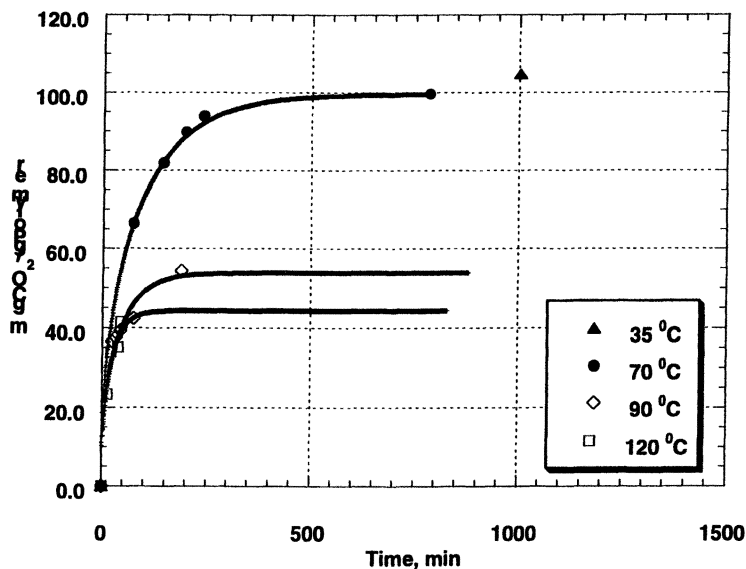


Figure 3. The solubility of CO_2 in poly(bisphenol A carbonate) at 138 bar. The polymer used for sorption at 35 and 70 °C was amorphous, while that for sorption at 90 and 120 °C had 25% crystallinity.

Table 2. Monomer Molar Ratios (DPC/BPA)^a and Molecular Weight^b before and after Solid State Polymerization^c in Supercritical CO₂

<i>DPC/BPA</i>	<i>M_w before SSP in CO₂</i>	<i>M_w after SSP in CO₂</i>
1.00	16100	58200
1.08	17300	78100

NOTE: *a.* monomer ratios at the beginning of melt polymerization. *b.* weight average molecular weight (g/mol), determined by GPC based on polystyrene standard. *c.* Solid state polymerization conditions: 207 bar, 15 mL/min of CO₂ flow, 160 °C, 2 hours; 180 °C, 2 hours; 200 °C, 2 hours; 220 °C, 2 hours, and 230 °C, 2 hours.

The temperatures used for synthesizing the polymers in Table 2 are quite low relative to those used in a conventional melt polymerization (11,12). For example, for the polymer with *M_w* of 78,000, the highest temperature during the melt polymerization was 230 °C, and the highest temperature during SSP was 230 °C. The properties of these polymers may be different than “conventional” poly(bisphenol A carbonate), and are currently being evaluated.

Conclusions

Solid state polymerization of poly(bisphenol A carbonate) was successfully carried out with scCO₂ as the sweep fluid to efficiently remove the reaction condensate (phenol) and obtain high molecular weight polymer. Both the forward chemical reaction rate constant and the phenol diffusion coefficient inside the polymer particle during SSP in scCO₂ were significantly higher than that in atmospheric N₂. The rate enhancement from scCO₂ appears to be a consequence of increased end group mobility and free volume due to the plasticization of the polymer by dissolved CO₂. High molecular weight polymers can be synthesized using short reaction times and lower reaction temperatures when SSP is carried out in scCO₂.

Acknowledgements

This work was performed while the author (C.S.) held a National Research Council Research Associateship Award at the US Army Research Office. The authors acknowledge additional financial support from the STC program of the National Science Foundation under Agreement CHE-9876674. The authors

would also like to thank Ms. Zhilian Zhou at University of North Carolina at Chapel Hill for running the NMR.

References

1. LeGrand, D. G.; Bendler, J. T. *Handbook of Polycarbonate Science and Technology*; Marcel Dekker: New York, **2000**.
2. Iyer, V. S.; Sehra, J. C.; Ravindranath, K.; Sivaram, S. *Macromolecules* **1993**, *25*, 186.
3. Gross, S. M.; Roberts, G. W.; Kiserow, D. J.; DeSimone, J. M. *Macromolecules* **2000**, *33*, 40.
4. Shi, C.; DeSimone, J. M.; Kiserow, D. J.; Roberts, G. W. *Macromolecules* **2001**, *34*, 7744.
5. Shi, C.; Gross, S. M.; DeSimone, J. M.; Kiserow, D. J.; Roberts, G. W. *Macromolecules* **2001**, *34*, 2060.
6. Goodner, M. D.; DeSimone, J. M.; Kiserow, D. J.; Roberts, G. W. *Ind. Eng. Chem. Res.* **2000**, *39*, 2797
7. Shi, C.; Roberts, G. W.; Kiserow, D. J. *J. Polym. Sci., Part B: Polym. Phys.* **2003**, *41*, 1143.
8. Chan, A. H.; Paul, D. R. *Polym. Eng. Sci.* **1980**, *20*, 87.
9. Chang, S. H.; Park, S. C.; Shim, J. J. *J. Supercrit. Fluids* **1998**, *13*, 113.
10. Zoller, P. *J. Polym. Sci., Polym. Phys. Ed.* **1982**, *20*, 1453.
11. Brunelle, D. J.; Smigelski, P. M. *Polymer Preprints*, **2003**, *44*, 740.
12. King, J. A. U. S. Patent 5,319,066, **1994**.

Poly(bisphenol A carbonate) Copolymers

Chapter 8

Copolycarbonate of Bisphenol and 4, 4'- Dihydroxydiphenyl

Alexander Karbach¹, Doris Drechsler¹, Claus-Ludolf Schulte¹,
Ute Wollborn¹, Melanie Moethrath², Michael Erkelenz²,
James Y. J. Chung³, and James P. Mason³

¹Bayer Industry Services GmbH & Company OHG, Analytics, 47829
Krefeld, Germany (Alexander.Karbach.AK@bayerindustry.de)

²Bayer Material Science AG, Innovation, 47829 Krefeld, Germany

³Bayer Material Science AG, Business Development, Pittsburgh, PA 15205

A copolycarbonate (DOD-co-PC) (*1*) of bisphenol A and 4, 4'-dihydroxydiphenyl (DOD) with defined amounts of DOD has an outstanding balance of optical, mechanical, thermal and impact properties. In particular, it has high light transmission, high glass transition and heat-distortion temperatures, and high notched Izod impact strength at thick section and low temperatures. Furthermore, it is unusually resistant to embrittlement after heat aging. For further understanding of the structure property relationships, DOD-co-PC with different amounts of DOD are investigated.

Introduction

Certain copolycarbonates of bisphenol A and 4, 4'-dihydroxydiphenyl (DOD) were reported in the literature to have high transparency and glass transition temperature (2, 3), high surface hardness and electrical insulation properties (2). For samples with more than 60mol% DOD liquid crystalline

properties were obtained (4). Bayer Polymers recently carried out extensive evaluations of copolycarbonates of bisphenol A with different amounts of DOD (Figure 1). In the present paper, experimental results of a copolycarbonate (DOD-co-PC) with defined amounts of DOD are discussed with those of a bisphenol A polycarbonate (BPA-PC) (5) of a comparable molecular weight. The copolycarbonate was synthesized by interfacial phosgenation (5).

In the first chapter, the technical properties of DOD-co-PC are presented. The second chapter gives an overview on their morphology and their supramolecular structure; the results are discussed in combination with in situ deformation experiments.

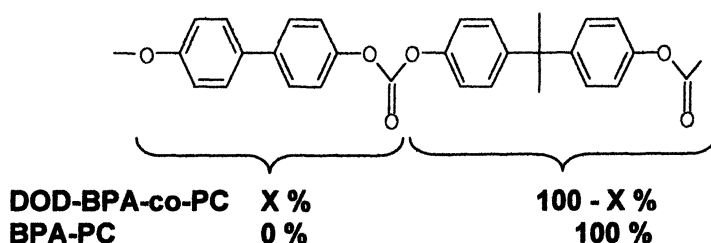


Figure 1. Structures of DOD-BPA-co-PC and BPA-PC.

Experimental Results

The following experiments were carried out on DOD-co-PC with 30 mol% DOD.

Optical, Thermal, Physical and Mechanical Properties

Optical Properties

DOD-co-PC is transparent with a high light-transmission comparable to BPA-PC. A refractive index of DOD-co-PC is slightly higher than that of PC. Also, DOD-co-PC has a higher birefringence than BPA-PC as shown in Figure 2a. The birefringence of DOD-co-PC is more persistent during heat aging (annealing) than that of BPA-PC. For instance, annealing DOD-co-PC at 130 °C lower temperature (120 °C) for 8 days significantly reduced the birefringence.

Table I. Optical properties of DOD-co-PC and BPA-PC.

	<i>Refractive Index</i> <i>ISO 489-A</i>	<i>Yellowness Index</i> <i>ASTM</i>	<i>Haze</i> <i>ASTM</i> [%]	<i>Transmission at 4.0 mm</i> <i>ISO 5036-1</i> [%]	<i>Theoretical Transmission at 1.0 mm</i> <i>ISO 5036-1</i> [%]
DOD-co-PC	1.599	3.0 – 5.0	0.5	86	89.91
BPA-PC	1.585	1.8 – 3.0	0.3 – 0.8	88	90.26

Table II. Thermal properties of DOD-co-PC and BPA-PC.

	<i>Glass Transition Temperature</i> <i>ISO 11357-2, DMA</i> °C	<i>Heat Distortion Temperature</i> <i>ISO 75, Method Af at 1.80MPa</i> °C	<i>Heat Distortion Temperature</i> <i>ISO 75, Method Af at 0.45MPa</i> °C	<i>Vicat Softening Temperature</i> <i>ISO 306, 50N/50K/h</i> °C
DOD-co-PC	163	134	149	156
BPA-PC	155	128	141	147

Thermal Properties

In comparison to BPA-PC, DOD-co-PC has higher glass transition, heat distortion and Vicat softening temperatures by 6 to 9 °C.

Physical and Mechanical Properties

Density, tensile and flexural properties of DOD-co-PC and BPA-PC are shown in Tables III, IV and V, respectively. DOD-co-PC has a higher density than PC. However, compared to BPA-PC, DOD-co-PC has a lower- tensile modulus, - yield stress, and - elongation at break, while its elongation at yield is higher. Similarly, the flexural modulus of DOD-co-PC is lower than that of the BPA-PC, and its flexural strain at yield is higher.

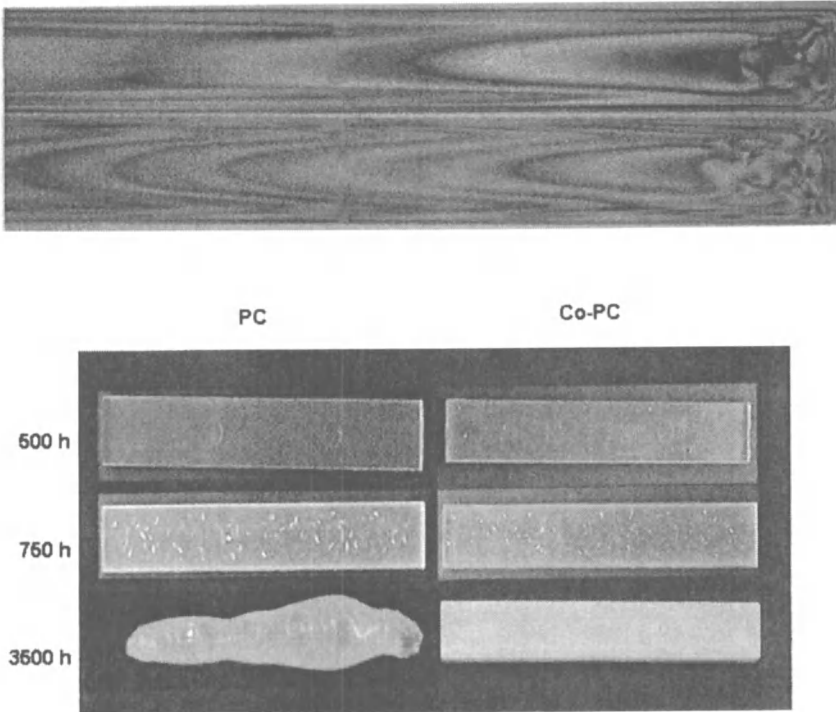


Figure 2. a) Injection molded samples of BPA-PC (top) and DOD-co-PC (bottom) shown under polarized light. b) Effect of boiling-water immersion on BPA-PC and DOD-co-PC. (See page 1 of color insert.)

Table III. Density of DOD-co-PC and BPA-PC.

<i>ISO 1183</i>	<i>Density</i> [kg/dm ³]
DOD-co-PC	1.217
BPA-PC	1.200

Table IV. Tensile properties of DOD-co-PC and BPA-PC.

<i>ISO 527</i>	<i>Tensile modulus</i> [MPa]	<i>Yield Stress</i> [MPa]	<i>Yield Strain</i> [%]	<i>Stress at break</i> [MPa]	<i>Strain at break</i> [%]
DOD-co-PC	2200	60	7.0	81	95
BPA-PC	2400	65	6.0	70	115

Table V. Flexural properties of DOD-co-PC and BPA-PC.

<i>ISO 178</i>	<i>Flexural modulus</i> [MPa]	<i>Yield Stress</i> [MPa]	<i>Flexural Strain</i> [%]	<i>Stress at 3.5% strain</i> [MPa]
DOD-co-PC	2200	98	8.1	66
BPA-PC	2400	97	7.0	73

*Notched Izod Impact Strength***Table VI. Notched Izod Impact Test (ISO 180/4A) with standard notch radius of 0.25 mm at various temperatures.**

<i>Test Temperature</i>	<i>23 °C</i> [kJ/m ²]	<i>-10 °C</i> [kJ/m ²]	<i>-20 °C</i> [kJ/m ²]	<i>-30 °C</i> [kJ/m ²]	<i>-40 °C</i> [kJ/m ²]	<i>-50 °C</i> [kJ/m ²]	<i>-60 °C</i> [kJ/m ²]
DOD-co-PC	82	60	57	56	52	52	50
BPA-PC	90	90	15	15	<10	<10	<10

At 23 and -10°C DOD-co-PC has slightly lower impact strength than BPA-PC. However, at -20°C and below BPA-PC is brittle with very low impact strength, whereas DOD-co-PC is ductile with high impact strength even at -60°C. Visually, the ductile fracture surfaces of both DOD-co-PC and BPA-PC show extensive shear yielding.

As shown in Table VII, reduction in notch radius from 0.25 mm to 0.1 mm reduces the Izod impact strengths of both DOD-co-PC and BPA-PC. BPA-PC is brittle even at 23 °C with an impact strength of <10 kJ/m. In contrast, DOD-co-PC is ductile at 23 and 10 °C with the impact strengths of 39 and 37 kJ/m², respectively. At 0 and -20 °C, DOD-co-PC shows brittle breaks even though its impact values are still high (37 and 35 kJ/m², respectively).

Table VII. Notched Izod Impact Test (ISO 180/4A) with notch radius of 0.1 mm at various temperatures.

<i>Test e</i>	23 °C	10 °C	0 °C	-20 °C
<i>Temperatur</i>	[kJ/m ²]	[kJ/m ²]	[kJ/m ²]	[kJ/m ²]
DOD-co-PC	39	37	35	35
	tough	tough	brittle	brittle
BPA-PC	<10 brittle	<10 brittle	<10 brittle	<10 brittle

As shown in Table VIII, the critical thickness of the DOD-co-PC for ductile to brittle transition in notched Izod impact test with a notch radius of 0.25 mm at room temperature is higher (6.8 vs. 4.9 mm) than that of the BPA-PC.

Table VIII. Critical thickness ductile to brittle transition at standard notch radius of 0.25 mm and 23 °C.

<i>ISO 180</i>	<i>BPA-PC</i>	<i>DOD-co-PC</i>
Critical Thickness (mm)	4.9	6.8

Heat aging (annealing) of DOD-co-PC at 135 °C for up to 480 hours did not cause brittle break in notched Izod impact test, while BPA-PC became brittle after annealing for only 2 hours at the same temperature.

Table IX. Effect of heat aging on notched Izod Impact Strength of DOD-co-PC and BPA-PC at 23 °C and 0.25 mm notch radius.

<i>Impact Strength (ISO 180/4A)</i>	<i>DOD-co-PC</i> [kJ/m ²]	<i>BPA-PC</i> [kJ/m ²]
Heat Aging at 135 °C for:		
0 (Control) Hour	82	90
2 Hours	52	15
24 Hours	52	10
46 Hours	52	7.7
168 Hours	54	5
480 Hours	52	5

Table X. Burning Behavior, TGA Pyrolysis-Residue, Glow Wire Temperatures, and Limiting Oxygen Index of DOD-co-PC and BPA-PC.

	<i>Burning Behavior at 3.0 mm</i>	<i>Burning Behavior at 6.0 mm</i>	<i>TGA Pyrolysis Residue</i>	<i>Glow wire test at 1.0 mm</i>	<i>Glow wire test at 2.0 mm</i>	<i>Glow wire test at 3.0 mm</i>	<i>Limiting Oxygen Index</i>
	<i>UL94</i>	<i>UL94</i>	<i>IEC-695-2-1</i>	<i>IEC-695-2-1</i>	<i>IEC-695-2-1</i>	<i>ISO 4589</i>	
	<i>Class</i>	<i>Class</i>	<i>[%]</i>	<i>passed [°C]</i>	<i>passed [°C]</i>	<i>passed [°C]</i>	<i>[%]</i>
DOD-co-PC	V2	V0	32.5	800	900	960	35
BPA-PC	HB	HB	29.4	850	850	900	28

Flame Resistance

Compared to BPA-PC, DOD-co-PC has better UL94 flame-resistance ratings, larger TGA pyrolysis residues, higher glow-wire temperatures at thick sections (2 and 3 mm), and a higher limiting oxygen index.

Table XI. Stress Crack Resistance of DOD-co-PC and BPA-PC to ASTM reference fuel C (*) for 30 min. at 23 °C. Unnotched Charpy Impact values of the chemical exposure.

Applied Flex. Strain (%)	0.2	0.4	0.8	1.2
DOD-co-PC	No Break	No Break	2.9** kJ/m ²	1.6** kJ/m ²
BPA-PC	No Break	Cracked	Cracked	Cracked

* 50% Toluene/50% Isooctane by Volume; ** per ISO 179/1D Impact Test

Environmental Stress Crack Resistance

DOD-co-PC is somewhat more stress-crack resistant to ASTM reference fuel than BPA-PC. As can be seen in Figure 2b, DOD-co-PC is also more resistant to boiling water than BPA-PC in terms of dimensional stability and flitter (sparkling micro-cracks) formation.

Analytical Results

To shed some light on the significant differences in the aforementioned properties of the DOD-co-PC and BPA-PC at the microscopic level, the morphology and the supramolecular structure of different copolycarbonates were investigated using nuclear magnetic resonance spectroscopy (NMR) (6), X-ray diffraction (XRD) (7), atomic force microscopy (AFM) (8, 9) and differential scanning calorimetry (DSC) (10, 11). The polymer molecular-weight characterization was done with gel permeation chromatography (GPC) (12, 13). The chemical structure of oligomers was investigated by Matrix-assisted-laser-desorption time-of-flight mass-spectroscopy (MALDI TOF MS) (14).

NMR Data

The ¹H-NMR spectra were recorded using a Bruker DPX 400 spectrometer equipped with a QNP probe head operating at 400.13 MHz for ¹H in CDCl₃ solutions.

Figure 3 shows ¹³C-NMR spectra of the DOD-BPA-copolycarbonates with 30 mole% of DOD and 12.6 mole% of DOD for comparison. The average chain length of the DOD-carbonate blocks is in a range of 1.8 units calculated from the peak intensities of DOD-carbonate and BPA-carbonate. The relative intensities

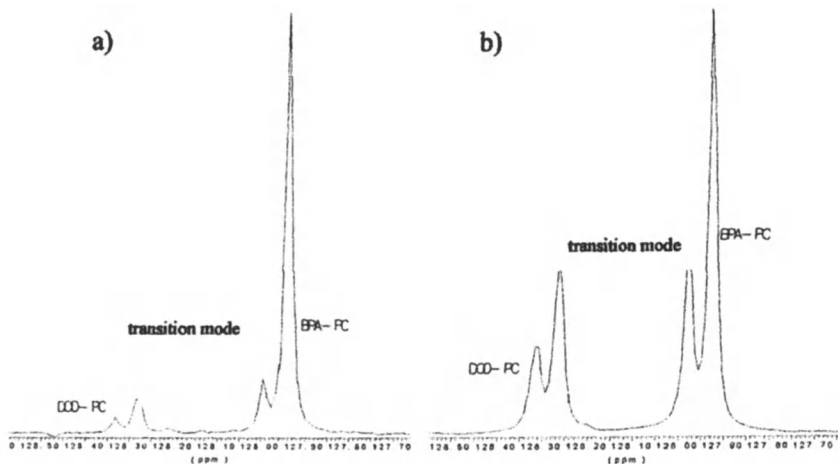


Figure 3. ^{13}C -NMR of Aromatic CH Groups of DOD-BPA-copolycarbonates with 12.6 and 30 mole % of DOD (a and b, respectively) (See page 1 of color insert.)

DSC

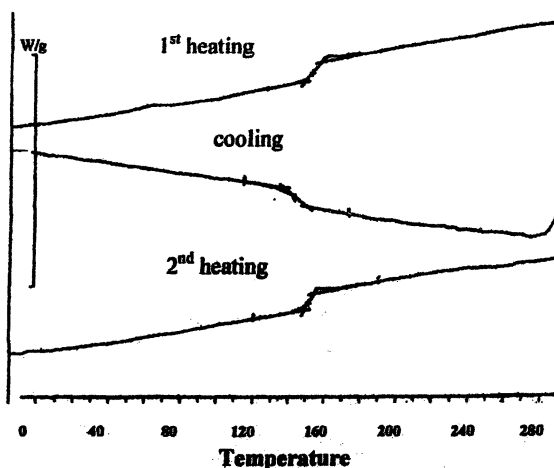


Figure 4 DSC measurements of DOD-BPA-copolycarbonate.

of the DOD-carbonate blocks compared to those of the transition (DOD-carbonate-BPA and BPA-carbonate-DOD) peaks are independent of the BPA-carbonate block length.

The DSC measurements were done on a Mettler DSC 30 at a heating and cooling rate of 20°C/min. As shown in Figure 4, there is no evidence for

crystalline or semi-crystalline structures. Only a glass transition with a T_g of 150 °C can be detected for DOD-co-PC.

X-Ray Diffraction Spectra

The XRD measurements of injection-moulded bars were done using Bruker GADDS (Karlsruhe, Germany) in reflection mode with Cu- K_α -radiation. In Figure 5a the spectra of various DOD-BPA-copolycarbonate samples with various amounts of DOD as well as PC are given. All the samples show halos indicating no crystallinity. Another interesting point is that a peak maximum is shifted toward higher d-values as the amount of DOD in the samples is increased. For instance, a shift of the peak maximum of the copolycarbonate with 50 mol% of DOD from that of PC is in the range of 0.3 Å.

Radial Distribution Function

Radial distribution functions (Figure 5b) of the interatomic vector length between the C-C atoms of BPA-PC and DOD-co-PC were obtained after energy minimization of 100 units each of BPA- and DOD-carbonate chains by using Dreiding Force Field (Cerius 3.5, MSI, San Diego). There is a shift of 0.3-0.4 Å from BPA-PC to DOD-co-PC, which is caused by the exchange of the more bulky BPA units through the shorter DOD units.

AFM

AFM measurements of the microtomed sample surfaces were performed with NanoScope IIIa (Dimension 3000, Digital Instruments/Veeco Metrology Group, Santa Barbara, USA) in tapping mode with Si-tips attached on 225 µm cantilevers at resonance frequencies of about 60 kHz.

As can be seen in Figure 6, BPA-PC sample shows homogenous phase distribution, whereas various copolycarbonate samples show micro phase separation with dark-soft areas in a range of 20-30 nm and look like a network.

It is informative that the phase contrast is increased as function of DOD content. For instance, as shown in Figure 7a, a copolycarbonate with 40mol % of DOD shows a sharp phase-separation in hard and soft regions with diameter of 10-20 nm. The soft region must not be understood as a rubber phase or a modifier. The soft region means easily moveable under the AFM tip or a region with low stiffness and elasticity. Accordingly, bright regions are attributed to the hard BPA-rich areas, while the dark regions are attributed to the soft DOD-rich

areas. The DOD-rich phases appear to be assembled into microdomains, which are separated by BPA-rich areas as interstitial material.

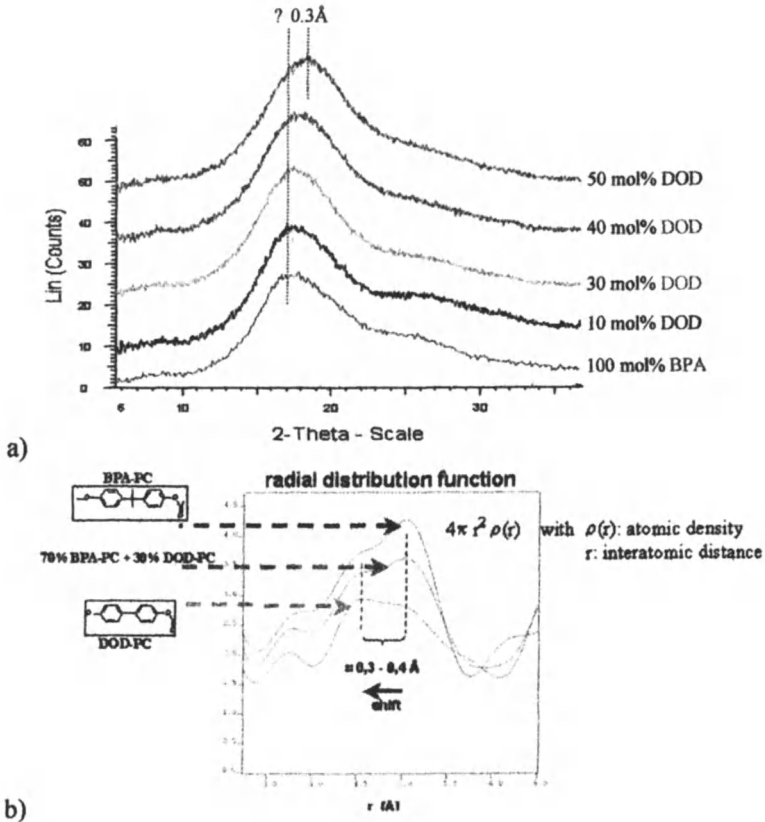


Figure 5. a) XRD Spectra measurements of DOD-BPA-copolycarbonates, b) Radial Distribution Function of DOD-co-PC. (See page 2 of color insert.)

The evaluation of the phase shift offers a possibility for the quantification of the micro phase separation. Figure 7b shows a plot of the half width (HW) of the detected phase angle vs. the molar composition of the investigated samples. The diagram indicates that the higher the HW of the DOD portion is, the higher the molecular separation.

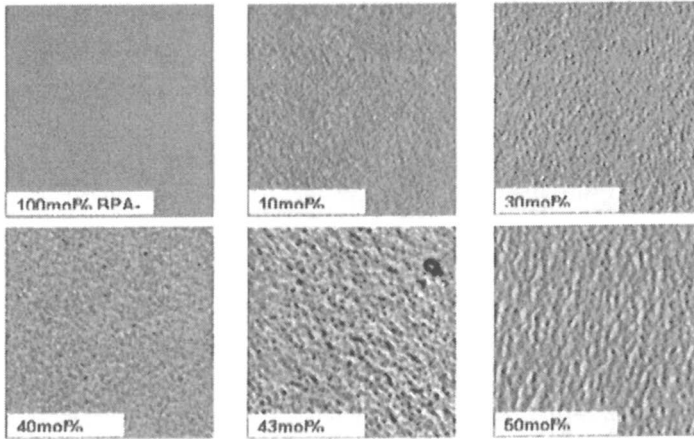


Figure 6. AFM phase contrast images of different compounds. Scan size: $1 \mu\text{m}^2$.
(See page 2 of color insert.)

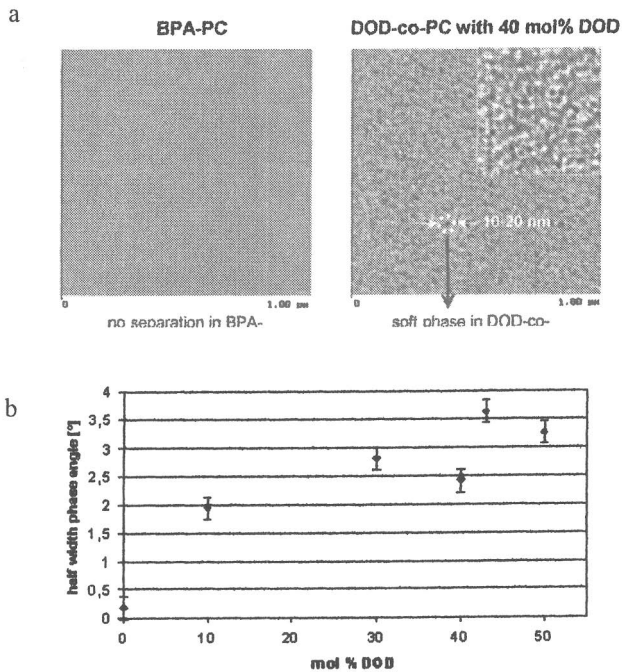


Figure 7. a) AFM phase contrast images of the BPA-PC and the 40 mol% DOD-co-PC. (See page 3 of color insert.)
b) Quantification of the micro phase separation.

GPC

The molecular weight distributions of DOD-BPA copolycarbonates were measured by Viscotec 2000 using triple detection techniques (refractive index-, light scattering-, viscosity-detection). Figures 8a and 8b show a comparison of samples with different amounts of DOD measured on refractive index- and light scattering traces.

The triple detection permits an absolute molecular weight calibration of the SEC and the direct evaluation of the Mark-Houwink constants for DOD-co-PC with different content of DOD. For a given molecular weight the radius of gyration R_g increases slightly with increasing amount of DOD in the polymer, and the formation of small amounts of high molecular parts can be detected.

The light scattering detector is very sensitive to very small amounts of high molecular structures in the polymers which cannot be detected by other detectors like refractive index (RI) or UV. In DOD containing copolymers the formation of small amounts of high molecular parts can be detected.

The DOD copolymers show no significant chemical dispersion along the molecular weight distribution. This behaviour was evaluated by $^1\text{H-NMR}$ measurements on GPC-fractions taken at different molecular weights of the copolymer. A typical example (40 mol% DOD-co-PC) is demonstrated in Figure 8c.

MALDI-TOF

The characterization of oligomers from DOD-BPA-copolycarbonates were performed with a MALDI-TOF Bruker Biflex III. The oligomers were investigated within a molecular range of about 900 to 3000 g/mol.

From the molecular weights of the individual components it is possible to evaluate the chemical composition of these components in terms to their BPA- and DOD-contents as well as their end groups. Starting from pure BPA-PC where only cyclic and linear oligomers are detected terminated on both sides with end groups. With an increasing DOD content in the samples the formation of DOD containing cyclic and linear oligomers occur. In the molecular weight range investigated, the DOD oligomers were mainly containing only one DOD-unit, even in copolymers with DOD concentrations up to 30 mol% DOD.

Compared with BPA-PC in which cyclic oligomers form a major part of the oligomers, the formation of DOD containing cyclic oligomers is decreased compared with their linear species.

A typical MALDI-TOF spectrum of an oligomer taken from a DOD-co-PC (29 mol% DOD) is given in Figure 9.

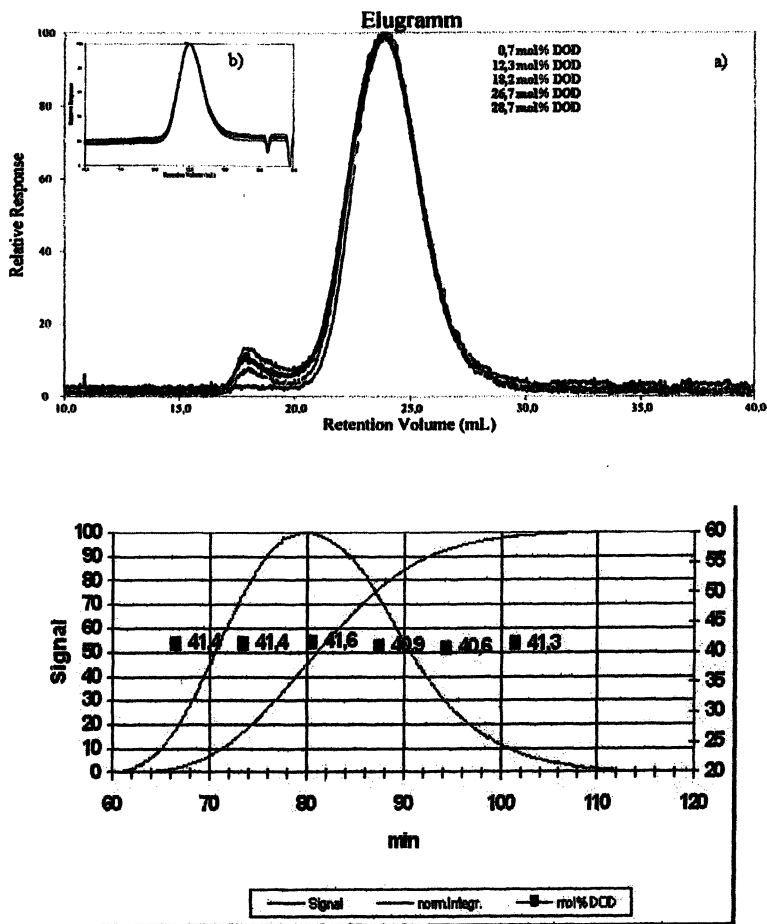


Figure 8. GPC chromatogram of DOD-BPA copolycarbonates a) RI-detection b) LS-detection. c) GPC chromatogram, chemical composition (NMR) as a function of molecular weight. (See page 3 of color insert.)

The chemical composition of the main components given in Figure 9 can be evaluated from their molecular weights of the Li-adducts in terms to their BPA- and DOD units as well their end groups. The chemical composition of the species labeled in Figure 9 are summarised in Table XII.

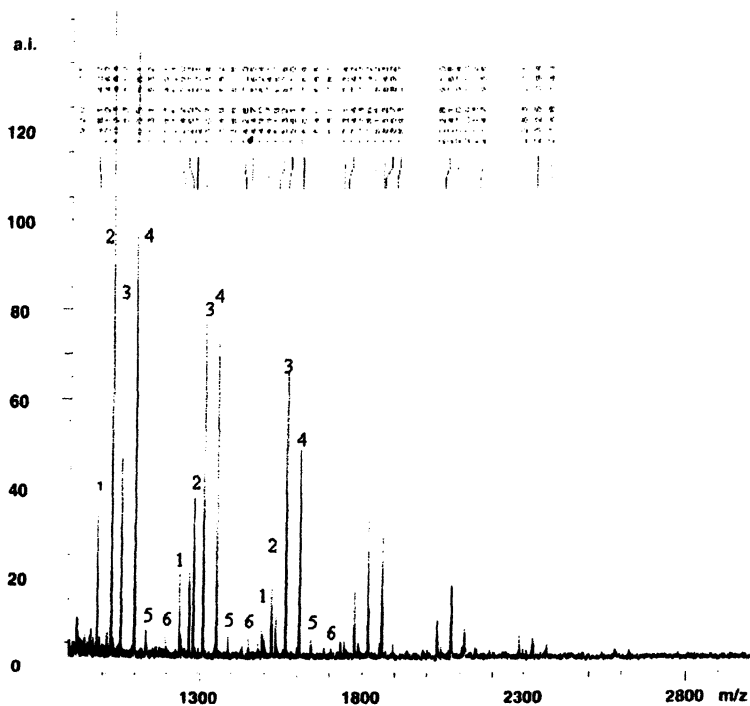


Figure 9. MALDI-TOF spectrum of an oligomer taken from a DOD-co-PC (29 mol% DOD).

Table XII. MALDI TOF MS: chemical composition of the species.

	<i>BPA</i>	<i>DOD</i>	<i>Type</i>
1	3-5	1	cyclus
2	4-7	0	cyclus
3	2-5	1	BUP/BUP terminated
4	3-6	0	BUP/BUP terminated
5	3-5	1	BUP/OH terminated
6	3-4	2	cyclus

BUP: ter.- butylphenol end group

OH: OH-endgroup

Conclusion

The copolycarbonate (DOD-co-PC) of bisphenol A and 4,4'-dihydroxydiphenyl (DOD) with 30 mol% of DOD has an outstanding balance of transparency, heat resistance, stiffness and notched Izod impact strength under a variety of test conditions. It also has an improved resistance to the Reference Fuel C and boiling water over BPA-PC.

References

1. Sakashita, T.; Shimoda, T.; Kishimura, K.; EP 544407 A1, GE, Prio 29.10.1991
2. Sakamoto, H.; Morishita, H.; Myamoto, H.; Nagao, T.; *Japan Kokai Tokkyo Koho* 1993, 05-339390
3. Koenig, A.; Wehrmann, R.; DE 197 44 693 A 1, 1999
4. Legrand, D.G.; Bendler, J.T.; *Handbook of Polycarbonate Science and Technology*, Marcel Dekker, Inc., New York, 2000, pp. 87-89
5. Schnell, H.; *Chemistry and Physics of Polycarbonates*, Polymer Reviews,; John Wiley and Sons, Inc.; 1964; Vol. 9
6. Emsley, J.W.; Feeney, J.; Sutcliffe, L.H., *High Resolution Nuclear Magnetic Resonance Spectroscopy*; Pergamon Press, 1966
7. Klug, H. P.; Alexander, L.E.; *X-Ray Diffraction Procedures*; John Wiley & Sons, New York, 1974
8. Binnig, G.; Quate, C.F.; Gerber, C.; *Phys. Rev. Let.* 1986, 56, 930
9. Krüger, D.; Anczykowski, B.; Fuchs, H.; *Ann. Physik* 1997, 6, 341
10. Mathot, V. B. F.; *Calorimetry and thermal Analysis of polymers*; Hanser Publishers, 1993
11. Höhne, G; Hemminger, W.; Flammersheim, H.-J.; *Differential Scanning calorimetry*, Springer Verlag, 1995
12. Yau, W.W.; Kirkland, J.J; Bly, D.D.; *Modern size-exclusion liquid chromatography*; John Wiley Sons, 1979
13. Mori, S.; Barth, H. G.; *Size Exclusion chromatography*, Springer Verlag, 1999
14. Lehmann, W. D.; *Massenspektrometrie in der Biochemie*, Spektrum, Akademischer Verlag, 1996

Chapter 9

Mechanical and Morphological Properties of the Copolycarbonate of Bisphenol A and 4, 4'-Dihydroxydiphenyl

Alexander Karbach¹, Doris Drechsler¹, Claus-Ludolf Schultz¹,
Ute Wollborn¹, Melanie Moethrath², Michael Erkelenz²,
James Y. J. Chung³, and James P. Mason³

¹Bayer Industry Services GmbH & Company OHG, Analytics, 47829 Krefeld, Germany (Alexander.Karbach.AK@bayerindustry.de)

²Bayer Material Science AG, Innovation, 47829 Krefeld, Germany

³Bayer Material Science AG, Business Development, Pittsburgh, PA 15205

A copolycarbonate (DOD-co-PC) (*1*) of bisphenol A and 4, 4'-dihydroxydiphenyl (DOD) with defined amounts of DOD has an outstanding balance of optical, mechanical, thermal and impact properties. In particular, it has high light transmission, high glass transition and heat-distortion temperatures, and high notched Izod impact strength at thick section and low temperatures. Furthermore, it is unusually resistant to embrittlement after heat aging. For further understanding of the structure property relationships, DOD-co-PC with different amounts of DOD are investigated.

Introduction

Bayer Polymers recently carried out extensive evaluations of copolycarbonates of bisphenol A with different amounts of 4, 4'-dihydroxydiphenyl (DOD) (Figure 1) (*1-4*). The preceding chapter discussed the technical properties of DOD-co-PC. In this chapter, we present an overview on their morphology and their supramolecular structure; the results are discussed in combination with in situ deformation experiments.

Results

In-Situ Bending Measurements

In Figure 1a the 3-point bending module (Kammrath and Weiss GmbH, Germany) and a schematic sketch is shown. It can be directly adjusted under the microscopes. The sample is clamped in the middle of the module, directly on the anvil. Under this anvil is a cell for force measurements. The outer frame, driven by a DC-motor, bends the ends of the sample down. With this technique it is guaranteed that the middle of the sample stays at constant height which makes it possible to investigate the sample surface *in situ* in the light microscope and the AFM. In the following measurements three point bending tests at room temperature in air were performed. Injection moulded bars (45 mm x 10 mm x 4 mm) were investigated after notching the sample, with the notch oriented opposite the anvil.

For quantitative analysis the force displacement curve is recorded. It can be seen that the BPA-PC compared to the 30 mol% DOD has the higher modulus as expected (Figure 1b).

The sample was notched with a razor blade in the centre of the bar about 200 μm deep. Under the notch we get a defined point of fracture.

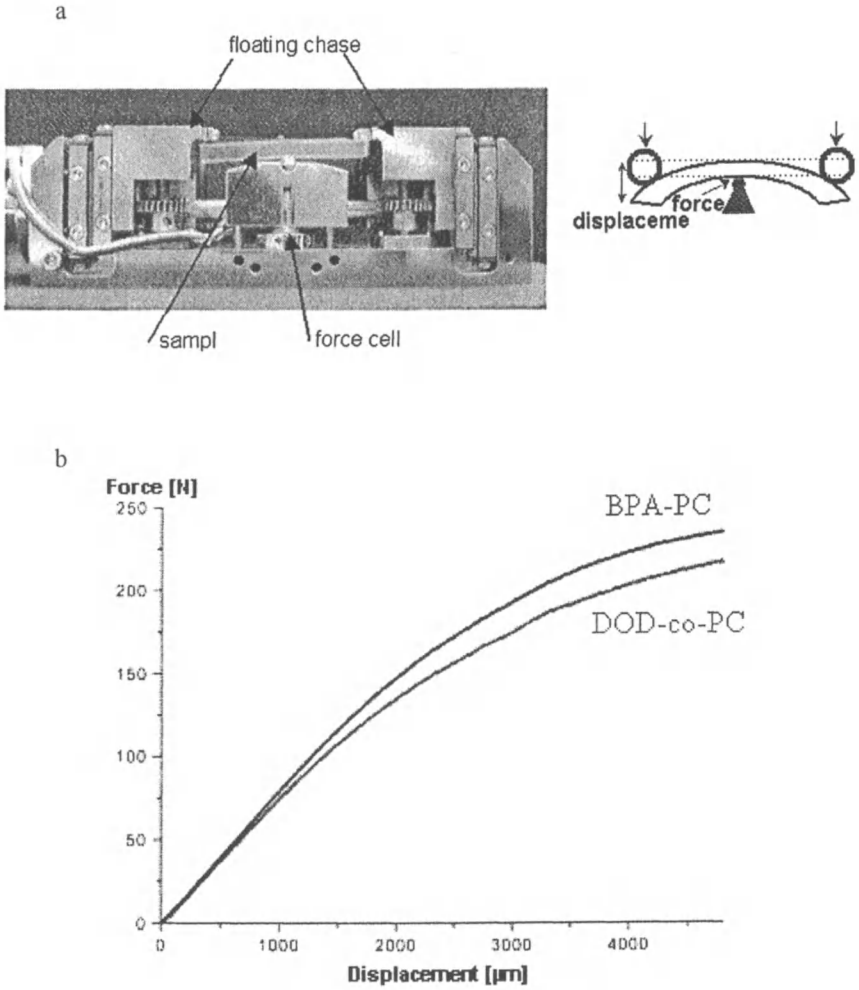
The bending speed was 1.2 mm/min and the bending rate was 2.4 min^{-1} respectively. During the AFM measurements of 15 min a stress relaxation of the sample has to be taken into account.

The polarising light microscopy of the BPA-PC sample shows the typical stress fringes due to the deformation of the material (Figure 2).

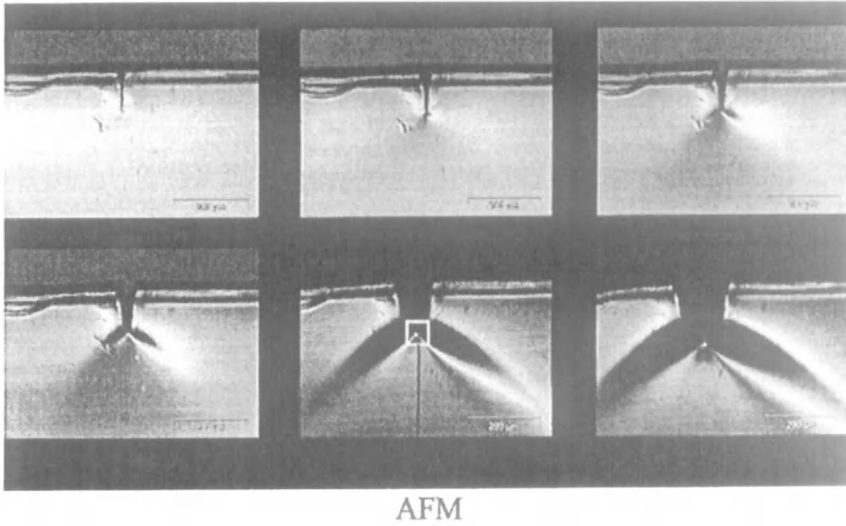
For AFM investigations the tip was positioned at the end of the notch at the small side of the bar. The AFM investigations, done at the end of the notch on the microtomed surface, show that there is no cracking below and even no crazes are visible. The shutter of the microtome knife indicate the high strained material under the notch (Figure 3).

In Figure 4a an overview of the sample with 30 mol% DOD ($5 \mu\text{m}$)² of the region under the notch at a displacement of 3,5 mm is shown. The bending stress causes the notch to broaden and in the matrix the formation of crazes vertical to the stress direction is visible. The crazing process can be seen more clearly in the zoomed images of the same sample position. At a bending of 3,5 mm a lot of crazes are visible in the vertical axis. Simultaneously, in the stress direction the micro domains are not growing. Deformation morphology like the crossing shear bands of the yielding materials is not visible.

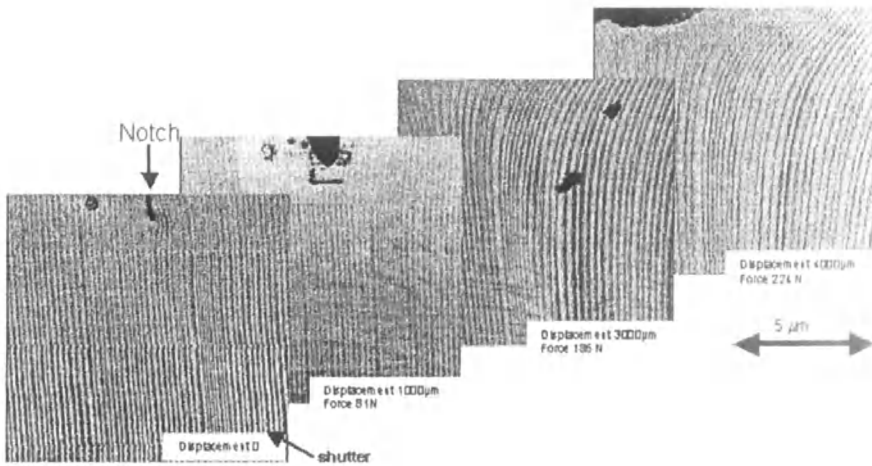
Comparing the crazing in the BPA-PC sample and the DOD-co-PC sample, the materials show different behaviour during stress. The craze width depending on the displacement is shown in Figure 4b. The craze width in the BPA-PC sample during the bending grows depending of the displacement. In contrast, the craze width in the DOD-co-PC stays only in the range of the micro domains. Therefore, the micro domains of DOD-rich regions limit the crazing width.



*Figure 1. a) 3-Point-Bending-Module (See page 4 of color insert.)
b) Force-Displacement-Curve of the injection moulding bars.*



*Figure 2. Light microscopy of BPA-PC in 3-point-bending-test.
(See page 4 of color insert.)*



*Figure 3. AFM of BPA-PC in 3-point-bending-test.
(See page 5 of color insert.)*

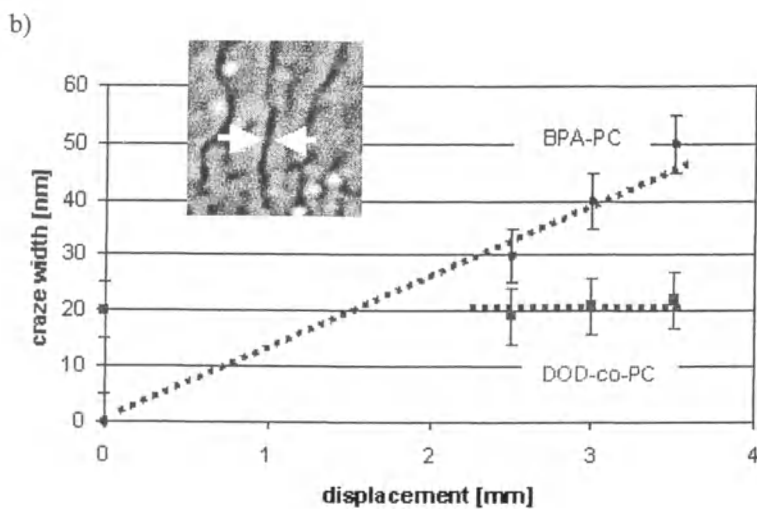
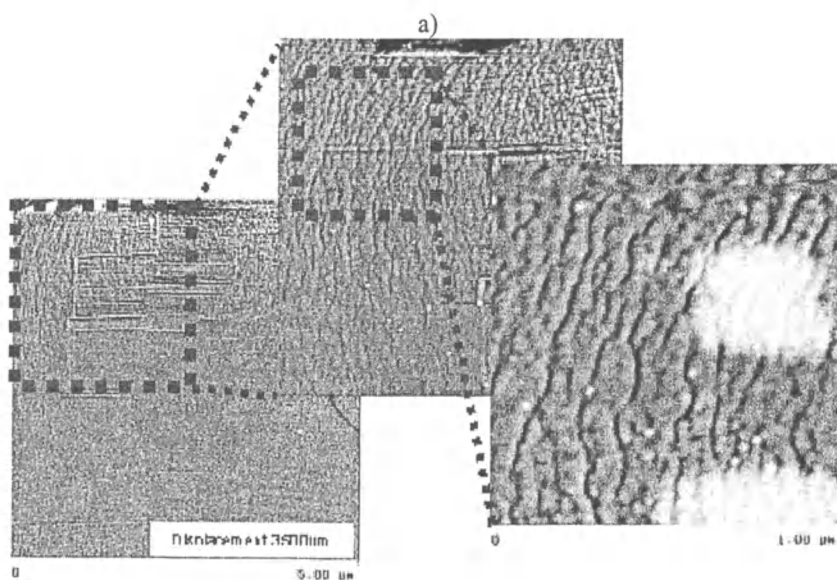


Figure 4. a) AFM phase contrast of 30 mol% DOD-co-PC in 3-point-bending-test. b) 3-Point-bending, crazing in BPA-PC compared to DOD-co-PC. (See page 5 of color insert.)

Discussion

To shed some light on the significant differences in the aforementioned properties, these differences are further discussed in terms the analytical characterization data and molecular structure analysis.

Morphological Structure of DOD-co-PC

Figure 5 shows the proposed morphological structure of the DOD-co-PC based on the XRD, NMR and AFM results together with the molecular dynamics data as discussed below.

The molecular dynamics study using CERIU3.5 (MSI, San Diego) was performed with Dreiding Force Field at 300 K on a single molecule of DOD-co-PC with DOD-blocks of two DOD units with Dreiding Force Field to get information about their molecular dimensions. The length of a DOD unit is in a range of 3 nm. A lateral arrangement of DOD-co-PC chains containing DOD-blocks of two DOD units leads to DOD rich areas with a diameter of 10nm. Taking into account a DOD-co-PC chain with MW=25000 g/mol, 70 mol% BPA (MW=254 g/mol), and 30 mol% DOD (MW=212 g/mol) leads to 104 units with average molecular weight of 241 g/mol per unit. Approximately 15 polymer chains containing DOD-blocks of two DOD-units belong to the so-called soft regions. The so-called soft region of 10 nm is then formed by 15 neighbored DOD-blocks, containing 2 DOD-units.

Deformation Mechanism

A model of the deformation mechanism is shown in Figure 6. The region between the micro domains perpendicular to the stress direction opens up crazing regions. These crazes grow towards the microdomains but their diameter stay unchanged.

Optical Properties

DOD-co-PC is transparent and amorphous as also indicated by its DSC data and X-ray scattering pattern. However, its AFM pictures show very small domains (10 to 20 microns) of heterogeneity, which are attributed to the presence of DOD with an average block length of about 1.8 in the polymer chains. Since these domains are significantly larger than an estimated domain size (2 to 3 nm) of a DOD-carbonate-DOD block, they are tentatively attributed

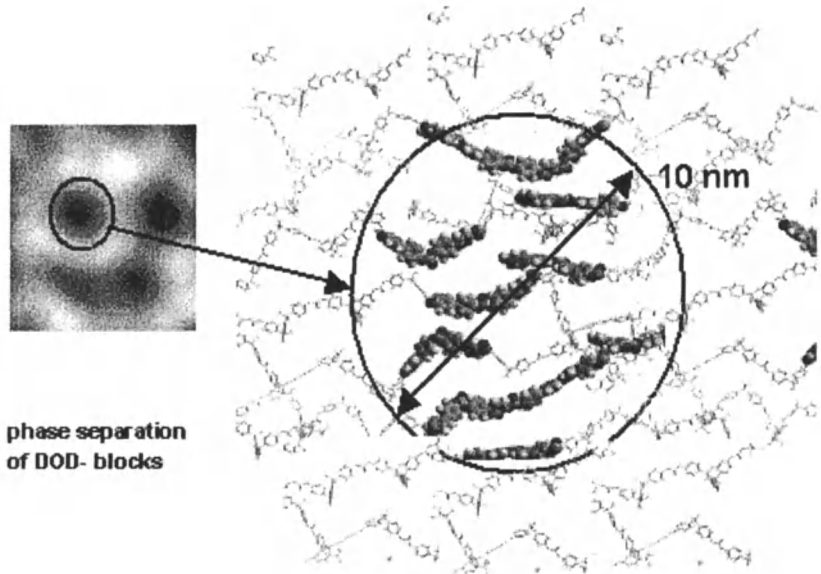


Figure 5. Proposed morphological structure of the DOD-co-PC (DOD-blocks: balls, BPA-units: sticks). (See page 6 of color insert.)

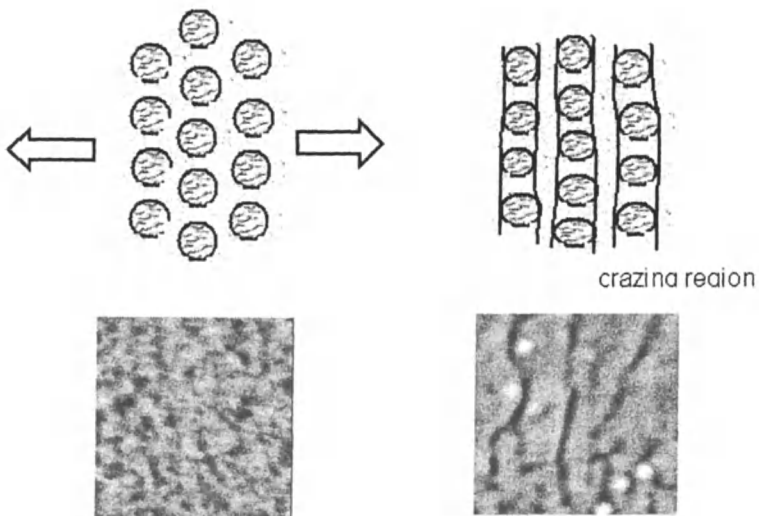


Figure 6. Model of deformation mechanism of DOD-co-PC. (See page 6 of color insert.)

to the short intra-chain and/or inter-chain alignments of DOD-carbonate-DOD blocks due to the linearity of diphenylene units. These chain alignments are also likely to be responsible for the high birefringence of DOD-co-PC.

Thermal Properties and Density

The higher thermal properties and density of DOD-Co-PC than those of PC are attributed to the linearity and rigidity of diphenylene units.

Flexural and Tensile Properties

Compared to BPA-PC, DOD-co-PC has a lower tensile yield stress, flexural and tensile modulus but higher tensile and flexural strains both at yield. These data are explained (5) in terms of DOD-co-PC's higher propensity to shear yield under a applied stress due to the presumably lower rotational energy barriers of phenylene rings around the axis of "inter-ring" C-C bonds in the diphenylene units in the DOD-co-PC than those of phenylene rings in the PC chains. This presumption on the lower rotational-energy barriers is based on the literature (6, 7, 8) of the respective model compounds.

Notched Izod Impact Strength

The high notched Izod impact strength of DOD-co-PC under a variety of test conditions is also attributed (4) to the outstanding efficiency of diphenylene unit's shear yielding. Conversely, in the view of the DOD-co-PC's high impact strength and low yield stress, it can be mentioned that the diphenylene units in DOD-co-PC act as a stress dissipator.

Flame Resistance

DOD-co-PC has a higher LOI and better UL94 ratings than PC. This is attributed to its higher aromatic content of DOD-co-PC and thus more char formation during burning.

Resistance to Hydrolysis and Reference Fuel

The improved resistance of DOD-co-PC over PC is rationalized with the short chain alignments of DOD units.

Conclusion

The copolycarbonate (DOD-co-PC) of bisphenol A and 4,4'-dihydroxydiphenyl (DOD) with 30 mol% of DOD has an outstanding balance of transparency, heat resistance, stiffness and notched Izod impact strength under a variety of test conditions. Figure 7 gives a comparison of some mechanical, optical and thermal data of the DOD-co-PC with a BPA-PC.

The analytical data leads to the following conclusion.

NMR gives an average chain length of the DOD-CoPC blocks in a range of 1.8 DOD units. X-ray and DSC- measurements show no crystallinity.

AFM shows a microphase separation of the DOD-blocks in a range of 10-20 nm. By *in situ* bending and tensile tests it is possible to assign macroscopic mechanical properties and microscopic deformations at the same time.

The proposed model allows further understanding how the chemical structure of the polymer chains influence via mesoscale the macroscopic properties of the polymer. The small DOD-blocks in the DOD rich phase controls the deformation behaviour of the DOD-co-PC, because they act as dissipator.

On the molecular level the outstanding properties of DOD-co-PC could be attributed to the linearity, rigidity and low rotational-energy barriers of diphenylene units in the DOD-co-PC chains, which absorb impact energy.

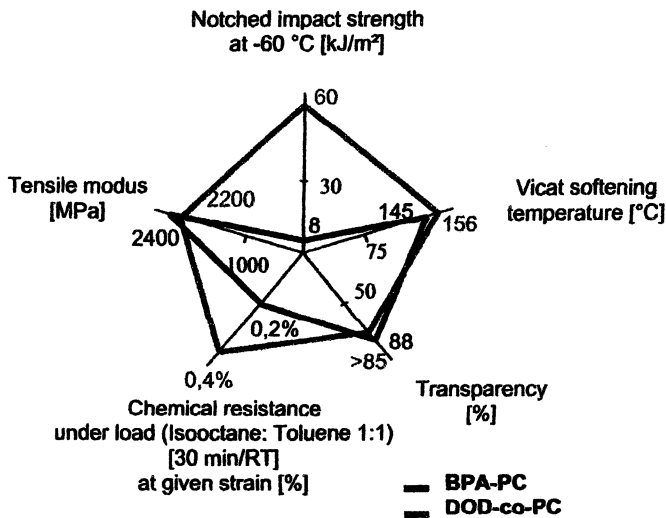


Figure 7. Comparison of properties of the DOD-co-PC with BPA-PC.
(See page 7 of color insert.)

References

1. Sakashita, T.; Shimoda, T.; Kishimura, K.; EP 544407 A1, GE, Prio 29.10.1991.
2. Sakamoto, H.; Morishita, H.; Myamoto, H.; Nagao, T.; *Japan Kokai Tokkyo Koho* **1993**, 05-33939.
3. Koenig, A.; Wehrmann, R.; DE 197 44 693 A 1, 1999.
4. Legrand, D.G.; Bendler, J.T.; *Handbook of Polycarbonate Science and Technology*, Marcel Dekker, Inc., New York, 2000, pp. 87-89.
5. Chung, J. Y. J.; Paul, W. G.; *60th Annual Tech. Conference/Society of Plastics Engineers* **2002**, 174.6
6. Mayo, R. E.; Goldstein, J. H.; *Mol. Phys* **1966.**, 10, 30.
7. Almenningen; Bastiansen, O.; Fernholt, L.; Cyvin, B.; Cyvin, S.; Samdal, S.; *Molecular Structure* **1985**, 128, 59.
8. Laskowski, C.; Yoon, D. Y.; McLean, D.; Jaffe, R. L.; *Macromolecules*, **1988**, 21, 1629.

Chapter 10

Ductile Polycarbonates Containing Bisaryl Units: Theory and Modeling

John T. Bendler¹ and David A. Boyles²

¹Physics Department, U.S. Naval Academy, Annapolis, MD 21402

²Department of Chemistry and Chemical Engineering, South Dakota School of Mines and Technology, Rapid City, SD 57701

Abstract

Theoretical arguments suggest that polymer segment geometries and, in particular, molecular aspect ratios play an important role in controlling bulk polymer ductility. Under tensile loading, competition between crazing and shear flow determines the ultimate failure mechanism of a glassy polymer. Shear yielding stresses are less variable from polymer to polymer than are craze initiation stresses and craze strengths. Craze strengths are strongly influenced by the entanglement densities and overall polymer molecular weight. A quantitative relationship has been proposed by Fetters et al. relating the entanglement molecular weight, M_e , to the monomer shape or packing length, p . This correlation indicates that incorporation of tetraaryl units into a polycarbonate chain can lead to a higher entanglement density and craze strength, and hence improved bulk toughness, as well as enhanced heat and solvent resistance. A novel synthetic route to these new polymers has been found and ductility measurements are planned.

Introduction

Amongst the useful properties of bisphenol A polycarbonate (BPA-PC), of particular interest is its notable impact toughness and ductility which can persist to -40°C for high molecular weights. Numerous analogues of BPA-PC have been synthesized which display higher heat or improved solvent resistance, but to date all new variants of BPA-PC exhibit poorer ductility. Unraveling the secret of BPA-PC's glass state ductility could, in principle, result in a new generation of engineering polymers with useful properties well-suited to electronic, automotive, medical and military applications. In recent years, both theory and molecular simulations have broadened and deepened our knowledge of mechanical behavior of polymers, so that now, perhaps, the first steps towards "arm-chair" design of new polymers may soon become practical.

In this article we review several theoretical ideas and computational results which suggest that overall monomer geometries play a significant role in controlling glassy state fracture strengths, entanglement densities and ultimately bulk polymer toughness. These ideas have been applied to the example of biaryl units incorporated into a polycarbonate backbone, with the implication that incorporation of such units can improve craze strength and bulk toughness. Recently a successful synthetic route has been found to make these polymers, so that soon the predictions can be directly tested in the laboratory.

Monomer Geometries and Polymer Toughness

Polymers exhibit two principal modes of mechanical failure, shear yielding and brittle fracture. All glassy thermoplastics are ductile in compression, when the hydrostatic component of the stress is negative. All glassy polymers fail by craze formation and subsequent brittle fracture if the cavitation component of the stress is positive and sufficiently large relative to the octahedral shear stress. Brittle failure is the less desirable mode since the energy absorbed is much smaller than that found for shear yielding. This difference in energy absorption is chiefly due to the relatively small fraction of the total polymer volume that participates in brittle (i.e., craze) failure compared with the large fraction of the polymer sample involved in shear yielding. Vincent was one of the first to characterize the ductile-brittle transition (in tension) for polymers in terms of the ratio of the tensile brittle strength to the tensile yield stress.^(2,3) He noted that the shear yield mechanism in a polymer glass involves substantial long range reorganization and molecular motion of the polymer chains which causes yielding to be quite sensitive to temperature. Brittle fracture, on the other hand, is initiated locally (often by dirt or imperfections), and though brittle strength is

influenced directly by molecular weight and molecular orientation, it is relatively sensitive to temperature. Vincent defined the ductile-brittle transition, T_{DB} , as the temperature at which the yield stress becomes equal to the brittle strength.(3) Since it becomes increasingly difficult to rearrange the chains as thermal energy is reduced, the yield stress continues to rise with falling temperature, and so at temperatures below T_{DB} the polymer fails in a brittle mode, since now the brittle strength has become smaller than the yield stress.

Vincent noted that polymers with bulky side groups, such as polystyrene and polycyclohexyl methacrylate, generally have lower brittle strengths than chains without side groups, and he finally concluded that brittle strengths were correlated with the average molecular cross-sectional area (MCSA) of a polymer chain measured perpendicular to the chain axis.(2,3) He defined the average MCSA (per mole) of a chain as;

$$MCSA = \frac{\text{Mass of the repeat unit}}{\text{density} \times \text{length of the repeat unit}} \quad (1)$$

Vincent considered a number of polymers for which he had measured both yield stresses and brittle strengths, and found a convincing correlation between MCSA and brittle strength. He interpreted this result as meaning that the chain backbone acts as a reinforcement for the polymer. When tensile stress is applied to the solid polymer, those chain backbones crossing each unit area parallel to the stress (see Figure 1) help support the load and therefore increase the brittle strength. The smaller is the polymer's MCSA, the more chain backbones will cross each unit area, and the stronger will be the polymer:

$$\text{Brittle strength} \propto \text{number of bonds per unit area} \propto \frac{1}{MCSA}$$

Vincent's correlation did not attract wide theoretical attention, but it was employed in an interesting software program developed by Seitz and coworkers at Dow(4) and it was used to estimate and calculate solid state and melt polymer properties.

A more recently introduced parameter related to the molecular geometry of a polymer chain repeat unit is the packing length, p .(5,6) The packing length is defined as the total occupied volume of a chain divided by the mean-squared end-to-end distance of the chain; thus(5)

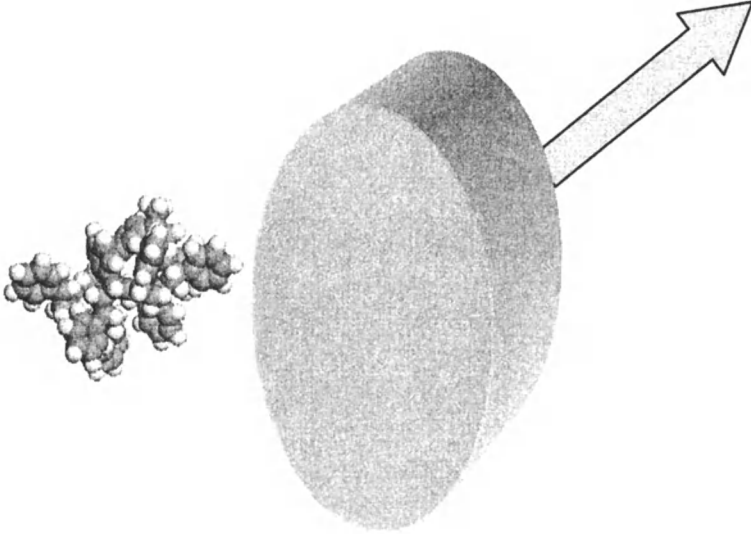


Figure 1. Illustrating Vincent's idea that the molecular cross sectional area (MCSA) of the backbone determines the number of polymer chains that cross each unit area normal to the direction of a uniaxial applied stress, σ .

$$p = \left[\frac{M}{\langle R^2 \rangle_0 \rho N_a} \right] = \frac{V_C}{\langle R^2 \rangle_0} \quad (2)$$

where M is the molecular weight of the chain, N_a is Avogadro's number, $\langle R^2 \rangle_0$ is the mean-squared unperturbed end-to-end distance, ρ is the density of the polymer, and V_C is the chain volume equal to $M/\rho N_a$. The packing length defined in equation 2 has been successfully correlated with entanglement spacings in the melt for a wide variety of different polymers.(5,6) The entanglement molecular weight M_e of a polymer and the plateau modulus G_N^0 in the melt are related by

$$M_e = \frac{\rho RT}{G_N^0} \quad (3)$$

where R is the universal gas constant, ρ is the density of the melt, and T is the absolute temperature. The packing length p has resulted in a widely-used correlation between $\langle R^2 \rangle_0$, M_e , ρ and G_N^0 . These correlations have been termed "universal" (5,6) for flexible linear chains and may be written

$$G_N^0 = \frac{kT}{n_t^2 p^3} \quad (4)$$

and

$$M_e = \rho N_a n_t^2 p^3 \quad (5)$$

where n_t (a constant approximately equal to 21) corresponds to the number of entanglement strands in a cube having the dimensions of the tube diameter, d_t . The correlations in equations 4 and 5 have been extended by Fetters et al. to include the critical molecular weight, M_C , which is the molecular weight at which the influence of entanglements begins to be felt on the viscosity. Knowledge of p , in principle, allows useful estimates to be made for G_N^0 , M_e , M_C and the tube diameter, d_t , for a polymer which has not yet been synthesized, or which has not been synthesized in sufficient quantity for testing, but for which p is known or perhaps can be estimated from molecular models.

The physical meaning of the packing length p is not immediately evident from equation 2. In one paper, Fetters et al. describe the packing length as a quantity that may be "likened to the molecular diameter of the repeat unit in a polymer chain." (4) This description of p suggests that the quantity $\pi(p/2)^2$ should be comparable to Vincent's MCSA. Figure 2 shows a plot of p versus

$2\sqrt{\frac{MCSA}{\pi}}$ for eight linear flexible polymers, where the data has been taken

from the literature. (4,5,7) While one might suspect that p and MCSA are quite different descriptors of chain geometry, Figure 2 shows a surprisingly good correlation ($R=0.85$), especially since the MCSA is a very local parameter and is determined completely by the volume and length of the monomer unit, while the

packing length p , depends strongly on $\langle R^2 \rangle_0$, and therefore reflects the intrinsic long range chain flexibility of the chain.

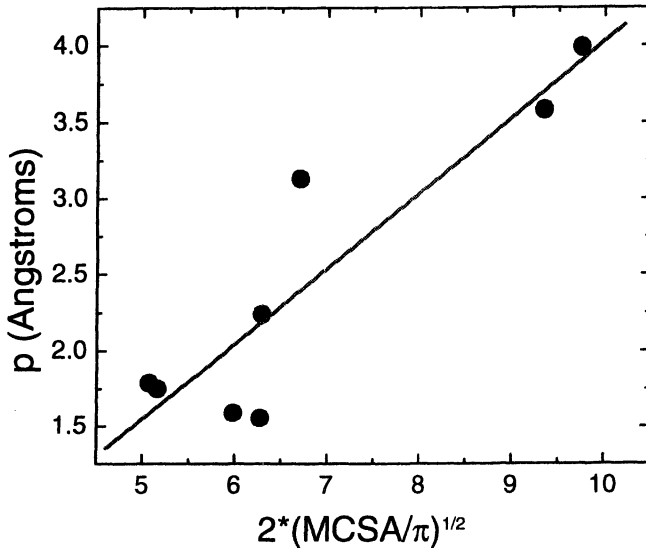


Figure 2. Plot of the packing length, p , versus $2\sqrt{\frac{MCSA}{\pi}}$ for eight polymers, including PS, PMMA, PVC, BPA-PC, PP, PET, PE, and PTFE. Data is taken from References 5,6 and 7.

The correlation in Figure 2 suggests that there is roughly a factor of 2 difference between p and $2\sqrt{\frac{MCSA}{\pi}}$. While further work is needed to clarify

the relationship between these two measures of chain dimensions, it is obvious that both parameters are related to polymer chain thickness, and that qualitatively, an increase in entanglement density (i.e., small p) should be related to Vincent's fracture strength (i.e., small MCSAs).

Entanglements play a crucial role in craze growth and breakdown, and are thus also directly related to brittle strength and toughness in polymers. Yield stresses and craze initiation stresses do not display significant molecular weight dependencies,(8) so that the principal role of entanglements is to enhance the load-bearing capabilities of crazes once formed. Tensile stresses that lead to

craze initiation and crack formation increase the volume of the polymer through creation of craze voids containing oriented fibrils. Entanglements act as chemical crosslinks to limit the volume expansion to the extension ratio, λ , that corresponds to chain segments $1/3$ the distance between entanglements being fully stretched.(9) Polymer chains with low entanglement densities expand to a greater degree forming thin, weak craze fibrils that are less effective in blunting the craze-crack growth. Highly entangled polymers, such as BPA-PC, form thick, strong fibrils that can support large tensile loads until shear yielding can commence.(10)

Molecular cross sectional areas (MCSAs) and chain packing lengths (p) may influence brittle strengths in separate but complementary ways. Craze initiation may be suppressed by small MCSAs since a high density of chain backbones per unit area are parallel to the principal tensile stress direction opposing extension and void formation. In spite of this substantial craze initiation resistance, some crazes will invariably form due to the presence of dirt or adventitious flaws. Then craze growth and fibril thinning will be inhibited by a high entanglement density due to the small packing length, p .

Tetraaryl Polycarbonate

Past efforts to design new polycarbonates have often opted for large, bulky substituents on the BPA unit to enhance and improve heat resistance.(11) As the discussion above suggests, this strategy could be expected to lead to brittle materials with limited impact strength or toughness, which it invariably did. A recognition that ductility requires glassy state mobility lead to efforts to correlate low temperature motions such as the γ process to toughness.(11,12) While this approach is sensible and leads to improved properties and performance, it also presumes that ductility is most sensitive to relative ease of shear flow. On the other hand, there are indications that ease of craze initiation and growth are more sensitive to chemical structure variations than shear flow.

With these ideas in mind, it was decided to attempt to study polycarbonates which were intentionally designed to have small MCSAs, while still retaining good molecule mobility in the glass. Since a practical driver for new polycarbonate structures is higher heat and solvent resistance, small MCSA polycarbonates with aliphatic hydrocarbon segments in the backbone were not considered promising. Instead, a new polycarbonate, TABPA-PC, with extended bisaryl units was chosen for study:

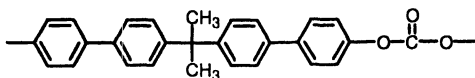


Figure 3. Chemical structure of the tetraaryl polycarbonate (TABPA-PC).

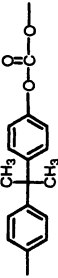
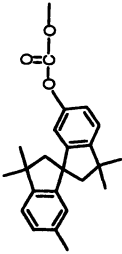
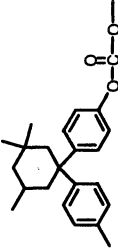
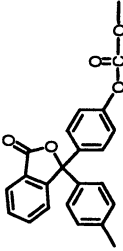
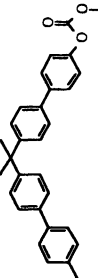
The preliminary results for TABPA-PC were promising;(14,15) the polymer showed good heat resistance, having a T_g greater than 190°C for copolymers with BPA-PC, and the ability to form amorphous, tough films. Unfortunately, the synthetic route was difficult and would not allow a scale-up of the synthesis to take place. Only recently has a viable synthesis been found, enabling quantities of TABPA-PC polymer adequate for mechanical testing to be prepared.(1,16)

Table 1 shows calculation results for the MCSA and packing length p for TABPA-PC along with analogous results for BPA-PC and several other polycarbonates. The radii of gyration of the polymer samples were evaluated using molecular dynamics simulations. Typically, the molecular weight of the polymer studied in the simulations was 12,000 amu, which corresponds to about 50 monomers of BPA-PC and 30 monomers of TABPA-PC. The calculations were performed using Accelrys Materials Studio 3.0, Amorphous Cell and Discover modules. The forcefield was the Compass Forcefield, that has been developed by Accelrys and tested for polycarbonates against Xray and *ab initio* results. The calculations for BPA-PC agreed well with experimental results. The MCSAs were determined using molecular volumes from Connolly solvent accessible surfaces, and the monomer lengths were taken from the molecular dynamics simulation samples.

As expected, the MCSA for TABPA is smaller than BPA-PCs, though not by a large amount. What is striking is the significant difference between the MCSAs for BPA-PC and TABPA-PC and the other less ductile polymers. Likewise, the packing lengths for BPA-PC and TABPA-PC are lower than those for the other three polymers. In the last column of the Table is the calculated entanglement molecular weight for each polymer, using the packing length correlation. These values show that the entanglement density in BPA-PC, for example, is three times greater than that of the spirobiindane (SBI) polymer and more than twice the density for the other two polycarbonates. The TABPA-PC is predicted to have an entanglement density which is more than 25% greater than that of BPA-PC.

The calculation results in Table 1 show that TABPA-PCs craze toughness and brittle strength should be acceptable, but what evidence is there that shear yielding might be readily achieved as well? Figure 4 shows dynamic mechanical results for a 25-75 copolymer of TABPA-BPA polycarbonate, along with the results for a 100% BPA-PC polymer. (The results were obtained by Mr. James

Table 1. Properties of various polycarbonates

Polycarbonate	Chemical Structure	Monomer Volume $\text{\AA}^3(3)$	Length \AA	MCSA $\text{\AA}(2)$	$\left(\frac{\langle R_g^2 \rangle}{M}\right)^{1/2}$	Pack. Length \AA	M_c
Bisphenol A		211	11.50	18.3	0.86	1.55	1680
Spirobiindane(17)		1.28	7.7	32.1	0.45	3.20	5100
Isophorone(18)		1.27	10.1	30.9	0.78	2.60	3840
Phenolphthalein(19)		1.31	11.9	25.5	0.83	2.10	4110
Tetraaryl BPA		333	19.0	17.5	1.20	0.92	1130

F. Kelley and Dr. William Richards of GE Global Research, Schenectady, N.Y., who kindly gave permission for us to use them.) The low temperature loss peaks in both polymers are identical in intensity and frequency. As expected, incorporation of tetraaryl units in the backbone does not interfere with the low temperature motions, so that the shear yield stress should not be too different from BPA-PCs.

Figure 4 is noteworthy since the *a priori* expectation is that smaller p and smaller MCSA will lead to better packing, and hence lower “free volume”. The extra phenyl rings in the backbone increase the polymer cohesive energy, raise the T_g and stiffen the structure. Generally, p and free volume will decrease together so that complementary efforts must be made to sustain molecular mobility.

In summary, theoretical evidence has been presented which indicates that polymer chain geometries, and in particular chain backbone diameters, play an important role in bulk toughness and ductility. A new family of low-MCSA polycarbonates has been developed, and efforts are currently underway to evaluate their mechanical properties, especially ductility.

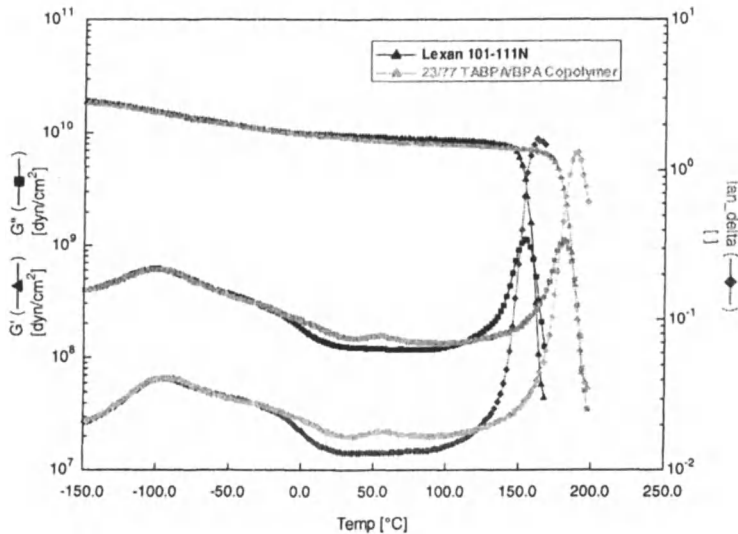


Figure 4. Dynamic mechanical data for BPA-PC and a 25-75 copolymer of TABPA and BPA showing identical low-temperature loss peaks. (Courtesy of James F. Kelly and William D. Richards.)

Acknowledgements

We gratefully acknowledge the financial support of the National Science Foundation (Grant No. DMR-98-15957) Department of Defense-Army Research Office (Grant No. DAAD19-01-1-0482), the Army Research Laboratory (Grant No. DAAD19-02-2-0011), NSF (ILI Grant No. USE-9052345 for the NMR used in this work). This material is also based in part upon work supported by the National Science Foundation/EPSCoR Grant #EPS-0091948 and by the State of South Dakota. Thanks are due to Dan Brunelle and Bill Richards for valuable advice and assistance.

References

1. Boyles, D.A., et. al., *Polymer Preprints* 44, 1, (2003)753.
2. Vincent, P.I.; *Polymer* **1972**, 13, 558.
3. Vincent, P.I.; *Nature* (Phys. Sci.) 1971, 233, 104.
4. *Synthia*, 2.2OS, Biosym Technologies, San Diego, CA., 1993.
5. Fetters, L.J.; Lohse, D.J.; Graessley, W.W. *J. Polymer Sci. B. Polym. Phys.* **1999**, 37, 1023.
6. Fetters, L.J.; Lohse, D.J.; Milner, S.T.; Graessley, W.W. *Macromolecules*, **1999**, 32, 6847-6851.
7. *Polymer User Guide, Part 2*, 6.0, Biosym Technologies, San Diego, CA., **1993**; Table 10.9, page 10-30.
8. Kambour, R.P.; Farraye, E.A. *Polymer Comm.* **1984**, 25, 357-360.
9. Rottler, J.; Robbins, M.O. *Phys. Rev. Lett.* **2002**, 89, 195501-1-195501-4.
10. Kramer, E.J. *Adv. Polymer Sci.* **1983**, 52/53, 1.
11. Bendler, J.T.; *Comput. Theoret. Polym. Sci.* **1998**, 8, 83.
12. Schmidhauser, J.; Sybert, P.D. "Nonbisphenol A Polycarbonates" in LeGrand, D.G.; Bendler, J.T. *Handbook of Polycarbonate Science and Technology*, pgs. 61-105; New York: Marcel Dekker, Inc. **2000**.
13. Yee, A.F.; Smith, S.A. *Macromolecules* **1981**, 14, 54-64.
14. Bendler, J.T.; Schmidhauser, J.C.; Longley, K.L. Polycarbonate from bis[4'-(4-hydroxyphenyl)-phenyl]alkanes. U.S. Patent 5,281,689, January 25, **1994**.
15. Bendler, J.T.; Schmidhauser, J.C.; Longley, K.L. Bis[4'-(4-hydroxyphenyl)-phenyl]alkanes and polycarbonates prepared therefrom. U.S. Patent 5,319,149, June 7, **1994**.
16. Boyles, D.A., et. al.; see companion paper this proceedings.
17. Steuben, K.C. *J. Polym. Sci. A* **1965**, 3209.
18. Freitag, D.; Fengler, G.; Morbitzer, L. *Angew. Chem. Int. Ed* **1991**, 30, 1598.
19. Baggett, J.M. *US Patent 4,210,741* **1980**, The Dow Chemical Company.

Chapter 11

Synthesis of 1,1-Dichloro-2,2-bis[4-(4'-Hydroxyphenyl)phenyl]ethene and Its Incorporation into Homo- and Heteropolycarbonates

David A. Boyles¹, Tsvetanka S. Filipova¹, John T. Bendler²,
Maria J. Schroeder³, Rachel Waltner¹, Guy Longbrake¹,
and Josiah Reams¹

¹Department of Chemistry and Chemical Engineering, South Dakota School of Mines and Technology, Rapid City, SD 57701

²Physics Department and ³Chemistry Department, U.S. Naval Academy, Annapolis, MD 21402

Polycarbonates from 1,1-dichloro-2,2-bis-(4-hydroxyphenyl)-ethylene (BPC) constitute a highly flame-resistant family of engineering thermoplastics. The preparation of polycarbonates from BPC was first reported in 1964 as a copolymer with bisphenol A (BPA). A new monomer analogue of BPC has been synthesized which has a higher aspect ratio than BPC. This monomer has been polymerized to polycarbonates with the goal of improved ductility and heat-resistance. An efficient synthesis of the monomer 1,1-dichloro-2,2-bis[4'-(4-hydroxyphenyl)phenyl]ethane (TABPC) is reported, as are the molecular weights and glass transition temperatures of homo- and heteropolycarbonates of TABPC.

Introduction

Since first synthesized in 1898 by Einhorn,⁽¹⁾ polycarbonates have not only been commercialized but have continued to be actively investigated both by theoreticians as well by synthetic organic chemists. From a theoretical standpoint the origin of ductility in commercial polycarbonate remains yet unknown and new and ductile polycarbonates which can withstand higher temperatures than current materials are of interest in aircraft, automotive, electronic, and medical applications, as well as in military applications such as transparent armor.

Bisphenol C polycarbonate (BPCPC) from the monomer 1,1-dichloro-2,2-bis(4-hydroxyphenyl)ethene (BPC) in Figure (1), was developed by Porejko's group (2,3) at Warsaw Technical University. The patent on this material first appeared in 1964 with subsequent publication in 1968. The 1970's literature on the polymer focused primarily on the self-extinguishing properties of this material. (4-9) Rusanov (10) has written an extensive review on the polymers of BPC. As recently as 2000, Ramirez (11) proposed a mechanism for the exothermic decomposition of these materials which leads to char yields responsible for their self-extinguishing properties. As noted by Lyon,⁽¹²⁾ General Electric was at one time interested in this polymer but downselected to the polyetherimide (ULTEM) polymer instead, due to the better fire and temperature-resistant properties of the latter. In spite of the retirement of the bisphenol C polycarbonate, bisphenol C itself continues to find many uses, and is derivatized to epoxies, cyanate esters, polyarylates, and other usual bisphenol-derived materials. Interest in many of these materials has recently been shown by the Federal Aviation Agency (FAA)⁽¹²⁾ owing to the fire-resistant properties and ability of these materials to meet property requirements for aircraft interiors.

Our interest in this polymer involves the synthesis of bisphenol A analogues having high aspect ratio monomers such as the tetraarylbisphenol C (TABPC) compound also shown in Figure (1). Synthesis of this material and its polymers and copolymers may provide new additions to the already-extensive library of polycarbonate compounds and literature, as well as insights into dynamic mechanical processes of similar compounds.

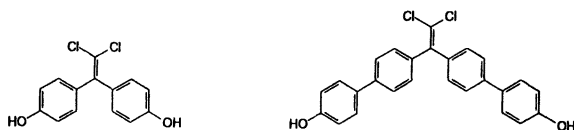


Figure 1. Bisphenol C and target monomer tetraarylbisphenol C (TABPC).

Structural Considerations

Several notable structure-property comparisons can be made from the brief list of polycarbonates shown in Figure (2). The phenyl rings of bisphenol A polycarbonate (BPAPC) undergo 180° phenyl ring flips in the glassy state at an activation energy similar to that of the mechanical γ process which occurs at -100° C.¹³ Ring flips for this material have also been observed by solution NMR.^(14,15) That the polymeric material remains ductile down to -40° C has evoked speculation that the ring flip process, the γ process, and ductility are correlated with each other. Yee, for example, has indicated that the gamma peak is "related to motions of the phenylene ring" although he concludes that "On the whole...it appears likely that the γ dispersion arises from motions involving the displacement of the entire monomer unit."⁽¹⁶⁾ While each of the polycarbonates in the list exhibits a γ process, unlike the others, the spirobiindane analogue is locked into rigid conformation and is therefore unable to undergo phenyl ring flipping.

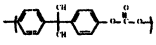
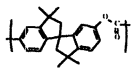
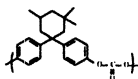
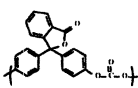
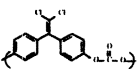
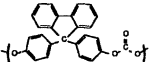
		T_g °C	γ Transition °C
Bisphenol A		150	-100
Spirobiindane		225	-105
Isophorone		245	-100
Phenolphthalein		280	-95
Bisphenol C		160	-105
Fluorenone		275	-100

Figure 2: Comparison of T_g and γ transition data for known polycarbonates.

BPAPC and BPCPC show center groups of similar size, the latter compound having an sp^2 center in its aryl bridging dichlorovinylidene unit compared to the sp^3 center of the isopropylidene unit in bisphenol A. This difference has a relatively minor effect on the properties of these corresponding polycarbonates: it is generally recognized that BPCPC is similar to BPAPC in terms of both

dynamic NMR studies as well as mechanical results.(17) The two materials that exhibit remarkably similar properties in terms of glass transition temperature (150 °C versus 168 °C), flexural modulus (336 ksi versus 376 ksi), flexural strength (16,300 psi versus 16,200 psi), tensile yield strain (10% versus 11%) and amorphous character. Also, the glass transition temperatures of BPAPC and BPCPC are close, and BPCPC is the only polycarbonate with a ductility near that of BPAPC. On the other hand, BPCPC has been shown by solution NMR to have phenylene rings that have a relaxation time twice that of the BPA-PC.(18)

Unlike the polymers depicted in Figure (2), polycarbonates exist which differ structurally from those having bulky center group substitution. Polycarbonates of the 2,2-bis[4-(4-hydroxyphenyl)phenyl]alkanes in particular have glass transition temperatures which are 30-40°C higher than those of BPAPC,(19,20) as do many of the polycarbonates in Figure (2). Among these is a polycarbonate containing the bisphenol monomer tetraarylbisphenol A (TABPAPC) first reported by Bendler and Schmidhauser (19,20) (Figure (3)) While retaining the increased molecular mass of repeat units having spherical center groups, tetraarylbisphenol A polycarbonate (TABPAPC) is distinguished from them by its higher aspect-ratio repeat units which effectively distribute the molecular weight outwardly in the direction of the *para* position of the aryl ring, resulting in linearly rigid but rotatable biphenyl units. Thus, the monomer center-of-mass distance is small and the aspect ratio large. Such linear profiles are characteristic of mesogenic units found in liquid crystalline materials as well as in liquid crystalline homo- and copolycarbonates.(21)

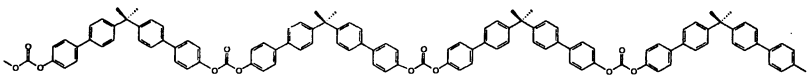


Figure 3: A polycarbonate with high aspect-ratio tetraaryl repeat units: tetraarylbisphenol A polycarbonate (TABPAPC).

The striking ductility and higher glass transition temperatures resulting from the incorporation of these high aspect-ratio repeat units into polycarbonates may bear out the observations of Vincent (22) over 40 years ago that polymer chain cross-sectional area is inversely proportional to brittle toughness, and that the latter property may be enhanced upon an increase of intermolecular cohesive attractions. Clearly, the easiest way to increase cross-sectional area is to increase molecular mass not by structural modifications which tend toward sphericity of repeat units as has been commonly the case, but by modifications which tend toward monomer elongation. Synthetically, this means introducing potentially rotatable rigid rod elements in the form of biphenyl units. Such mesogenic units are similarly found in liquid crystalline materials, including various copolymer

polycarbonates containing 4,4'-biphenol as reviewed by Schmidhauser and Sybert.(21)

It was with these considerations that we sought to synthesize polycarbonates from BPC which had additional phenyl rings with the goal of understanding whether the properties of polycarbonates prepared from such monomers would parallel those of the tetraarylbisphenol A polycarbonate (TABPAPC). Rings furthest removed from the repeat unit center may undergo lower energy threshold ring rotation because of less steric inhibition. Conceivably, this could afford a molecular dissipation mechanism by which impact energy could be converted into phenyl ring rotation, perhaps enhancing ductility and polymer toughness, and in resisting fracture upon impact.

Synthesis

Synthesis of Monomeric Bisphenols

Our group has previously demonstrated the synthesis of several high aspect ratio bisphenols using a Suzuki reaction sequence (Figure (4)).(23-26)

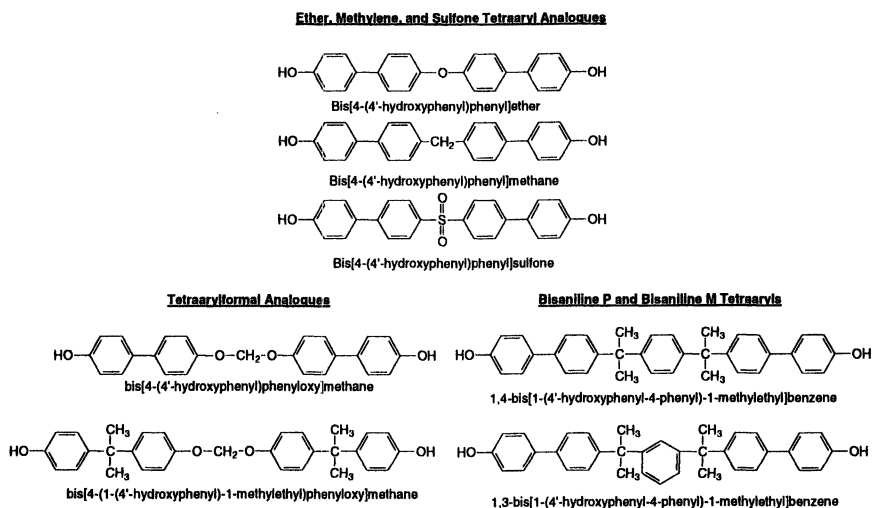
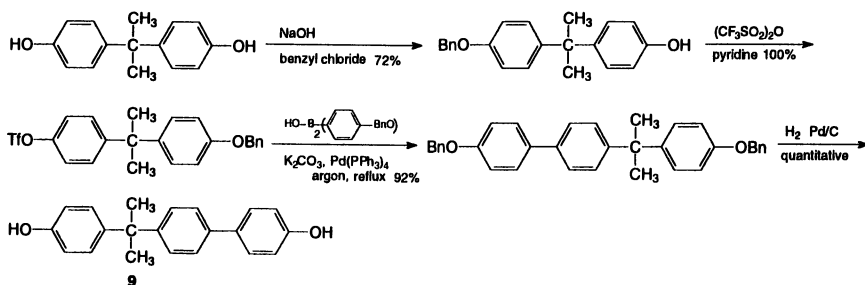


Figure 4: Tetraarylbisphenols synthesized by the Suzuki reaction.

In addition to the synthesis of these tetraarylbisphenolic systems, the utility of the Suzuki reaction has been demonstrated by the synthesis of unsymmetrical triaryl systems, namely, the synthesis of a bisphenol A analogue which has a single additional aryl ring, 2-(4'-hydroxyphenyl)-2-[4'-(4-hydroxyphenyl)phenyl]propane **9** shown in Scheme (1). Tetrakis(triphenylphosphine)-palladium(0) was used in this reaction due to the lower reactivity of the triflate substrate compared to that of aryl iodides.(27) The monomer has since been polymerized to afford a polycarbonate of M_w 57,010 and M_n 26,070, which had a glass transition temperature of 150° C.(28)

Scheme 1: Suzuki synthesis of asymmetric bisphenol A analogue.



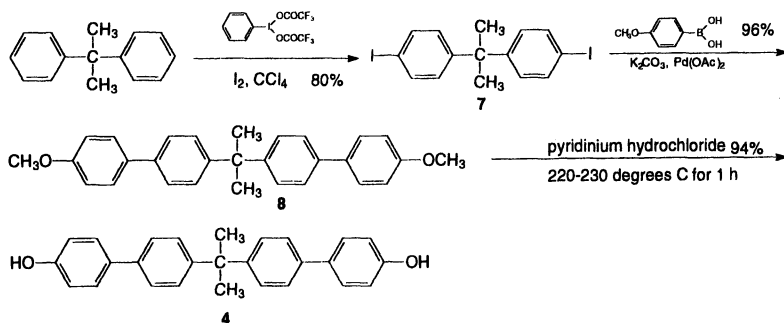
New Synthesis of Tetraarylbisphenol A (TABPA)

Also, whereas the patented synthesis (19,20) of TABPA relies on the use of a ligand-mediated Stille coupling sequence of a tri-*n*-butylorganostannane and the ditriflate of bisphenol A, we successfully synthesized TABPA by a less expensive, ligandless Suzuki reaction procedure. As depicted in Scheme (2), 2,2-bis(4-iodophenyl)propane **7** was synthesized from commercially available 2,2-diphenylpropane. The diiodo product was reacted in aqueous acetone with palladium acetate under ligandless conditions as described by Goodson, et al., (29) providing 2,2-bis[4-(4-methoxy-phenyl)phenyl]propane **8**. Demethylation was accomplished in high yield using pyridinium hydrochloride under melt conditions to afford TABPA **4**.

Synthesis of Tetraarylbisphenol C (TABPC)

It was thus that we turned our attention to the synthesis of the desired bisphenol C tetraaryl analogue, the 1,1-dichloro-2,2-bis[4-(4'-hydroxyphenyl)phenyl]ethene (TABPC). Since the Suzuki reaction most reliably required either

Scheme 2: Ligandless Suzuki coupling using aryl iodide with polymerization of monomer.



triflates or halides for one of the two reaction partners, the known compounds in Figure (5) were considered candidate reaction substrates. The dihydroxy compound (a demethylated 1,1,1-trichloro-2,2-bis(4-methoxyphenyl)ethane known as “methoxychlor”) could have been used as its corresponding triflate, with subsequent Suzuki conditions as had been done previously. Likewise, the bromo- and chloro- substrates could have been used. However, our previous use of iodosubstrates and their reaction under exceptionally mild conditions made the choice of the 1,1,1-trichloro-2,2-bis(4-iodophenyl)ethane most attractive.(30)

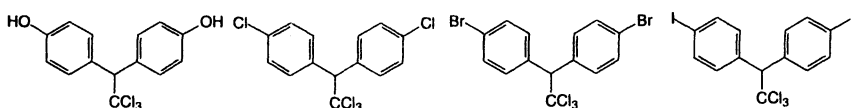
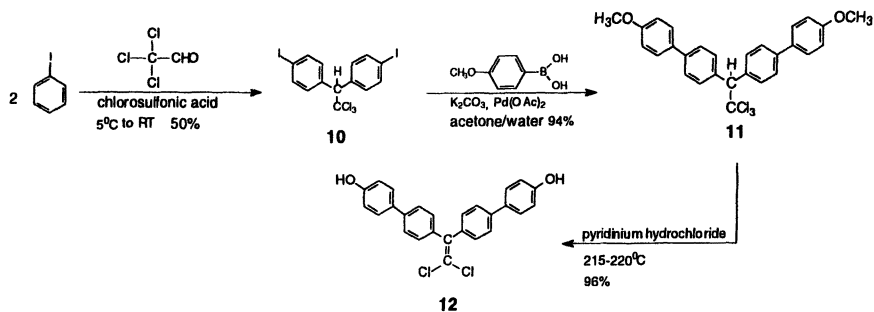


Figure 5: Possible substrates for elaboration to tetraaryl bisphenol C (TABPC).

The synthesis was undertaken as indicated in (Scheme (3)). Iodobenzene was condensed with chloral in the presence of chlorosulfonic acid as dehydrating agent, affording an unoptimized 50% yield of the desired Suzuki partner 1,1,1-trichloro-2,2-bis(4-iodophenyl)ethane **10**. Next, we used the mild Suzuki conditions of Goodson (29) with 4-methoxyphenylboronic acid to procure the desired dimethyl-protected tetraaryl product **11**. It was notable that no dehydrohalogenation occurred in the presence of carbonate base used for the

Suzuki reaction step. Finally, treatment under the melt conditions of Lesiak (31) afforded the demethylated product which simultaneously underwent the desired dehydrohalogenation to afford TABPC 12. Polar impurities were removed using silica gel to afford a recrystallized product in 96% yield (84% yield from flash chromatography with methylene chloride/acetone eluent, 12.5:1).

Scheme 3: Synthetic route for tetraaryl bisphenol C target monomer.



In this manner the complementary set of the isomeric *ortho*, *meta*, and *para*-TABPA analogues was also synthesized, as was that of the isomeric *ortho*, *meta*, and *para*-TABPC analogues indicated in Figure (6). (32)

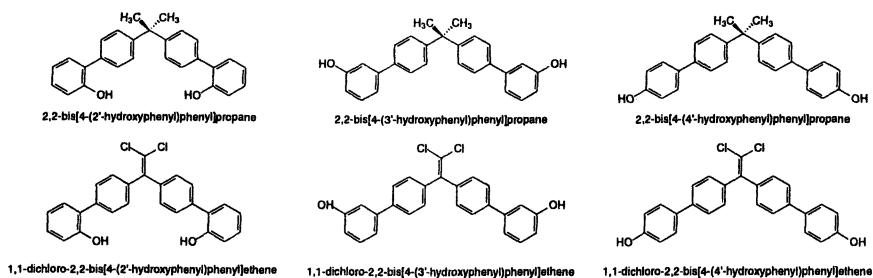


Figure 6: Positional isomers synthesized.

For polycarbonate synthesis we used the triphosgene method of Sun, et al.,³³ with pyridine to dissolve the difficultly-soluble TABPC. Likewise we prepared several copolymers including those of bisphenol A (BPA), bisphenol C (BPC), 4,4'-(hexafluoroisopropylidene)diphenol (HFBPA) and 4,4'-sulfonylbiphenol (SBPA) as indicated in Table (1). The molecular weights are dependent on stoichiometry as shown, and although the polydispersities are narrow, the degree of polymerization is also low. In subsequent polymerizations we have utilized

phosgene gas to produce materials having superior molecular weights. For example, we have synthesized the 75/25 copolymer of bisphenol A with tetraarylbisphenol C using *para-t*-butylphenol as end-cap, obtaining $M_w=84,380$, $M_n=50,930$ and polydispersity of 1.66. The T_g of the copolymer was $181.58\text{ }^\circ\text{C}$. We continue to optimize the syntheses of the polymers in Table 1 to obtain higher molecular weights.

Table 1: Stoichiometry and molecular weight data for polymers synthesized.

PC	Diol 1-Diol 2	Mol Ratio Diol 1-Diol 2	TP* mol	Yield %	M_w g/mol	M_n g/mol	PD I	T_g $^\circ\text{C}$
1	<i>p</i> -TABPC	100	0.60	88	20,083	6,305	3.1	138.94
2	<i>p</i> -TABPC-BPC	50/50	0.32	60	6,250	3,547	1.5	139.22
3	<i>p</i> -TABPC-BPC	25/75	0.42	95	10,100	6,458	1.6	157.82
4	<i>p</i> -TABPC-BPC	50/50	0.42	96	7,900	5,436	1.4	152.09
5	<i>p</i> -TABPC-BPC	75/25	0.42	91	3,786	2,883	1.3	146.36
6	<i>p</i> -TABPC-BPA	50/50	0.37	88	6,500	4,771	1.3	148.56
7	<i>p</i> -TABPC-BPA	50/50	0.42	85	7,143	4,948	1.4	154.40
8	<i>p</i> -TABPC-HFBPA	50/50	0.42	91	7,713	5,644	1.4	158.98
9	<i>p</i> -TABPC-SBPA	50/50	0.42	93	4,126	3,050	1.4	156.79
10	<i>m</i> -TABPC*	100	0.37	99	-	-	-	135.94
11	<i>m</i> -TABPC-BPA	25/75	0.34	97	7,474	4,009	1.9	149.18
12	<i>o</i> -TABPC*	100	0.37	99	-	-	-	137.94
13	<i>o</i> -TABPC-BPA	25/75	0.34	98	10,590	5,144	2.1	151.37

¹Triphosgene; HFBPA = hexafluorobisphenol A, SBPA = bisphenol S; (* not all dissolved, cloudy solution).

Experimental Section

Materials. All reagents were of commercial quality and were purchased from the Aldrich Chemical Co. 4-Methoxyphenylboronic acid was purchased from Optima Chemical Group, LLC. Chloral was obtained upon dehydration of chloral hydrate by mixing with twice its weight of sulfuric acid and subsequent separation. Solvents were dried and purified by standard procedures.

Instrumentation. IR spectra were determined on a BIO-RAD FT-40 spectrophotometer, using KBr pellets. ^1H NMR spectra were recorded with a GE-QE300 operating at 300 MHz. ^1H chemical shift were reported as δ values (ppm) relative to the used solvent CDCl_3 (7.24) or DMSO-d_6 (2.49). Molecular weights, relative to narrow polystyrene standards, were measured using a Shimadzu HPLC-GPC system consisting of a LC-10AD pump, SIL-10AF autosampler and Wyatt Mini DAWN light scattering detector. The measurements were taken with THF as mobile phase on two PLgel $5\mu\text{m}$ MIXED-D columns with flow rate of 1 mL min^{-1} . Samples were also run using a Waters 510 Pump and Controller, HPLC-grade THF, filtered, flow rate: 1.0 mL/min with a Styragel HMW6E and Phenogel 5 100A column using a Waters 410 Refractive Index Detector. Millennium software was used for data analysis. EasiCal polystyrene standards were used for calibration. Elemental analyses were performed by Midwest Microlab, LLC, 7212 N.Shadeland Avenue, Suite 110, Indianapolis, IN 46250.

Synthesis of 2,2-bis(4-iodophenyl)-1,1,1-trichloroethane, I-DDT.

Chloral (16.2 g, 0.11 mol) was mixed with iodobenzene (40.8 g, 0.20 mol), and the mixture was stirred and cooled to 5°C . Chlorosulfonic acid (12 mL, 0.18 mol) was added at a rate of a few mL every 10 min and the temperature was maintained at 5°C . The reaction mixture was allowed to warm and after reaching room temperature, then stirred for 2 h. The dark purple mixture was poured over ice, whereupon it formed pink crystals. The crystals were filtered and washed with water ($3 \times 150\text{ mL}$), then taken into ethyl acetate, washed with dilute sodium bisulfite solution (150 mL) and then with brine (150 mL). The organic layer was dried (Na_2SO_4) and concentrated. The residue was recrystallized from ethanol to afford the title compound I-DDT (26.9 g, 50%) as white needles, mp $179\text{--}180^\circ\text{C}$. ^1H NMR (300 MHz, CDCl_3) δ 7.65-7.70 (d, $J=8.5\text{ Hz}$, 4H, ArH), 7.28-7.33 (d, $J=8.5\text{ Hz}$, 4H, ArH), 4.95 (s, 1H, CH). Anal. Calcd for $\text{C}_{14}\text{H}_9\text{Cl}_3\text{I}_2$: C, 31.29; H, 1.69; Cl, I, 47.23. Found: C, 31.22; H, 1.68; I, 47.41.

Synthesis of 1,1,1-trichloro-2,2-bis[4'-(4-methoxyphenyl)-phenyl]ethane, p-TADDT.

1,1,1-trichloro-2,2-bis(4-iodophenyl)ethane (26.9 g, 0.05 mol) and 4-methoxyphenylboronic acid (16.7 g, 0.11 mol) were dissolved in acetone (90 mL). A solution of potassium carbonate (34.6 g, 0.25 mol) in water (90 mL) was then added and reaction mixture was stirred 5 min to gentle reflux. After evacuation and flushing with argon, palladium(II)acetate (10 mg) was added and the suspension was then heated for 10 h under reflux and a positive argon pressure. It was then cooled to room temperature and extracted with ethyl acetate ($4 \times 200\text{ mL}$), washed with water ($2 \times 100\text{ mL}$) and brine ($1 \times 150\text{ mL}$). The combined organic layers were dried (Na_2SO_4) and concentrated under reduced

pressure. The residue was recrystallized from ethanol to afford the title compound (23.4 g, 94%) as white crystals, mp 148-150 °C. IR (KBr, cm^{-1}): 3065, 3026, 2973, 2909, 2836, 1608, 1581, 1525, 1498, 1462, 1441, 1249, 1179, 1041, 824. ^1H NMR (300 MHz, CDCl_3): δ 7.68-7.70 (d, $J=8.0$ Hz, 4H, ArH), 7.50-7.53 (m, 8H, ArH), 6.95-6.98 (d, $J=8.1$ Hz, 4H, ArH), 5.13 (s, 1H, CH), 3.84 (s, 3H, OCH_3). ^{13}C NMR (75 MHz, CDCl_3): δ : 159.3 (C- OCH_3), 140.4 (ArC quat.), 136.6 (ArC quat.), 132.9 (ArC quat.), 130.5 (ArCH), 128.2 (ArCH), 126.6 (ArCH), 114.3 (ArCH), 101.8 (C- Cl_3), 70.6 (CH), 55.4 (OCH_3). Anal. Calcd for $\text{C}_{26}\text{H}_{23}\text{Cl}_3\text{O}_2$: C, 67.55; H, 4.66; Cl, 21.36. Found: C, 67.07; H, 4.71; Cl, 21.43.

Synthesis of 1,1-dichloro-2,2-bis[4'-(4-hydroxyphenyl)phenyl] ethene, p-TA-BPC.

1,1-dichloro-2,2-bis[4-(4'-methoxyphenyl)-phenyl]ethene (10.00 g, 0.020 mol) and pyridine hydrochloride (16.73 g, 0.138 mol) were placed in a beaker and slowly heated with stirring to 215-220 °C. Three additional 10 g portions of pyridine hydrochloride were added over the course of the reaction. The temperature was held at 215-220 °C for 30 min. Then the viscous, dark, red-brown liquid obtained was poured with stirring into 500 mL of water. The solid was collected by filtration and recrystallized from ethanol/water. The final product TA-BPC (8.34 g, 96%) was fine light yellow crystals, mp 220 °C. IR (KBr, cm^{-1}): 3520, 3300-2600, 3034, 1609, 1595, 1527, 1497, 1252, 1171, 1110, 960, 861, 823, 509. ^1H NMR (300 MHz, $\text{DMSO}-d_6$): δ 9.59 (br s, 2H, exchangeable with D_2O , OH), 7.56-7.59 (d, $J=8.6$ Hz, 4H, ArH), 7.45-7.49 (d, $J=8.4$ Hz, 4H, ArH), 7.30-7.34 (d, $J=8.7$ Hz, 4H, ArH), 6.80-6.82 (d, $J=8.2$ Hz, 4H, ArH). ^{13}C NMR (75 MHz, $\text{DMSO}-d_6$): δ 157.9 (C-OH), 140.9 (C= CCl_2), 140.4 (ArC quat.), 137.4 (ArC quat.), 130.5 (ArC quat.), 129.9 (ArCH), 128.3 (ArCH), 126.4 (ArCH), 118.3 (C= CCl_2), 116.3 (ArCH). Anal. Calcd for $\text{C}_{26}\text{H}_{18}\text{Cl}_2\text{O}_2$: C, 72.07; H, 4.19; Cl, 16.36. Found: C, 70.89; H, 4.64; Cl, 15.61.

Synthesis of homopolycarbonate (TABPCPC)

Homopolycarbonate (PC TABPC) was synthesized in accordance with the literature method.(33) TABPC (0.217 g, 0.5 mmol) was dissolved in 5.8 mL of pyridine and the solution was cooled to 0 °C. A solution of triphosgene (0.062 g, 0.21 mmol) in methylene chloride (2 mL) was added dropwise and the reaction mixture was vigorously stirred at 0-5 °C for 15 min. The solution became viscous and saturated with pyridine-hydrochloride after this time and was subsequently warmed to room temperature. The suspension was then stirred for an additional 4 hours. A 5% aqueous hydrochloric acid (10 mL) was used to neutralize the reaction mixture. The polymer was extracted with methylene chloride (3x20mL), washed with water (3x20mL), and the combined organic layers were dried (MgSO_4) and concentrated. The viscous residue was poured

into methanol. The precipitated polymer was filtered, washed with methanol and dried at 40 °C under vacuum for 24 h (0.20 g, 88% yield). IR (KBr) 3032, 1771, 1610, 1590, 1494, 1225, 1185, 1161, 1005, 974, 860, 821, 514 cm⁻¹. ¹H NMR (300 MHz, CDCl₃) δ 7.35-7.41 (m, 8H, ArH), 7.55-7.58 (d, J=7 Hz, 4H, ArH), 7.62-7.65 (m, J=7.6 Hz, 4H, ArH).

Synthesis of copolycarbonates

Bisphenol A (BPA), bisphenol C (BPC), 4,4'-(hexafluoroisopropylidene)diphenol (HFBPA) and 4,4'-sulfonylbiphenol (SBPA) were used as co-monomers. All copolymers (PC TABPC-BPA, PC TABPC-BPC, PC TABPC-HFBPA and PC TABPC-SBPA) were prepared using triphosgene similar to the above method for the synthesis of the homopolymer. The copolycarbonates were characterized by IR, ¹H NMR and HPLC-GPC using laser light scattering for molecular weight determination.

Conclusions

More than 40 years after the synthesis of the polycarbonate of BPC by Porejko we have synthesized a novel tetraarylbisphenol--1,1-dichloro-2,2-bis[4-(4'-hydroxyphenyl)phenyl]ethene (TABPC). The title monomer TABPC is an analogue of the 2,2-bis[4-(4-hydroxyphenyl)phenyl]propane (TABPA) of Bendler and Schmidhauser. The unique, high aspect ratio profile of these monomers makes them a separate category of computationally-designed bisphenols for polycarbonate. The synthetic conditions for the title compound and its positional isomers involved a mild, ligandless Suzuki procedure using an aryl iodide substrate which is easily accessible. Structure has been confirmed by IR, and 300 MHz proton and carbon-13 nuclear magnetic resonance spectroscopy. Solution polymerization was performed using triphosgene to give both homopolymer and heteropolymers. In spite of the lower molecular weights of the products the T_g's are relatively high; Flory-Fox calculations as well as polymerization of the monomers with phosgene to obtain high molecular weight polymers continue. Dynamic NMR studies of these materials are in progress, as are dynamic mechanical analyses to ascertain thermal properties and scale-up for mechanical testing of the new polymers. Since bisphenol A finds use in a variety of resins (epoxies and cyanate resins, for example) the synthetic strategies outlined herein additionally provide the possibility for not only interesting polycarbonate materials, but for a wide range of useful materials. Work continues in these areas.

Acknowledgements

We gratefully acknowledge the financial support of the National Science Foundation (Grant No. DMR-98-15957) Department of Defense-Army Research Office (Grant No. DAAD19-01-1-0482), the Army Research Laboratory (Grant No. DAAD19-02-2-0011), NSF (ILI Grant No. USE-9052345 for the NMR used in this work). This material is also based in part upon work supported by the National Science Foundation/EPSCoR Grant #EPS-0091948 and by the State of South Dakota.

References

1. Einhorn, A. *Liebigs. Ann. Chem.* **1898**, 300, 135.2. Porejko, S.; Brzozowski, Z.K.; Maczynski, C.; Wielgosz, Z. Pol. Patent 1964, 48, 893.
3. Porejko, S.; Wielgosz, Z. *Polimery* **1968**, 13, 55.
4. Brzozowski, Z.K.; Porejko, S. Self-Extinguishing Epoxy Resins of Low Viscosity, Polish Patent 53,272 (Cl.C08g), June 28, 1967, Applied February 24, 1965.
5. Brzozowski, Z. K.; Porejko, S. Low-Viscosity, Self-Extinguishing Epoxy Resins, Polish patent 56 079 (Cl.C08 g), 10 October 1968, Applied 10 August 1965, 2 pp. Addition to Po. 47 344.
6. Brzozowski, Z.K.; Kielkiewicz, J. *Plaste and Kautschuk*, **1971**, 12, 887-889.
7. Brzozowski, Z.K.; Brzozowska-Jania, T.; Florianczyk, T. *Polimery*, **1972**, 17(8), 419-22.
8. Brzozowski, Z. K.; "Epoxide Resins With Reduced Inflammability From Chlorobisphenol-Derivatives of Chloral," *Polimery*, **1986**, 31, (3-4) 99-103.
9. Factor, A.; Orlando, C.M. *J. Polym. Sci., Polym. Chem. Ed.* **1980**, 18, 579-592.
10. Rusanov, A.L. *Condensation Polymers Based on Chloral And Its Derivatives*, Progress In Polymer Science, **1994**, 19, 589-662.
11. Ramirez, M. "Thermal Decomposition Mechanism of 2,2-bis-(4-hydroxy-phenyl)-1,1-dichloroethylene-based polymers." Report No. DOT/FAA/AR-00/42; Federal Aviation Administration: Atlantic City, New Jersey, February 2001.
12. Lyon, R.E. "Fire Resistant Polymers Based on Bisphenol-C." <http://www.fire.tc.faa.gov/2001conference/html/materials/advanced.htm> (accessed March 2003).
13. Inglefield, P.T.; Jones, A.A.; Lubianez, R.P.; O'Gara, J.F. *Macromolecules*, **1981**, 14, 288-292.
14. Spiess, H.W. *Colloid Polym. Sci.*, **1983**, 261, 193-209.
15. Schaefer, J.; Stejskal, E.O.; McKay, R.A.; Dixon, W.T. *Macromolecules*, **1984**, 17, 1479-1489.
16. Yee, A.F.; Smith, S.A. *Macromolecules* **1981**, 14, 54-64.
17. Jones, A.A.; Bisceglia, M. *Macromolecules* **1979**, 12, 113
18. O'Gara, J.F.; Desjardins, S.G.; Jones, A.A. *Macromolecules* **1981**, 14, 64.
19. Bendler, J.T.; Schmidhauser, J.C.; Longley, K.L. Polycarbonate from bis[4'-(4-hydroxyphenyl)-phenyl]alkanes. U.S. Patent 5,281,689, January 25, 1994.

20. Bendler, J.T.; Schmidhauser, J.C.; Longley, K.L. Bis[4'-(4-hydroxyphenyl)-phenyl]alkanes and polycarbonates prepared therefrom. U.S. Patent 5,319,149, June 7, 1994.
21. Schmidhauser, J.; Sybert, P.D. "Nonbisphenol A Polycarbonates" in LeGrand, D.G.; Bendler, J.T. *Handbook of Polycarbonate Science and Technology*, pgs. 61-105; New York: Marcel Dekker, Inc. **2000**.
22. Vincent P.I. *Polymer*, **1960**, 1, 425-444.
23. Hao, J., Boyles, D.A. "Synthesis and Suzuki Reaction of Bis(4-benzyloxyphenyl)borinic acid with the Ditriflate of Bisphenol A," Presented at the 224th ACS National Meeting, Boston, MA, August 20, 2002, Poster 453.
24. Hao, J.; Boyles, D.A.; Bendler, J.T. Synthesis of 4,4'-Bisphenolformal. Presented at the 225th ACS National Meeting, New Orleans, LA, March 26, 2003, Poster 497.
25. Hao, Jiangtao. Synthesis and Polymerization of Novel Biphenyl Mesogenic Monomers and New Suzuki Reaction Methodology Development. Ph.D. Dissertation, South Dakota School of Mines and Technology, Rapid City, SD, April 2003.
26. Filipova, T.S.; Boyles, D.A.; Bendler, J.T.; Schroeder, M. Synthesis of Bis[4-(4'-hydroxyphenyl)phenyl]propane and Novel Polycarbonates Prepared Therefrom. 225th ACS National Meeting, New Orleans, LA, March 25, 2003, Poster 550.
27. Beller, M.; Fischer, H.; Herrmann, W. A.; Ofele, K. *Angew Chem. Int. Ed.* **1995**, 34, 1848-1849.
28. Unpublished work.
29. Goodson, F.E.; Wallow, T.I.; Novak, B.M. *Organic Syntheses*, **1997**, 75, 61.
30. The dihydroxydiphenyl compounds was made by Elbs, K. *J. prakt. Chem.* **1893**, 47, 44. Dibromo- and dichlorodiphenyltrichloroethanes (DDT) were made by Zeidler, O. *Ber.* **1874**, 7(2), 1180-1181 and Ter Meer, E. *Ber.* **1874**, 7, 1201. Diiododiphenyltrichloroethane was first claimed to have been made by Chattaway, F.D.; Muir, R. J. K. *J. Chem. Soc. (London)* **1934**, 701-703 (no experimental provided).
31. Lesiak, T., Nowakowski, J. *J. prakt. Chem.* **1981**, 323 (4), 684-690.
32. Manuscript in preparation.
33. Sun, S.J.; Hsu, K.Y.; Chang, T.C. *Poly. J.* **1997**, 29, 25-32.

Poly(bisphenol A carbonate) Blends and Composites

Chapter 12

Composites of Polycarbonate with Multiwalled Carbon Nanotubes Produced by Melt Mixing

Petra Pötschke¹, Arup R. Bhattacharyya^{1,3}, Andreas Janke¹,
and Harald Goering²

¹Institute of Polymer Research at Dresden, Hohe Strasse 6, 01069 Dresden, Germany

²Federal Institute for Materials Research and Testing, Unter den Eichen 87, 12200 Berlin, Germany

³Current address: Department of Metallurgical Engineering and Materials Science, Indian Institute of Technology at Bombay, Powai, Mumbai 400076, India

Composites of polycarbonate (PC) with varying amount of multiwalled carbon nanotubes (MWNT) were prepared by diluting a PC based masterbatch containing 15 wt% MWNT using melt mixing technique. Electrical resistivity data showed percolation of MWNT between 1 and 1.5 wt%. Near the percolation threshold longer mixing at low rotation speed seems to be favorable. The formation of network-like structures also could be detected by oscillatory rheometry and visual observations of the composite dispersions in a PC-solvent. Transmission electron microscopy and atomic force microscopy were used to characterize the state of MWNT dispersion and indicated no pronounced orientation in extrusion direction. The mechanical reinforcement aspect of MWNT is also regarded in context with the masterbatch diluting technology. It was found that molecular weight reduction of PC takes place due to the high shear forces in presence of nanotubes during the masterbatch preparation. This leads to changes in glass transition temperature and counteracts the effects originating from the nanotube addition.

Polycarbonate (PC) is a versatile engineering thermoplastic with a wide range of useful properties like high tensile strength, stiffness, high heat distortion temperature (dimensional stability) with high optical clarity, and electrically insulating characteristics (1). However, for some applications special properties like electrical conductivity or antistatic discharge behavior may be desired. Such properties are important for the application of materials for housings, automotive parts, and in electronic devices. By using conductive filler materials, insulating polymers can be modified to be conductive or antistatic. New opportunities arise when using nanoscaled conductive fillers, especially carbon nanotubes (CNT) which exhibit excellent electrical properties (CNT are as conductive as copper) with distinct fibrous shape with very high aspect ratio p ($p = L/D$, where $L = 1-50 \mu\text{m}$ and $d = 1-50 \text{nm}$).

It is well known that the aspect ratio is correlated with the percolation concentration, i.e., the filler concentration at which a network of conductive filler is formed through the matrix which manifests in changes of resistivity over decades. According to theoretical calculations on cylindrical shape fillers (2), percolation on CNT/polymer composites can be expected starting at about 0.05 vol% of filler (assuming an aspect ratio of 1000). The lowest amounts reported in literature are 0.04 wt% for epoxy/multiwalled carbon nanotube (MWNT) composite (3) and 0.05 wt% found for polypropylene/MWNT films (4). However, most experimental studies on polymer/MWNT composites show percolation between 1-5 vol% (5-8). On the other hand, putting nanotubes into polymers homogeneously is quite difficult. To achieve a homogeneous distribution is difficult because of the existence of synthesis induced tangled intertwined aggregates and due to the high intermolecular van der Waals interactions between the nanotubes.

In most cases, melt mixing is the preferred method of composite formation. The tendency of MWNT to form aggregates may be minimized by appropriate application of shear stress during melt mixing (7,9). This contribution presents composites of polycarbonate with varying amounts of MWNT produced by melt mixing. In this study, the technology of diluting a masterbatch containing a high amount of MWNT by mixing with pure PC is used and the electrical properties are studied in dependence on MWNT content and processing conditions.

For PC, the use of glass fibers and carbon fibers is common and reported to increase tensile and flexural strength, modulus, and impact strength (1). The incorporation of nanotubes which exhibit modulus and strength levels in the range of 200-1000 GPa and 200-900 MPa, respectively (10-12), is expected to enhance the mechanical properties at low filler contents. In this contribution, the mechanical reinforcement aspect of MWNT is regarded in context with the masterbatch diluting technology.

Experimental

Materials and Composite Preparation

A masterbatch of 15 wt% MWNT in PC (equivalent to 10.4 vol% assuming a MWNT density of 1.75 g/cm^3 (5)) was obtained in the form of granules from Hyperion Catalysis International, Inc. (Cambridge, USA) (5, 8). Two sets of experiments were performed in order to dilute the masterbatch. In set 1, one-kilogram mixtures of PC with the masterbatch were extruded using a co-rotating, intermeshing twin screw extruder (HAAKE, Germany; length $D=30 \text{ mm}$, $L/D=10$) to obtain concentrations of 0.5 wt%, 1 wt%, 2 wt%, and 5 wt% MWNT in PC 1 (Iupilon E-2000, Mitsubishi Engineering Plastics) (8). Compounding of set 1 was carried out using a barrel temperature of $240 \text{ }^\circ\text{C}$, a screw speed of 280 rpm, and a feed rate of 980 g/h. The granules were compression molded into bars with the dimension $65 \times 13 \times 3 \text{ mm}^3$. In addition, the masterbatch was diluted with a lower viscosity PC 2 (the same as used for the masterbatch preparation) using melt mixing in a DACA Micro Compounder (DACA Instruments, Goleta, USA) at $260 \text{ }^\circ\text{C}$ (13). In set 2, a rotational speed of 50 or 150 rpm was applied for 5 or 15 min. Here, the concentration of MWNT was selected in a smaller interval to get more exactly the percolation composition.

Electrical Conductivity

The volume conductivity was measured for compression molded samples. For set 1, compression molded bars (length 40 mm) were used. For set 2 thin sheets (diameter 60 mm, thickness 0.35 mm) were prepared from the extruded strands. A Keithley electrometer Model 6517 was used which was either equipped with a 8002A High Resistance Test Fixture (set 1) or with a 8009 Resistivity Test Fixture equipped with ring electrodes (set 2) to investigate the high resistance samples at 500 V. A four point test fixture combined with a Keithley electrometer Model 2000 was used for samples with MWNT level higher than 1.5 wt%. Strips with the size of $20 \text{ mm} \times 3 \text{ mm}$ were cut from the sheets.

Rheological Measurements

Melt rheological properties were obtained using an ARES oscillatory rheometer (Rheometric Scientific, USA) at $260 \text{ }^\circ\text{C}$ under nitrogen atmosphere. Frequency sweeps were carried out between 0.1 and 100 rad/s at strains within the linear viscoelastic range using a parallel plate geometry (plates with

diameter of 25 mm, gap of 1 to 2 mm). Measurements are presented for set 1 where parts of compression molded bars were placed between the preheated plates.

Microscopic Techniques

Scanning electron microscopy (SEM) was performed using a LEO 1530 scanning electron microscope (Leo Elektronenmikroskopie, Oberkochen, Germany) after gold sputtering of a fractured surface of a masterbatch pellet.

For transmission electron microscopy (TEM) thin sections of relatively high thickness (~ 200 nm) were prepared perpendicular and parallel to the extrusion direction from the middle part of the strand using a Reichert Ultracut S ultramicrotome (Leica, Austria) at room temperature. A diamond knife with a cut angle of 35° (Diatome, Switzerland) was used. This thickness was chosen in order to get good balance between a high amount of structure elements in the section and a suitable sample transparency. The EM 912 (Zeiss, Germany) operated at 120 kV was used and the micrographs were taken in defocusing contrast in order to visualize the nanotubes.

Test specimens for atomic force microscopy (AFM) were prepared by cutting a strand piece parallel and perpendicular to extrusion direction using a Leica RM 2155 microtome (Leica, Germany) equipped with a diamond knife at room temperature. The AFM measurements were carried out in the tapping mode by a Dimension 3100 NanoScope IV (Veeco, USA) (14).

Dissolving Experiments on PC-MWNT Composites

In order to obtain a qualitative view of the state of MWNT dispersion within the composites, the composites were dissolved in tetrahydrofuran (THF) for about 2 weeks at room temperature. Small pieces of the extrudates (corresponding to 1.2 mg MWNT) were immersed in about 50 ml THF without additional shaking. From these dispersions of nanotubes in the PC-THF solution, photographs were taken and the appearance of the dispersion is discussed.

Dynamic Mechanical Analysis (DMA) and Differential Scanning Calorimetry (DSC)

The dynamic mechanical properties of the extruded strands were measured in accordance to EN ISO 6721-2 using a freely oscillating torsion pendulum at a frequency of 1 Hz under N₂ atmosphere. Samples of 50 mm length were cut from extruded strands and a gauge length 40 mm was used for the testing. The

samples were rapidly cooled down to about $-196\text{ }^{\circ}\text{C}$ and oscillated with constant deformation amplitude smaller than 1 %. The heating rate was 2 K/min. The temperature position of the main $\tan \delta$ peak maximum is defined as the glass transition temperature of PC (T_g).

DSC measurements were conducted with a DSC7 Perkin Elmer (equipped with Pyris-Software, Version 4.0) for 8 mg sample at a scan rate of ± 20 K/min under N_2 atmosphere in the temperature range from 25 to 275 $^{\circ}\text{C}$. The glass transition temperature of PC was determined from the derivative heat flow of the second heating using the inflection point method.

Stress-Strain-Behavior

Tensile tests were performed on the compression molded bars of set 1 using a gauge length of 18 mm. A Zwick 1456 testing machine was used and a speed of 50 mm/min was applied. About 7 samples were measured for a particular composition, samples with break at the clamps were omitted.

Results and Discussion

Electrical Properties and Percolation in PC/MWNT Composites

In our studies the percolation was found between 1.0 and 2.0 wt% MWNT in PC 1 for set 1 produced using the Haake extruder (8) and between 1.0 and 1.5 wt% MWNT for set 2 mixed with PC 2 using the Micro Compounder (13) (Figure 1). In this range, the volume conductivity changes over more than 10 decades and the composites with nanotube contents higher than 1.5 wt% can be regarded as electrically conductive. Increasing amount of MWNT increases the volume conductivity only marginally. The results show that the used small scale extruder has a mixing efficiency comparable to that of a larger scale extruder.

For concentrations of MWNT near the percolation threshold the processing conditions (screw speed and mixing time) were varied in set 2. Increasing the mixing time and screw speed at 1.0 wt% MWNT (below the percolation concentration) increases electrical conductivity which can be ascribed to a better distribution and dispersion of the nanotubes within the volume (15). At MWNT contents slightly above the percolation concentration (1.5 wt% and 2 wt%), the increase in screw speed at low mixing time also increases conductivity but longer mixing time at high screw speed led to unchanged (2.0 wt%) or even lower conductivity value (1.5 wt%). The latter can be a result of breakage of the MWNT due to high melt viscosity of these composites as discussed by Andrews et al. (4). At higher MWNT concentrations the influence of mixing conditions

becomes less important. The number of contacts between MWNT is so high that small changes in distribution and dispersion do not show significant effects. These relationships were studied in more detail by Pötschke et al. in (16) using complex permittivity and related AC conductivity measurements in the frequency range between 10^{-4} to 10^7 Hz.

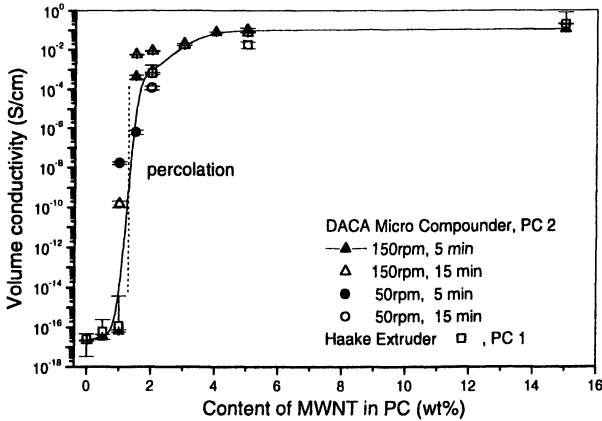


Figure 1. Volume conductivity vs. MWNT content for PC-MWNT composites

The formation of network-like structures of MWNT also could be detected by oscillatory rheometry as shown in Figure 2 for set 1 (8).

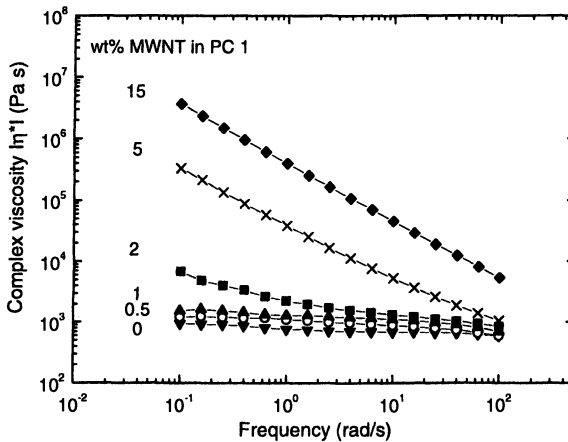


Figure 2. Complex melt viscosity at 260°C vs. frequency for PC 1-MWNT composites (Reproduced with permission from ref. 8. Copyright 2002 Elsevier)

Pure polycarbonate and composites with MWNT up to 1 wt% show similar frequency dependencies of the complex viscosity and reach a Newtonian plateau at low frequencies. Starting from 2 wt% nanotubes, the qualitative behavior of viscosity vs. frequency changes significantly. The viscosity curves exhibit a much greater increase with decreasing frequency and exhibit non-Newtonian behavior at much lower frequencies. Therefore, 2 wt% MWNT may be regarded as a 'rheological threshold' composition. The increase in viscosity is accompanied by an increase in the elastic melt properties, represented by the storage modulus G' , which shows a plateau at low frequencies as presented in (8). This change of rheological behavior can be associated with the formation of a network-like structure of the MWNT and coincidences with the electrical percolation composition. It is known from anisotropic fillers that a structure formation leads to significant changes in the qualitative melt rheological behaviour indicating an increase in viscosity with lowering the test frequency in oscillation tests (17). This was found also for micrometer sized fibres and montmorillonite nanoclay fillers.

In addition, dissolving tests of the composites were performed (8,13). It was reported (18,19) that dissolving experiments showing the state of nanotube dispersion in a good solvent for the matrix polymer material can be useful to give information also about the state of dispersion which was achieved in the solid structure. Visual observation of dissolved composite samples of PC 2-MWNT composites in THF is shown in Figure 3.

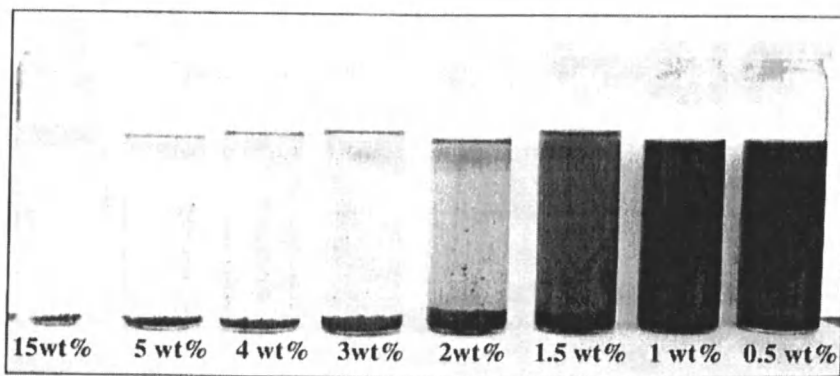


Figure 3. Photographs of the composite dispersions in THF to characterize the state of MWNT dispersion in PC 2, from left to right: 15 wt%, 5 wt%, 4 wt%, 3 wt%, 2 wt%, 1.5 wt%, 1 wt%, 0.5 wt% MWNT. MWNT amount in each vial 1.2 mg (Reproduced with permission from reference 13. Copyright 2003 VSP)

The samples with 0.5 and 1.0 wt% MWNT appear as homogeneous black solutions, indicating homogeneous distribution of individual tubes or only small

aggregates of MWNT. Starting with 1.5 wt%, a black sediment is visible which corresponds to remains of the interconnected nanotube structure which can not be destroyed under the dissolving conditions. Thus, the existence of a sediment and the brightness appearance of the solution are indicating the existence of a percolated MWNT structure. The volume of the sediment decreases with increasing MWNT content which can be related to a higher compactness of the agglomerated tubes. Similar results were found when using chloroform as solvent.

Dispersion and Orientation of MWNT in Composites with PC

The structure of the masterbatch consisting of PC 2 with 15 wt% MWNT is shown in Figure 4. It is visible from the SEM micrograph that the MWNT form a highly entangled (interconnected) structure in the PC matrix. A similar kind of interlocked structure has been reported in poly (vinyl alcohol) /MWNT composite at 50 wt% MWNT content (5). The MWNT used in this study exhibit a distinct curved shape in all three dimensions which can be described as 'spaghetti' like structure.

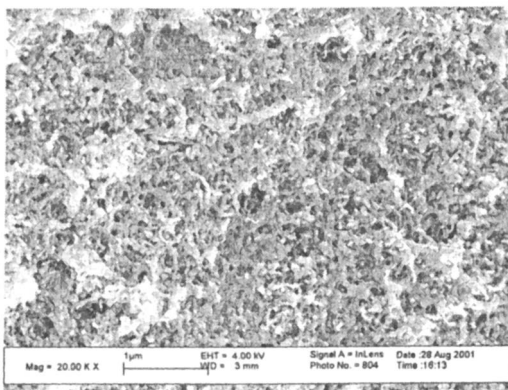


Figure 4. SEM micrograph of PC 2- 15 wt% MWNT composite (masterbatch)

Figures 5a to 5d show the TEM micrographs of composites of PC 2 with varying concentrations of MWNT. The samples were cut in the extrusion (flow) direction. In Figure 5b the sample was cut perpendicular to the extrusion direction is shown for 5wt% MWNT. In order to assess the state of dispersion, a low magnification was selected.

It is found that the dispersion of MWNT is almost homogeneous at 5, 2 and 1 wt% concentration of MWNT. At 5 wt% level (Figures 5a,b), the tubes appear uniformly dispersed in the entire volume of the matrix, without significant

agglomeration or clusters. The tubes are found as single tubes and are less entangled than in the masterbatch. The occurrence of 'electrical percolation' between 2 wt% and 1 wt% caused by connection of neighboring tubes to each other in three dimensionally seems to be visible from the TEM micrographs, even considering the need to visualize all segments of the tubes within a composite thickness of 200 nm.

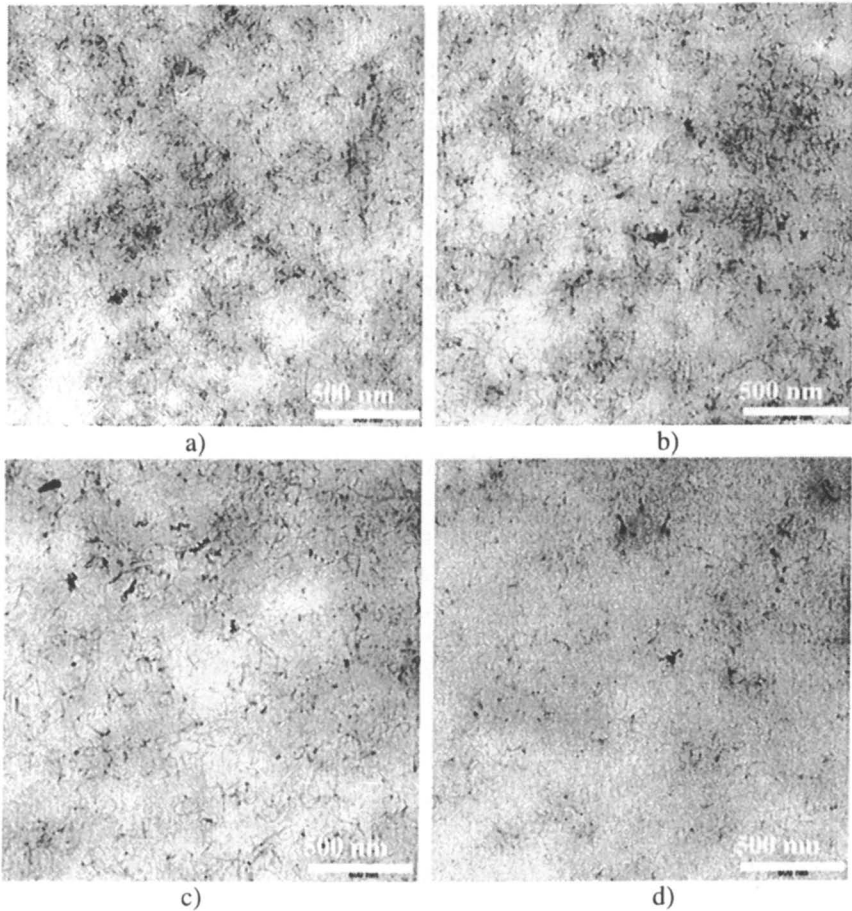


Figure 5. TEM micrographs of PC 2-MWNT composites, cut along extrusion direction: a) 5 wt% MWNT, c) 2 wt% MWNT, d) 1 wt% MWNT. b) 5 wt% MWNT, cut perpendicular to extrusion direction

In addition, AFM investigations were performed in order to characterize a possible orientation or alignment of the tubes along extrusion direction. By

comparing samples which were cut perpendicular and along the extrusion direction, as shown in Figure 5a,b (TEM) and Figure 6a,b (AFM) for the PC-5 wt% MWNT composite, no significant difference in the appearance of the MWNT dispersion could be observed.

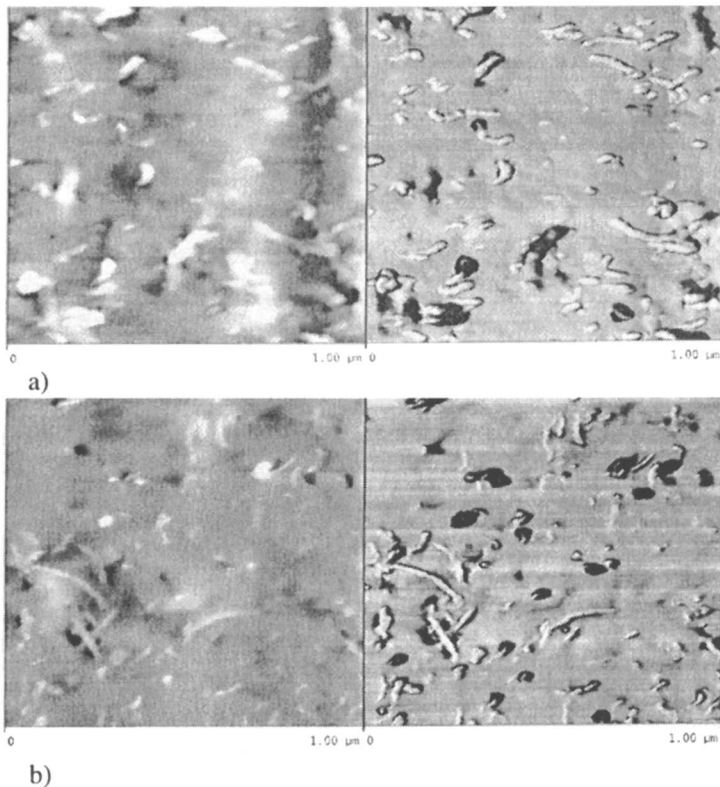


Figure 6. AFM images of PC-5 wt% MWNT: a) along, b) perpendicular to the extrusion direction (Adapted with permission from reference 14. Copyright 2004 Elsevier)

According to the schema shown in Figure 7, orientation should be clearly visible by comparing cuts made along extrusion direction (A) with cuts made perpendicular (B) to extrusion direction. In the extrusion direction more long tube segments should be visible, whereas in the perpendicular direction spots of cut tubes should dominate. Since the micrographs obtained in both directions appear similar, we can conclude that the nanotubes are not significantly oriented.

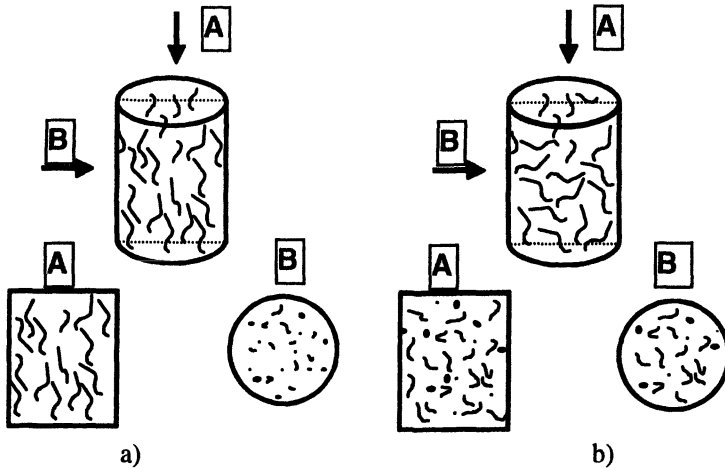


Figure 7. Illustration of the effects of nanotube alignment on the appearance of micrographs taken of thin sections (TEM) or at cut surfaces (AFM): a) aligned tubes, b) tubes distributed statistically. (Reproduced with permission from reference 14. Copyright 2004 Elsevier)

Mechanical Reinforcement Aspect

It is one of the expectations for CNT that their incorporation into polymeric matrices leads to a mechanical reinforcement. An increase in G' measured by DMA was reported for several CNT/polymer systems (4,5,20). The shear storage modulus G' for selected PC 2-MWNT combinations is shown in Figure 8. It is seen that there is an increase in G' with nanotube contents. This increase is shown more in detail in Figure 9 representing G' in dependence on MWNT concentrations for selected temperatures below and above T_g .

At 25 °C, the increase in G' is quite low. However, at temperatures above the T_g the increase in G' is much more pronounced, which is in accordance to findings by several authors (5). Figure 8 shows in addition the temperature dependence of $\tan \delta$ indicating the β , α' and α relaxation of PC by the corresponding $\tan \delta$ maxima (according to Bauwens-Crowet (21)). It is obvious that the relaxation intensities as well as the temperature positions are only slightly changed with increasing content of nanotubes. Only the α -relaxation (T_g) shows changes which can be correlated to the existence of nanotubes within the PC. The peak intensity is decreased with nanotube content resulting from the lower amount of relaxing PC matrix and the T_g differs slightly.

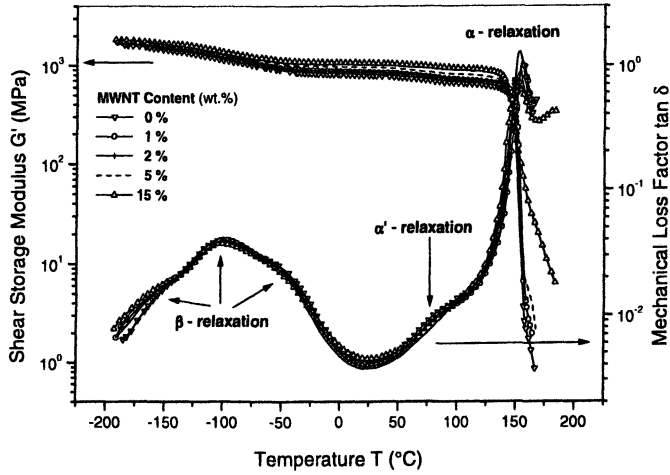


Figure 8. Shear storage modulus G' and loss factor $\tan \delta$ for composites of PC 2 with different amounts of MWNT (Reproduced with permission from reference 13. Copyright 2003 VSP).

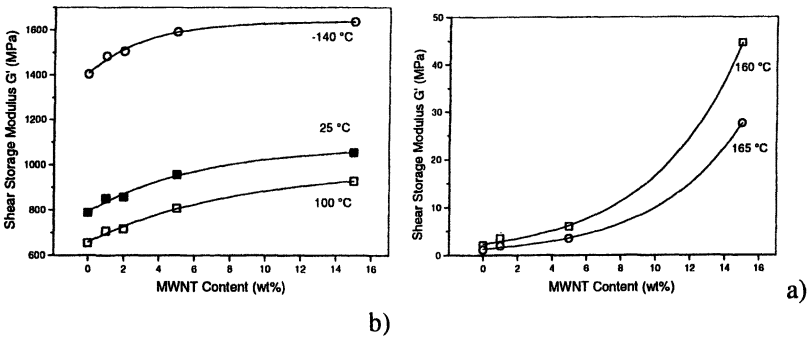


Figure 9: Shear storage modulus G' versus MWNT content at different temperatures: a) below T_g , b) above T_g (Reproduced with permission from reference 13. Copyright 2003 VSP).

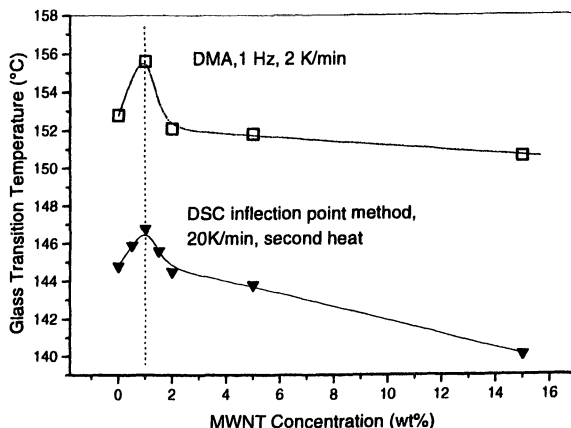


Figure 10. Glass transition temperature T_g versus MWNT content in PC 2 (Reproduced with permission from reference 13. Copyright 2003 VSP)

It is expected from a theoretical point of view that the T_g of the matrix material in systems with nanofillers is increased due to the fact that polymer chains near the nanofiller surface are less mobile and therefore show an increased T_g in case of strong interfacial interactions between the nanofiller and the polymeric matrix. In nanofilled systems the amount of immobile material is very high because of the very high surface area. For our system, changes of T_g as detected by DMA and DSC are shown in Figure 10.

At 1 wt% MWNT an increase in T_g as compared to extruded PC can be observed. However, with increasing nanotube concentration the T_g is decreasing and the value measured for the 15 wt% MWNT sample (masterbatch) is about 5 K lower than that for the pure PC. In set 1, we found a continuous decrease in T_g with MWNT content measured by DSC and DMA. This behaviour is unexpected and can not be explained only by the incorporation of the nanotubes.

To look into this phenomenon more in detail GPC experiments were conducted as described in detail in (13). It was found that the PC phase in the masterbatch has a lower molecular weight as compared to pure PC used for the masterbatch preparation and used as diluting polymer. This lower molecular weight can be attributed to molecular changes of the PC during the masterbatch preparation process and results from the high shear forces due to the increase in the melt viscosity of the composite after the nanotube adding (see Fig. 2). Thus, in these composites prepared by dilution of masterbatch two effects are counteracting: (i) the effect of reinforcement due to the nanotube addition, (ii) the effect of adding degraded PC that leads to lowered mechanical properties.

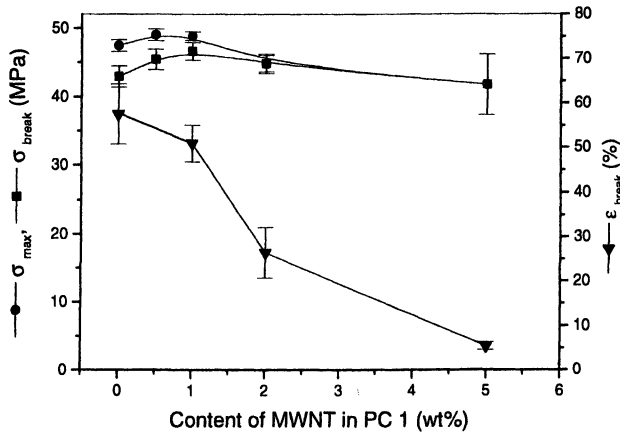


Figure 11. Maximum strength σ_{max} , strength at break σ_{break} , and elongation at break ϵ_{break} for PC 1-MWNT composites.

These results contribute to explain the change in mechanical properties with MWNT content (Figure 11) for PC 1-MWNT composites. There is only a small increase in tensile strength and strength at break up to 1 wt% MWNT as compared to the pure extruded PC. Starting at 2 wt% MWNT the values decrease slightly. Elongation at break is reduced significantly at all compositions after incorporation of MWNT. However, the highest drop in elongation at break occurred after reaching the percolation composition indicating that the network-like structure of MWNT hinders the typical deformation behavior of the PC. In order to achieve significant enhancement of Young's modulus and strength, good interfacial interactions leading to high phase adhesion may be a necessary requirement as shown by Cooper et al. (22) and Gojny et al. (23) for epoxy/MWNT composites. This may require chemical modification of the nanotube surface.

Summary and Conclusion

In this study, composites of polycarbonate (PC) with varying amount of multi wall carbon nanotubes (MWNT) were prepared by diluting a PC based masterbatch containing 15 wt% MWNT (Hyperion Catalysis, Inc.) using melt mixing technique. Electrical conductivity measurements indicated percolation of MWNT between 1 and 1.5 wt%. Near the percolation threshold longer mixing at low rotation speed seems to be favorable. Percolation also could be detected by oscillatory rheology and visual observations of the composite dispersions in a PC-solvent. Transmission electron microscopy and atomic force microscopy

showed a excellent dispersion of the MWNT and indicated no pronounced orientation of MWNT in extrusion direction.

Differential scanning calorimetry and dynamic mechanical analysis were applied to detect changes in the glass transition temperature of PC as a result of MWNT interactions with the PC matrix and of processing. DMA confirmed the reinforcement effect of the nanotubes. During the masterbatch preparation, the addition of the nanotubes increased the melt viscosity significantly due to network formation. The shear forces during mixing were very high because of the high viscosity of the PC-MWNT masterbatch composite which led to chain degradation of PC as indicated by a decrease of molecular weight. As a result, the glass transition temperature of the PC was decreased and mechanical properties of the PC part in the masterbatch were lowered. Thus, in the diluted composites strength was not increased significantly.

Acknowledgement. We would like to thank Hyperion Catalysis International, Inc. for supplying PC and the masterbatch. P.P. thanks Prof. D. R. Paul (University of Texas, Austin, USA) for the initiation of this work and his kind support. In addition, we are grateful for the GPC measurements performed by Mr. D. Voigt and the DSC measurements made by Dr. G. Pompe (both from IPF Dresden). Dr. M. Abdel-Goad (IPF Dresden) is thanked for helpful discussions.

References

1. Brydson, J. A. *Plastics Materials*, 5th edition, Butterworths, London, 1989, pp 521-545.
2. Balberg, I. *Philos Mag B* **1987**, *56*, 991.
3. Sandler, J.; Shaffer, M.S.P.; Prasse, T.; Bauhofer, W.; Schulte, K.; Windle, A.H. *Polymer* **1999**, *40*, 5967.
4. Andrews, R.; Jacques, D.; Minot, M.; Rantell, T. *Macromol. Mat. Eng.* **2002**, *287*, 395.
5. Shaffer, M.S.P.; Windle, A. H. *Adv. Mat.* **1999**, *11*, 937.
6. Safadi, B.; Andrews, R.; Grulke, E.A. *J. Appl. Poly. Sci.* **2002**, *84*, 2660.
7. Hagerstrom, J.R.; Greene, S.L. Electrostatic dissipating composites containing Hyperion fibril nanotubes. Commercialization of Nanostructured Materials, Miami, USA, April 7, **2000**.
8. Pötschke, P.; Fornes, T.D.; Paul, D.R. *Polymer* **2002**, *43*, 3247.
9. Hagenmueller, R.; Gommans, H.H.; Rinzler, A.; Fischer, J.E.; Winey, K.I. *Chem. Phys. Lett.* **2000**, *330*, 219.
10. Salvétat, J.P.; Briggs, G.A.D.; Bonard, J.M.; Bacsa, R.R.; Kulik, A.J.; Stöckli, T.; Burnham, N.A.; Forró, L. *Phys. Rev. Lett.* **1999**; *82*, 944.

11. Walters, D.A.; Ericson, L.M.; Casavant, M.J.; Lui, J.; Colbert, D.T.; Smith, K.A.; Smalley RE. *Appl. Phys. Lett.* **1999**, *74*, 3803.
12. Li, F.; Cheng, H.M.; Bai, S.; Su, G.; Dresselhaus, M.S. *Appl. Phys. Lett.* **2000**, *77*, 3161.
13. Pötschke, P.; Bhattacharyya, A.R.; Janke, A.; Goering, H. *Comp. Interf.* **2003**, *10*, 389.
14. Pötschke, P.; Bhattacharyya, A.R.; Janke, A. *Eur. Polym. J.* **2004**, *40*, 137.
15. Ferguson D.W., Bryant E.W.S., Fowler H.C. ESD thermoplastic product offers advantage for demanding electronic applications, ANTEC'98, **1998**, 1219.
16. Pötschke, P.; Alig, I.; Dudkin, S. *Polymer* **2003**, *44*, 5023.
17. Utracki, L.A. Rheology and Processing of Multiphase Systems. In: Ottenbrite, R.M.; Utracki, L.A.; Inoue, S., editors. Current Topics in Polymer Science, vol. II. Rheology and Polymer Processing/Multiphase Systems. Carl Hanser: Munich, Vienna, New York **1987**, 7-59.
18. Bandyopadhyaya, R.; Nativ-Roth, E.; Regev, O.; Yerushalmi-Rozen, R. *Nanoletters* **2002**, *2*, 25.
19. Barraza, H.J.; Pompeo, F.; O'Rear, E.A.; Resasco, D.E. *Nanoletters* **2002**, *2*, 797.
20. Jin, Z.; Pramoda, K. P.; Xu, G.; Goh S. H. *Chem. Phys. Lett.* **2001**, *43*, 337.
21. Bauwens-Crowet, C. *J. Mat. Sci.* **1999**, *34*, 1701.
22. Cooper, C.A.; Rohen, S.R.; Barber, A.H.; Wagner, H.D. *Appl. Phys. Lett.* **2002**, *81*, 3873.
23. Gojny, F.H.; Nastalczyk, J.; Roslaniec, Z.; Schulte, K. *Chem. Phys. Lett.* **2003**, *370*, 820.

Chapter 13

Melt-Mixed Blends of Carbon Nanotube-Filled Polycarbonate with Polyethylene

**Petra Pötschke¹, Arup R. Bhattacharyya^{1,3},
Mahmoud Abdel-Goad¹, Andreas Janke¹, and Harald Goering²**

¹Institute of Polymer Research at Dresden, Hohe Strasse 6, 01069 Dresden, Germany

²Federal Institute for Materials Research and Testing, Unter den Eichen 87, 12200 Berlin, Germany

³Current address: Department of Metallurgical Engineering and Materials Science, Indian Institute of Technology at Bombay, Powai, Mumbai 400076, India

Blends of polycarbonate (PC) and polyethylene (PE) were prepared by melt mixing using nanotubes as conductive fillers. Multiwalled carbon nanotubes (MWNT) are first introduced into polycarbonate using a masterbatch dilution technology. This blending strategy is intended to produce conductive blends containing less MWNT than required for the pure PC by using the concept of double percolation through the formation of co-continuous morphologies.

In melt mixed blends with PE, fully co-continuous morphologies could be obtained in the composition range between 25 to 90 vol% of the filled PC phase. The co-continuous structures are very fine with ligaments in the range of 1 μm and show only marginal differences in phase size with blend composition. Significantly increased conductivity values of the blends could be achieved in the same composition range in that PC forms a continuous phase, i.e. starting at compositions of 25 vol% filled PC. Here, the total MWNT content in the blend is only 0.34 vol%.

Blending of polymers is a common way to modify the properties of a given polymer in order to get tailor-made materials. For polycarbonate (PC), next to structural changes achieved by modified synthesis routes, melt blending with different polymers is reported to enhance processability and impact strength (1-5). Common blends based on PC are those with polyalkenes, styrenics, acrylics, polyvinyl chloride and thermoplastic polyurethane, and engineering plastics (1). If conductive or antistatic materials are desired, addition of conductive fillers is a suitable way. Recently, carbon nanotubes (CNT) have been shown to be attractive fillers for achieving electrical conductivity of polymers at relatively low CNT contents. Amounts lower than 1 wt% are reported to be sufficient to get conductive polymers (6,7). This efficient behavior of CNT is caused by the excellent electrical properties in combination with the very high aspect ratio, as high as 1000 (8). Thus, it is also promising to use CNT as additives in polymer blends for electrically conductive or antistatic applications and achieving, at the same time, the well-known advantages of polymer blending for tailor-made material properties. This is especially effective when using the double percolation phenomena, first introduced by Sumita et al. (9) for carbon black (CB) filled blends. Here, the first percolation is arising due to CB in one phase which itself form a continuous phase in the blend (second percolation). Much lower contents of the conductive fillers are necessary when both phases form a co-continuous structure and the filled phase has low volume content. In addition, it was shown that co-continuous structures often lead to synergistic improvement of blend properties (10).

Thus, in this contribution melt blending of CNT filled PC with high density polyethylene (PE) is performed in order to fulfill two tasks simultaneously: (i) to get conductive or antistatic material at very low nanotube contents by creating co-continuous blend structures using the double percolation concept and (ii) to use the advantage of (co-continuous) polymer blends concerning the enhancement of mechanical properties. The work combines our experiences in melt mixing of CNT filled PC (11-15) and in the field of polymer melt blending (10,16-19) which is to our knowledge, the first work reported on this topic (10,20). Polyethylene was chosen as a model polymer because of its incompatibility with PC in order to test the applicability of the double percolation concept to multiphase co-continuous blends containing carbon nanotubes excluding additional effects, like compatibilization. On the other hand, polyolefins were also shown to be potential partners in blends with PC. Kunori and Geil (3,4) studied in detail the mechanical effects of adding HDPE and LDPE to PC on modulus, tensile and impact strength and correlated the results with the blend morphology. Li et al. (5) reported on blends of PC with ethylene-1-octene copolymers (POE) which had improved impact strength at low temperatures. The use of an ionomer as compatibilizer refined the dispersed phase morphology in PC/POE=80/20 blends with improved tensile strength and elongation at break.

Experimental

Materials, Composite and Blend Preparation

High density polyethylene (PE, Lupolen® 4261A, BASF AG, Germany) was blended with a composite of polycarbonate (PC) containing 2 wt% multiwalled carbon nanotubes (PC-2NT) at different compositions. A DACA Micro Compounder with a capacity of 4.5cm³ operated at 260 °C, 50 rpm and a mixing time of 5 min was used. The PC-2NT composite was produced in a Haake-extruder using the masterbatch diluting technology. A PC based masterbatch containing 15 wt% multiwalled carbon nanotubes (MWNT) supplied by Hyperion Catalysis International, Inc. (Cambridge, USA) was melt mixed with PC Iupilon E 2000 (Mitsubishi Engineering Plastics, Japan) as described in (11).

Electrical Conductivity

The volume conductivity was measured on compression molded samples. Thin sheets (diameter 60 mm, thickness 0.35 mm) were prepared from the extruded strands. For low conductivity samples, a 8009 Resistivity Test Fixture combined with a Keithley electrometer Model 6517 was used. For samples with higher conductivity, a four point test fixture combined with Keithley electrometer Model 2000 or Model 6517A was applied using strips with the size of 20 mm x 3 mm cut from the sheets.

Rheological Measurements

The rheological measurements were performed using an ARES oscillatory rheometer (Rheometric Scientific, USA) at 260 °C over frequency range varying from 100 to 0.05 rad/s under nitrogen atmosphere. A parallel plate geometry was used (plate diameter of 25 mm, gap of about 1 mm) and the strain was chosen within the linear viscoelastic range.

Microscopic Techniques

Scanning electron microscopy (SEM) was performed using a LEO VP 435 scanning electron microscope (Leo Elektronenmikroskopie, Oberkochen, Germany) after gold sputtering. For some investigations, a low voltage Zeiss Gemini DSM 982 scanning electron microscope (Zeiss, Germany) was used without sample sputtering. Extruded strands of the blends were cryofractured and investigated without or with selective dissolution of the PC part in

chloroform (4 d at RT). Test specimens for atomic force microscopy (AFM) were prepared by cutting a strand piece perpendicular to extrusion direction using a Leica RM 2155 microtome (Leica, Germany) equipped with a diamond knife at about -60 °C. The AFM measurements were carried out in the tapping mode by a Dimension 3100 NanoScope IV (Veeco, USA) (13).

Dynamic Mechanical Analysis (DMA)

The dynamic mechanical properties of the extruded strands were measured in accordance to EN ISO 6721-2 using a freely oscillating torsion pendulum at a frequency of 1 Hz under N₂ atmosphere. Samples of 50 mm length were cut from extruded strands and a gauge length 40 mm was used for the testing. The samples were rapidly cooled down to about -196 °C and oscillated with constant deformation amplitude smaller than 1 %. The heating rate was 2 K/min.

Continuity of PC in Blends by Selective Extraction of PC

After drying at 80 °C for 8 h strands of the blends (about 2 cm length, two for each composition) were immersed in 50 ml chloroform at room temperature for 4 days. After the first day the solution of the dissolved part of PC was replaced by fresh chloroform. The extracted strands were rinsed in fresh chloroform and dried at 105 °C until constant weight. The continuity (C) was calculated as $C = \text{dissolvable PC part} / \text{PC part in the blend}$, in which the 'dissolvable PC part' is the weight difference between the sample before and after extraction. The continuity gives a measure which part of the PC is involved in the continuous PC phase.

Results and Discussion

Morphology of Blends of PC-2 wt% MWNT with PE

The aim of blending a conductive PC composite with PE was to obtain a conductive blend at low contents of CNT. For this purpose, the PC-2 wt% MWNT (PC-2NT) composite was selected due to its conductive nature (11). In order to get conductive blends, a continuous structure of the filled PC phase is necessary. In other words, the filled PC should form the matrix of a dispersed blend or exhibit a continuous phase in a co-continuous blend. To achieve co-continuity in melt-mixed blends at low concentrations of one phase, this phase should have the lower melt viscosity under mixing conditions (10). Therefore, a high viscosity PE was selected (see Figure 8).

Fully co-continuous morphologies could be obtained in the composition range between 25 to 90 vol% of the filled PC phase. This was checked by morphological analysis and selective extraction of the PC from the extruded strands. Examples of the co-continuous morphology are shown in Figure 1 for SEM of cryofractured surfaces and in Figure 2 for AFM of a cryocut surface.

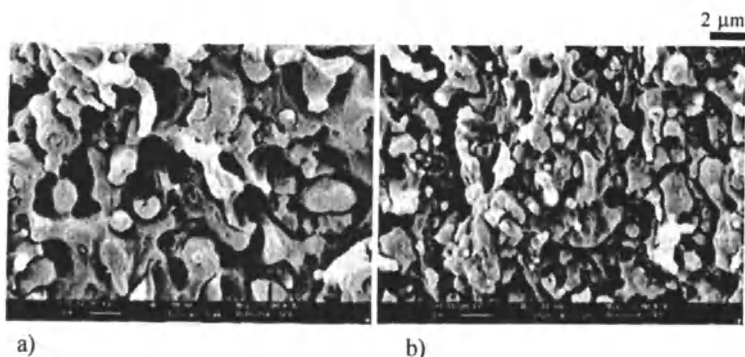


Figure 1. SEM of cryofractured strands of blends of PE with 45 vol% PC-2NT prepared at a) mixing speed of 50 rpm, b) mixing speed of 150 rpm

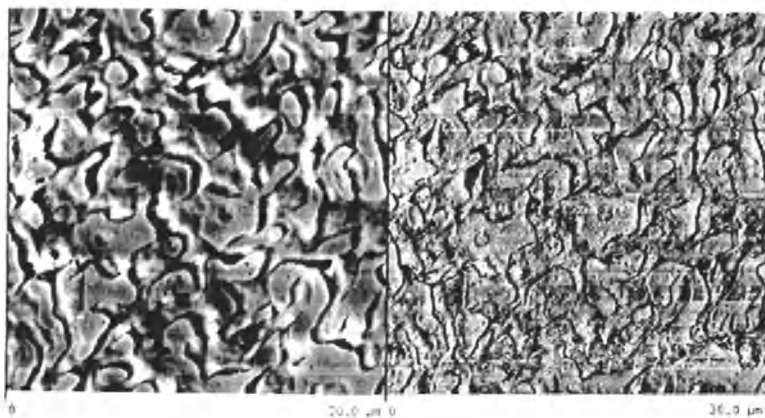


Figure 2. AFM of the blend PC-2NT/PE = 45/55 vol% (left height image, right phase image) (Reproduced with permission from reference 20. Copyright 2003 Elsevier)

From the AFM micrograph it evidences that the structure elements with the smoother surface having higher stiffness represent the PC. After selective extraction in chloroform for 4 days, the shapes of the strand pieces were unchanged for all blend compositions prepared and the dissolving experiment

was nearly quantitative (>90 %) starting at 25 vol% PC-2NT. However, even at 20 vol% PC-2NT 80 wt% of the PC take part in a continuous PC-phase. The continuity as calculated from the extraction experiments is shown in Figure 3.

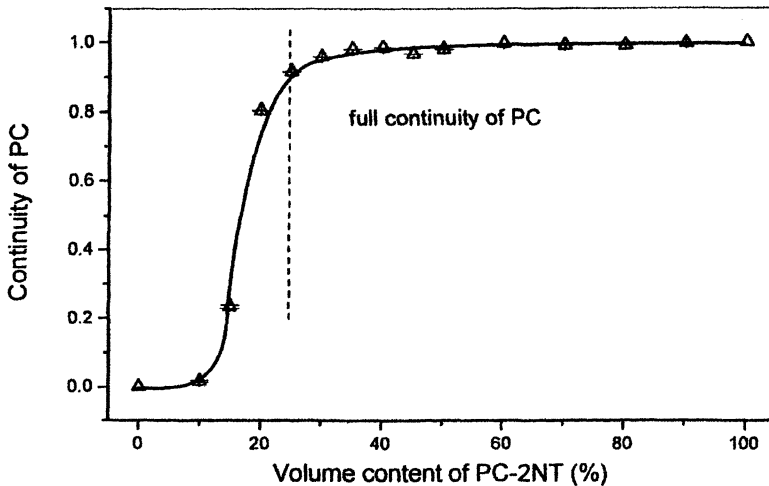


Figure 3. Continuity of PC in blends of PC-2NT with PE as calculated from selective extraction experiments

Figure 4 shows SEM micrographs of cryofractured extracted strands over the whole range of composition. It is seen, that the co-continuous structures are very fine with ligaments in the range of 1 μm . In addition, the fineness of the structure does not differ very much over composition.

Interestingly, even if the MWNT had been incorporated in the PC phase, the tubes are still visible in the extracted blends. The extruded strands have a black color even after extraction of the PC, whereas the dissolved part in chloroform did not show any black appearance. This indicates that the MWNT are still inside the extracted samples. According to the morphology as shown in Figure 5 some MWNT bridge the PC and PE phase with their ends. In the extracted blend samples, tubes are visible at the surface of the cryofractured strand. In Figure 5a), the tubes are partially visible in their whole length and in a stretched way. The true length can be seen much more clearly than in the AFM micrographs of composites (13) which is more than 10 μm for some tubes (20).

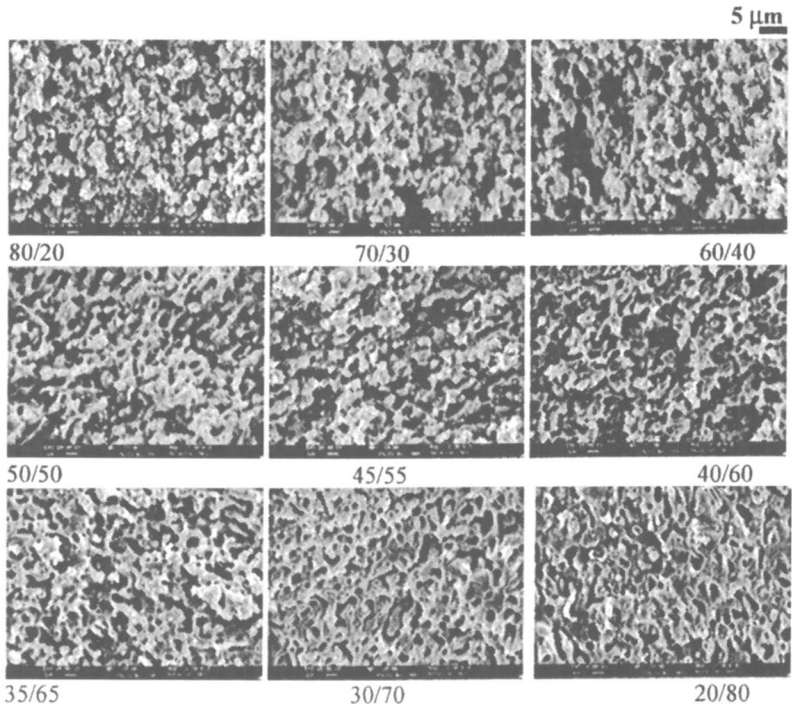


Figure 4. SEM micrographs of cryofractured extracted strands of different PC-2NT/PE (vol%) blends

Figure 5b shows that the observed tubes are not an artifact produced by cryofracturing the extracted strand. Here, AFM micrographs of cryocut surfaces are shown which indicate that the nanotubes bridging between the phases is already visible in the nonextracted cut sample as indicated by the circle (Fig. 5c). This bridging behavior indicates that the tubes were not aligned in the flow direction during the morphology development of the co-continuous blends during mixing. As we have shown in a previous paper (13), in composites of PC with MWNT the nanotubes do not align within the PC phase in extruded strands under the extrusion conditions selected. Even if the phase size of the PC is much lower in the blends with PE (about 1 μm) we may also assume that the MWNT fail to align within the PC phase in the co-continuous blends. In addition, there may be a tendency of nanotube migration towards the PE phase owing to their good affinity for polyolefins (9, 21,22).

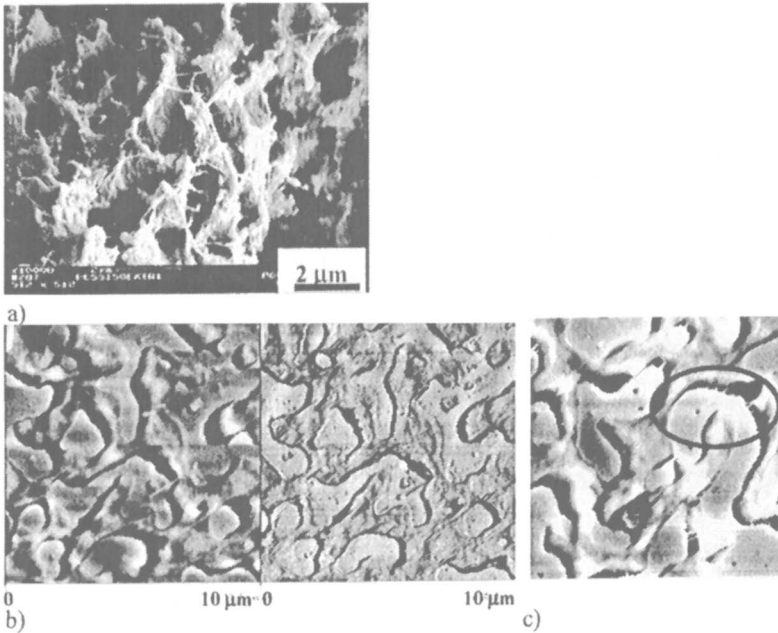


Figure 5. Nanotubes bridging the PE and PC phases in PC-2NT/PE=45/55 (vol%) blend. a) SEM micrograph of cryofractured extracted sample b), c) AFM micrographs of cut surface before extraction (left height image, middle phase image, right height image with picture frame $8 \times 7.7 \mu\text{m}$)

According to investigations on the mechanism of formation of co-continuous structures by melt mixing, the morphology development can be imagined as a breakup process of thin sheets of both components into a lacy like structure, to fibrous filaments or droplets (10). This breakup mechanism seems to be delayed by the nanotubes which enhances the viscosity of the filled component as well as hinder the breakup mechanically. The latter effect can be understood by the length dimensions of the tubes which is higher than the phase sizes (ligament sizes) in the blends. In addition, coalescence effects can be reduced in blends with a filled phase due to the viscosity enhancement (23). These stabilizing effects for the co-continuous morphology could be the reason that the co-continuous composition range is very broad in this system and that the morphology fineness does not differ very much at different compositions.

Figure 6 shows the effect of mixing time on the morphology. As it was shown in Figure 1, enhanced screw speed produces the same type of morphology but smaller phase sizes. Prolongation of the mixing time from 5 min to 15 min indicates that the co-continuous morphology is not an intermediate structure as a

result of a phase inversion process but a stable morphology type. The morphology fineness is nearly unchanged, however, it appears that the bridging behavior of the MWNT is reduced indicating nanotube breaking.

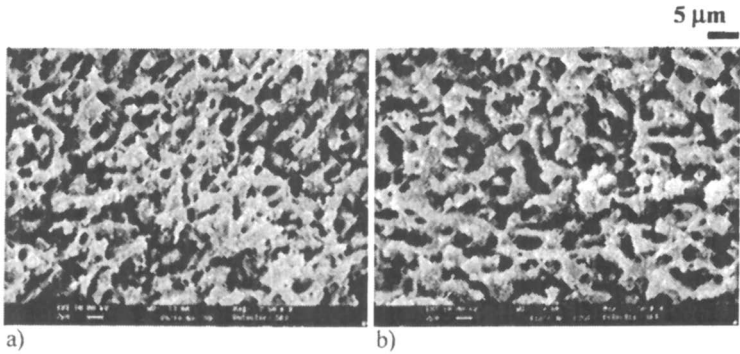


Figure 6. SEM of cryofractures of extracted PC-2NT/PE = 45/55 (vol%) blends a) mixed at 50 rpm for 5 min b) mixed at 50 rpm for 15 min

Electrical Conductivity in Blends of PC-2 wt% MWNT with PE

Electrical conductivity measurements revealed that the conductivity of the blends is strongly related to the type of morphology. As shown in Figure 7, a significant increase in conductivity by about 9 decades was observed starting at 25 vol% PC-2NT which correlates to the lowest PC-2NT composition of the fully co-continuous range.

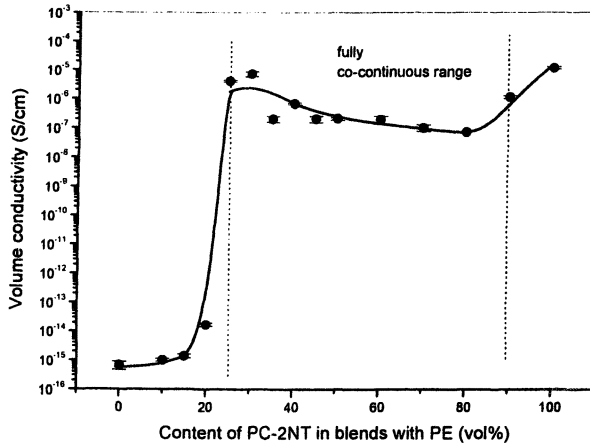


Figure 7. Volume conductivity vs. PC-2NT content in blends with PE

The conductivity values of the co-continuous blends are lower than that of the PC-2NT phase itself maybe due to the penetration of parts of the nanotubes in the high viscous PE phase which results in reducing the number of nanotube-nanotube contacts. In addition, nanotube breakup can also be assumed to occur during the melt blending procedure. The reduction in conductivity of the PC-2NT ($2 \cdot 10^{-3}$ S/cm) after the additional blending extrusion step (10^{-5} S/cm) is an indication of the above mentioned assumption. As shown in (20) conductivity values of the blends are decreased when using longer mixing time during the blending. This is in accordance with the observation in Figure 6 that the nanotube bridging effect seems to be reduced after longer mixing. Such nanotube shortening may occur also at short mixing times and seems to occur not only in bulk of the PC phase but predominantly at the interface between both phases leading to breakage of the bridging MWNT. The tendency of decreasing conductivity values between 25 and 80 vol% PC-2NT indicates that the MWNT attrition in the co-continuous blends is probably more pronounced at higher PC-2NT content.

Similar results of a significant decrease in the filler content required to achieve a certain conductivity value by using co-continuous blend morphologies were recently reported by Meincke et al. (24) on a PA6/ABS = 50/50 blend system. To get conductivity values of 10^{-7} S/cm (as obtained in our study over a broad composition range) about 6 wt% of the same kind of MWNT as used in our study were needed in pure PA6 but only about 2.5 wt% in case of a co-continuous PA6/ABS = 50/50 wt% blend in which the MWNT were first melt mixed into PA6 using the masterbatch dilution technology.

Rheological Behavior of Blends of PC-2 wt% MWNT with PE

The dynamic spectrum of shear storage modulus, G' , of two selected blends, and the blend components at 260°C is logarithmically plotted against the angular frequency in Figure 8. The storage modulus is the reflection of the sample elasticity. Figure 8 shows a significant increase in G' of PC by the incorporation of 2wt% MWNT into neat PC due to the percolation structure formation. This increase is more noticeable at low frequency and G' of PC-2NT becomes nearly flat. The addition of 30 and 70 vol % PE to PC-2NT increases the G' modulus in particular more significantly at low frequency. In addition, at very low frequency, the values of G' of the blends with 30 and 70 vol% PE are higher than that of neat PE. This is related to the co-continuous structure formation as reported in the literature (10). Moreover, G' of neat PE is higher than this of neat PC and PC-2NT. In Figure 9, the complex viscosity, $|\eta^*|$, of blends and blend components is presented as a function of frequency. In the case of neat PC, at low frequency the Newtonian plateau is clearly seen at which the viscosity is independent on the frequency, in contrast to $|\eta^*|$ of PC-2NT and the blends. The

complex viscosity of PC-2NT and blends rises with decreasing the frequency due to the percolation and co-continuous formation as discussed before in G' .

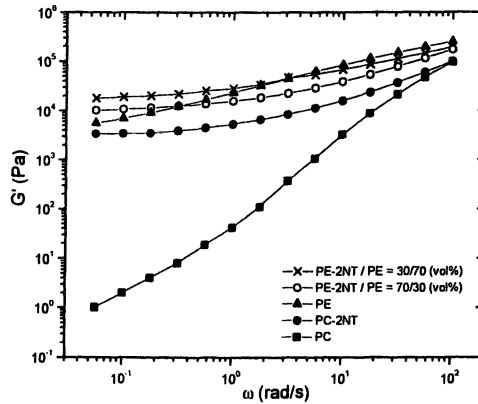


Figure 8: G' vs. frequency for PE/PC-2NT blends and blend components

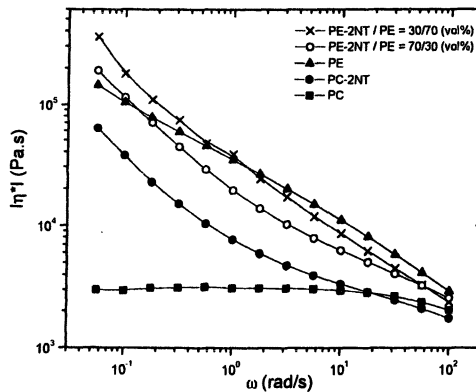


Figure 9: $|\eta^*|$ vs. frequency of PE/PC-2NT blends and blend components

Dynamic Mechanical Behavior of Blends of PC-2 wt% MWNT with PE

Figures 10 and 11 show the dynamic mechanical behavior of two selected blend compositions and the blend components. It is clearly seen that the blends are immiscible. In the blends, the glass transition (T_g) of PE and of PC appear at temperatures corresponding to those of the blend components. The β -relaxation of PC is visible as a shoulder in the blends due to the similar temperature position in relation to the T_g of PE. On the other hand, the melt region of

crystallites of PE (T_m) and α' -relaxation of PC appear very close to each other and show a common transition in the blends which is visible as a slightly moved T_m peak of PE with a shoulder at the high temperature side corresponding to the PC part. But the changes in the shape and position of the relaxation of the PE in this region are also can be caused by morphological modifications (crystallinity, size of crystallites) during blending.

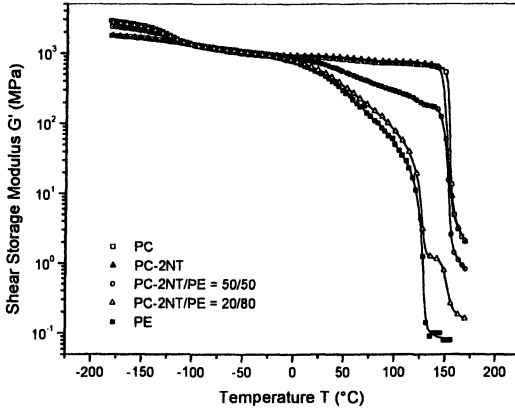


Figure 10. Shear storage modulus G' of PE, PC, PC-2NT, and two blends

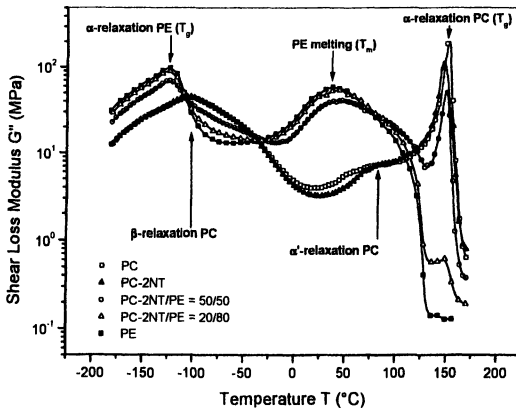


Figure 11. Shear loss modulus G'' of PE, PC, PC-2NT, and two blends (relaxation processes of PC were assigned according to Bauwens-Crowet (25))

The addition of 2 wt% MWNT to PC leads to a small increase in G' up to 150°C and a slight decrease in T_g of PC. The PC-2NT/PE=50/50 blend clearly shows that PC forms a continuous phase since a sharp drop in G' starts at the

glass transition temperature corresponding to PC and PC-2NT. At the T_m of PE, only a small drop of G' appears. From the G' behavior it is also visible that some amount of the PC-2NT in the blend with 80 vol% PE forms a continuous structure. After the decrease in G' at the temperature typical for PE melting, a small plateau appears up to the temperature where the α -relaxation of the PC occurs. This is in accordance to the result from the selective extraction, where it was found that about 80 wt% of the filled PC contributes to a continuous PC structure. These results indicate that the nanotube addition does not lead to a compatibilization effect in the blend system even if the nanotubes contribute to bridge the phases mechanically.

Summary and Conclusion

Blends of polycarbonate filled with MWNT and polyethylene have been prepared. The aim of blending a conductive PC composite with PE was to obtain a conductive blend at low contents of carbon nanotubes by using the double percolation concept and forming co-continuous blend morphologies. For this purpose, a composite of PC with 2 wt% MWNT was selected due to its conductive nature. In the melt mixed blends, fully co-continuous morphologies could be obtained in the composition range between 25 to 90 vol% of the filled PC phase which was checked by selective extraction of the PC from the extruded strands. The co-continuous structure is very fine with ligaments in the range of 1 μm and shows only marginal differences in phase size with blend composition.

Significantly enhanced conductivity of the blends could be achieved exactly in the same composition range where PC forms a continuous phase, i.e. starting at 25 vol% filled PC. Even if the blends conductivity values are not in the range of 'conductive materials' ($>10^{-4}$ S/cm) their conductivity is in the range of dissipative materials. At a composition of 25 vol% filled PC the total content of MWNT in the blend is only 0.34 vol%. Thus, the concept of double percolation also works for co-continuous blends with carbon nanotubes in one phase.

Interestingly, even if the MWNT had been incorporated in the PC phase, nanotubes are still visible in samples after extraction of PC. SEM investigations revealed, that some of the MWNT are found to bridge the PC and PE phase at least with their ends. This can be understood by the length dimensions of the tubes which is higher than the phase sizes in the blends and a tendency of the tubes to migrate to the PE phase. The bridging effect and the high melt viscosity of both components leads to excellent blend stability and a broad co-continuous composition range. The MWNT bridging the phases seem to have a higher breakage tendency during processing, thus leading to lower conductivity values as compared to the MWNT filled PC component. The results showed also that the storage modulus and complex viscosity are increased by the incorporation of MWNT into PC and with the blending of PC composite with PE.

Acknowledgement. We thank Hyperion Catalysis International, Inc. for supplying the masterbatch and Dr. T. D. Fornes (University of Texas at Austin, USA) for preparing the composite of PC with 2 wt% MWNT by extrusion.

References

1. Utracki, L. A. Polycarbonate blends, chapter 18 in: Commercial Polymer Blends Chapman & Hall, 1st ed. London, **1988**, 384ff.
2. Li, F.; Cheng, H.M.; Bai, S.; Su, G.; Dresselhaus, M.S. *Appl. Phys. Lett.* **2000**, *77*, 3161.
3. Kunori, T.; Geil, P. H. *J. Macromol. Sci.-Phys.* **1980**, *B18*, 93.
4. Kunori, T.; Geil, P. H. *J. Macromol. Sci.-Phys* **1980**, *B18*, 135.
5. Li, C.; Zhang, Y.; Zhang, Y.; Zhang, C. *Europ. Polym. J.* **2003**, *39*, 305.
6. Sandler, J.; Shaffer, M.S.P.; Prasse, T.; Bauhofer, W.; Schulte, K.; Windle, A.H. *Polymer*, **1999**, *40*, 5967.
7. Andrews, R; Jacques, D.; Minot, M.; Rantell, T. *Macromol. Mat. Eng.* **2002**, *287*, 395.
8. Hagerstrom, JR.; Greene, S.L. Electrostatic dissipating composites containing Hyperion fibril nanotubes. Commercialization of Nanostructured Materials, Miami, USA, April 7, **2000**.
9. Sumita, M.; Sakata, K.; Asai, S.; Mijasaka, K.; Nagakawa, H. *Polymer Bulletin* **1991**, *25*, 265.
10. Pötschke, P.; Paul, D.R. *J. Macromol. Sci.: Polymer Reviews* **2003**, *C43*, 87.
11. Pötschke, P.; Fornes, T.D.; Paul, D.R. *Polymer* **2002**, *43*, 3247.
12. Pötschke, P.; Bhattacharyya, A.R.; Goering, H. *Comp. Interf.* **2003**, *10*, 389.
13. Pötschke, P.; Bhattacharyya, A.R.; Janke, A. *Eur. Polym. J.* **2004**, *40*, 137.
14. Pötschke, P.; Alig, I.; Dudkin, S. *Polymer* **2003**, *44*, 5023.
15. Pötschke, P.; Bhattacharyya, A.R.; *Polym. Prepr.* **2003**, *44*(1), 760.
16. Pötschke, P.; Paul, D.R. *Macrom. Symp.* **2003**, *198*, 69.
17. Jafari, S.H.; Pötschke, P.; Stephan, M.; Warth, H.; Alberts, H. *Polymer* **2002**, *43*, 6985.
18. Jafari, S.H.; Pötschke, P.; Stephan, M.; Pompe, G.; Warth, H.; Alberts, H. *J. Appl. Polym. Sci.* **2002**, *84*, 2753.
19. Pötschke, P.; Wallheinke, K.; Stutz, H. *Polym. Engng. Sci.* **1999**, *39*, 1035.
20. Pötschke, P.; Bhattacharyya, A.R.; Janke, A. *Polymer* **2003**, *44*, 8061.
21. Gubbels, F.; Blacher, S.; Vanlathem, E.; Jérôme, R.; Deltour, R.; Brouers, F.; Teyssié, Ph. *Macromolecules* **1995**, *28*, 1559.
22. Zhang, C.; Han, H.F.; Yi, X.S.; Asai, S.; Sumita, M. *Comp. Interf.* **1999**, *6*, 227.
23. Roland, C.; Böhm, G.G.A. *J. Polym. Sci. , Polym. Ed.* **1984**, *22*, 79.
24. Meincke, O.; Kaempfer, D.; Weickmann, H.; Friedrich, C.; Vathauer, M.; Warth, H. *Polymer* **2004**, *45*, 739.
25. Bauwens-Crowet, C. *J. Mat. Sci.* **1999**, *34*, 1701.

Modeling of Poly(bisphenol A carbonate)

Chapter 14

Advanced Solution Characterization of Polycarbonate Materials across the Molecular Weight Distribution

Arno Hagens^{1,3}, Bernard Wolf², and Christian Bailly^{1,*}

¹Laboratoire des Hauts Polymères, Université Catholique de Louvain,
1348 Louvain-la-Neuve, Belgium

²Institut für Physikalische Chemie der Universität Mainz, Jakob-Welder
Weg 13, 55099 Mainz, Germany

³Current address: GE Plastics, Plasticslaan 1, 4612PX Bergen op Zoom,
The Netherlands

The microstructure of polycarbonate homo- and copolymers is investigated across the molecular weight distribution with the help of narrowly dispersed fractions obtained by Continuous Polymer Fractionation (CPF). The experimental distribution of branching units in melt-polymerized polycarbonate is compared with predictions obtained from a simulation model. Experiments and simulations with mixed fractions are also used to study redistribution processes affecting melt-polymerized polycarbonate. The applicability limits of CPF for the fractionation of copolymers is evaluated for the first time by a study on PC-siloxane copolymers. Copolymers with statistically distributed segments can be fractionated without compositional bias only to the extent that all chains have the same average composition, which is not the case for chains carrying a small number of long comonomer segments.

Introduction

Many important chemical and physical characteristics of polymers containing structural heterogeneities (e.g. branching units, co-monomers or functional groups) are strongly dependent on details of the molecular microstructure. Unfortunately, this effect is often compounded with the influence of molecular weight distribution (MWD). It is therefore highly desirable to gain access to the distribution of microstructural features across the MWD instead of relying on one "global" structure index. It is even more interesting to obtain sizable amounts of narrow molecular weight fractions since it then becomes possible to test the fractions separately or in combination and hence clarify the interplay between microstructure, molecular weight and properties.

While structure-property relationships have been thoroughly investigated for industrially important classes of polymers such as polyolefins and polyesters based on the characterization of narrowly dispersed fractions obtained from preparative fractionation techniques like Temperature Rising Elution Fractionation (TREF) and Successive Solution Fractionation (SSF), no such systematic studies have been carried out for polycarbonate materials. Bisphenol-A based polycarbonate (BPA-PC, Figure 1) is an especially interesting polymer to study for a number of reasons. Firstly, it is an important thermoplastic engineering material which has uses in a wide range of applications including building and construction, automotive, electronic and consumer products. Secondly, BPA-PC can be made via different polymerization routes and its chemical microstructure can be modified in various ways through incorporation of branching units, co-monomers and functional groups. Hence, a large variety of microstructurally different PC materials is readily available for research. In addition, the amorphous structure of BPA-PC simplifies its chemical characterization.

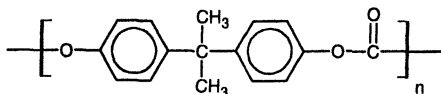


Figure 1: BPA-PC structure.

BPA-PC synthesis

Currently, BPA-PC is produced on an industrial scale either by interfacial phosgenation or melt-transesterification processes [1]. In the interfacial process, an aqueous solution containing BPA and an organic solvent containing phosgene are mixed, whereupon polycarbonate is formed at the interface between the two immiscible phases. In the melt-transesterification process, BPA and diphenyl carbonate (DPC) are reacted as pure components under reduced pressure and at high temperatures. The melt-transesterification technology has several advantages over the interfacial process since the use of large volumes of organic solvents and highly toxic phosgene is avoided. Moreover, the final resin contains a much lower level of residual contaminants and has a more consistent colour. In contrast, the elevated temperatures used during the melt-polymerization process may lead to side reactions resulting in the formation of branching products. The most widely accepted mechanism for thermal rearrangements of PC in the melt is a base-catalyzed Kolbe-Schmitt reaction [2]. The following structures have been shown to result from this mechanism: phenyl salicylate (PhSAL, structure I), phenyl salicylate phenyl carbonate (PhSALPhC, structure II) and phenyl-*o*-phenoxy benzoate (Ph-*o*-PhxBz, structure III) [2-4]. The corresponding PC structures are shown in Figure 2. PhSALPhC structures are being formed upon reaction between the hydroxyl group of a PhSAL unit and a carbonate group of an arbitrary polycarbonate chain. Ph-*o*-PhxBz structures are being formed in a concerted rearrangement reaction of polymer chains with the concomitant release of CO₂.

In addition, interfacially and melt-polymerized PC show two significant structural differences:

1. Interfacial PC is normally fully end-capped (usually with phenyl carbonate end-groups). By contrast, melt-polymerized PC contains a significant residual concentration of uncapped end-groups (bisphenol monocarbonate) [2].
2. Due to fast redistribution reactions occurring during polymerization melt-polymerized PC is characterized by a "thermodynamic" most probable Flory molecular weight distribution (MWD) whereas interfacial polymerization is kinetically controlled, leading to a different (although similar) distribution [1].

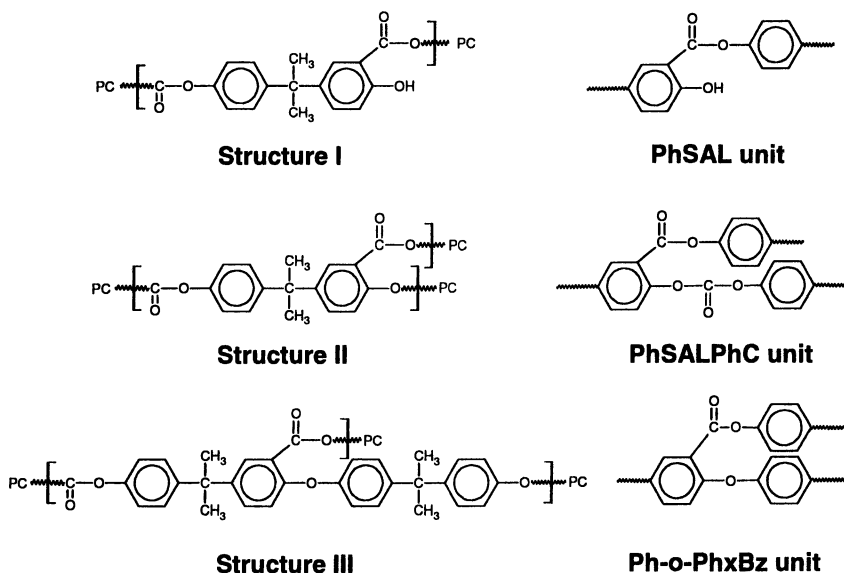


Figure 2: Polycarbonate melt rearrangement structures.

Polycarbonate-Siloxane Copolymers

Polycarbonate-siloxane (PC-Si) copolymers were first introduced in the mid 1960's and are characterized by an outstanding thermal stability, good weathering properties, excellent flame retardancy and high impact resistance at low temperature [5-9]. PC-Si materials are now used in numerous applications including windows, roofing, contact lenses and gas-permeable membranes. A large group of bisphenol end-capped oligo-siloxanes are known to form useful copolymers with polycarbonate. A particularly interesting polysiloxane block is obtained by reacting hydrosilane-capped oligo-dimethylsiloxane with eugenol (4-allyl-2-methoxyphenol) using the well known hydrosilation reaction. Eugenol is readily available as a synthetic or as a natural product. The resulting α,ω -capped polysiloxane can be copolymerized with bisphenol-A to form a PC-Si copolymer [10,11]. The general structure of a PC/Eugenol-siloxane (PC-EuSi) copolymer is shown in Figure 3. PC-Si copolymers can be made via different synthetic routes including interfacial phosgenation and melt polymerization processes [5].

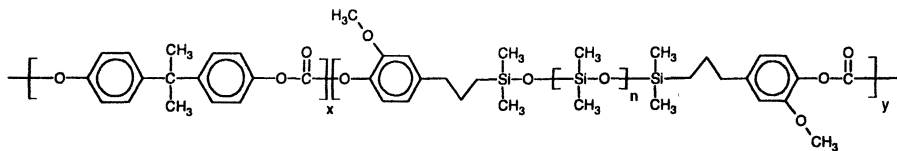


Figure 3: Generic structure of a BPA-Polycarbonate/Eugenol-siloxane copolymer.

Objectives

In this paper, we review our recent studies on the fractionation and structural characterization across the MWD of PC homopolymers and siloxane copolymers [12-14]. The assessment of the branching structure distribution across the MWD is discussed for BPA-PC materials made via a melt transesterification process. Experimental results are compared with predictions obtained from a simulation model. Thermally induced processes affecting the MWD of BPA-PC materials made via interfacial phosgenation and melt transesterification processes are also addressed. The general applicability of CPF for the fractionation of copolymers is discussed, based on the results obtained of the PC-siloxane copolymers.

Preparative Fractionation of Polycarbonate

In the early years of polymer research, fractionation was mainly applied for determination of the molecular weight distribution of polymers, a property that nowadays can be satisfactorily obtained by using chromatographic techniques such as Size Exclusion Chromatography (SEC). At present, the interest in polymer fractionation mainly lies in obtaining preparative quantities of narrowly dispersed fractions that can be used for further analysis. The large scale fractionation of polymers presents typical problems such as the necessity to use large volumes of solvents, very long fractionation times and the need for specially designed equipment [15-17].

In many cases, a particular polymer can be fractionated by more than one method and its choice depends on the desired objectives of the fractionation, i.e. the number of fractions, fraction distribution and fraction size. Polycarbonate can be fractionated by most common fractionation methods (Table I).

Table I: Fractionation methods for polycarbonate materials.

<i>Fractionation method</i>	<i>Reference</i>
Precipitation fractionation	18-31
Film extraction fractionation	2,32
Stepwise elution column fractionation	33-36
Baker-Williams fractionation	37
Coacervate fractionation	33
Preparative Size Exclusion Chromatography	38
High Osmotic Pressure Chromatography	39
Continuous Polymer Fractionation	40

For the work presented in this paper, narrowly dispersed, multi-gram size fractions of controlled molecular weight were desirable. Continuous Polymer Fractionation fulfills these requirements the best and was selected as method of choice.

Continuous Polymer Fractionation

Continuous polymer fractionation (CPF) has been developed as a technique capable of producing large quantities of narrowly distributed molecular weight fractions. Theoretical principles for CPF were first exposed by Englert and Tompa [41] while Wolf and co-workers developed the actual technique in practical form and applied it to different classes of polymers [42,43]. In CPF, fractions of increasing molecular weights are removed from a concentrated polymer solution by a countercurrent liquid-liquid extraction with a single solvent or solvent/non-solvent mixture.

Experimental

Samples

PC1 and PC2 are lab-synthesized polycarbonate samples made by a melt-transesterification (MT) process from BPA and diphenyl carbonate, using literature-described procedures [44,45]. PC3 is an industrial sample obtained

from an interfacial phosgenation (IP) process. Characterization data for the three samples are given in Table II.

PC-SIL1 and PC-SIL2 are lab synthesized PC/Eugenol-siloxane copolymers obtained from an interfacial phosgenation process. PC-SIL1 contains 10 weight % Eugenol capped siloxane oligomer with a degree of polymerization of 2 ($n=0$ on average in Figure 3) and PC-SIL2 contains 5 weight % Eugenol capped siloxane oligomer with a degree of polymerization of 23 ($n=21$ on average in Figure 3). Characterization data for both samples are given in Table III.

Table II: Characterization data for PC homopolymers.

<i>Sample name</i>	<i>Polym. process</i>	<i>M_w</i> (g/mol)	<i>M_n</i> (g/mol)	<i>D</i>	<i>Modified units</i>		<i>Hydroxyl Endgroups</i> (ppm)
					<i>PhSAL</i> (ppm)	<i>PhSALPhC</i> (ppm)	
PC1	MT	21,700	9,520	2.28	n.d.	1250	570
PC2	MT	23,700	9,210	2.57	1795	3465	1185
PC3	IP	23,200	9,270	2.50	n.d.	n.d.	<20

Table III: Characterization data for PC/Eugenol-siloxane copolymers.

<i>Sample name</i>	<i>M_w</i> (g/mol)	<i>M_n</i> (g/mol)	<i>D</i>	<i>w%</i> <i>Siloxane</i>	<i>Siloxane block length</i>
PC-SIL1	49,400	21,200	2.33	10.1	2.2
PC-SIL2	69,600	24,800	2.81	5.3	23.3

Continuous Polymer Fractionation

Details of the equipment and operating conditions have been reported elsewhere [12,13].

Size Exclusion Chromatography (SEC), NMR and thermal analysis

Experimental details on the SEC and NMR methods have been reported in reference [12] for PC homopolymers and [13] for PC-siloxane copolymers. Details on the thermal analysis method have been reported in reference [14].

Results and Discussion

CPF of PC Homopolymers

Samples PC1 to -3 (cf. Table II) were fractionated using CPF. Previous studies have shown that a solvent/non-solvent mixture consisting of methylene chloride (MCH) and diethylene glycol (DEG) is a suitable system for the fractionation of linear PC materials [46].

After each fractionation step, a high MW gel fraction and a low MW sol fraction were collected. For subsequent fractionation steps, either the gel phase was used directly or after isolation of the polycarbonate fraction. Finely dispersed PC powders were obtained from sol and gel fractions by subsequent evaporation of MCH and extraction of DEG using methanol. Fractionation efficiency is in the range of 90-95% for all samples. Samples PC1, PC2 and PC3 were fractionated into three, four and three fractions respectively.

It will be outlined later in this section, that the fractionation of PC1 and -2, which contain branching units, is carried out solely according to MW and is *not* influenced by the branching architecture.

Characterization data for the fractions of PC1 (PC1F1 to 3), PC2 (PC2F1 to 4) and PC3 (PC3F1 to 3) are given in Table IV.

CPF of PC-Siloxane Copolymers

Copolymers are especially difficult materials to fractionate because their solubility not only depends on molecular weight, like for homopolymers, but also on differences in chemical composition (CC). In addition, copolymers with the same overall CC but differing in microstructure might have a different solubility behaviour. If the effect of CC is small, fractionation can be carried out analogously to the fractionation of a homopolymer. If both CC and MW

influence fractionation, changes in temperature or solvents may lead to different results and fractions are obtained that differ in MW as well as CC.

Table IV: Characterization data for PC homopolymer fractions.

<i>Sample name</i>	<i>M_w</i> (g/mol)	<i>M_n</i> (g/mol)	<i>D</i>	<i>Modified units</i>	
				<i>PhSAL</i> (ppm)	<i>PhSALPhC</i> (ppm)
PC1	21,700	9,520	2.28	n.d.	1250
PC1F1	11,400	6,590	1.73	n.d.	760
PC1F2	17,700	11,570	1.53	n.d.	1220
PC1F3	31,900	24,100	1.32	n.d.	1870
PC2	23,700	9,210	2.57	1795	3465
PC2F1	11,900	6,330	1.87	1670	2045
PC2F2	22,100	14,120	1.57	1820	3535
PC2F3	28,900	19,090	1.51	1760	4005
PC2F4	39,200	24,950	1.57	1855	5190
PC3	23,200	9,270	2.50	n.d.	n.d.
PC3F1	13,200	6,110	2.16	n.d.	n.d.
PC3F2	23,600	15,150	1.56	n.d.	n.d.
PC3F3	37,700	26,550	1.42	n.d.	n.d.

No methods for the large scale fractionation of PC-siloxane copolymers are described in literature. As a starting point for the CPF experiments conducted here, experimental conditions as applied for the fractionation of PC-homopolymers were taken. The combination of methylene chloride and diethylene glycol appeared to be a suitable solvent mixture. PC-SIL1 and PC-SIL2 were fractionated into six and four fractions respectively.

As will become clear in the section on the characterization of PC-siloxane copolymers, PC-SIL1 was fractionated by MW only while PC-SIL2 was fractionated by both MW and CC.

Characterization data for the fractions of PC-SIL1 (PC-SIL1F1 to 6) and PC-SIL2 (PC-SIL2F1 to 4) are given in Table V.

Table V: Characterization data for PC/Eugenol-siloxane copolymer fractions.

<i>Sample name</i>	<i>M_w</i> (g/mol)	<i>M_n</i> (g/mol)	<i>D</i>	<i>w%</i> <i>Siloxane</i>	<i>Siloxane</i> <i>block length</i>
PC-SIL1	49,400	21,200	2.33	10.1	2.2
PC-SIL1F1	24,100	11,500	2.10	10.1	2.3
PC-SIL1F2	25,300	13,700	1.85	10.1	2.3
PC-SIL1F3	27,500	14,100	1.96	9.8	2.3
PC-SIL1F4	72,700	50,400	1.44	9.7	2.3
PC-SIL1F5	16,700	9,700	1.72	10.1	2.3
PC-SIL1F6	37,900	26,200	1.45	9.6	2.4
PC-SIL2	69,600	24,800	2.81	5.3	23.3
PC-SIL2F1	87,100	52,300	1.67	4.0	22.1
PC-SIL2F2	25,300	11,100	2.28	8.0	24.8
PC-SIL2F3	31,000	12,300	2.51	7.0	24.8
PC-SIL2F4	66,800	38,900	1.71	4.3	23.0

Determination of the Branching Distribution of Melt-polymerized PC

It is well-known that branching can have a significant influence on the rheological and mechanical properties of polymers and a detailed understanding of the branching distribution is therefore of major importance. For melt-polymerized PC, this distribution has never been studied in detail.

In PC1 and PC2, only PhSAL and PhSALPhC structures are present as evidenced by NMR analysis; Ph-*o*-PhxBz structures were not detected. For an accurate determination of the branching structure distribution, the fractionation should be carried out solely according to MW and not to some extent also according to branching architecture. Two indications confidently guarantee that this is indeed the case. Firstly, the overall branching density of the investigated PC samples is very low (the number of branching units per chain is less than 0.5 for unfractionated polymers and derived fractions [12]). Secondly, as will become clear from simulation experiments discussed later in this section, there is an excellent agreement between experimental and simulated branching densities of the samples.

Figure 4 shows the concentration of PhSAL and PhSALPhC units as a function of number average molecular weight for PC1 and -2 and derived fractions. The concentration of PhSAL units in PC2 is fraction MW independent indicating homogeneous incorporation in the polymer i.e., the thermal rearrangement reaction leading to PhSAL structures is not molecular weight dependent. The concentration of PhSALPhC units however increases quasi-linearly with MW indicating that PhSALPhC branching units are not homogeneously distributed across the molecular weight distribution.

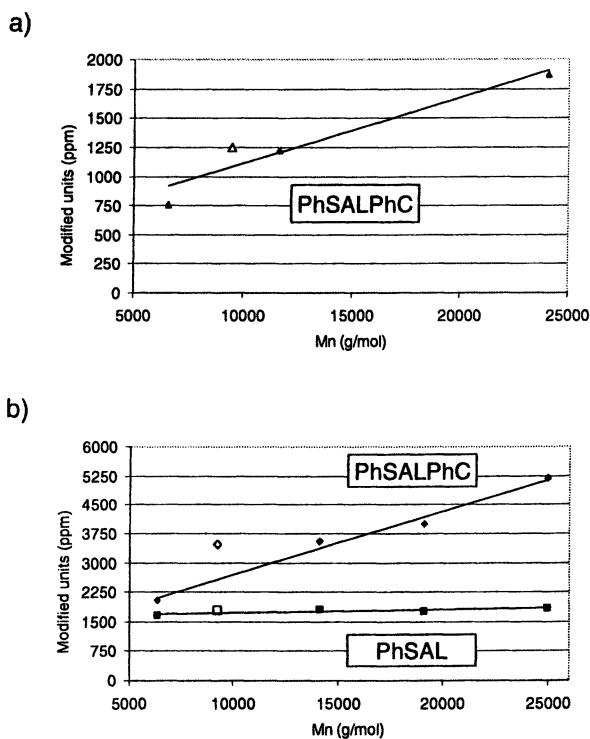


Figure 4: PhSAL and PhSALPhC concentration as a function of Mn for a) PC1 and b) PC2; closed symbols denote the fractions, open symbols the unfractionated polymer.

Simulations

In order to validate experimental results, a Monte Carlo simulation model was developed based on a random sampling technique (details in reference [12]). The molecular weight, endgroup and branching data of samples PC1 and PC2 were used as input parameters for the model. The polymers were then "rebuilt" by a statistical simulation process. Figure 5 compares the simulated branching density for PC1 as a function of molecular weight (solid line) with the experimental data (dots). The branching density initially increases with MW and reaches a plateau for very high molecular weights. The results are qualitatively identical for PC2. The simulation results for PC are similar to literature described models for branching density distributions of addition polymers despite the fact that the branching mechanisms are quite different [47,48]. Excellent agreement is obtained between experimental and simulated data.

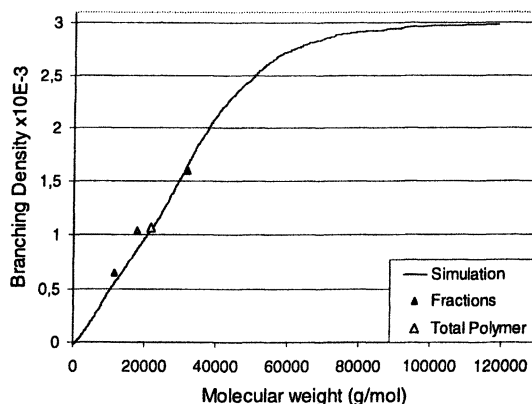


Figure 5: Simulated and experimental branching density as a function of molecular weight for the total (unfractionated) polymer and fractions of PC1.

The observed branching density and concentration of branching units with increasing MW reflects that under statistical "thermodynamic" control, branched chains will "on average" be longer than linear chains, thus concentrating branching points in the high MW fractions. As can be derived from Figure 5, this effect only disappears at very high MW, beyond the experimental reach for PC.

Thermally Induced Redistribution of Fractionated PC

In a typical redistribution process, polymer chains split and recombine continuously, resulting in a visible MWD change until the most probable Flory distribution ($D=2$) is reached. There is no net change in the total number of chains and, as a result, the number average molecular weight, M_n , remains unaffected. Redistribution in polycarbonate can take place via hydroxyl end-groups and by carbonate interchange. The interchange route usually proceeds extremely slowly and PC-redistribution mainly occurs via hydroxyl end-groups.

Redistribution of mixed BPA-PC fractions made via the interfacial process

PC3 fractions 1 (low MW) and 3 (high MW) were mixed in a 1:1 w/w% ratio and subjected to thermal treatment in order to visualize and quantify redistribution processes (see reference [14] for details). The original bimodal MWD of the fraction mixture remains unaffected under all experimental conditions, indicating that no significant redistribution has taken place. Due to the very low hydroxyl end-groups concentration of interfacial PC, redistribution can only take place via the slow carbonate interchange route which, if occurring at all, does not modify the MWD under the used conditions.

Redistribution of mixed BPA-PC fractions made via melt-transesterification

When 1:1 w/w% mixtures of the lowest and highest MW fractions of PC1 and PC2 respectively were subjected to thermal treatment, the initial bimodal MWD gradually shifted to a unimodal distribution indicating that redistribution had taken place. Figure 6 shows experimental results for PC2 upon prolonged thermal treatment at 225°C. Most of the visible shift occurs within the first minutes, suggesting a very fast redistribution rate

Simulations

A Monte Carlo model was implemented to simulate redistribution processes (details in reference [14]). In a number of simulation cycles an "attacker" chain attacks at a random monomer of a "victim" chain and two chains with new individual lengths are formed while the combined length remains unchanged. To provide a correct picture of the process kinetics, care has to be exercised to give the correct statistical weights to the "attackers" and "victims". The total number of chains and, hence, M_n has to remain constant which allows for an internal check of the simulation.

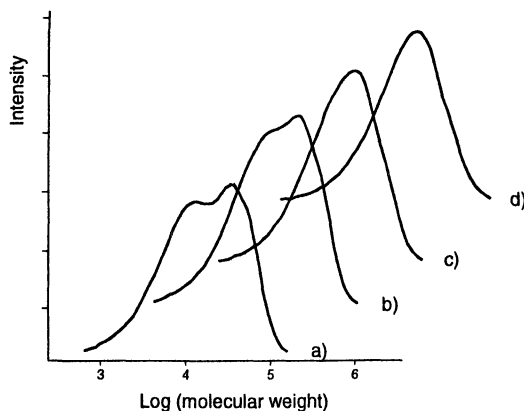


Figure 6: MWD for a 1:1 w/w% mixture of PC2 fractions 1 and 4 heated at 225°C, a) t = 0 min., b) t = 1 min., c) t = 3 min., d) t = 6 min.

Figure 7 shows the simulated MWD of a 1:1 w/w% mixture of fractions 1 and 4 of PC2 for an increasing number of simulation cycles. The bimodal MWD of the fraction mixture rapidly changes to a unimodal peak which remains unchanged when a polydispersity of 2 has been reached, i.e. the Flory distribution.

Matching of the experimental and simulated MWD was found to be only feasible for short heating times and temperatures not higher than 250°C. Under more abusive conditions, competing post-condensation and hydrolysis reactions obscure the effects of pure redistribution.

From experimental and simulation data, it can be calculated that approximately half a percent of all carbonate groups reacts per minute at 250°C. This conclusion is valid for PC1 as well as PC2.

Characterization of Fractionated Polycarbonate-Siloxane Copolymers

Characterization of unfractionated copolymers

Microstructure of the unfractionated copolymers was determined using ¹³C-NMR. The measured composition for PC-SIL1 and PC-SIL2 samples is very close to the theoretical composition for completely statistical copolymers [13]. The distribution of siloxane species across the MWD was assessed using on- and off-line SEC-IR hyphenating techniques.

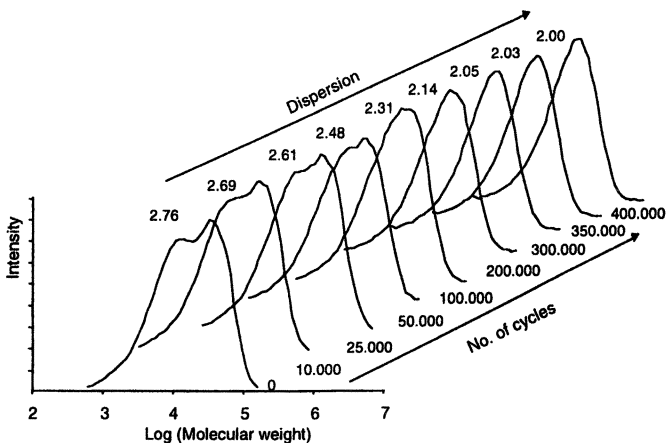


Figure 7: Simulated MWD for a 1:1 w/w% mixture of PC2 fractions 1 and 4 at an increasing number of simulation cycles.

Using off-line SEC-FTIR, the copolymers were analyzed for peak height at 1051 cm^{-1} for the siloxane and at 1082 cm^{-1} for the BPA-PC component in the FTIR spectrum. A plot of peak intensity vs. time is called a chemigram. The chemigram for PC-SIL2 is shown in Figure 8. BPA-PC and siloxane peaks show complete overlap indicating no significant composition drift across the MWD. This is confirmed by on-line SEC analysis, where BPA-PC and siloxane traces also match across the entire MWD.

For PC-SIL1, similar results were obtained, i.e. a complete overlap of BPA-PC and siloxane traces as determined by both on- and off-line SEC-IR techniques.

These combined results indicate that the siloxane blocks of both copolymers are statistically distributed on chains of all lengths.

Characterization of fractions

Siloxane contents and block lengths of the fractions were determined using proton-NMR. Figure 9 shows the siloxane concentration as a function of fraction number average MW for the investigated copolymers. For PC-SIL1, the measured siloxane concentration is constant for all fractions. For PC-SIL2, the siloxane concentration decreases with increasing MW of the fractions implying a CC drift during fractionation.

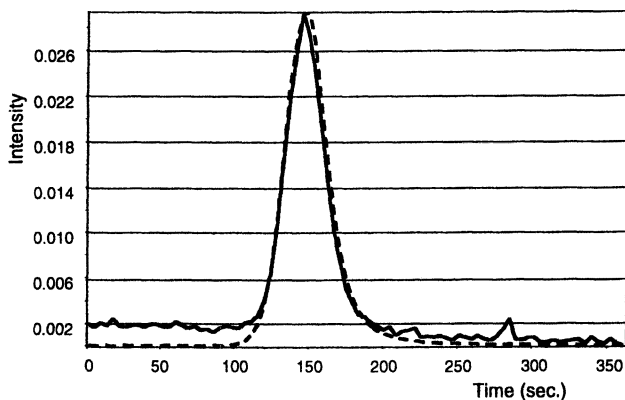


Figure 8: Off-line SEC-IR analysis of PC-SIL2: chemigrams for BPA-polycarbonate (dotted line) and Eugenol-siloxane (solid line).

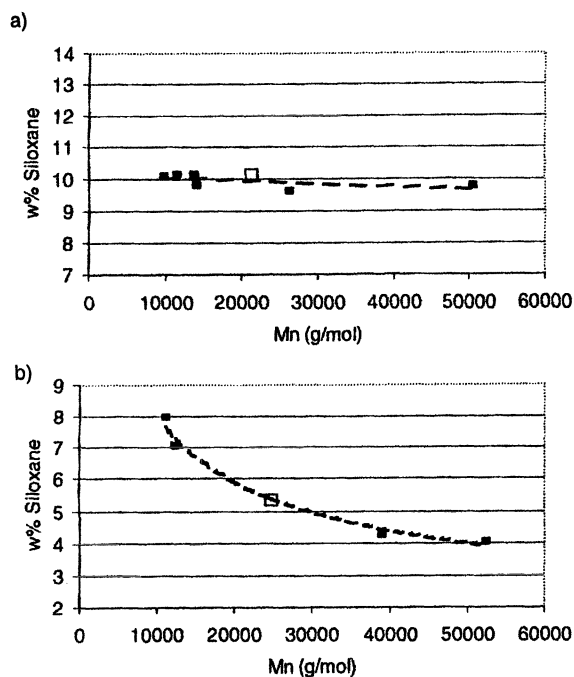


Figure 9: Siloxane concentration as a function of the number average molecular weight for a) PC-SIL1 and b) PC-SIL2; closed symbols denote the fractions, open symbols the unfractionated polymer.

At first sight, there seems to be a contradiction between the NMR/SEC-IR findings that PC-SIL2 is compositionally homogeneous and the variation in siloxane concentration for the fractions. The statistical nature of PC-SIL2 should lead to fractionation according to MW only. However, it can be derived from SEC and NMR data that for all fractions, the number of siloxane blocks built in PC-SIL2 chains is very low (less than 3 on the average). This means that many polymer chains are free of siloxane blocks or contain a very small number of them. The solubility differences between chains containing no vs. one or several siloxane blocks is probably responsible for the CC drift during fractionation. This effect is especially pronounced for low MW chains (cf. Figure 10). Since the solubility of PC-EuSi copolymers is higher in MCH/DEG mixtures than the solubility of pure PC (as could be concluded from orienting dissolution experiments), it is logical that a higher than average siloxane content is found in the low MW fractions which are extracted in the sol phase and a lower than average siloxane content in the high MW fractions which are extracted in the gel phase in the fractionation process.

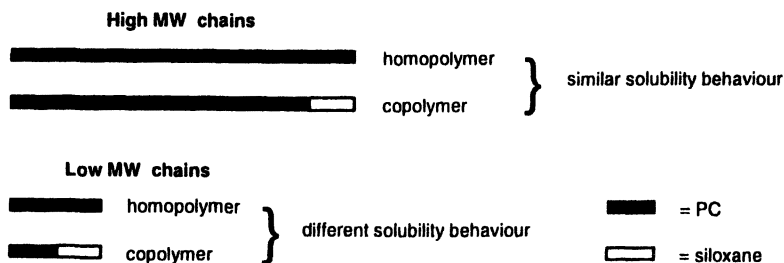


Figure 10: Effect of incorporation of a low number of siloxane blocks on the solubility of low and high molecular weight copolymer chains.

Conclusions

Linear and lightly branched BPA-homopolycarbonate samples and BPA-polycarbonate/Eugenol-siloxane copolymer samples have been fractionated using the Continuous Polymer Fractionation (CPF) method. Preparative size fractions with narrow dispersions have been obtained from methylene chloride/diethylene glycol solvent/anti-solvent mixtures.

Fractions, obtained from CPF experiments, have been used to assess the distribution of branching structures across the MWD for melt-polymerized PC materials. The overall low level of branching ensures that fractionation has occurred according to molecular weight only. PhSALPhC branching units are incorporated heterogeneously across the MWD as determined by NMR and SEC

analysis. This reflects the fact that, under thermodynamic control of the MWD, branched chains will be longer on the average than linear ones. Experimentally determined branching densities of the fractions are in good agreement with results obtained from a Monte-Carlo simulation.

Thermally induced redistribution reactions in fractionated BPA-PC materials made via melt-transesterification and interfacial polymerization processes have been studied. Redistribution effects were visualized by monitoring changes in the MWD upon thermal treatment of mixed fractions. While interfacially polymerized PC does not undergo significant redistribution, predominantly because of the low amount of hydroxyl end-groups, fast redistribution reactions occur in melt-polymerized PC. The first stages of redistribution can be simulated using a Monte Carlo model. At 250°C, approximately 0.5% of all carbonate groups are involved in a redistribution exchange reaction per minute for the systems studied.

Fractions obtained from CPF experiments were used for determination of the PC/Eugenol-siloxane copolymer microstructure and distribution of siloxane species across the MWD. The contrasting behaviour of the two samples studied highlights the applicability and limits of CPF for copolymers. The results show that copolymers with statistically distributed segments can be fractionated according to MW using CPF only to the extent that all chains have the same average composition, which is not the case for short chains carrying a small number of comparatively long comonomer segments.

Acknowledgements

The authors are indebted to W.-J. Goddrie, J.J. Pesce, A. Schneider (University of Mainz, Germany) and J.C. Carnahan (GE Corporate Research, Schenectady, NY, USA), for performing some of the analyses and simulations. They would also like to thank Prof. J. Devaux (Université catholique de Louvain, Belgium) and Dr. G. de Wit (Technical University of Eindhoven, The Netherlands) for helpful discussions.

References

1. King Jr., J.A., in: Handbook of Polycarbonate Science and Technology (Legrand, D.G., and Bendler, J.T. (eds.)), Marcel Dekker, New York, 2000, Chapter 2.
2. Schnell, H., Chemistry and Physics of Polycarbonates, Wiley-Interscience, New York, 1964.
3. Katsuji, S., Jap. Patent 9-59371 (to Teijin LTD), 1997.

4. Bailly, Ch., Daumerie, M., Legras, R., and Mercier, J.P., *J. Polym. Sci., Phys. Ed.* 23 (1985) 493-507.
5. Schmidhauser, J., and Sybert, P.D., in: *Handbook of Polycarbonate Science and Technology* (Legrand, D.G., and Bendler, J.T. (eds.)), Marcel Dekker, New York, 2000, Chapter 5.
6. Vaughn Jr., H.A., *J. Polym. Sci., Part B*, 7 (1969) 569-572.
7. Kambour, R.P., *J. Polym. Sci., Part B*, 7 (1969) 573-577.
8. LeGrand, D.G., *J. Polym. Sci., Part B*, 7 (1969) 579-585.
9. Grigo, U., Kircher, K., and Müller, P.R., in: *Kunststoff Handbuch 3/1* (Becker, G.W., and Braun, D. (eds.)), Hanser, München, 1992, Chapter 3.
10. Hoover, J.F., US Patent 6,072,011 (to General Electric Co.), 2000.
11. Ogawa, N., Tajima, J., Takarada, M., and Tanaka, M., US Patent 5,916,980 (to Mitsubishi Gas Chemical Co. and Shin-Etsu Chemical Co.), 1999.
12. Hagenaars, A.C., Pesce, J.-J., Bailly, Ch., and Wolf, B.A., *Polymer* 42 (2001) 7653-7661.
13. Hagenaars, A.C., Schneider, A., Bailly, Ch., and Wolf, B.A., *Polymer* 43 (2002) 2663-2669.
14. Hagenaars, A.C., Goddrie, W.-J., and Bailly, Ch., *Polymer* 43 (2002) 5039-5045.
15. Cantow (ed.), M.J.R., *Polymer Fractionation*, Academic Press, New York, 1967.
16. Tung (ed.), L.H., *Fractionation of Synthetic Polymers*, Marcel Dekker, New York, 1977.
17. Francuskiewicz, F., *Polymer Fractionation*, Springer, Berlin, 1994.
18. Schnell, H., *Angew. Chem.* 68 (1956) 633-640.
19. Schulz, G.V., and Horbach, A., *Makromolek. Chem.* 29 (1959) 93-116.
20. Tomikawa, M., *Chem. High Polym. (Tokyo)* 20 (1963) 11-16.
21. Lunak, S., and Bohdanecky, M., *Coll. Czech. Chem. Commun.* 30 (1965) 2756-2770.
22. Sitaramaiah, G., *J. Polym. Sci.: part A*, 3 (1965) 2743-2757.
23. Moore, W.R., and Uddin, M.A., *Europ. Polym. J.* 3 (1967) 673-679.
24. Moore, W.R., and Uddin, M.A., *Europ. Polym. J.* 5 (1969) 185-193.
25. Berry, G.C., Nomura, H., and Mayhan, K.G., *J. Polym. Sci., A2*, 5 (1967) 1-21.
26. Bartosiewicz, R.L., and Booth, C., *Eur. Polym. J.* 10 (1974) 791-798.
27. Bartosiewicz, R.L., Booth, C., and Marshall, A., *Europ. Polym. J.* 10 (1974) 783-789.
28. Hoare, H.C., and Hillman, D.E., *Brit. Polym. J.* 3 (1971) 259-262.
29. Robertson, A.B., Cook, J.A., and Gregory, J.T., *Advan. Chem. Ser.* 128 (1973) 258-273.
30. Tsuji, T., Norisuye, T., and Fujita., *Polym. J.* 5 (1975) 558-569.

31. Bailly, C., Daoust, D., Legras, R., Mercier, J.P., Strazielle, C., and Lapp, A., *Polymer* 27 (1986) 1410-1415.
32. Baumann, G.F., and Steingiser, S., *J. Polym. Sci. A1* (1963) 3395-3406.
33. Turska, E., Dems, A., and Siniarska, M., *Bull. Acad. Polon. Sci. Ser. Sci. Chim.* 13 (1965) 189-193.
34. Turska, E., and Siniarska-Kapuscinska, M., *Eur. Polym. J. – Supplement* (1969) 431-439.
35. Turska, E., and Wróbel, A.M., *Polymer* 11 (1970) 408-414.
36. Dobrescu, V., *Mater. Plast. (Bucharest)* 15 (1978) 14-17.
37. Glöckner, G., *Plaste und Kautschuk* 12 (1965) 96-102.
38. Ekmanis, J.L., "Preparative Gel Permeation Chromatography", presentation given at the 1985 Pittsburgh conference, New Orleans, 1985. Also published as *Waters Lab Highlights LAH 0326*, Waters Millipore Corp., Milford, 1986.
39. Luo, M., and Teraoka, I., *Macromolecules* 29 (1996) 4226-4233.
40. Weinmann, K., Wolf, B.A., Rätzsch, M.T., and Tschersich, L., *J. Appl. Polym. Sci.* 45 (1992) 1265-1279.
41. Englert, A., and Tompa, H., *Polymer* 11 (1970) 507-532.
42. Wolf, B.A., *Makromol. Chem., Macromol. Symp.* 61 (1992) 244-247.
43. Wolf, B.A., *Adv. Mat.* 6 (1994) 701-704.
44. Hersh, S.N., and Choi, K.Y., *J. Appl. Polym. Sci.* 41 (1990) 1033-1046.
45. Kim, Y., and Choi, K.Y., *J. Appl. Polym. Sci.* 49 (1993) 747-764.
46. Weinmann, K., Ph.D. Thesis, University of Mainz, Germany, 1992.
47. Tobita, H., *Macromol. Theory Simul.* 5 (1996) 129-144.
48. Tobita, H., and Hamashima, N., *J. Polym. Sci., Polym. Phys.* 38 (2000) 2009-2018.

Chapter 15

Ring-Opening and Branching in Polycarbonates: A Density Functional–Monte Carlo Study

R. O. Jones¹, J. Akola¹, and P. Ballone^{1,2}

¹Institut für Festkörperforschung, FZ Jülich, D–52425 Jülich, Germany

²Dipartimento di Fisica, Università di Messina, I–98166 Messina, Italy

Density functional calculations of the structures, potential energy surfaces, and reactivities for systems closely related to bisphenol A-polycarbonate (BPA-PC) provide the basis for a model describing the ring opening polymerization of its cyclic oligomers by nucleophilic molecules. The model comprises a fixed number of difunctional particles and harmonic bonds, and includes a low concentration ($0.01\% \leq c_a \leq 0.36\%$) of mono-functional active particles able to modify pattern of the bonds without changing the total number. Monte Carlo simulations using this model show that in 2D and 3D there is a transition from unpolymerized cyclic oligomers at low density to a system of linear chains at high density. Entropy in the distribution of inter-particle bonds drives chain formation. The effects of branching defects are investigated by adding trifunctional units (of concentration c_3). At sufficiently high density and c_3 values, the linking of polymer chains by trifunctional units gives rise to an aggregate (*gel*) incorporating most of the system mass.

Introduction

The outstanding mechanical, optical and thermal properties of polycarbonates underlie their diverse industrial applications, which motivate the continuing interest by experimental and computational research groups. Although polycarbonates have been produced on an industrial scale for decades, important questions remain concerning the relation between their macroscopic properties and the atomic structure. An example is the polymerization of cyclic oligomers of bisphenol

A polycarbonate (BPA-PC) to long chains and rings, whose size distribution is crucial to the thermal and mechanical properties. The linear structure of BPA-PC can be modified by branching centers arising from parasitic reactions, impurities, or additives. The resulting cross-links can alter greatly the polymer size distribution and the dynamical (e.g., diffusion, viscosity) and mechanical properties.^{1,2} Branching can also result in transitions to qualitatively new phases such as gels and rubber.³

A detailed understanding of the molecular size distribution and of the effects of branching requires a multifaceted investigation covering electronic and structural properties, chemical kinetics, and statistical mechanics. We describe here two examples of such computational investigations: the first explores the ring-opening polymerization (ROP) of BPA-PC starting from its cyclic oligomers and using small nucleophilic catalysts,⁴ the second analyzes the influence of branching centers on the molecular structure and size distribution.

The basic reaction step leading to the ROP of BPA-PC has been investigated by combined density functional (DF)/ molecular dynamics computations,⁵ which provide reliable predictions of reaction pathways and energies for these systems. The effect of many such reactions occurring in a condensed environment has then been investigated by Monte Carlo (MC) computations for a model based on the DF results, which provide key parameters. The model consists of structureless particles representing BPA monomers, with harmonic springs representing covalent bonds among them. It also includes catalyst particles and a bond interchange mechanism mimicking the reaction investigated by DF. The model describes fully flexible chains and rings, and thus provides an idealized view of BPA-PC. Moreover, our assumption of equilibrium polymerization allows us to use standard statistical mechanics approaches like MC, and to compare our results to those of previous studies for equilibrium (“living”) polymers.⁶

The role of branching defects on the equilibrium structure has been investigated following the same strategy used to study polymerization. First, the chemical pathways leading to branching defects have been analyzed by DF computations.⁷ The equilibrium properties of fluid mixtures of di- and trifunctional units have then been determined by Monte Carlo simulations as a function of density, temperature and concentration c_3 of the trifunctional monomers. Whenever the density and c_3 concentration are sufficiently high, the linking of polymer chains leads in 2D and 3D to a molecular aggregate (gel) comprising most of the system mass. This is a continuous transition analogous to percolation.

Reactions of phenoxides with cyclic tetramer

The ring-opening polymerization of cyclic oligomers of BPA-PC is catalyzed by nucleophilic molecules such as lithium and sodium phenoxide (LiOPh and NaOPh, respectively). The reactions have remarkably low exotherms, with enthalpy changes at the limit of the experimental resolution ($\Delta H \leq 0.3$ kcal/mol

in the case of LiOPh).⁸ Our DF calculations of the cyclic BPA-PC tetramer have shown that the local coordination of this molecule is very similar to that in the PC chains, and its reaction with LiOPh and NaOPh follows the path illustrated in Fig. 1.⁹ An attack involving the (positively charged) metal atom is most likely at the carbonate group, as confirmed by experimental studies on a number of functionalized bisphenols using a variety of catalysts.¹⁰ Therefore, we have performed a constrained simulation using the distance R_C between the carbonyl C and the reactant O as the initial reaction coordinate.

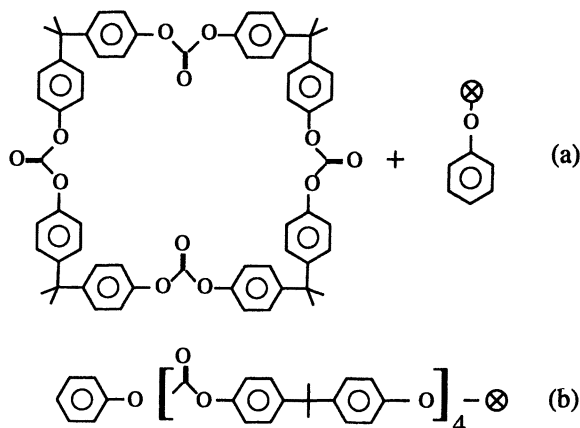


Figure 1. Schematic view of the first step in the ring opening polymerization of BPA-PC. The active site is an electropositive metal atom, identified by a cross.

Fig. 2 shows six snapshots of the trajectory for the reaction of LiOPh approaching from outside the cyclic tetramer.⁹ The reactants interact weakly for $R_C \sim 4$, with steric hindrances from neighboring phenyl rings giving rise to an energy barrier of 4 kcal/mol at $R_C = 3.8$ Å. For shorter separations, the Li-O attraction induces a rotation of the carbonyl group and a rapid decrease (~ 15 kcal/mol) in the potential energy [2(2)]. Smaller values of R_C lead to a C atom surrounded by four O atoms with approximately tetrahedral coordination [2(3)]. A reduction of R_C to 1.5 Å (corresponding to a second energy barrier of 4 kcal/mol) breaks the symmetric bonding of Li, and the Li is now attached to the tetrahedral O bound to a single C atom [2(4)]. This bond provides a 3-fold axis for rotations of the O-Li bond that result in very small energy variations.

Under normal thermodynamic conditions, the O-Li bond can then be oriented with equal probability along three directions. One relaxation gives rise to structure 2(6), which has a weak bond between Li and the new carbonyl O. This bond will break at room temperature, leading to the open chain with an active -C-O-Li termination. This configuration has essentially the same potential energy as the original reactants, in agreement with experimental evidence. Moreover, the chain termination reproduces the structure and chemical characteristics of the original LiOPh.

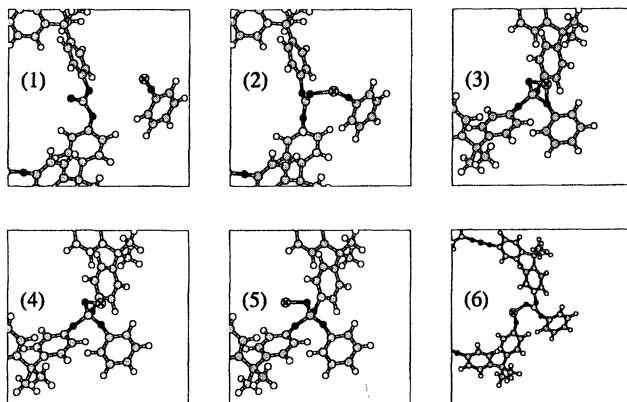


Figure 2. Reaction of LiOPh with cyclic tetramer of BPA-PC. The product (6) is a Li-terminated chain (Li atom crossed). Only part of the chain is shown.

It could catalyze the ring opening of further oligomers, giving rise to a “living polymer”. The extension of these computations to different reagent (diphenyl carbonate) and catalyst (tetraphenylphosphonium phenoxide) molecules¹¹ shows that the energy barrier and the energy difference between reagents and products can be tuned by an appropriate choice of the chemical species.

Additional DF results on the structure, energy and vibrational properties for molecules related to bisphenol carbonate (from saturated fragments to cyclic oligomers of up to four BPA monomers)¹² can be summarized as follows: structural and vibrational properties of covalent bonds are highly transferable from one BPA aggregate to another. The structures of cyclic dimer and trimer are strained, but the cyclic tetramer is remarkably strain-free and displays structural features similar to those of extended chains. Total energies and vibrational entropy *per monomer* should then depend weakly on the molecular weight above three monomers, provided the rearrangements do not change the number and type of bonds. The DF results for structure, energy and vibrational frequencies agree well with available experimental data.

Polymerization of PC: Model simulations

The analysis of the reaction between the cyclic tetramer and LiOPh and NaOPh clarifies the origin of their catalytic activity, and provides much information about the reaction mechanisms. However, it does not explain why cyclic oligomers polymerize under appropriate conditions, since reactants and products have nearly the

same potential energy. The vibrational properties that determine configurational entropy contributions also change little during the reaction. In addition, translational entropy (accounting for the ideal part of $S(T)$) favors a multitude of small molecules over a few large connected aggregates.

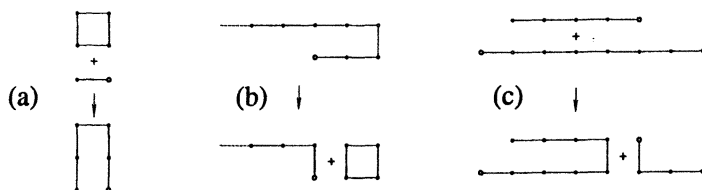


Figure 3. Model used to study polymerization: (a) chain formation from ring, (b) ring formation from chain, and (c) tail interchange between active chains. The active site is denoted by an open circle.

The polymerization process has been studied using a model, in which BPA-PC structural units are represented by Lennard-Jones (LJ) particles connected by harmonic springs representing the covalent bonds in the polymer backbone.^{13,14} Each particle forms one or two bonds, so that the system comprises open chains and rings without branching, and the catalyst is represented by *active* particles that can interchange bonds with a neighboring particle. The active particles can form only one bond, so that they must be at an end of a chain with at least two particles.

The rules for bond interchange are shown in Fig. 3, which illustrates the basic processes taking place: the incorporation [3(a)] and the separation [3(b)] of a ring from an open chain carrying an active head, and the interchange of segments between chains [3(c)]. Constant volume Monte Carlo simulations are performed by sampling the positions and bonding configuration using a Metropolis algorithm.

We have investigated systems in 2D and 3D over a wide range of densities and temperatures, focusing on the limit of low catalyst concentration (from 0.01 to 0.36 %). All computations were started by equilibrating a sample of 2500 cyclic tetramers before introducing a small number (from 1 to 36) of dimers, each with one active particle representing the metal termination of the M-OPh molecule. The primary role of the catalyst is to enhance the kinetics of the rearrangement of the covalent bonds. However, since the number of bonds is conserved during ring-opening polymerization of BPA-PC, the number of catalyst molecules also determines the number of free chain terminations (active or not), which is conserved during the polymerization process. We express densities in terms of the packing fraction η , defined as $\eta = \pi\rho\sigma^2/4$ and $\eta = \pi\rho\sigma^3/6$ in 2D and in 3D, respectively, where σ is the Lennard-Jones diameter of our particles. Energies and

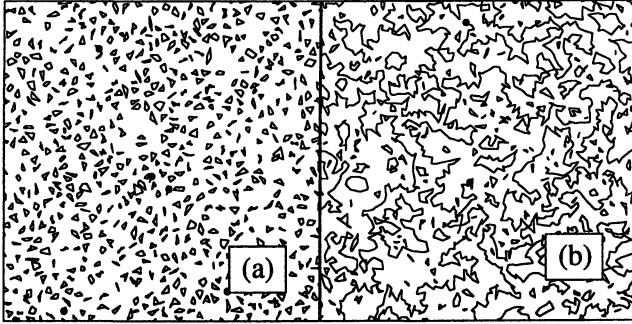


Figure 4. Snapshots of (a) the initial tetramer fluid, and (b) a configuration at equilibrium under the bond interchange mechanism. Simulation in 2D at $\eta = 0.4$ and $T = 3$. Solid dots identify active particles.

temperatures are measured in units of the LJ energy parameter ϵ . A temperature of $T = 3$ corresponds to 375 K for a typical molecular system with $\epsilon = 0.25$.

The addition of the catalyst influences the configuration dramatically in most cases, leading to long open chains with up to $\sim 50\%$ of the particles (see Fig. 4). The remaining particles are subdivided into an equilibrium population of rings, whose average size is much smaller than that of the chains.

We first discuss the results in 2D, which are less affected by finite-size effects than their 3D counterparts with the same particle number. In Fig. 5 we show the average length of the active chain N_a as a function of density for different concentrations of active particles. The degree of polymerization increases with increasing density, with a sharp rise at $\eta \sim 0.15$. The competition between active chains for the available monomers means that the average chain length decreases with increasing concentration of the active particles. The increasing average length with decreasing N_a makes the rise at $\eta = 0.15$ more pronounced, leading to a discontinuous transition in the limit of vanishing catalyst concentration.¹³

The equilibrium size distributions of rings and chains are characterized by the mass-fraction distributions $P_r(L)$ and $P_l(L)$, defined as the percentage of monomers belonging to a ring or a chain, respectively, of length L . The Zimm-Schulz distribution:

$$P_l(L) \propto L^\gamma \exp[-\gamma L/\langle L_l \rangle] \quad (1)$$

provides a fair fit to all curves, with an exponent ($1.1 < \gamma < 1.4$) close to the value predicted by analytic theories $\gamma = 43/32$.¹⁵ This fit may reflect simply the existence of a unimodal, broad, and relatively featureless $P_l(L)$ that decays exponentially for high L and scales simply with η and c_a . A similar

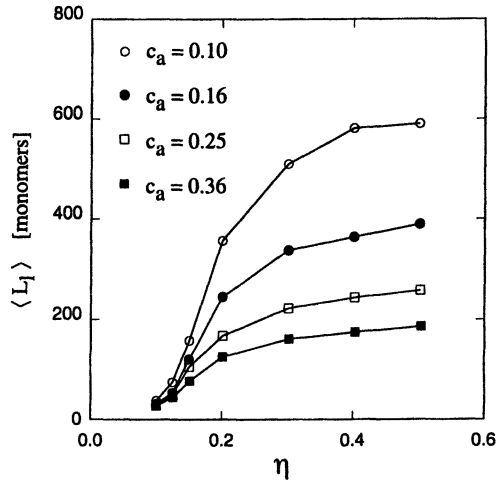


Figure 5. Average length of active chains as a function of packing fraction η for different concentrations (%) of active particles. Simulations in 2D (Reproduced with permission from reference 14a. Copyright 2002 American Institute of Physics.)

fit is provided by other expressions, including $P_l(L) \propto L \exp[-\gamma L/\langle L_l \rangle]$ and $P_l(L) \propto L^\gamma \exp[-L/\langle L_l \rangle]$. The distribution $P_r(L)$ for rings changes little over the range of η and c_a considered in our simulations.

Temperature also affects the average length of the chains, although less dramatically than the density. The monotonic rise of the polymerization degree with increasing T indicates that entropy is the driving force stabilizing the long chains. This is supported by the behavior of the average potential energy, which rises steadily during polymerization. Since the spontaneous evolution of every system is towards a state of lower free energy, the rise of the average potential energy per particle $\langle U \rangle$ must be over-compensated by the simultaneous increase of the system entropy. Moreover, the positive sign of both the potential energy and entropy changes upon polymerization ($\Delta U > 0$, $\Delta S > 0$) implies that the model displays a floor temperature T_f separating an unpolymerized phase (at $T < T_f$) from the polymerized phase at $T > T_f$. We have not observed the transition directly, because it appears to occur below the temperature range accessible to our simulations, which require a sufficiently fast relaxation of the bonding configurations to reach equilibrium.

The simulations in 3D and 2D show both similarities and differences. The tendency to polymerize is much stronger in 3D, with the average mass of the active chain generally being well above 80 % of the total, and the polymerization line occurs in 3D at a packing fraction an order of magnitude lower (see Fig. 6).

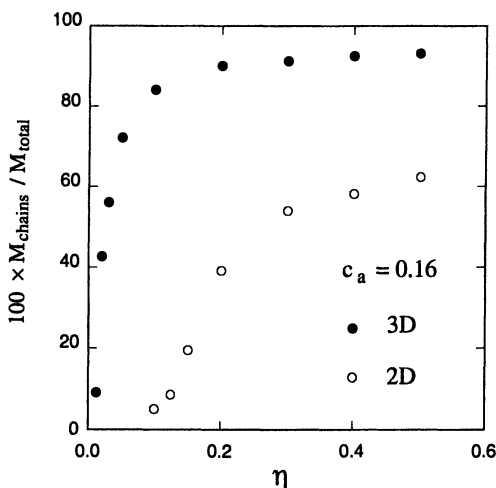


Figure 6. Fraction of system mass in open chains in 2D and 3D as a function of packing fraction η (Reproduced with permission from reference 14a. Copyright 2002 American Institute of Physics.)

The degree of polymerization in 3D decreases slightly but monotonically with decreasing T , as found in 2D. At $\eta = 0.3$ and $c_a = 0.16\%$, for example, open chains account for 91.3% of the total mass for $T = 3$, decreasing to 84.8% at $T = 0.6$. We did not observe a polymerization transition on changing T alone, so that the polymerization line in the $\eta - T$ plane must be a very steep function of η . In both 2D and 3D there is a systematic and significant increase of viscosity and a decrease in diffusion during polymerization.

Branching and polymerization in polycarbonates

The model discussed above has been extended by introducing LJ particles that form three bonds and give rise to branching, and Fig. 7 shows an example in the polycarbonate context.² The course of the reaction depends on density, T , and the concentration of additives and impurities, and the resultant polymer shows a shear sensitivity that is directly related to the amount of branching agent and inversely related to the amount of the initiator. As in our previous simulations, a low concentration c_a of active particles allows equilibration with respect to the bond configuration. The model emphasizes the role of entropy over potential energy, since all particles interact by the same LJ potential, all bonds are equivalent, and their number is conserved. We have performed simulations in 2D and 3D for concentrations of trifunctional units c_3 from 0.1 % to 32 % and densities covering the

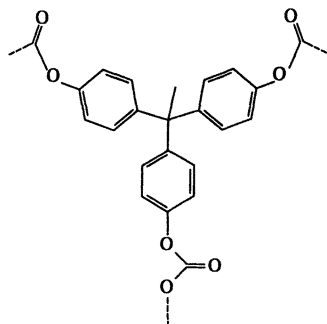


Figure 7. Schematic view of the branching center in bisphenol-A polycarbonate produced by the ring-opening polymerization of cyclic oligomers in the presence of small amounts of 1,1,1-tris(4-hydroxyphenyl)ethane, THPE [Ref. 14(b)].

polymerization line found for $c_3 = 0$. Only the lowest range of c_3 (up to a few percent) is relevant for industrial applications, but a much wider interval has been explored for completeness.

Aggregates with trifunctional units (see Fig. 8(a)) are much more compact than linear polymers of comparable size (see Fig. 8(b)), if other parameters (η , T , c_a and dimensionality) are equal. The reduced gyration radius affects, the dynamical and mechanical properties and the stability of large aggregates, since compact molecules carrying active heads are more likely to self-mutilate [Fig. 3(b)] than extended chains. This tends to reduce the average molecular weight, thus partially compensating the trend towards larger aggregates due to the linking of polymeric segments by trifunctional units. A more quantitative analysis of these effects is provided by monitoring the size distribution and the average size of molecules with one or more chain terminations ($\langle L_l \rangle$) or at least one trifunctional unit ($\langle L_3 \rangle$). These account for a large fraction of the total mass in the polymeric phase, and the analysis of either provides similar information.

Polymerization and gel transition in 2D

Simulations for 2D systems with $c_3 = 0$ showed^{13,14} that the polymeric phase is stable if $\eta \geq 0.16$, and intuition suggests that introducing a small number of trifunctional units could enhance polymerization by allowing the formation of interchain links and aggregates of chain segments. For 2D systems with $c_3 \sim 0.1 - 1\%$, however, the addition of trifunctional particles *lowers* the degree of polymerization significantly, resulting in a sizable reduction of the average size $\langle L_l \rangle$ for molecules with at least one chain termination. The apparent trend towards smaller aggregates is due to the reduction in the molecular extension by branching

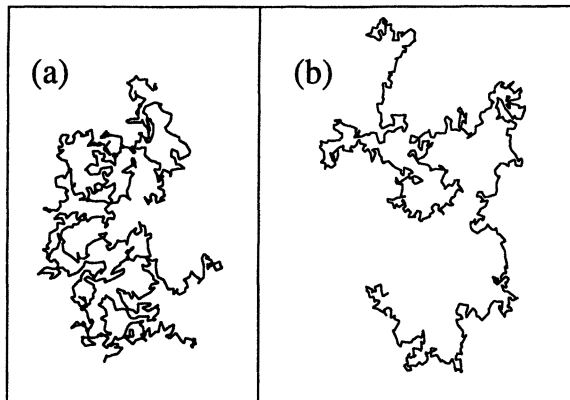


Figure 8. Typical molecular structures in 2D simulations at $\eta = 0.3$, $T = 3$ and $c_a = 0.16\%$. (a) $c_3 = 4\%$; (b) $c_3 = 0$.

centers described in the previous section. In 2D this decrease of polymerization upon addition of trifunctional units is a major effect, and only large concentrations of trifunctional units are able to reverse the depolymerization trend. Increasing further the c_3 concentration results in a new (gel) phase qualitatively different from the polymer found for $c_3 = 0$. The new phase is formed across a phase transition, which, together with the polymerization transition found previously,^{13,14} allows us to identify three distinct phases for the model: a fluid phase comprising oligomers; a gel, in which most of the mass is included in a single molecule; and a polymeric phase comprising several linear or branched aggregates of fairly large ($L \geq 100$ monomers) size. The gel forms via a continuous transition with increasing c_3 , resulting from the linking of aggregates with a wide range of sizes. The accompanying anomalous increase of size fluctuations supports both the continuous nature of the phase transformation and the connection to percolation.

Fig. 9 shows $P_l(L)$ for samples at $\eta = 0.5$, $T = 3$ and c_3 values covering the gel transition ($c_3 \sim 10\%$ for these conditions). In the absence of branching,¹⁴ $P_l(L)$ is approximated well by the Zimm-Schulz function $\propto L^\gamma \exp[-\gamma L/\langle L \rangle]$, with an exponent γ close to the value ($\gamma = 43/32$)¹⁵ for a model closely related to the present one.

The addition of branching centers affects $P_l(L)$ significantly for low c_3 , as indicated by the rapid decrease of $\langle L_l \rangle$ close to $c_3 = 0$: the peak of $P_l(L)$ moves towards lower sizes, while the tail of the distribution extends to higher sizes. The distribution deviates significantly from the Zimm-Schulz form, and an exponential form [$P_l(L) \propto \exp[-\alpha L/\langle L \rangle]$, $\alpha \sim 0.36$] is more appropriate in the c_3 range corresponding to a lower degree of polymerization (see the curve for $c_3 = 1\%$

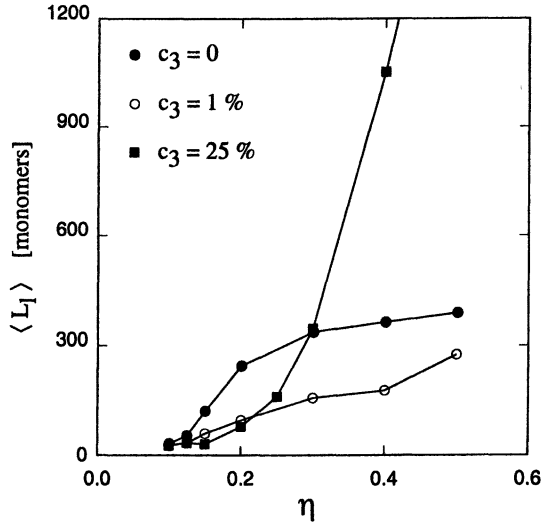


Figure 9. $\langle L_l \rangle$ as a function of η at three values of c_3 (Reproduced with permission from reference 14b. Copyright 2002 American Institute of Physics.)

in Fig. 10). $P_l(L)$ is bimodal in the gel, with the high- L peak centered at sizes ($L \sim 9000$ monomers) close to the total sample size (see the curve for $c_3 = 25\%$ in Fig. 10). At the gel transition ($c_3 = 10\%$), $P_l(L)$ is nearly constant over a wide size range, which explains the large fluctuations in $\langle L_l \rangle$.

Polymerization and gel transition in 3D

Many features observed in 2D systems are found in 3D, although the greater stability of the 3D polymer phase influences the properties of branched systems. The reduction of $\langle L_l \rangle$ at low c_3 is much less pronounced than in 2D, although it is evident in the c_3 dependence of $\langle L_l \rangle$. The rapid rise of $\langle L_l \rangle$ at higher c_3 values is accompanied by a large increase in the size fluctuations, which allows us to locate the gel transition at $c_3 \sim 2\%$ for these conditions of density and T .

The dependence of the molecular size distribution $P_l(L)$ on density and c_3 in 3D samples is greater than in 2D, reflecting the increased stability of both polymer and gel. Starting from a $P_l(L) \propto L \exp[-L/\langle L \rangle]$ for $c_3 = 0$, the addition of only 0.1–0.2% of trifunctional particles changes significantly the shape of $P_l(L)$, which is now approximated better by $P_l(L) \propto \exp[-\alpha L/\langle L \rangle]$ ($\alpha \sim 0.3$). With increasing c_3 , the height and the width of the first $P_l(L)$ peak decrease monotonically, while the large- L tail develops into a secondary peak at $L \sim 6000$ for $c_3 \sim 1\%$. At the gel point ($c_3 = 2\%$), identified here by the maximum in the

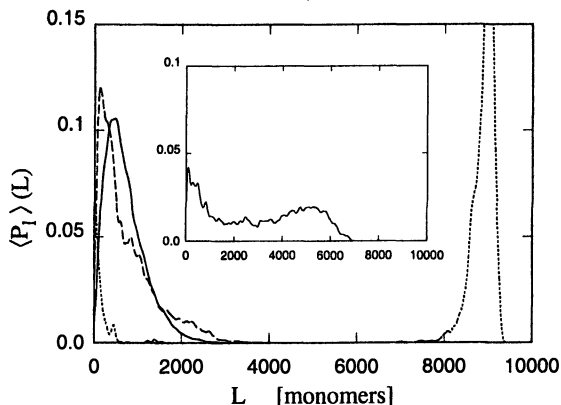


Figure 10. Mass fraction distribution $\langle P_l \rangle$ in 2D samples at $\eta = 0.5$ and $T = 3$. Full line: $c_3 = 0$; dashed line: $c_3 = 1\%$; dotted line: $c_3 = 25\%$. Inset: $c_3 = 10\%$, corresponding to the gel point (Reproduced with permission from reference 14b. Copyright 2002 American Institute of Physics.)

relative size fluctuations, $P_l(L)$ is clearly bimodal. For larger values of c_3 , most of the weight under the $P_l(L)$ curve belongs to the high- L peak, which moves towards larger sizes (saturating at $L \sim 9000$) and reduces its width.

As discussed above, the polymerization and gel transitions are driven by the entropy associated to the bonding configuration, and this is emphasized by the fact that polymerization becomes weaker with decreasing T . The analysis of snapshots, the mass-fraction distribution $\langle P_l(L) \rangle$, and the molecular size fluctuations all show the progressive loss of gel characteristics as T is lowered, and the gradual evolution of these properties with changing T prevents the precise determination of the transition point. The polymerization and gel transitions are less sensitive to temperature in 3D than in 2D, mainly because the relevant range of c_3 is lower.

Discussion and Concluding Remarks

A combination of DF computations and MC simulations has been used to investigate ring-opening polymerization in BPA-PC. Density functional calculations have been used to determine the energy balance, the energy barrier and the path for the basic reaction leading to polymerization. The results show that reactants and products have nearly the same energy, and the potential energy barrier is low when the reaction is catalyzed by LiOPh, and vanishes in the case of NaOPh. Vibrational properties do not change significantly, so that the vibrational entropy is nearly unchanged by the reaction. A model incorporating these ingredients and

energy parameters from the DF computations has been devised: BPA-PC structural units are represented by Lennard-Jones particles, and the covalent bonds in the polymer backbone are described by harmonic springs. Each particle forms one or two harmonic bonds, so that the system comprises open chains or rings without branching. The reaction is initiated by introducing a small number of *active* particles. These interact with the rest of the system via the same potentials as the other particles, but they mimic the behavior of the catalytic head in MOPh because (a) they form one and only one bond, and (b) bond exchanges occur only when at least one of the bonds involves an active particle.

Extensive MC simulations show that the model displays a strong tendency to form long chains that is enhanced by increasing density, temperature and dimensionality. Simple thermodynamic considerations show that the driving force towards polymerization is provided by the entropy of the bonding configuration, whose contribution to free energy rises with increasing temperature.

The role of branching defects has been investigated by including trifunctional monomers in the model used to study polymerization, and equilibrating the structure and bond configuration by MC simulations. The addition of trifunctional particles displaces the polymerization line and introduces a qualitatively new (*gel*) phase. Simulations have been performed here for 2D and 3D systems. In 2D systems the effect of branching centers on the molecular size distribution is different at low and high concentrations. At low concentrations the main effect is to reduce the gyration radius of the molecule, which limits the size of the aggregates. At densities slightly above the polymerization line the system may revert to the unpolymerized state over a wide range of c_3 . At high c_3 and in the polymer range of (η, T) , the linking of chains by trifunctional units increases the molecular size and leads to a gel at a critical concentration that depends on η , T , and dimensionality.

Most results for 2D systems remain qualitatively valid in 3D. Small concentrations of trivalent particles lower the degree of polymerization at densities $0.04 \leq \eta \leq 0.15$, although this effect is less important than in 3D and is not seen for $\eta \geq 0.15$. Higher concentrations of trifunctional particles lead to a continuous transition to a gel, which occurs with increasing c_3 and packing fraction η . The evolution of the size distribution with increasing c_3 is similar in 2D and in 3D.

Lowering T reduces the degree of polymerization even in the absence of branching, and trifunctional particles enhance greatly the sensitivity to temperature of both polymer and gel. The latter is affected more, and we observe a reversible transition between the polymer at low T and the gel at high T , for 2D samples at high density and high values of c_3 . The continuous nature of the transition hampers the determination of the transition point in this case. The effect of decreasing T is reduced in 3D for the range of c_3 studied here, although similar effects to those observed in 2D could also occur for larger values of c_3 . The changes in the system properties with changing temperature and density are fully reversible.

The calculations were performed in the FZ Jülich on a Compaq DS20E server and XP1000 workstations provided in part by the Bundesministerium für Bildung und Wissenschaft, Bonn, within the MaTech-Kompetenzzentrum "Werkstoffmodellierung" (03N6015). We thank D. Brunelle (G.E., Niskayuna, NY), S. Greer (University of Maryland, College Park, MD), and F. Bruder, S. Kratschmer, and M. Möhrath (Bayer AG, Krefeld, Germany) for helpful discussions.

References

1. See, for example, Clarke, S. M.; Hotta, A.; Tajbakhsh, A. R.; Terenjev, E. M. *Phys. Rev. E* **2001**, *64*, 061702.
2. Krabbenhoft, H. O.; Boden, E. P. *Makromol. Chem., Macromol. Symp.* **1991**, *42/43*, 167. Branching increases heat resistance and shear sensitivity.
3. de Gennes, P. G. *Scaling concepts in Polymer Physics*, Cornell University Press: Ithaca, 1979.
4. Brunelle, D. J. in: *Ring-opening Polymerization: Mechanisms, Catalysis, Structure, Utility*, Brunelle, D. J., Ed.; Hanser: München, Germany, 1993, pp. 1 and 309.
5. Car, R.; Parrinello, M. *Phys. Rev. Lett.* **1985**, *55*, 2471. We have used the CPMD program version 3.0, Hutter, J. *et al.*, Max-Planck-Institut für Festkörperforschung and IBM Research 1990-99.
6. For comprehensive reviews, see Greer, S. G. *Adv. Chem. Phys.* **1996**, *94*, 261; Greer, S. C. *J. Phys. Chem. B* **1998**, *102*, 5413; Greer, S. C. *Annu. Rev. Phys. Chem.* **2002**, *53*, 173.
7. Akola, J.; Jones, R. O. *Macromolecules* **2003**, *36*, 1355.
8. Brunelle, D. J.; Boden, E. P.; Shannon, T. G. *J. Am. Chem. Soc.* **1990**, *112*, 2399.
9. Ballone, P.; Montanari, B.; Jones, R. O. *J. Phys. Chem. A* **2000**, *104* 2793.
10. Brunelle, D. J.; Shannon, T. G. *Makromol. Chem., Macromol. Symp.* **1991**, *42/43* 155.
11. Ballone, P.; Jones, R. O. *J. Phys. Chem. A* **2001**, *105*, 3008.
12. Montanari, B.; Ballone, P.; Jones, R. O. *J. Chem. Phys.* **1998**, *108*, 6947; Montanari, B.; Ballone, P.; Jones, R. O. *Macromolecules* **1998**, *31*, 7784; Ballone, P.; Montanari, B.; Jones, R. O.; Hahn, O. *J. Phys. Chem. A* **1999**, *103*, 5387; Montanari, B.; Ballone, P.; Jones, R. O. *Macromolecules* **1999**, *32*, 3396.
13. Ballone, P.; Jones, R. O. *J. Chem. Phys.* **2001**, *115*, 3895.
14. (a) Ballone, P.; Jones, R. O. *J. Chem. Phys.* **2002**, *116*, 7724, (b) *ibid.* **2002**, *117*, 6841.
15. Schäfer, L. *Phys. Rev. B* **1992**, *46*, 6061; Gujrati, P. D. *Phys. Rev. B* **1989**, *40*, 5140.

Aliphatic Polycarbonates

Chapter 16

Synthesis and Physical Properties of Tetramethylcyclobutanediol Polycarbonates

A. Ersin Acar and Daniel J. Brunelle

GE Global Research, 1 Research Circle, Niskayuna, NY 12309

Polycarbonates from 1,1,3,3-tetramethylcyclobutane-2,4-diol (TMCBD) have been prepared via transesterification reactions with diphenyl carbonate, and evaluated as UV-transparent, weatherable polymers. Melting and glass transition behavior was found to be related to *trans* content in the polymer. In melt transesterifications, the *trans* content decreased with long reaction time, due to a ring-opening decomposition reaction. However, high *trans* content could be maintained by preparing oligomers in the melt, followed by solid state polymerization to high molecular weight.

Introduction

Polymers for outdoor applications are currently an item of interest in the polymer industry. Such polymers should have good chemical resistance, mechanical properties, good abrasion or scratch resistance and most importantly excellent weathering properties. The latter entails resistance to uv light, leading to gloss and color retention, and good hydrolytic stability. Most of the aromatic resins used for such applications are not stable under *uv*-light due to photooxidation reactions taking place and therefore often contain *uv* stabilizers. For a resin to be inherently weatherable it either needs to be *uv* transparent or should have built-in *uv*-stabilizer. Aliphatic polymers are good examples of *uv*

transparent polymers which do not contain any functional group that can absorb at shorter wavelengths. However, these systems often have low glass transition temperatures that render them difficult to use even at moderate temperatures (50- 70°C) where the part dimensional stability and integrity is important. It is of interest to find new aliphatic monomers and polymers with higher glass transition temperatures. It would also be desirable for such materials to have good chemical and scratch resistance for specific applications such as automotive exteriors.

We have investigated 1,1,3,3-tetramethylcyclobutane-2,4-diol (TMCBD) polycarbonate for potential high temperature outdoor applications. TMCBD has already been incorporated into different polyesters to increase their glass transition temperatures (T_g). (1,2) It is believed that the rigidity of TMCBD monomer decreases the degree of freedom in the polymer and therefore increases its glass transition temperature, relative to other aliphatic diols. The monomer itself is synthesized by pyrolysis of isobutyric acid or isobutyric anhydride to form dimethylketene, which spontaneously dimerizes to cyclic diketone. Hydrogenation of the latter gives TMCBD as a mixture of *trans* and *cis* isomers (Figure 1). (3)

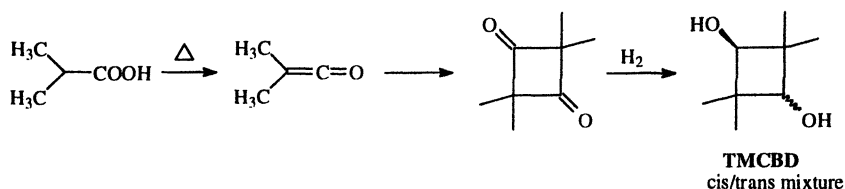


Figure 1. Synthesis of TMCBD monomer

TMCBD Polycarbonates have been previously reported in the literature. In these examples, polycarbonate formation was achieved either via direct phosgenation or ester interchange reactions using dialkyl carbonates or diaryl carbonates. (4,5,6) However, the synthesis can be problematic with both methods. Phosgenation reactions are slow, requiring refluxing in chlorobenzene for many hours. At the typical polymerization conditions for transesterification reactions, TMCBD decomposes and gives rise to poor polymer yields. Methods will be described to solve such problems and obtain high molecular weight, high yield TMCBD polycarbonates. Physical and rheology data of TMCBD polycarbonate will be presented and compared with other aliphatic systems.

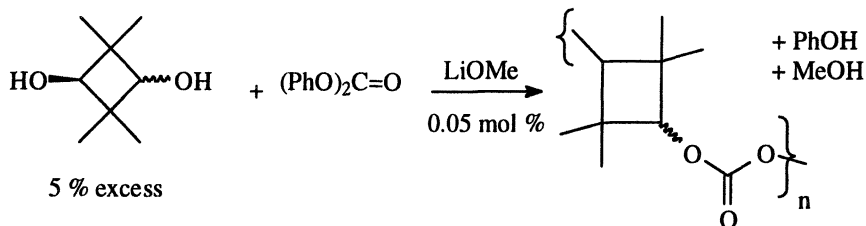


Figure 2. Structure and synthesis of TMCBD-Polycarbonate

Experimental

Chemicals: 2,2,4,4-tetramethyl-1,3-cyclobutanediol (TMCBD) was obtained from Eastman Chemical Company as a 55/45 cis/trans isomer mixture with >99% purity, or from TCI with a 35/65 cis/trans isomer ratio. Diphenyl carbonate (DPC) was supplied by GE Plastic Mt. Vernon, IN; LiOMe was purchased from Aldrich chemical Co. Bis-(2,2,2-trifluoroethyl)carbonate (TFEC) was prepared according to reference 9.

GPC: Analyses were performed on a Perkin Elmer instrument in chloroform containing 3 % isopropanol using a PLgel 5 μ Mixed-C column. A Hewlett Packard model HP1047A RI detector was used for polymer detection. Molecular weights by GPC were based on calibration with polystyrene standards.

DSC: The melt temperatures and crystallization temperatures were measured on a Perkin-Elmer DSC-7 with Pyris software. The typical DSC sample size was 5~10 mg and the DSC heating and cooling rates were 20 °C/min. The melting temperatures given in this report were taken from the endothermic peak of the second heating cycle. When double melting peaks were seen, the peak from the higher temperature was reported as T_m . The crystallization temperatures were taken from the exothermic peak of the second cooling cycle.

NMR: ^1H NMR spectra were run at 300 MHz on a GE NMR Instrument QE-300 or on a 400 MHz Bruker NMR spectrometer. Samples were prepared in CDCl_3 with TMS as an internal standard

Scratch Application: An apparatus to apply scratches reproducible in size to $\pm 0.1\mu\text{m}$ was built at GE Global Research Center. Scratches are made using a diamond-tipped indenter that moves along a sample surface under a constant applied normal load. The indenter is mounted on a Del-Tron air-bearing stage and this indenter assembly is moved in the vertical direction using a Parker Daedal Cross Roller Bearing stage. The air bearing stage allows for small vertical motions that compensate for sample tilt or curvature. X-Y motion is provided by two other Cross Roller Bearing stages. A Compumotor 4000 controller guides the three Roller Bearing stages. The normal force is applied

using dead weights that are placed on the indenter assembly. Typical loads are in the range of 400g to 2 Kg. The diamond indenters used in this study have a tip radius of 400Å with cone angles of 90°. The rate at which the scratch is applied is controlled by the speed of sample translation that is maintained at 0.1mm/second.

Scratch Size Measurement: Scratch dimensions are measured using an ADE Phaseshift Optical Interferometer with Mapvue Software. The total height of the scratch (h_{total}) and the width (w) were measured from the two-dimensional plot of the data as shown in Figure 3. The width is defined as the peak to peak distance and the total height is defined as the average of the peak to bottom distance of the two peaks.

Notched Izod Impact Test: Test was performed using a TMI Impact Tester (Model 43-02) for standard injection molded Izod bars. Notches (45° x 0.01" radius x 0.125" deep) were generated by a TMI Notcher (Model 43-15) with a single blade. Samples were equilibrated at a 40% relative humidity at room temperature for 48 hours before testing.

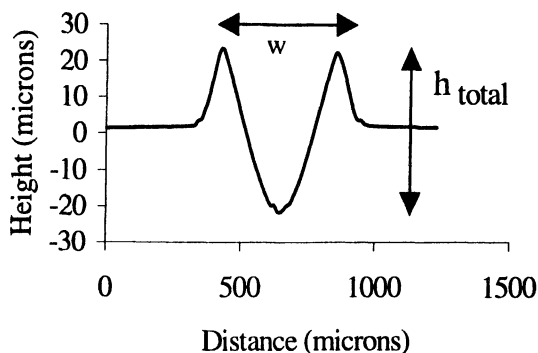


Figure 3: Two-dimensional representation of Interferometer data used to measure scratch dimensions.

Synthesis of TMCBD Polycarbonates

Melt polymerization with DMC and TFEC: TMCBD (65% *trans* content; 50 mmol; 7.211 g), bis-(2,2,2-trifluoroethyl)carbonate (55 mmol, 12.43g), and LiOMe (3.8 mg; 0.1 mmol) were combined and refluxed in 20 mL of dry toluene for one hour. The toluene and by-product trifluoroethanol were removed by distillation (pot temp = 150°C) for one hour, and replaced by 10 mL

of *o*-dichlorobenzene. The pot temperature was increased to 200°C, driving off the solvent and any remaining trifluoroethanol or trifluoroethyl carbonate. The product crystallized during the distillation. NMR analysis showed 62% *trans* content and a DP = 70. DSC showed T_m = 330°C and T_c = 280 °C.

Similar reaction using TMCBD with 50% *trans* content afforded TMCBD-PC with 48% *trans* content, M_w = 45,000, T_g = 118°C, T_m = 255°C, and T_c = 205°C.

Similar reaction using a mixture of 80% TMCBD with 65% *trans* content and 20% CHDM with 70% *trans* content led to 65% *trans* TMCBD-co-CHDM polycarbonate with T_g = 88°C, and T_m = 205°C.

Cylindrical Melt reactor: In order to prevent early solidification of the polymerization mixture, tubular reactors were used. It was believed that a better heat and mass transfer could be achieved with this type of reactor. 100 mL or 500 mL cylindrical glass reactors with a stainless steel stirring blade were used for high molecular weight TMCBD polycarbonate syntheses. Heating was achieved via a stainless steel-jacketed heating mantle. The temperature and pressure inside the reactor was computer controlled. A torquemeter was used to indirectly measure the viscosity increase during the polymerization.

Synthesis TMCBD polycarbonates via melt polymerization with diphenyl carbonate (DPC): DPC (63.43g, 1eq.), 2,2,4,4-tetramethyl-1,3-cyclobutanediol (TMCBD, 44.84 g, 1.05 eq) and LiOMe (5.6 mg, .0005 eq) were put into a tubular glass reactor fitted with a mechanical stirrer, a vacuum distillation adapter and a nitrogen inlet. The temperature of the mixture was adjusted to 130 °C. After starting materials were melt, the mixture was stirred at that temperature for 15-30 min. Then, temperature was raised stepwise to distill out phenol generated, and at each step solution was stirred for the times indicated; 180 °C (120 min), 210 °C (70 min), 230 °C (90 min) 253 °C (50-70 min). Then, vacuum was applied gradually where the pressure was dropped to 0.5-0.8 torr over 25-50 min. Polymerization was stopped when the viscosity stayed constant over 20 min as observed from torquemeter. A portion of the polymer was taken out by applying nitrogen pressure and collecting the strands from the bottom of the broken reactor. The polymer left in the reactor was dissolved in CHCl₃ and precipitated into MeOH, in order to collect the sample quantitatively.

TMCBD Decomposition product (2,2,4-trimethyl-pental) ¹H-NMR (CDCl₃): 9.62 (s, 1H); 5.65 (s, 1H); 9.62 (s, 1H); 5.65 (s, 1H); 9.62 (s, 1H); 5.65 (s, 1H).

Solid-state polymerization (SSP) of TMCBD polycarbonates: Oligomers with low molecular weight were synthesized as described above. Oligomers were then ground. Oligomer powder was put into a solid state polymerizer fitted with a collecting flask, where the phenol generated was carried out with hot nitrogen

and collected. SSP was carried out at 230 °C, under hot nitrogen flow. The final polymer powder was analyzed without further purification.

Results and Discussion

Synthesis of TMCBD Polycarbonates

A recent report by Kelsey, et al. (1) has shown that incorporation of TMCBD into polyesters can lead to dramatically increased glass transition temperatures. For example, a copolyester made from a 78/22 mole ratio of TMCBD/1,4-butanediol with dimethyl terephthalate raised the T_g of the polymer by nearly 100°C. Daly and Hahn report that TMCBD polycarbonate can be prepared via transesterification with diphenyl carbonate, using ~1.1% LiOH as catalyst. (7,8) Similarly, Walker, et al. (5) from Eastman Chemical have reported the preparation of TMCBD polycarbonate via transesterification with dimethyl carbonate, first forming the bis-methyl carbonate, followed by polymerization, removing dimethyl carbonate as the byproduct. However, in neither case were mechanical nor weathering properties of the polycarbonates reported. Therefore we began to pursue the synthesis of TMCBD polycarbonates containing 100% TMCBD, using a variety of methods. The goal of the study was to find a method which would give access to enough polycarbonate so that properties such as scratch resistance, impact resistance, chemical resistance and viscosity could be measured. A molecular weight of 60K and above was targeted for optimum physical properties. First, polymerizations with dimethyl carbonate or trifluoroethyl carbonate were investigated.

The procedure of Walker, et al. (5) calls for conversion of TMCBD to its bismethylcarbonate, via reaction with a large excess of dimethyl carbonate (5 eq.), followed by melt polymerization, affording 64-72% yield of the polymer. Although that procedure was straightforward, we found the polymerization, which must be driven by distillation of dimethyl carbonate, to be slow, and only afforded low molecular weight polymers (< 40,000) in our small scale reactions. Furthermore, yields were low due to decomposition processes, and a significant amount of *trans* content was lost, dropping from 65% *trans* in the monomer to 45% in the polymer.

Replacement of dimethyl carbonate with the activated bis-(2,2,2-trifluoroethyl) carbonate (9) (TFEC) allowed direct reaction with TMCBD (50% *trans*) using only a small excess (5%) of carbonate reagent, and basic catalysis: a white polymer with Mw = 45,000 was obtained. The TMCBD-PC, which had 48% *trans* content had T_g = 118°C, T_m = 255°C, and T_c = 205°C. A similar polycarbonate with a higher *trans* content was also prepared: TMCBD PC with 62% *trans* content had T_m = 330°C and T_c = 280°C. The polymer had Mn =

11,900 by nmr measurement of endgroups. Finally, an 80/20 copolycarbonate of TMCBD with 1,4-cyclohexanedimethanol (CHDM) was prepared, using the 65% *trans* TMCBD and 70% *trans* CHDM: the polymer had a low Tg (88°C), and Tm = 205°C.

Polymerizations with diphenyl carbonate

Because polymerization with dimethyl carbonate was difficult, yet polymers from trifluoroethyl carbonate looked promising, large scale polymerizations with diphenyl carbonate (DPC) were investigated next. Similar to previous work, melt polymerizations were carried out using base catalysis. LiOMe was employed as the catalyst so that the proton exchange would generate MeOH which is easily distilled from the polymerization mixture (Figure 3). A tubular reactor was used to better control heat flow, and to prevent premature crystallization, which had been observed in the work with trifluoroethanol using high *trans* content. Controlling the material balance was a challenge in this particular system. In addition to the instability of the TMCBD monomer mentioned earlier, it was known that DPC would sublime at the polymerization conditions. Therefore, initial polymerizations were carried out at various DPC and TMCBD feeding ratios, which indicated that high molecular weight TMCBD polycarbonates could be synthesized using a total of 5%-mol excess of TMCBD with respect to DPC (Table 1).

Table 1. TMCBD Polycarbonates synthesized by melt process (50 g scale)

Entry	Cat. conc. (mol%)	Mw $\times 10^{-3}$	PDI	Tg (°C)
1	0.1	64.2	1.83	123
2	0.01	50.5	1.70	120
3	0.05	78.3	2.01	124
4	0.05	93.2	1.86	124

In order to minimize the potential decomposition of the TMCBD monomer through base catalysis, the catalyst concentration was decreased substantially with respect to previous work (6,7) (>1%; Table 1). In all cases relatively high molecular weights could be achieved using the same feed ratios. Polymers obtained were slightly hazy. DSC analysis of the TMCBD-PC showed a Tg at 123 °C (lit. (5) DSC shows Tg = 105°C) and a melting point at 250 °C with 10.5 Cal/mol heat of crystallization (Entry 1, Table 1). The NMR spectrum of Entry 1 (Table 1) is shown in Figure 4.

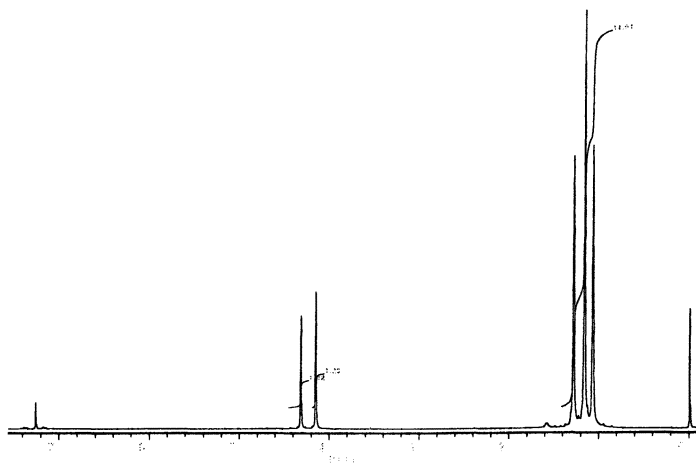


Figure 4. $^1\text{H-NMR}$ Spectrum of 57/43 cis/trans TMCBD-PC, Entry 1, Table 1

When polymers were isolated, approximately 10-15% of material was lost, similar to previous observations, and initially, this was attributed to multi-step isolation techniques. Since the glass transition temperature of the 64K polycarbonate was promising, we decided to scale up the polymerization. A total of 1 Kg TMCBD-PC was synthesized in four batches in which the molecular weight were controlled indirectly by torquemeter (Figure 5).

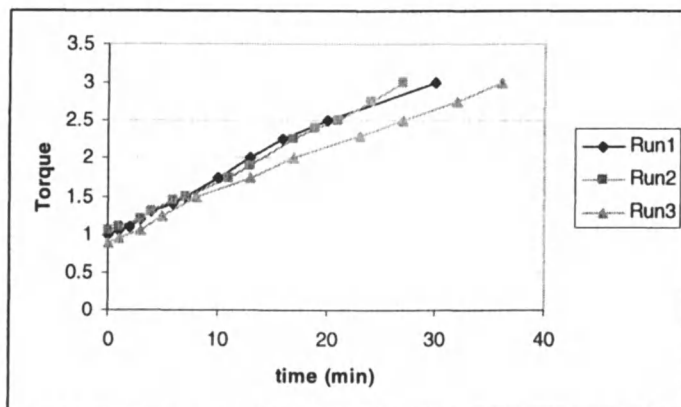


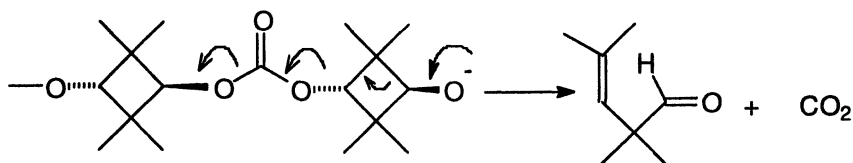
Figure 5. Molecular weight/torque increase during vacuum distillation as observed with torquemeter

Table 2. TMCBD-PC's Synthesized in 250 g scale

# RUN	M_w (10^3 g/mol)	PDI	T_g ($^{\circ}C$)	%Trans in Polymer	% Weight Loss
1	72	1.76	-	22	20
2	77	1.83	-	-	15
3	74	1.93	-	-	11
4	69	2.01	-	-	24
mix	70	1.83	125	23	-
Extruded	65	1.83	125	23	-
molded	60	1.81	126	23	-
65trans/35cis	125	1.86	122	24	40

Molecular weights obtained were surprisingly consistent. Interestingly, the isolated polymer yields were again 10 to 25 % less than theoretical values (Table 2). Unlike the previous experiences with smaller scale reactions, such loss could not be attributed to material loss due to isolation steps. In order to investigate the source of such material loss, materials distilling off the polymerization mixtures were investigated.

The vacuum line, dry-ice trap and the liquid nitrogen trap were filled with materials which proved *not* to be phenol. Further analysis of the solid indicated that it was a mixture of solidified CO_2 and the decomposition product of TMCBD, 2,2,4-trimethylpentenal. At this point it was interesting to determine the source of material loss from either monomer or polymer decomposition. If TMCBD monomer were decomposing, it seemed doubtful that high molecular weights could be achieved, since the correct TMCBD/DPC ratio would be lost. Decomposition in large scale reactions seemed to be higher than small scale reactions, but yet molecular weights were higher than that of the small scale analogues. When polymer samples were analyzed by 1H -NMR, it was found that *cis/trans* ratio of the TMCBD in the polymer (77/23) was higher than the initial ratio of 55/45, suggesting that *trans* TMCBD was decomposed preferentially.

Figure 6. Unzipping of TMCBD polycarbonate at sites containing *trans* isomer

When a similar polymerization was carried out using *trans*-rich TMCBD (Table 2, last entry, 65% *trans*), 40% of material was lost and *cis/trans* ratio increased up to 74/26. (last entry, Table 2). Despite such a high material lost, the molecular weight obtained was the highest ever achieved in our hands.

Results suggest that TMCBD decomposition and generation of CO₂ happens on the polymer or oligomer chain and not on the monomer. It is most probable that unzipping is fast at the sites containing the *trans*-isomer through a flip-flop mechanism favored by the anti-periplanar geometry of the leaving group, but slower when it reaches the *cis*-isomer (Figure 6). The remaining *cis*-TMCBD end groups can react further with DPC or phenyl carbonate end groups and form high molecular weight polycarbonates with a higher *cis* isomer content. Because of this unzipping reaction, it is difficult to prepare high molecular weight TMCBD-PC with a high level of *trans* content via melt chemistry. Interestingly, Daly and Hahn allude to decomposition only at 400°C, but do not discuss *cis* and *trans* isomer issues. (7)

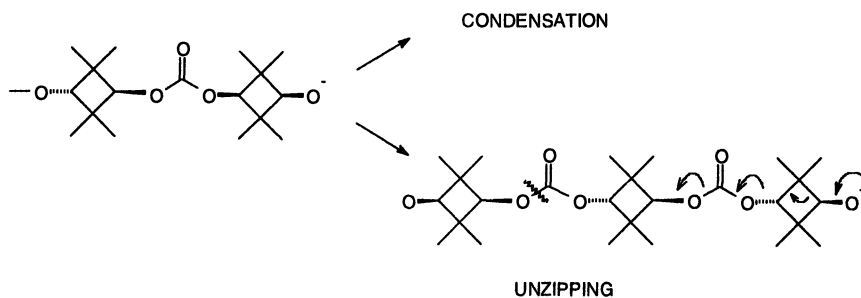


Figure 7. Competing reactions at high molecular weight

The unzipping process can also clarify another aspect of the polymerization. The significant drop in yield and decomposition of the *trans*-isomer was observed only when high molecular weights were targeted. This suggests a late decomposition of the polycarbonate chains. It is possible that as the polycarbonate chains reach high molecular weight, the concentration of the reactive end-groups decreases such that the intramolecular unzipping process takes precedence over the condensation reactions (Figure 7).

Changing or lowering the reaction temperature should, in principle, change the kinetics of both processes and possibly favor the condensation pathway. However, at lower temperatures due to the high melting point of TMCBD polycarbonate the polymerization mixture solidifies. Therefore, a solid state polymerization (SSP) technique was investigated next. In this approach, first low molecular weight oligomers were synthesized by the melt process using the same feeding ratio. Then, the resulting oligomers were subjected to solid state polymerization to give higher molecular weight polycarbonates. Using the SSP technique it was hoped that the yield of the polymerization and the *trans* isomer content could be increased significantly.

First, the optimum temperature for solid state polymerization was investigated. An oligomer with 24K molecular weight was subjected to SSP first at 220 °C (Figure 8). Polymerization proved to be slow at this temperature, and therefore temperature was raised to 230 °C at which temperature the molecular weight was built at a reasonable rate.

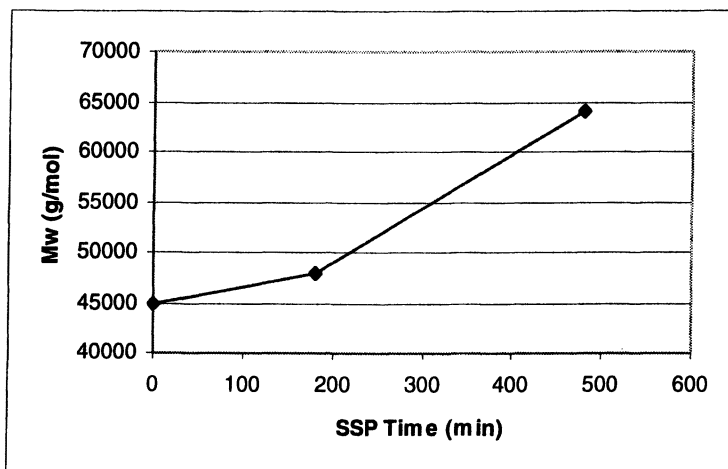


Figure 8. SSP of TMCBD-PC at 220 °C (up to 180 min) and 230 °C

Then a series of SSP were run under these conditions. As can be seen from in Table 3, the material loss was minimal, within experimental error range. It is important to note that the small amount of *trans*-isomer lost comes from the oligomerization step, the *trans/cis* ratio remained unchanged during SSP step, and was nearly twice the *trans* content that the melt polymerizations provided. Thus, combination of melt oligomerization and subsequent solid state polymerization of the oligomers increased the yield of TMCBD polycarbonate synthesis from 70-75% up to 90-93%, without optimization.

Table 3. TMCBD Polycarbonates synthesized by solid state polymerization

Olig Mw $\times 10^{-3}$	Mw $\times 10^{-3}$	PDI	Wt Loss (%)	Trans Loss (%)	Pzn. Temp °C
45	49	2.1	-	1	220
45	64	2.05	4	1	220-235
25	80	2.13	3	0	230
25	64	1.98	3	0	230
25	57	1.89	-	0	230

Physical Properties of TMCBD Polycarbonates

Impact and solvent resistance test with molded parts were carried out with the scaled TMCBD-PC with 77/23 *cis/trans* TMCBD content. TMCBD Polycarbonates showed very low impact resistance (Notched izod = 29.3 J/m, Stdev= 0.28). The polymers were readily soluble in organic solvents such as CH_2Cl_2 and CHCl_3 . When the molded bars were subjected to a gasoline test the TMCBD polycarbonates showed very poor performance. The polymer surface that contacted the gasoline washed away. The only samples that were resistant against gasoline were highly crystalline opaque samples.

The scratch resistance of TMCBD polycarbonate was also investigated. TMCBD polycarbonates showed better scratch resistance than PCCD and BPA-polycarbonate (Figure 9). Although based on one run it seems like the *trans/cis* ratio is important for the scratch resistance and higher *trans* content (TMCBD-PC 64K, 57/43 *cis/trans* TMCBD-PC, gives slightly better scratch resistance).

The viscosity of the TMCBD polycarbonates were higher than the PCCD polyesters with similar molecular weights. As expected the viscosity of TMCBD-PC (64K) decreases considerably above T_m (250 °C).

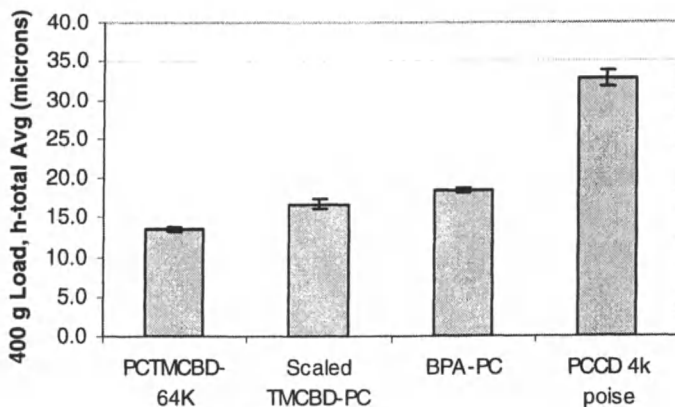


Figure 9. Scratch resistance of TMCBD-PC

Table 4. Melt viscosity of TMCBD-PC and PCCD

Polymer	Temperature (°C)	Viscosity
TMCBD-PC-64K	255	27,330
TMCBD-PC-64K	260	23,457
TMCBD-PC-64K	265	8,559
PCCD-2000 Poise	250	3,228
PCCD-4000 Poise	250	7,080

Conclusions

An efficient route for preparation of TMCBD polycarbonates using transesterification with diphenyl carbonate has been developed. Use of a combination of melt oligomerization and solid-state polymerization provides high molecular weight polymers with high *trans* content in high yield. Although the TMCBD Polycarbonates have high glass transition temperatures, high scratch resistance and are stable under weathering conditions, they show poor performance towards chemical and impact resistance. Their low impact and high solubility towards organic solvents require very specific applications where these would not be a problem.

Acknowledgement: We thank Steven Rice, James Kelley, Vicki Watkins, and Kay Longley for their significant experimental contributions.

References:

- ¹ Kelsey, D. R.; Scardino, B. M.; Grebowicz, J. S.; Chuah, H. H. *Macromolecules* **2000**, *33*, 5810. References cited therein.
- ² Sasaki, S.; Matsumoto, M.; JP 02,222,416, Kuraray Co. Ltd., Japan, **1990**.
- ³ Sumner, C. H. Jr.; Gustafson, B. L.; Knight, J. R., U.S. 5,169,994, Eastman Kodak Co., **1992**.
- ⁴ Matzner, M., U.S. Patent 3,527,734, Union Carbide Corporation, **1970**.
- ⁵ Walker, R. T.; Darnell, W.R.; Fleisher J. C.; US 6,037,436 **2001**.
- ⁶ Geiger, C. C.; Davies, J. D.; Daly, W.H., *Journal of Polymer Science: Part A Polymer Chemistry* **1995**, *33*, 2317
- ⁷ Daly, W.H.; Hahn, B.R. *Polymer Prep.*, **1989**, *30*(1), 337-338.
- ⁸ Geiger, C.C.; Davies, J.D.; Daly, W.H. *Jour. Poly. Sci. A: Polym. Chem.*, **1995**, *33*, 2317-2327.
- ⁹ Brunelle, D. J.; Smith, W.E. US Patent 4,217,438, General Electric, 1982.

Chapter 17

Synthesis of Novel Aliphatic Poly(ester-carbonates) Containing Pendent Olefin and Epoxide Functional Groups

Brian D. Mullen¹, Robson F. Storey^{2,*}, and Chau N. Tang²

¹GE Advanced Materials Mt. Vernon, Inc., One Lexan Lane, Mt. Vernon, IN 47620

²School of Polymers and High Performance Materials, Department of Polymer Science, The University of Southern Mississippi, Box 10076, Hattiesburg, MS 39406

The synthesis and polymerization of a novel cyclic carbonate monomer containing a pendent unsaturated ester group, 5-methyl-5-allyloxycarbonyl-1,3-dioxan-2-one (MAC) is reported. The random copolymerization of this cyclic monomer with *rac*-lactide was performed using stannous ethoxide (Sn(OEt)₂) as the catalyst/initiator. Random copolymers containing various amounts of MAC and *rac*-LA were synthesized to introduce unsaturated groups pendent to the polymer backbone for possible crosslinking, epoxidation, or addition reactions. In addition, oligomeric macroinitiators of MAC were synthesized, and ring-opening polymerization of *rac*-LA yielded near monodisperse poly(*rac*-LA) with multiple double bonds pendent to one end of the polymer chain. Post-polymerization epoxidation reactions of the copolymers were performed with *m*-chloroperoxy benzoic acid to yield poly(ester-carbonates) with epoxide groups randomly along the backbone (random copolymer) or at one end of the polymer chain (from the MAC oligomeric macroinitiator). The epoxide groups provide a pathway for more organic transformations with alcohols, carboxylic acids, and amines.

Introduction

The application and usefulness of synthetic biodegradable polymers has grown exponentially in the last few decades. The excellent degradation characteristics and environmental acceptability of polymers derived from *rac*-lactide (*rac*-LA), *L*-lactide (LLA), ϵ -caprolactone (CL), glycolide (GA), and trimethylene carbonate (TMC) have led to a number of commercial applications. Polymers prepared from lactic acid have found numerous uses in the biomedical industry, beginning with the first biodegradable sutures approved in the 1960's.(1) Presently, Cargill-Dow LLC has made investments to produce over 140,000 tons of PLLA annually for packaging applications, fibers, and coatings.(2) The market of bioabsorbable polymers exceeds \$300 million annually (> 95% from biodegradable sutures and drug delivery), for example, a GA-TMC copolymer (Maxon® by Tyco(®)) is used as a monofilament suture and microspheres of a *rac*-LA-GA copolymer (Leuprolide Depot® by TAP Pharmaceutical Co.) are used to deliver leuprolide in the treatment of prostate cancer.

The syntheses of new cyclic carbonates that contain pendent functionalities have been reported in the last few years and provide an important methodology for the development of biodegradable polycarbonates with unique morphological, degradative, and physical properties. Grimm and coworkers reported the synthesis of a protected six-membered hydroxy-functionalized cyclic carbonate derived from trimethylol propane and dialkyl esters of carbonic acid.(3) Additionally, Gross et al. reported the synthesis of polycarbonates containing pendent hydroxyl groups.(4-6) Cyclic carbonates containing pendent carboxylic acid groups have been synthesized by the Bisht and Storey research groups.(7-8) Bisht and co-workers also reported the synthesis of the monomer, 5-methyl-5-carboxy-1,3-dioxan-2-one (MCC), and created copolymers with TMC utilizing enzyme-catalyzed ring-opening polymerization.(9)

There are a few examples of the synthesis of six-membered cyclic carbonates with unsaturated groups and other functionalities. Hocker and coworkers synthesized cyclic carbonates with pendent cyanide groups, allyl functionalities, ethers, esters, and norbornenes.(10) Endo and coworkers have synthesized amino acid-functionalized six-membered cyclic carbonates derived from *L*-serine and *L*-threonine.(11) Additionally, Gross and McCarthy have reported the synthesis of a 6-membered cyclic carbonate which contained an unsaturated group that was oxidized to hydroxyl groups in a post-polymerization reaction.(6)

In this chapter, we report the synthesis of a new 6-membered cyclic carbonate containing double bond functionality, 5-methyl-5-allyloxycarbonyl-1,3-dioxan-2-one (MAC).(12) The random copolymerization of this monomer

with *rac*-lactide was performed using commercially available stannous ethoxide ($\text{Sn}(\text{OEt})_2$) as the catalyst/initiator, and the polymerizations were conducted in bulk or in toluene solution at elevated temperatures. Polymers containing the co-monomer MAC were synthesized to introduce reactive double bond functionality into the polymer backbone for possible crosslinking, epoxidation, or addition reactions. Also, soluble macroinitiators of MAC were synthesized, and the controlled ROP of *rac*-LA was accomplished to afford near monodisperse poly(*rac*-LA) with numerous double bonds on one end of the polymer chain. Post-polymerization oxidation reactions were carried out with *m*-chloroperoxy benzoic acid (*m*CPBA) to afford polymers with epoxide groups placed randomly along the backbone (random copolymer) or at one end of the polymer chain (from the MAC macroinitiator).

Experimental

Materials.

Toluene was refluxed over sodium pellets for 24-48 h and distilled under N_2 before use. Tetrahydrofuran (THF) was refluxed over sodium benzophenone for 24 h and distilled under nitrogen atmosphere. DOWEX 50WX2-200 (Dowex) resin was purchased from Aldrich and washed with concentrated HCl, water, acetone, and CH_2Cl_2 before use. Triethylamine (TEA) and methylene chloride (CH_2Cl_2) were distilled from calcium hydride under nitrogen atmosphere. 2,2-Bis(hydroxymethyl) propionic acid (*bis*-MPA), allyl bromide, potassium carbonate (anhydrous), ethyl chloroformate, 2,2-dimethoxy propane, and *p*-toluenesulfonic acid (PTSA) were purchased from Aldrich and used as received. 2,2-dimethyl-5-methyl-5-carboxy-1,3-dioxane (DMCD) was synthesized according to a previously published procedure.⁽¹³⁾

Characterization

^{13}C and ^1H NMR spectra were acquired using a Varian 300 spectrometer and 5 mm O.D. tubes. Either CDCl_3 or *D*₆-DMSO was used as solvent with internal reference tetramethylsilane (TMS); sample concentrations were ~10% (w/v) for ^{13}C and ~5% (w/v) for ^1H NMR spectra. The comonomer compositions for poly(*rac*-LA-*co*-MAC) were calculated using proton NMR. The calculations were based on the integration of the relative peak areas of the allyl protons ($-\text{CH}_2-\text{CH}=\text{CH}_2$) corresponding to the MAC repeat units (d, 4.62 ppm) and the methyl protons ($-\text{CH}(\text{CH}_3)\text{O}-$) corresponding to the lactide repeat units (d, 1.56 ppm).

Size exclusion chromatography experiments were performed to determine the molecular weights and polydispersities (PDI) of the polymeric materials as previously described.⁽⁹⁾

Synthesis

Allyl isopropylidene-2,2-bis(oxymethyl) propionate (AIP-bis-OMP). In a typical reaction, a 1 L round bottom flask containing 400 mL of ethanol was charged with 23.3 g of (DMCD) (0.144 mol) and 41.6 g anhydrous potassium carbonate (0.304 mol). The mixture was stirred at room temperature for 24 h. The excess K_2CO_3 was filtered, and the solvent was removed *in vacuo* to produce the white, solid, potassium carboxylate salt, which was dried *in vacuo* for 24 h; yield = 31.9 g (96.0 %). Subsequently, a 500 mL round bottom flask was charged with 31.9 g of the potassium carboxylate salt DMCD (0.151 mol), 22.5 mL of allyl bromide (0.260 mol), and 350 mL of acetone. The mixture was stirred at room temperature for approximately 1 h. Then, the reaction was placed into a silicone oil bath thermostatted at 45 °C and stirred for an 48 h. The solid KBr was filtered from the mixture. The filtrate was concentrated by removal of the solvent *in vacuo*. The crude product was a yellow viscous liquid, which was purified by stirring with activated carbon in CH_2Cl_2 . The activated carbon was removed by filtration, and the organic solvent was evaporated to produce a clear liquid; yield = 29.9 g (94.0 %) of AIP-bis-OMP. 1H NMR δ ($CDCl_3$): 1.2 (s, 3H, $-CH_3$), 1.3 – 1.5 (d, 6H, $-C(CH_3)_2$), 3.6-3.7 (d, 2H, $-OCH_2C-$), 4.1-4.3 (d, 2H, $-OCH_2C-$), 4.6-4.7 (d, 2H, $-OCH_2CH=$), 5.2-5.4 (m, 2H, $=CH_2$), and 5.8-6.0 (m, 1H, $=CH-$) ppm. ^{13}C NMR δ ($CDCl_3$): 18.6 ($-CH_3$), 22.7 ($-O-C(CH_3)_2-O-$), 24.6 ($-O-C(CH_3)_2-O-$), 41.8 (quat C), 65.2 ($O-CH_2-CH=$), 65.9 ($-CH_2-O-$), 97.9 ($-O-C(CH_3)_2-O-$), 117.9 ($-CH=CH_2-$), 132.0 ($-CH_2-CH=$), 173.7 ($-COO-$) ppm.

Allyl 2,2-bis(hydroxymethyl) propionate (A-bis-MP). Into a 500 mL Erlenmeyer flask containing 200 mL of methanol were charged 29.9 g of AIP-bis-OMP (0.140 mol) and 3.0 g of Dowex resin. The mixture was stirred at room temperature for 40 h. The resin was filtered, and the filtrate was concentrated to obtain a yellow viscous liquid. The product was diluted with 50 mL of THF, and 5.0 mL of triethylamine was added dropwise by syringe to scavenge any remaining HCl which may be present in the reaction mixture. Solid triethylammonium hydrochloride salt was filtered from the mixture, and the filtrate was purified by stirring with activated carbon and then filtered. Removal of the THF by rotary evaporation afforded 24.1 g of a clear oil (yield = 99.0 %). 1H NMR δ ($CDCl_3$): 1.07 (s, 3H, $-CH_3$), 3.4-3.5 (d, 2H, $-CH_2-OH$), 3.6-3.8 (d, 2H, $-CH_2-OH$), 3.8-3.9 (d, 2H, $-O-CH_2-CH=$), 5.2-5.4 (m, 2H, $-CH=CH_2$), 5.8-6.0 (m, 1H, $-CH_2-CH=$) ppm. ^{13}C NMR δ ($CDCl_3$): 17.6 (CH_3), 49.6 (quat C), 65.8 $-O-CH_2-CH=$, 67.2 ($-CH_2-OH$), 118.5 ($-CH=CH_2$), 131.9 ($-CH=CH_2$), 175.6 (C=O) ppm.

5-methyl-5-allyloxycarbonyl-1,3-dioxan-2-one (MAC). Into a 1 L 3-necked round-bottom flask containing 500 mL of THF were charged 16.8 g Allyl-bis-MP (0.096 mol) and 27.6 mL of ethyl chloroformate (0.289 mol). The reactants

were mixed at 0 °C for 15-20 min. Triethylamine (40.3 mL, 0.289 mol) was added drop-wise to the stirring reaction mixture via a 100 mL addition funnel over a period of 15 min. The ice bath was removed and the contents of the reaction were stirred at room temperature for an additional 2 h. The TEA-HCl solid was filtered. The filtrate was concentrated by rotary evaporation of the volatiles to obtain a viscous liquid, which crystallized upon cooling. The solid was washed with diethyl ether (100 mL) to obtain 13.3 g (69.0 %) of a white crystalline solid. M.P. = 66-67 °C. ¹H NMR δ (CDCl₃): 1.3 (s, 3H, -CH₃), 4.2-4.3 (d, 2H, -O-CH₂-C-), 4.67-4.73 (d, 2H, -O-CH₂-C-), 4.73-4.75 (s, 2H, -O-CH₂-CH=), 5.2-5.4 (m, 2H, -CH=CH₂), 5.6-5.8 (m, 1H, -CH=CH₂) ppm. ¹³C NMR δ (CDCl₃): 17.5 (-CH₃), 40.1 (quat C), 66.5 (-O-CH₂-CH=), 72.8 (-O-CH₂-C-), 119.2 (-CH=CH₂), 130.7 (-CH=CH₂), 147.2 (-O-CO-O-), 170.5 (-COOR) ppm. Elemental analysis calculated for C₉H₁₂O₅: C, 54.0; H, 6.0; O, 40.0. Found: C, 53.7; H, 6.0; O, 40.2.

Polymerization Techniques

Homopolymerization and random copolymerization were carried out within a dry-N₂ glove box at 115 °C in the bulk or at 95 °C in freshly distilled toluene.⁽¹²⁾ In a typical polymerization, 5.315 g of MAC (26.5 mmol), 10.190 g of *rac*-LA (71.0 mmol), and 0.085 g of Sn(OEt)₂ (0.40 mmol) were placed into a 100 mL round bottom flask. The flask and contents were placed into an oil bath thermostatted at 115 °C. The reaction contents were stirred with an overhead mechanical stirrer, and after polymerization (< 2 h), the polymer was precipitated into methanol. The polymer was dried *in vacuo* for 24 h prior to characterization.

Sn-MAC Macroinitiator Adduct. In a typical experiment, carried out within a dry-N₂ glove box, 1.0 g of MAC (5.0 mmol), 0.050 g of Sn(OEt)₂ (0.24 mmol), and 3.95 g of toluene were placed into a 50 mL round-bottom flask. The flask and contents were heated at 95 °C in a thermostatted oil bath for approximately 10 min. The flask was stoppered and the macroinitiator, Sn-MAC, with an approximate degree of polymerization, DP, equal to 10, was stored in the dry-N₂ glove box at room temperature until used to initiate polymerization.

Sn-Rac-LA Macroinitiator Adduct. In a typical experiment, carried out within a dry-N₂ glove box, 1.2 g of *rac*-LA (8.3 mmol), 0.060 g of Sn(OEt)₂ (0.29 mmol), and 4.2 g of toluene were placed into a 50 mL round bottom flask. The flask and contents were heated at 95 °C in a thermostatted oil bath for approximately 10 min. The flask was stoppered and the macroinitiator, Sn-*rac*-LA, with an approximate degree of polymerization, DP, equal to 14, was stored in the dry-N₂ glove box at room temperature until used to initiate polymerization. Subsequent polymerization of *rac*-LA was performed.

Epoxidation of the Allyl groups of the Poly(ester-carbonates). In a typical reaction, a 100 mL round-bottom flask was charged with 3.0 g of poly(*rac*-LA-co-MAC), 2-4 molar excess of *m*-chloroperoxybenzoic acid (*m*CPBA 70 % max purity) with respect to the double bonds of MAC, and 50 mL of CHCl₃. A reflux condenser was fitted to the round-bottom flask, and the mixture was refluxed for 8 h. The contents of the flask were allowed to cool in the refrigerator. The solution was filtered and precipitated into hexane. The polymer was rinsed with hexanes and allowed to dry 24 h *in vacuo*.

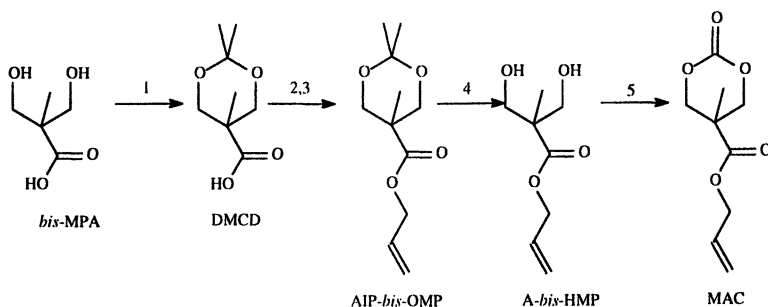
Results and Discussion

The five-step synthetic strategy of the new cyclic carbonate monomer, MAC, is outlined in Scheme 1.(12) A number of synthetic transformations of the starting material *bis*-MPA into multi-functional initiators, dendrimers, and cyclic carbonates have been reported.(8-10,13) An acetonide diol protecting group was utilized to prevent side reactions of the hydroxyl and carboxylic acid groups of *bis*-MPA during esterification of the carboxylic acid group. The protected intermediate, DMCD, was synthesized in 89 % yield by reacting 2,2-dimethoxypropane with *bis*-MPA. The acetonide protecting group was chosen because of its stability toward basic reagents and its quantitative de-protection with mild acidic resin. After protection of the diol, the potassium carboxylate salt was synthesized by reaction of DMCD with excess potassium carbonate (quantitative yield) in ethanol solution. The excess potassium carbonate was removed by vacuum filtration, and the potassium carboxylate salt of DMCD was reacted with allyl bromide in acetone to afford AIP-*bis*-OMP in good yield (94%). The diol-protecting group of AIP-*bis*-OMP was cleaved with DOWEX 50W-X2, to liberate the 1,3-diol, A-*bis*-HMP (99% yield); deprotection was monitored by the disappearance of the methyl protons (δ 1.3-1.4 ppm) of the acetonide group. The diol, A-*bis*-HMP, was reacted with ethyl chloroformate to yield the cyclic carbonate monomer containing an unsaturated moiety, MAC (69% yield). The NMR spectra of MAC are illustrated in Figure 1.

The copolymerization of MAC with *rac*-LA was performed either in the melt or in toluene solution in the presence of stannous ethoxide, which served as initiator/catalyst (Scheme 2). Polymerizations were maintained at or below 115 °C to minimize side reactions such as, trans-esterification and trans-carbonation.(12) However, at higher incorporations of MAC, the synthetic polymers displayed relatively broad polydispersities, and the experimental number average molecular weights (SEC) were higher than those predicted based on the monomer/initiator ratio and the assumption of a living polymerization. These results were consistent with our previous findings for tin-catalyzed ROP of similar cyclic carbonates, and are attributed to branching involving the ester side-group,(9) however, decreasing the polymerization

temperature to 95-110 °C and making the polymerization reaction homogeneous by the addition of a solvent decreased the polydispersity of the final polymers, and only decreased monomer conversion slightly.

Scheme 1^a



^a Conditions of experiment: (1) PTSA, 2,2-dimethoxy propane, acetone, 25 °C, 8h; (2) anhyd. K₂CO₃, EtOH, 25 °C, 8h; (3) allyl bromide, acetone, 25 °C, 4 h; 45°C, 48 h, (4) DOWEX 50W-X2 H⁺, MeOH, 25 °C, 8h; (5) ethyl chloroformate, TEA, THF, 0 °C 30 min, 25 °C 2h.(12)

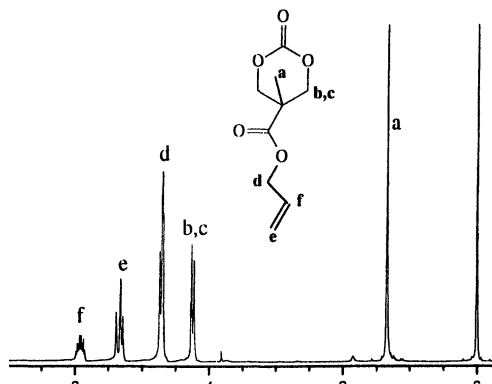
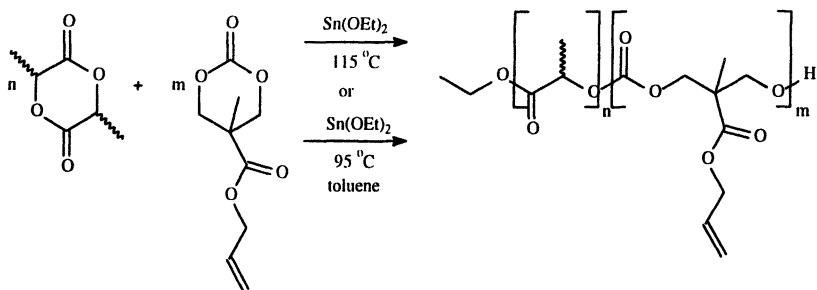


Figure 1. ¹H NMR spectrum of MAC.

Scheme 2



The copolymerization of MAC and *rac*-LA was accomplished utilizing a range of comonomer ratios in the feed; Table 1 summarizes the results.⁽¹²⁾ Monomer conversions were calculated by integrating the relative peak areas of the monomer (18.2-19.6 mL elution volume) and polymer (< 18 mL elution volume) peaks from the refractive index chromatogram of the SEC system. In general, monomer conversions were > 95% conversion after approximately 2 h of reaction time. NMR was utilized to calculate the copolymer compositions by integrating the relative peak areas of the allyl ($-\text{CH}_2\text{-CH}=\text{CH}_2$) protons corresponding to the MAC repeat units (δ , 4.62 ppm) and the methyl ($-\text{CH}(\text{CH}_3)\text{O}-$) protons corresponding to the lactide repeat units (δ , 1.56 ppm). In general, the incorporation of MAC into the copolymer was slightly less than the amount charged into the feed, possibly due to the higher reactivity of *rac*-LA toward ROP with $\text{Sn}(\text{OEt})_2$.

Comonomer incorporation into the copolymers appeared to be random according to NMR and thermal analysis. The carbonate region of the MAC repeat unit and the ester region of the *rac*-LA repeat unit also demonstrated sensitivity toward monomer sequencing. Figure 2 displays the carbonate carbonyl region of three *rac*-LA-MAC copolymers containing different fractions of MAC and *rac*-LA. The carbonate carbon corresponding to the MAC-MAC dyad displayed a chemical shift at 154.4 ppm, and the carbonate carbon corresponding to the MAC-*rac*-LA dyad displayed an upfield chemical shift at 154.1 ppm. As expected for random copolymers, the carbonate carbon corresponding to the MAC-*rac*-LA dyad increased with increasing incorporation of *rac*-LA in the final copolymer.

Table I. Molecular characteristics of Random Copolymers of *Rac*-LA and MAC Initiated by Sn(OEt)₂ in the Bulk or in Toluene

Entry	$f_{\text{MAC}}^{\text{a}}$	$F_{\text{MAC}}^{\text{b}}$	$M_{\text{n,th}}^{\text{c}}$	$M_{\text{n,exp}}$		Conversion ^e (%)	Temp. (deg. C)	Time (min)
				SEC ^d	$M_{\text{w}}/M_{\text{n}}$			
1	0.05	0.02	90,738	88,200	1.6	95	110 ^f	60
2	0.1	0.06	16,280	18,800	1.7	>99	115 ^f	120
3	0.1	0.1	46,319	40,800	1.6	96	95 ^g	60
4	0.2	0.2	23,858	37,600	3.1	>99	115 ^f	120
5	0.25	0.2	30,840	31,600	1.6	95	95 ^g	60
6	0.3	0.2	3,152	6,000	1.7	>99	115 ^f	120
7	0.3	0.3	19,372	24,700	4.0	>99	115 ^f	120
8	0.7	0.5	15,951	28,300	10.1 ⁱ	>99	115 ^f	120
9	1.0	1.0	---	13,700	1.8	98	40 ^h	20

^aMolar fraction of MAC in the comonomer feed. ^bMolar fraction of MAC in the random copolymer (determined by ¹H NMR analysis). ^cTheoretical molecular weight for a living polymerization. ^dExperimental molecular weight determined by SEC/MALLS. ^eConversions calculated using SEC (ratio of the polymer peak area to the monomer peak area from the refractive index chromatogram). ^fBulk polymerizations. ^gPolymerizations were conducted in toluene (co-monomer conc. = 1.4-1.5 M) solution at 95°C. ^hBulk polymerization conducted under vacuum without added initiator or catalyst (35 in. Hg). ⁱPolydispersity was very broad, and ASTRA™ software had difficulty calculating the polydispersity (PDI = 10.1) and displayed an error percentage of 15%, which is relatively a large % error.

SOURCE: Reproduced from reference 12 with permission from John Wiley & Sons © 2003.

Table II. Molecular Characteristics of Polymers initiated by Sn(II) Macroinitiators in Toluene (1.4 M) at 95 °C

Entry	Macroinitiator	Monomer	$M_{n,th}^a$	$M_{n,exp}$	
				SEC ^b	M_w/M_n
1	MAC	<i>rac</i> -LA	30,726	32,700	1.2
2	<i>rac</i> -LA	<i>rac</i> -LA	30,492	30,100	1.1

^aTheoretical molecular weight determined using the following equation:

$$\overline{M}_n(\text{theory}) = \frac{([M]_0 - [M])M_p}{2[\text{Sn}(\text{OR})_2]} + \overline{X}_A M_A + M_{\text{EtOH}} \quad \text{where, } [M]_0 = \text{initial monomer}$$

concentration in polymerization, $[M]$ = final monomer concentration in polymerization, M_p = molecular weight of monomer used in polymerization, $[\text{Sn}(\text{OR})_2]$ = concentration of macroinitiator in polymerization, \overline{X}_A = number average degree of polymerization of macroinitiator per ethoxide initiating moiety, M_A = molecular weight of monomer used in macroinitiator formation, M_{EtOH} = molecular weight of ethanol.¹² ^bDetermined using SEC/MALLS.

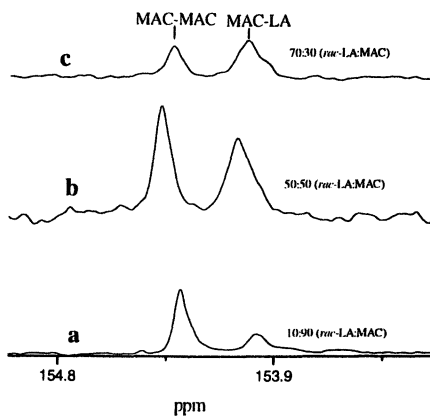


Figure 2. ¹³C NMR displaying the carbonate region of (a) Entry 1, Table II; (b) Entry 8, Table I; and (c) Entry 7, Table I. Reproduced from reference 12 with permission from John Wiley & Sons © 2003.

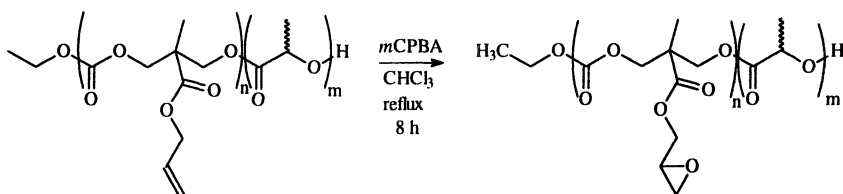
The *rac*-LA-MAC copolymers were analyzed by DSC and found to display a single glass transition temperature, indicative of a random copolymer. Figure 3 shows the experimental glass transition data (closed squares) and theoretical Flory-Fox line(15) (open squares) of poly(*rac*-LA-co-MAC) plotted as a function of wt% MAC; the experimental T_g data are nearly equivalent to the theoretical values. The copolymers were found to be completely amorphous.

In an earlier study, we reported the controlled polymerization of cyclic esters and carbonates using macroinitiators derived from stannous ethoxide and a cyclic ester, including LLA, *rac*-LA, and CL,(16) however, the use of a cyclic carbonate macroinitiator was not reported. The use of MAC as a macroinitiator offers the synthetic polymer chemist a technique to functionalize one end of the polymer backbone with numerous pendent groups, which contain double bonds for grafting or other post-polymerization modifications.

Table 2 displays the results of the ring opening polymerization of *rac*-LA or MAC utilizing Sn-*rac*-LA or Sn-MAC adduct. The Sn-MAC macroinitiator (Entry 1, Table 2), with an approximate degree of polymerization equal to approximately 10 MAC units per initiating fragment was used for the controlled polymerization of *rac*-LA; thus, in these cases, utilizing MAC as a macroinitiator provided 10 double bonds per poly(*rac*-LA) chain. The experimental molecular weights of the polymers produced from the macroinitiators were nearly equivalent to the theoretically predicted molecular weights, and the polydispersities of the poly(*rac*-LA) were ≤ 1.2 . The Sn-*rac*-LA macroinitiator (Entry 2, Table 2) was used for the ROP of *rac*-LA and provided approximately 14 repeat units of *rac*-LA per polymer chain. The theoretical number average molecular weights were nearly equivalent to the experimental molecular weights determined by SEC/MALLS. As predicted from earlier results,(16) the polydispersity of poly(*rac*-LA) initiated by Sn-*rac*-LA was very narrow (PDI = 1.1), indicative of a controlled ROP.

Scheme 3 displays the epoxidation scheme for the MAC-copolymers. The oxidation reactions were performed in refluxing chloroform for 4-8 h. Figure 4 displays carbon NMR spectra of poly(MAC) before and after epoxidation with *m*CPBA, and Figure 5 shows the SEC. Nearly quantitative oxidation occurred at a reaction time of 8 h, and oxidation was easily monitored by the disappearance of the olefinic carbons at chemical shifts of 118.4 ppm and 131.6 ppm and the appearance of the two epoxidized carbons at 44.6 ppm and 49.3 ppm. Many of the poly(*rac*-LA-co-MAC) materials and poly(*rac*-LA) initiated by the Sn-MAC macroinitiator adduct were subjected to epoxidation to afford poly(ester-carbonates) with pendent epoxide groups.

Scheme 3.



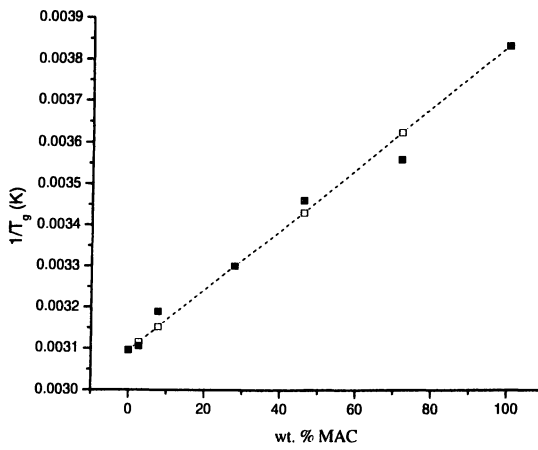


Figure 3. Plot of wt% MAC vs. $1/T_g$ (K), (\square) = experimental data; (\blacksquare) = theoretical data. Reproduced from reference 12 with permission from John Wiley & Sons © 2003.

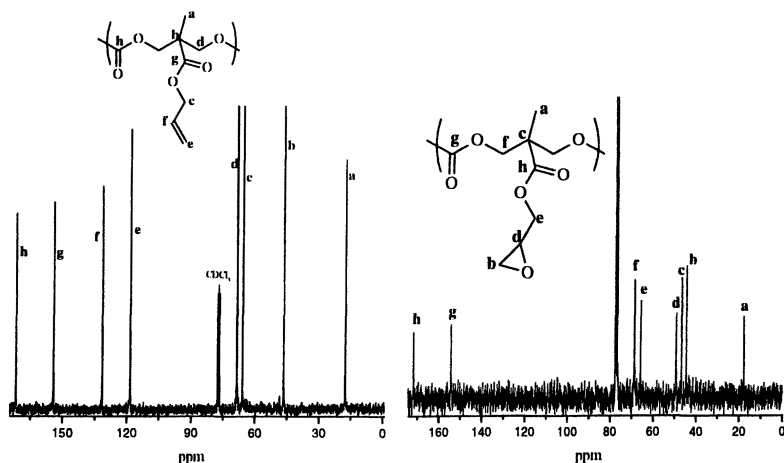


Figure 4. ^{13}C NMR spectra of (a) poly(MAC) and (b) poly(MAC) after epoxidation of the double bonds. Reproduced from reference 12 with permission from John Wiley & Sons © 2003.

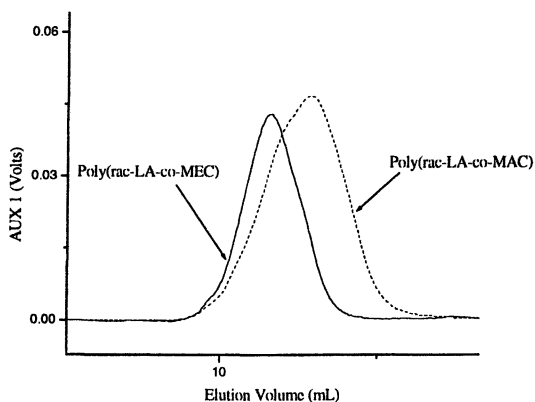


Figure 5. SEC traces of poly(rac-LA-co-MAC) (Entry 4, Table I) before and after epoxidation of the double bonds of MAC. Reproduced from reference 12 with permission from John Wiley & Sons © 2003.

Conclusions

The synthesis of a new cyclic carbonate containing double bond functionality, 5-methyl-5-allyloxycarbonyl-1,3-dioxan-2-one (MAC) has been reported in this chapter. Homopolymerization and copolymerization with *rac*-LA was accomplished using stannous alkoxide catalyst/initiators. The amount of double bonds was controlled by the molar fraction of MAC in the comonomer feed. The polymerizations were random in nature, and the controllability of the polymerization was related to reaction temperature, the amount of MAC in the feed, and whether the polymerization was homogeneous. Macroinitiators of MAC and *rac*-LA were synthesized with $\text{Sn}(\text{OEt})_2$ in toluene. These macroinitiators enabled the controlled polymerization of *rac*-LA. Post-polymerization oxidation of the allyl groups of the MAC-containing polymers provided epoxide groups along the polymer chain. Epoxide groups provide a pathway for reaction of the polymer backbone with any number of nucleophilic reagents (alcohols, amines, carboxylic acids, etc.). These further modifications might be used to favorably influence the thermal properties and/or solubility of the polymer depending on the choice of nucleophile. Finally, the epoxide groups offer sites for crosslinking or possibly for drug attachment/delivery applications.

Acknowledgments

The research upon which this material was based was funded by the Office of Naval Research Grant No N00014-01-1-1047. The authors would like to thank Dr. William Jarrett and Heidi Assumption for their technical assistance with the NMR experiments. Additionally, the authors would like to thank the editors/organizers for their hard work and effort during the Advances in Polycarbonates A.C.S. Symposium Series and the preparation of this book.

References

1. Middleton, J.C.; Tipton, A.J. In *Medical Plastics and Biomaterials* **1998**, 5(2).
2. <http://www.cargilldow.com/product.asp>.
3. Grimm, H. Buyusy, H.J. *EU Patent* 57,360, **1984**.
4. Chen, X.H., McCarthy, S.P.; Gross, R.A. *J. Appl. Poly. Sci.* **1998**, 67, 547.
5. Gross, R.A.; Chen, X.; McCarthy, S.P. *US* 6,093,792, **2000**.
6. Gross, R.A.; Kumar, R. *US* 6,316,581, **2001**.

7. Al-Azemi, T.F.; Bisht, K.S.; *Macromolecules* **1999**, *32*, 6536.
8. Storey, R.F.; Mullen, B.D.; Melchert, K.M. *J. M. S., Pure Appl. Chem.* **2001**, *A(38)*, 9, 897.
9. Al-Azemi, T.F.; Bisht, K.S. *J. Polym. Sci., Part A: Poly. Chem.* **2002**, *40*, 1267.
10. Keul, H.; Höcker, H. *Macromol. Rapid Commun.* **2000**, *21*, 869.
11. Sanda, F.; Kamatani, J.; Endo, T. *Macromolecules*, **2001**, *34*, 1564.
12. "New Aliphatic Poly(ester-carbonates) based on 5-methyl-5-allyloxycarbonyl-1,3-dioxan-2-one." Mullen, B.D.; Storey, R.F.; Tang, C.N. *J. Polym. Sci., Part A: Poly. Chem.*, *41*, 1978, Copyright © 2003. Reprinted by permission of John Wiley & Sons, Inc.
13. Ihre, H.; Hult, A.; Frechet, J.M.J.; Gitsov, I. *Macromolecules* **1998**, *31*, 13, 4061.
14. Messman, J.M.; Storey, R.F. *ACS Div. Polym. Chem. Polym. Preprs.* **2002**, *43*, 948.
15. Fox, T.G. *Bull. Am. Chem. Soc.* **1956**, *1*, 123.
16. Storey, R.F.; Mullen, B.D.; Desai, G.S.; Sherman, J.W.; Tang, C.N. *J. Polym. Sci.; Part A: Polym. Chem.* **2002**, *40*, 3434.

Chapter 18

Ammonolysis of Polycarbonates with (Supercritical) Ammonia: An alternative for Chemical Recycling

Werner Mormann* and David Spitzer

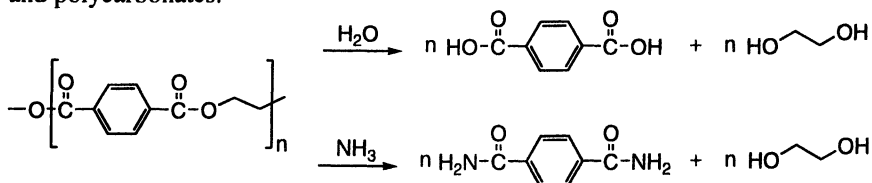
Universität Siegen, FB 8, Laboratorium für Makromolekulare Chemie,
57068 Siegen, Germany

*Corresponding author: mormann@chemie.uni-siegen.de

Ammonolysis of aliphatic and aromatic polycarbonates in liquid or in supercritical ammonia has been studied. Reaction products are alcohols (phenols) and urea. Ammonolysis of bisphenol A polycarbonate (BPA-PC) proceeds at room temperature at a high rate depending on the size and surface of particles. BPA-PC in composites like compact discs or car windows, consisting of a sandwich of glass layers bounded with a polyurethane adhesive to a polycarbonate, can be selectively ammonolyzed. Aliphatic poly(1,6-hexanediyl carbonate) can be fractionated without ammonolytic degradation in liquid ammonia up to 100 °C while ammonolysis occurs under supercritical conditions. If residence time and temperature (rate of reaction) are properly adjusted controlled degradation to oligomers is possible.

Recycling of polymers is possible by materials recycling, chemical recycling or energy recycling. Materials recycling is the preferred method for non-contaminated thermoplastics. Chemical recycling to monomers or to appropriate starting materials for re-synthesis of polymers is the method of choice for step condensation or step addition polymers. It is the only choice when these materials are contaminated with other polymers or inorganic material or when they are part of a composite with complex structure. Chemical recycling includes depolymerisation, pyrolysis and solvolytic cleavage of polymers. Solvolysis of polyesters, polycarbonate and polyurethanes has been done mostly by hydrolysis or glycolysis [1, 2].

Hydrolysis products of polyesters are the corresponding acids and alcohols as shown in Scheme 1. Glycolysis gives hydroxyalkyl esters and alcohols, while ammonolysis yields acid amides and alcohols as final reaction products which is also shown in Scheme 1. Acid amides cannot be used as such for the synthesis of polymers; this is why ammonolysis as a method of chemical recycling is restricted to step polymers that contain derivatives of carbonic acid in the main chain. Examples of important commercial plastics of this type are polyurethanes and polycarbonates.



Scheme 1: Hydrolysis and ammonolysis of poly(ethylene terephthalate)

Hydrolysis and glycolysis of polyurethanes have been reported and a paper appeared on ammonolysis of polyurethanes [3]. Ammonolysis of Bisphenol-A-polycarbonate using aqueous solutions of ammonia has been described [4, 5]. The method basically includes swelling or dissolution of the polymer in an organic solvent, e.g. dichloromethane followed by treatment with an aqueous solution of ammonia, which necessitates separation of solvents and isolation of the components from the different phases.

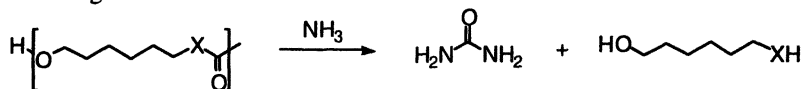
Supercritical fluids or condensed gases as reaction media have gained increasing interest during the past twenty years. Solvent properties and the ease of work up by simply releasing pressure and evaporating the gas or low boiling liquid are the main advantages. Carbon dioxide is by far the most frequently used solvent for supercritical extraction and chemical reactions [6, 7]. Ammonia - also a gas under normal conditions - has been used much less; application as reaction medium or as solvent for extractions is limited by its high reactivity towards a number of functional groups present in organic and biomolecules. It can participate in a number of nucleophilic displacement and acid - base reactions.

Ammonia has some unique properties as solvent. The dipole moment of ammonia (1.65 Debye) is only slightly lower than that of water or methanol (1.8 and 1.65 Debye), while carbon dioxide has no dipole moment. The dielectric constant of ammonia (16.9) is only one fifth that of water and even lower than that of ethanol. Like water ammonia can act as hydrogen bond acceptor and donor. These properties may be the reason why ammonia can dissolve a number of inorganic salts (halides, cyanides, thiocyanates, nitrates or nitrites). Even more remarkable is that it is miscible with water as well as polar organic compounds (alcohols, amines, esters) on one side and on the non polar end with hydrocarbons like cyclohexane. This allows running reactions under homogeneous conditions, which are heterogeneous in other solvents [8].

The higher critical temperature of ammonia (132.4 °C) with respect to carbon dioxide (31.3 °C) includes the option to work in liquid ammonia up to 130 °C, which may be convenient in terms of equipment as the vapor pressure is only 8.6 bar at 20 °C and 62.5 bar at 100 °C. The critical pressure of ammonia is 112.8 bar and the critical density is 0.235 g/cm³ [9].

Ammonolytic reactions of polycarbonate and poly(ethylene terephthalate) with ammonia, mainly in aqueous solution, have been reported [5, 10, 11]. Ammonolytic cleavage of polyurethanes in supercritical ammonia also has been reported [3].

Ammonolysis of polymers with functional groups of carbonic acid in the main chain will result in the formation of urea as "acid amide", a compound which among others can be used as fertilizer.



Equation 1

In the present article we report on the ammonolysis of aliphatic and aromatic polycarbonates using ammonia as reaction medium and reagent.

Materials, equipment, techniques

Makrolon[®] 2400: Bisphenol-A-polycarbonate; Bayer AG, Leverkusen (cylindrical pellets with 2 mm diameter and 3 mm length). Poly(1,6-hexanediyl carbonate); Bayer AG, Leverkusen (flakes).

Experiments under pressure were performed in stainless steel autoclaves or in a tubular reactor with continuous flow of ammonia.

Autoclaves used were of the type shown in Figure 1. They were sealed with flanges and o-rings. Up to 120 °C o-rings from perbunan were used and o-rings from teflon up to 200 °C. They were equipped with thermocouple, pressure

gauge, valve for filling and sampling. Heating was provided either with an electric heating jacket or with a fluid pumped through a heating jacket. The autoclaves had glass windows for visual observation of the contents. Mixing of components was achieved either with a mechanical stirrer powered by an electro motor, with a magnetic stirring bar or with steel balls.

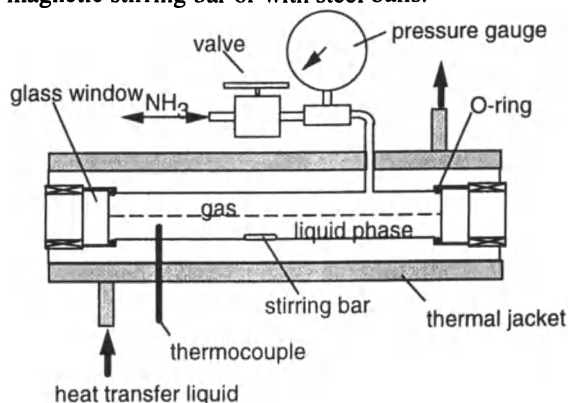


Fig. 1: Autoclave for visual observation (28 and 90 mL)

The **continuous flow reactor** is schematically shown in Figure 2. It consists of a pressure vessel as reservoir for ammonia which is heated to 35 °C to ensure sufficient pressure for the delivery of ammonia to the pump. The pump is an HPLC-pump with flow-rates from 0.01 to 9.99 mL/min. The reactor tubes have sintered metal filters at both ends, an inner diameter of 7.6 mm and variable length to provide volumes between 3.6 and 13.6 mL. Temperature is controlled and monitored with thermocouples at both ends of the reactor tube and at the outlet, pressure is controlled at the pump and monitored with a high pressure transmitter after the reactor. The whole set up after the pump is contained in a temperature controlled oven.

Samples can be taken with pressure vessels or with (semi)continuous flow of material which is enabled with a constant position of a needle valve or by intermittent opening and closing. This procedure is accompanied by a pressure drop but pressure is always far above the vapor pressure of ammonia.

Solubility of polymers and of expected ammonolysis products was determined in the autoclave for visual observation. Saturated solutions were prepared at a given temperature; samples were taken from the fluid phase. Ammonia was removed, the sample dried, weighed and characterised. Solubilities are included in Table 1.

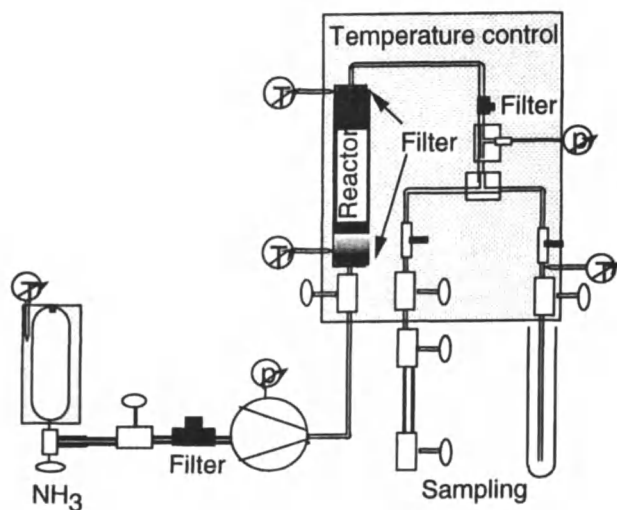


Fig. 2: Tube reactor (extractor) with continuous flow of ammonia

Table 1: Solubility of expected ammonolysis products of polycarbonates

Compound	T /°C	p /bar	Solubility /wt. %
Bisphenol-A	18	8	48.0
	90	51	> 92.0
Urea	31	12	58.1
	66	30	80.7
	109	74	91.5
1,6-Hexanediol	20	9	∞
	100	75	∞

Ammonolysis of Bisphenol-A-Polycarbonate (BPA-PC)

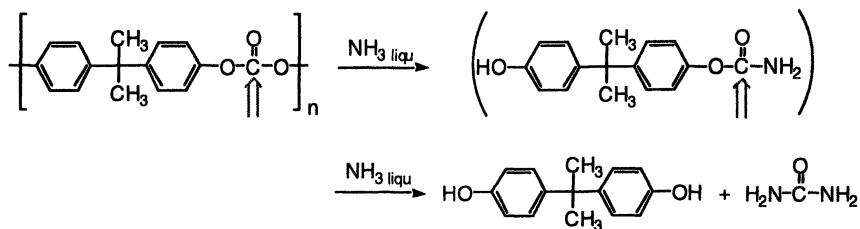
Bisphenol-A-polycarbonate has an annual production of 2 million tons which makes working on methods of recycling worthwhile. One of the applications that is not suitable for materials recycling is compact discs and DVD-discs. Another big market for polycarbonates are body panels for automotive applications.

Ammonolysis experiments of BPA-PC in organic solvents [5] had shown that under these conditions reaction took place at reasonable rates. Ammonolysis

of bisphenol-A-polycarbonate was carried out at room temperature with liquid ammonia in an autoclave using cylindrical pellets of virgin material with 2 mm diameter and 3 mm in length. Pellets had completely dissolved after 15 minutes.

After evaporation of excess ammonia the white solids were triturated either with water or with tetrahydrofuran. Bisphenol-A is insoluble in cold water and soluble in THF, while urea is easily soluble in water but insoluble in THF. THF-soluble or water insoluble fractions were analysed by SEC, HPLC and IR-spectroscopy. Reaction conditions and results of ammonolysis experiments of bisphenol-A-polycarbonate are collected in Table 2.

Samples from incomplete reactions had carbonyl bands at 1724 cm^{-1} and two peaks in the HPLC in accordance with bisphenol-A and a carbamate as shown in Scheme 2. Analysis of the liquid phase revealed that it did not contain any oligomeric or polymeric material; only bisphenol-A and urea were detected.



Scheme 2: Ammonolysis of bisphenol-A-polycarbonate

Reaction rate was decreased in one experiment to shed light on the possible mechanism of the ammonolysis of BPA-PC. The experiment was made at the boiling temperature of liquid ammonia ($-33\text{ }^{\circ}\text{C}$). Samples taken from the liquid phase again did not contain polycarbonate. Apart from urea and BPA only bisphenol-A-carbamate could be detected. Under these conditions it took 6 h until complete ammonolysis had taken place. Solid material that was separated from the solution after 15 min was analyzed by size exclusion chromatography. The molecular weight distribution curves shown in Figure 3 reveal that the high molecular weight part is unchanged with respect to virgin material while the low molecular weight part of the curve is shifted to lower values.

Obviously there is degradation by ammonolysis on the surface while the bulk of the pellets is unchanged. These results suggest that the rate-determining step in ammonolysis of BPA-PC is swelling of the polymer rather than ammonolytic cleavage of the carbonate moieties. As soon as ammonia has access cleavage takes place at such a rate that no carbonate functions can be detected with the methods used.

Depending on the reaction conditions ammonium cyanate was found besides urea. These results suggest a mechanism different from that outlined in Scheme 2

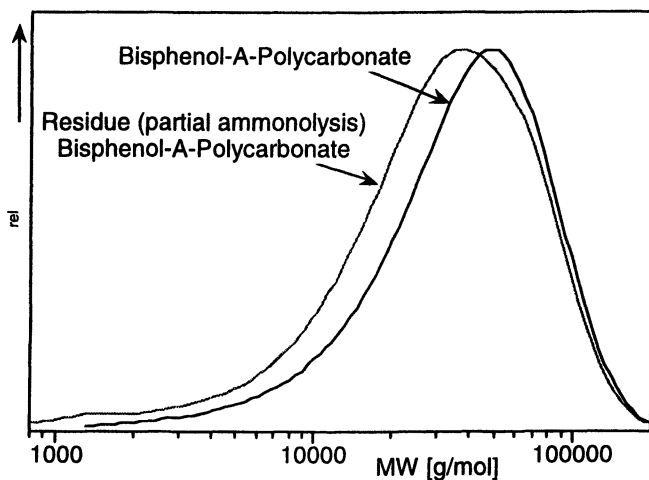


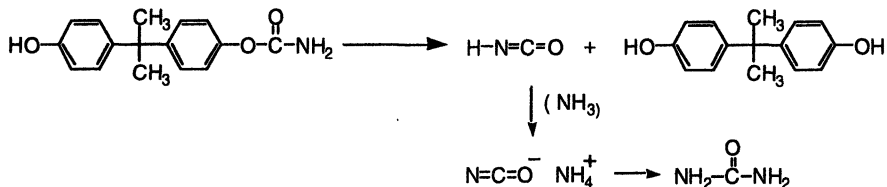
Fig. 3: Molecular weight distribution of BPA-PC solid fraction after partial ammonolysis

Table 2: Conditions and results of bisphenol-A-polycarbonate ammonolysis

PC (g)	NH (g)	T (°C)	p (bar)	t (min)	Products
27	51.1	20	8.6	5 ^a	bisphenol-A, urea, carbamate
				15	bisphenol-A, urea
30	26.6	20	8.6	15	bisphenol-A, NH ₄ NCO, urea
25	100.0	-33		15	bisphenol-A, NH ₄ NCO, urea

a: Sample from supernatant solution of PC pellets

for the cleavage of the carbamate functions. This step, to a significant extent, consists of elimination of cyanic acid followed by neutralization with ammonia rather than of a second addition elimination sequence leading to urea and phenol. During solubility studies of urea no ammonium cyanate had been detected, hence cyanic acid must have been cleaved off from the carbamate as shown in Scheme 3. This also explains why aromatic polycarbonates unlike aliphatic polycarbonates cannot be obtained from bisphenols and urea [12].



Scheme 3: Ammonolysis of bisphenol-A-polycarbonate

Recycling of BPA-PC based composites

Chemical recycling of BPA-PC not blended with other plastic materials or contaminated with non-polymeric material is second to materials recycling. The ease of ammonolytic cleavage of bisphenol-A-polycarbonate with liquid ammonia, however, can be used for selective degradation and chemical recycling of more complex structures like blends and composite materials containing BPA-polycarbonate.

One type of such composites are compact disks having an aluminum layer on one side and a protective coating on the other. Car windows made from a polycarbonate inner layer to which thin glass layers are attached with a polyurethane adhesive that are under development constitute another potential application that will have a large impact in terms of consumption and also in terms of a method for recycling.

Compact discs were crushed into pieces of less than 10 mm length, brought into an autoclave and covered with ammonia. The car window consisted of an inner layer of BPA-PC with 4 mm thickness to which glass layers of 0.5 mm thickness were glued with a polyurethane adhesive. The window was crushed to pieces of approximately the same size and treated in a similar way. When the reactions were finished, the liquid phase was pumped into another autoclave through a sinter metal filter, the solid residue was rinsed with ammonia and the combined filtrates were brought to ambient pressure to allow evaporation of ammonia. The residual white solids were analyzed in the usual way.

The insoluble part of the compact discs consisted of aluminum flakes and of transparent lumbers of the flexible coating. The residues of the car windows contained the glass with adherent polyurethane swollen by ammonia. Under the reaction conditions the polyurethane did not react with ammonia as more severe conditions are required [3]. The polyurethane could also be separated from the glass by dissolving it in dimethylformamide.

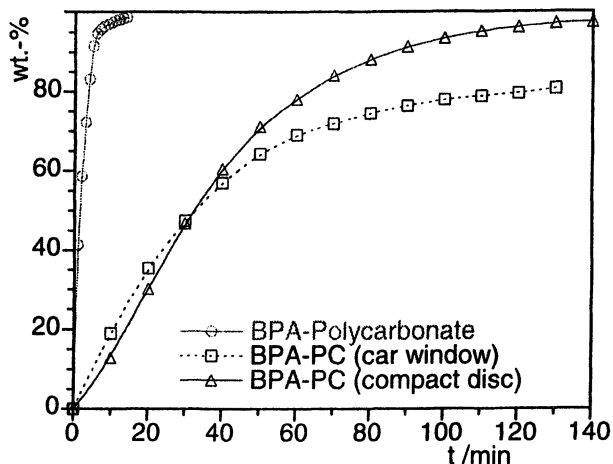


Fig. 4: Effect of accessible surface on the rate of ammonolysis of BPA-PC composites

Ammonolysis of compact disks as well as of car windows was also studied in the continuous flow setup. At 50 °C and 150 bar with an ammonia flow rate of 0.5 ml/min. Extracts consisted of BPA and urea. Results of the extracted fraction as a function of time are displayed in Figure 4. Pure BPA-PC is completely degraded after 15 min, the sandwiched materials require ten times longer or more for complete ammonolysis. This is due to the limited accessibility of ammonia through the impermeable cover layers. For a competitive process, the particle size will have to be decreased beyond 10 mm.

Based on the results reported above a process for recycling of BPA-polycarbonate can be designed. A schematic flow diagram of such a process with its essential steps is shown in Figure 5. Materials are crushed to a suitable particle size, filled into an autoclave, floated with ammonia and reacted at temperatures between 30 and 50 °C. The soluble fraction containing ammonia, BPA and urea is pumped into another vessel. The residue is rinsed with ammonia, leaving behind glass and polyurethane adhesive or aluminum and the coating in case of the compact disks. Ammonia then is allowed to evaporate from the liquid phase and condensed again for further use, leaving behind a solid mixture of BPA and urea. From this mixture either urea is separated by

trituration with water or BPA by trituration with tetrahydrofurane. The colorless BPA can be used for the synthesis of polycarbonate.

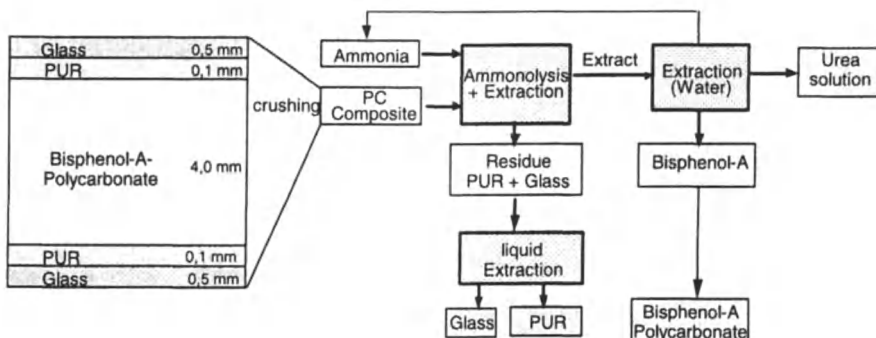
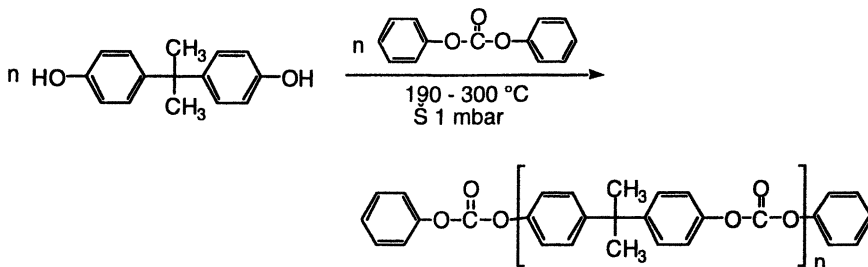


Fig. 5: Recycling of car windows (schematic flow diagram)

Re-synthesis of BPA-PC from recycled bisphenol-A

To fully complete the cycle BPA recovered from ammonolysis of a car window was distilled in vacuum and used for the synthesis of BPA-PC by melt transesterification polycondensation with diphenyl carbonate. The material obtained had properties of a CD-grade polycarbonate in terms of color, less than 5 ppm nitrogen, MVR: 77 cm³/10 min (300 °C/1.2 kg), while Makrolon CD2005 had 65 cm³/10 min.



Equation 2

These results prove that ammonolysis is a viable method for chemical recycling of polycarbonates.

Interaction of ammonia with poly(1,6-hexanediyl carbonate)

Poly(1,6-hexanediyl carbonate) (HD-PC) is a fully aliphatic analogue of BPA-PC. Part of these results has been previously published [13]. Solubility of this polymer could be determined since the reactivity is rather low in liquid ammonia. In addition to determination of solubility in the liquid phase in an autoclave continuous extraction was used in order to determine molar mass of the fractions. Samples were collected in the intermittent mode over 10 minutes and studied by SEC after evaporation of ammonia. Results from extraction are by 1 mass percent lower than those from the autoclave as shown in Figure 6. The dotted curve in Figure 6 already shows that solubility does not increase in a linear fashion above 100 °C as suggested by the solubility measured in the autoclave.

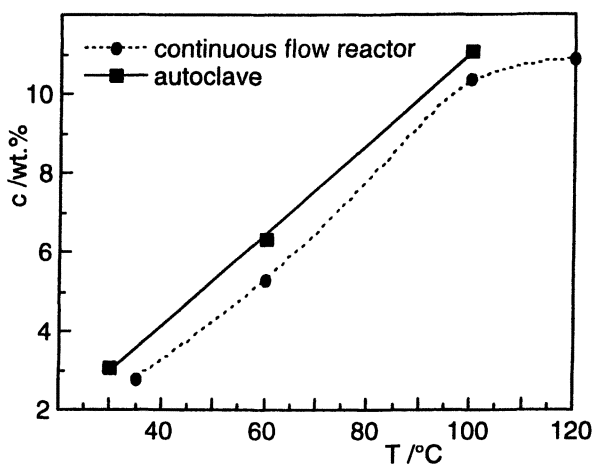


Fig. 6: Solubility of poly(1,6-hexanediyl carbonate)

Analysis of extracts with SEC revealed that not only the amount of the soluble fraction increases with temperature but also the molecular weight. This is demonstrated in Figure 7 with the molecular weight distribution curves of the soluble fractions at 35, 60 and 100 °C obtained from SEC. Similar curves from different fractions of extraction at 100 °C are shown in Figure 8. It can be seen that separation takes place according to molar mass and also that higher homologues become soluble with increasing temperature. Oligomers are extracted first and molar mass of extracts increases with time.

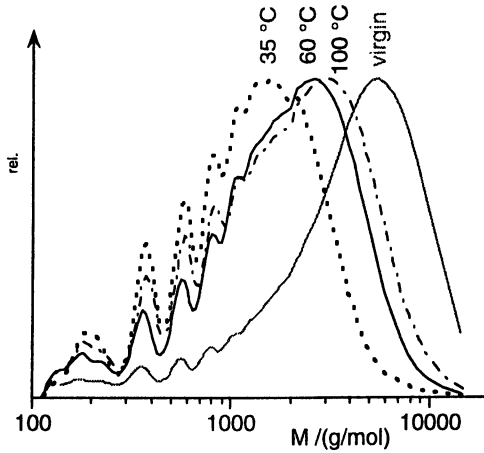


Fig. 7: Molecular weight of ammonia-soluble fractions of poly(1,6-hexanediyl carbonate) at 35, 60 and 100 °C

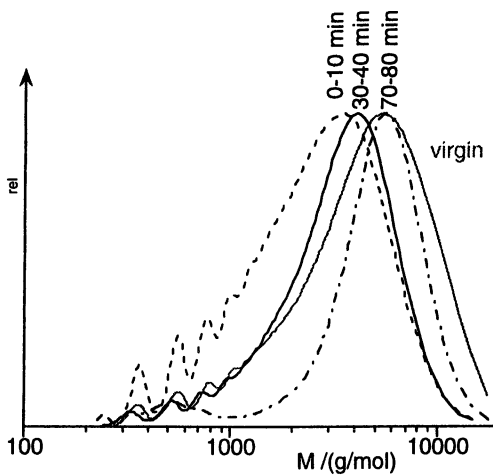


Fig. 8: Molecular weights of extracts of poly(1,6-hexanediyl carbonate) at 100 °C

A systematic study of solubility as a function of time and temperature was made with poly(1,6-hexanediyl carbonate). The continuous reactor was charged with a sample of polycarbonate at a given temperature, ammonia was pumped through and fractions were collected in the intermittent mode. All fractions were analyzed by size exclusion chromatography.

In Figure 9 a series of curves of the extracted mass after different times are plotted for temperatures from 35 to 180 °C. From 35 to 100 °C the extracted fraction increases from 25 to more than 90 percent and decreases with further increase of temperature. This indicates lower critical solution behavior of the aliphatic polycarbonate. Under supercritical conditions solubility further decreases and the shape of the curves also changes in the sense that solubility increases with time. This is due to ammonolytic degradation of the polymer.

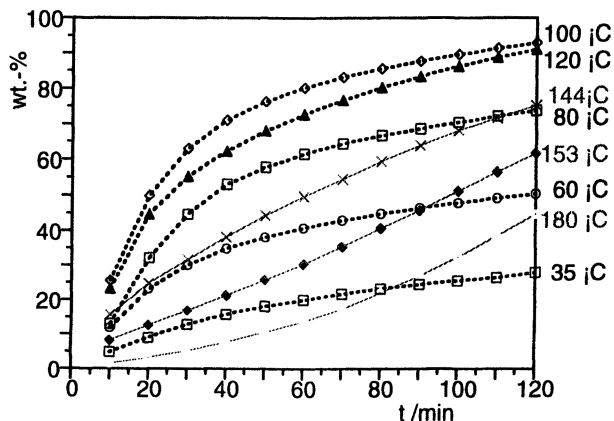


Fig. 9: Extracts from poly(1,6-hexanediyl carbonate) at different temperatures (Reproduced with permission from reference 13. Copyright 2004.)

In Figure 10 number average molar masses of the fractions of Figure 9 at those temperatures where ammonia is in the liquid state (35 to 120 °C) are displayed. Up to 120 °C molar mass of fractions increases with time, solubility, however, decreases above 100 °C.

Polydispersities of the fractions from Figure 10 obtained at 35, 80 and at 120 °C are shown in Figure 11. The first fractions more or less have a polydispersity of 2 corresponding to that of the virgin material. Only at 35 °C the first fraction has a polydispersity of 1.65. These values are due to the fact that the first fraction contains the soluble part of the given temperature. Subsequent fractions have lower polydispersities as they contain only small amounts of less soluble homologues. Polydispersities approach a limiting value which is in the order of 1.3 to 1.4 as long as no ammonolytic degradation occurs. With beginning ammonolysis at 120 °C polydispersity increases to approximately 1.5.

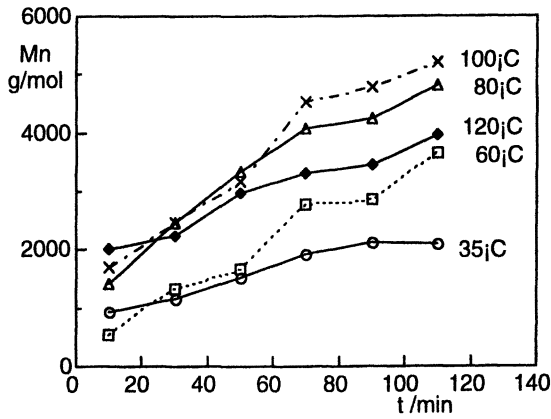


Fig. 10: Molecular weights of poly(1,6-hexanediyl carbonate) extracts (extraction with liquid ammonia) (Reproduced with permission from reference 13. Copyright 2004.)

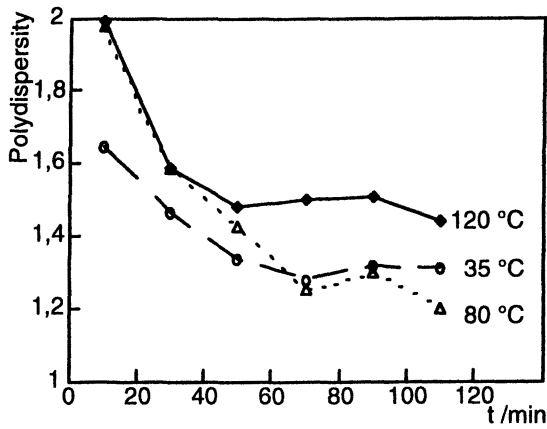


Fig. 11: Polydispersities of fractions from extraction of HD-PC at different temperatures

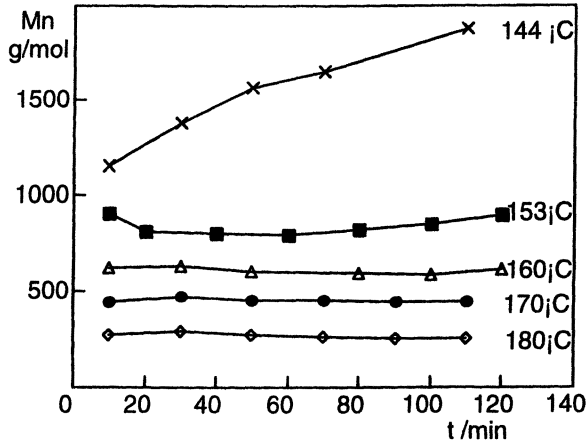
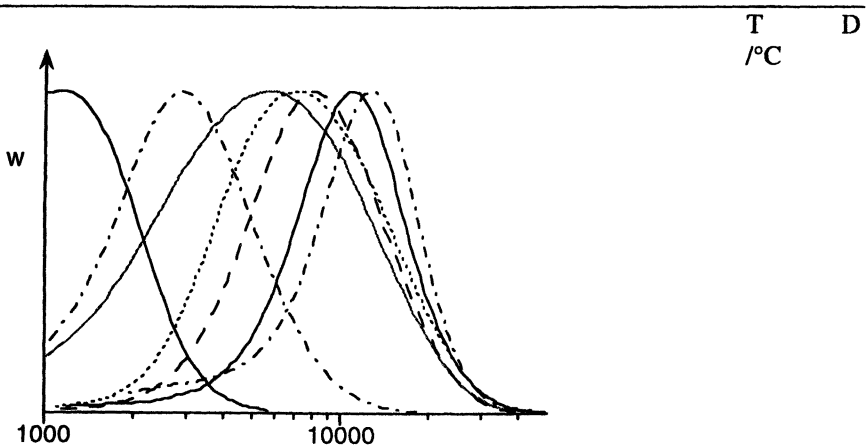


Fig. 12: Molecular weights of poly(1,6-hexanediyl carbonate) extracts (extraction with supercritical ammonia) (Reproduced with permission from reference 13. Copyright 2004.)

Under supercritical conditions above 150 °C molecular weight of extracts is practically constant with time for a given temperature as shown in Figure 12. This allows to degrade poly(1,6-hexanediyl carbonate) in a controlled fashion to molecular weights of 1000 or less.

Table 3: Molecular weight distribution (SEC) and polydispersity (D) of residues from extraction of poly(1,6-hexanediyl carbonate) at different temperatures



Molecular weights of residues of extraction support these results. They increase up to 100 °C. With further increase of temperature molar mass of residues decreases due to ammonolytic degradation. Up to 100 °C polydispersity of the residues decreases due to fractionation, it increases above 120 °C caused by random cleavage of the polymer chains (cf. Table 3).

Complete ammonolysis of poly(1,6-hexanediyl carbonate)

To study complete ammonolysis of poly(1,6-hexanediyl carbonate) a 20 percent mixture in ammonia was reacted at 200°C and 1000 bar for 2h in an autoclave. Samples were taken after the times given in Figure 13. A shift to lower molecular weight with time is observed and the amount of hexanediol increases. After 2 h only hexanediol can be found in the SEC-chromatogram according to equation 3.

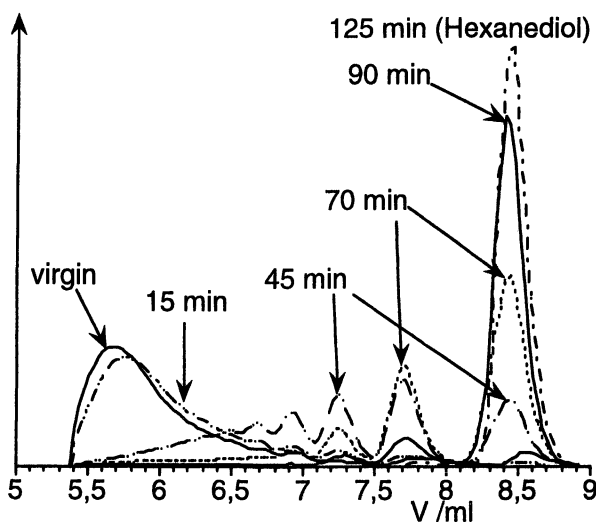
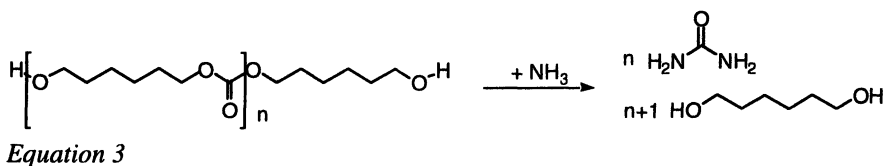


Fig. 13: SEC curves of ammonolysis of poly(1,6-hexanediyl carbonate); 200°C, 1000 bar

Conclusions

Behavior of an aromatic and an aliphatic polycarbonate towards liquid and supercritical ammonia has been investigated.

Aromatic bisphenol-A-polycarbonate readily undergoes ammonolysis to urea and bisphenol-A even at room temperature, both of which are easily soluble in ammonia. Ammonolysis can be used for chemical recycling of bisphenol-A-polycarbonate containing composites like compact disks or car windows. Inorganic material (glass, aluminum) and inert polymers (acrylate based protective coatings, polyurethanes) remain in the insoluble fraction. This process constitutes a new method for chemical recycling.

In liquid ammonia aliphatic polycarbonates can be separated according to molar mass. Solubility increases with temperature up to 100 °C (LCST behavior). At 120 °C and more pronounced under supercritical conditions ammonolysis takes place. Ammonolysis under supercritical conditions can be used for controlled degradation with proper residence time and flow rate.

Poly(1,6-hexanediyl carbonate) can be fractionated by extraction below 100 °C and degraded in a controlled manner under supercritical conditions.

Acknowledgement

The work presented in this paper has been supported by the Deutsche Forschungsgemeinschaft DFG (German research council), Forschungsschwerpunkt "Überkritische Fluide". We are indebted to Dr. Axel Grimm for carrying out some of the experiments and to Dr. Hähnsen Bayer AG, Krefeld for support in the re-synthesis of bisphenol-A-polycarbonate.

References

1. Frisch, K. C. *Polimeri*, **1998**, *43* (10), pp. 579-589
2. Xantos, M.; Patel, S. H. *NATO ASI Series, Series E: Applied Science*, **1998**, *351*, pp. 425-436
3. Lentz, H.; Mormann, W. *Makromol. Chem., Macromol. Symp.*, **1992**, *57*, pp. 305-310
4. EP 816,315 A2 (US 5,675,044) (1997), to General Electric Company, invs. Eijsbouts, P.; De Heer, J.; Hoogland, G.; Nanguneri, S.; De Wit, G. *Chem. Abst.*, **1997**, *127*, 294276x
5. US 4,885,407 (1989), to General Electric Company, invs. Fox, D. W.; Peters, E. N. *Chem. Abstr.*, **1990**, *112*, 200223t

6. Leitner, W. *Acc. Chem. Res.*, **2002**, *9*, pp. 746-756
7. Cooper, A. I. *J. Mater. Chem.*, **2000**, *2*, pp. 207-234
8. Mormann, W.; Wagner, T. *J. Polym. Sci.: Part A: Polymer Chemistry*, **1995**, *33*, pp. 1119-1124
9. Wilke, G.; Zosel, K.; Hubert, P.; Vitzthum, O. G.; Schneider, G. M., Lenz, H.; Franck, U.; Stahl, E.; Schilz, W.; Schütz, E.; Willing, E.; Klesper, E.; Peter, E.; Brunner, G.; Eggers, R. *Angew. Chem.*, **1978**, *90*, pp. 747-803
10. IN 154,774 (1984), to Nirlon Synthetics Fibers and Chemicals Ltd. *Chem. Abstr.*, **1986**, *104*, 51243e
11. JP 74,132,027 (1974), to Teigin Ltd., invs. Kawase, S.; Kobayashi, T.; Inata, H.; Kurisu, S.; Shima, T. *Chem. Abstr.*, **1975**, *83*, 44005y
12. Heitz, W.; Ball, P.; Füllmann, H. *Angew. Chem.*, **1980**, *92*, pp. 742-746
13. Mormann, W.; Spitzer, D. *e-Polymers* **2004**, no. 009

Indexes

Author Index

- Abdel-Goad, Mahmoud, 164
Acar, A. Ersin, 216
Akola, J., 200
Bailly, Christian, 180
Ballone, P., 200
Bendler, John T., 122, 133
Bhattacharyya, Arup R., 148, 164
Boden, Eugene P., 8
Boyles, David A., 122, 133
Brunelle, Daniel J., 1, 8, 216
Chung, James Y. J., 96, 112
DeSimone, Joseph M., 86
Drechsler, Doris, 96, 112
Erkelenz, Michael, 96, 112
Filipova, Tsvetanka S., 133
Goering, Harald, 148, 164
Gross, Stephen M., 86
Hagenaars, Arno, 180
Janke, Andreas, 148, 164
Johnson, B. F., 22
Jones, R. O., 200
Karbach, Alexander, 96, 112
Kiserow, Douglas J., 86
Korn, Michael R., 39, 58, 70
Longbrake, Guy, 133
Mason, James P., 96, 112
Moethrath, Melanie, 96, 112
Mormann, Werner, 244
Mullen, Brian D., 229
Pötschke, Petra, 148, 164
Pressman, E. J., 22
Reams, Josiah, 133
Roberts, George W., 86
Schroeder, Maria J., 133
Schultz, Claus-Ludolf, 96, 112
Shafer, S. J., 22
Shi, Chunmei, 86
Smigelski, Paul M. Jr., 8
Spitzer, David, 244
Storey, Robson F., 229
Tang, Chau N., 229
Waltner, Rachel, 133
Wolf, Bernard, 180
Wollborn, Ute, 96, 112

Subject Index

A

- A-bis-MP. *See* Allyl 2,2-bis(hydroxymethyl) propionate
- Acid catalyzed processes
 - condensation, phenol with acetone, BPA synthesis, 28–35
 - cracking in recovery/purge process, BPA synthesis by phenol-acetone condensation, 35
 - decomposition, cumene hydroperoxide in phenol and acetone production, 28
 - BPA isomerization, 33–34
- Acyl ammonium salts, side reactions in bisphenol polycarbonate formation, 11–12
- AFM. *See* Atomic force microscopy
- AIP-bis-OMP. *See* Allyl isopropylidene-2,2-bis(oxymethyl) propionate
- Aliphatic poly(ester carbonates) with pendent olefin and epoxide functional groups, synthesis, 229–243
- Allyl 2,2-bis(hydroxymethyl) propionate (A-bis-MP), synthesis, 232
- Allyl isopropylidene-2,2-bis(oxymethyl) propionate (AIP-bis-OMP), synthesis, 232
- Amine-catalyzed, interfacial process, commercial polycarbonate synthesis, 9–13
- Aminopropyl bonded column, LC/APCI-MS, 77
- Ammonia
 - interaction with poly(1,6-hexanediyl carbonate), 254–260
 - solvent properties, 246
 - supercritical, ammonolysis of polycarbonates, 244–261
- Ammonolysis
 - bisphenol-A-polycarbonate, 248–251
 - compact disks and car windows, 252–253
 - general polymers, 246
 - poly(1,6-hexanediyl carbonate), 259
- Ammonolysis and hydrolysis, poly(ethylene terephthalate), 245
- Annealing. *See* Heat aging
- APCI. *See* Atmospheric pressure chemical ionization
- Arcyl carbonates in synthesis end-functionalized polycarbonates, 42–43
- Arrhenius relationship, forward reaction rate constant, solid state polymerization, 89, 90*f*
- Asymmetric bisphenol A analogue, Suzuki synthesis, 138
- Atmospheric pressure chemical ionization (APCI) mass spectrometry
 - compared to other analytical tools, 83–84*f*
 - end-functionalized polycarbonate oligomers, 75–79
- Atomic force microscopy (AFM)
 - bisphenol-A and 4,4'-dihydroxydiphenyl copolycarbonate, 105–107*f*, 113, 115*f*–116*f*
 - multiwalled carbon nanotubes in polycarbonate composites, 151, 156–158
 - polyethylene blend with polycarbonate composite with multiwalled carbon nanotubes, 167, 168–169
- Autoclave, schematic, 246–247*f*

- Average molecular cross-sectional area (MCSA)
 correlation to brittle strength, 124, 125*f*, 136
 methods for increase, 136–137
 polymer chain, definition, 124
 tetraaryl polycarbonate, 129–130*t*
- Average property methods in characterization, end-functionalized polycarbonate oligomers, 58–69
- B**
- Base catalyzed cracking in recovery/purge process, in BPA synthesis by phenol-acetone condensation, 34–35*f*
- Bending measurements, 4,4'-dihydroxydiphenyl and bisphenol A copolycarbonate, 113–116*f*
- Biodegradable polymer applications, 230
- Biodegradable polymer copolymerization, *rac*-lactide with 5-methyl-5-allyloxycarbonyl-1,3-dioxan-2-one, 233–239
- 1,3-Bis[1-(4'-hydroxyphenyl-4-phenyl)-1-methylethyl]benzene, structure, 137*f*
- 1,4-Bis[1-(4'-hydroxyphenyl-4-phenyl)-1-methylethyl]benzene, structure, 137*f*
- Bis[4-(1-(4'-hydroxyphenyl)-1-methylethyl)phenoxy]methane, structure, 137*f*
- Bis[4-(4'-hydroxyphenyl)phenyl]ether, structure, 137*f*
- Bis[4-(4'-hydroxyphenyl)phenyl]methane, structure, 137*f*
- Bis[4-(4'-hydroxyphenyl)phenyl]sulfone, structure, 137*f*
- Bis[4-(4'-hydroxyphenyl)phenoxy]methane, structure, 137*f*
- 2,2-Bis(4-iodophenyl)-1,1,1-trichloroethane, (I-DDT), synthesis, 142
- Bisaryl units in ductile polycarbonates, 122–132
- Bischloroformates in bisphenol polycarbonate syntheses, 12–13, 19–20
- Bisphenol A. *See* BPA
- Bisphenol A polycarbonate. *See* BPA polycarbonate
- Bisphenol C, co-monomer in copolycarbonates, 144
- Bisphenol C polycarbonate, development and structural data, 134–136
- Blends, morphology, conductive polycarbonate composite with polyethylene, 167–172
- Bond interchange, rules in polymerization, 204
- BPA and 4,4'-dihydroxydiphenyl, copolycarbonates
 mechanics and morphology, 112–121
 structure with BPA polycarbonate structure, 97*f*
 technical properties, 96–111
- BPA as co-monomer in copolycarbonates, 144
- BPA polycarbonate
 ammonolysis, 248–251
 chemical structure and properties, 1, 130*t*, 135*f*, 181
 development overview, 1–4
 dynamic mechanics compared to TABPA-BPA polycarbonate, copolymer, 129, 131*f*
 end-functionalized oligomers, 39–57
 T_g and γ transition data, 135*f*–136

- BPA polycarbonate-based composites, recycling, 251–253
- BPA polycarbonate production
 by cyclic oligomers, 15–16
 commercial melt phase synthesis, 13–15, 23–35
 commercial solvent based synthesis, 9–13
 industrial scale production, 182–183*f*
 interfacial phase transfer catalyst process, 19
 re-synthesis from recycled BPA, 253
 synthesis by solid state polymerization, 17
- BPA synthesis, 27–35
- Branching and polymerization in polycarbonates, simulations, 207–211
- Branching distribution determination, melt-polymerized polycarbonate, 189–191
- Brittle strength compared to yield stress in polymers, temperature dependence, 124
- Brittle strength correlation to average molecular cross-sectional area (MCSA), 124, 125*f*
- Bulk promoter, thiols, 29
- Byproducts in phenol-acetone condensation in BPA synthesis, 32, 33*f*
- C**
- ¹³C NMR studies
 bisphenol-A and 4,4'-dihydroxydiphenyl copolycarbonate, 103–104
 double bond epoxidation spectra, 241
 phenyl end group ratio determination, 89
 polycarbonate-siloxane copolymer characterization, 193
 presence/absence of end groups, determination, 65
- Calibration standard correction in gel permeation chromatography, 60–61
- Car window, recycling, 251–253
- Carbon dioxide. *See* Supercritical carbon dioxide
- Carbon nanotubes (CNT) filled polycarbonate with polyethylene, melt-mixed blends, 164–177
- Catalysis, acid catalyzed condensation, phenol with acetone, BPA synthesis, 29–30
- Catalytic effect of metal phenoxides on ring-opening polymerizations, 204–205
- Cation exchange resins in BPA production, 30–32
- Chain extension, 40
- Chemical resistance, bisphenol A and 4,4'-dihydroxydiphenyl, 119, 120*f*
- Chloroformate activation *via* acyl ammonium salt, 10, 11*f*
- CNT. *See* Carbon nanotubes
- Co-continuous structures, formation mechanism, 171
- Commercial applications, overview, polycarbonates, 2–4
- Compact disks, recycling, 251–252
- Composites, bisphenol A polycarbonate-based, recycling, 251–253
- Continuous flow reaction, schematic, 247, 248*f*
- Continuous polymer fractionation for characterization, siloxane-polycarbonate copolymers, 185, 187–188*t*, 193–196
- Copolycarbonate, bisphenol-A and 4,4'-dihydroxydiphenyl mechanics and morphology, 112–121

- structure property relationships, 96–111
- Copolycarbonates, synthesis, 144
- Copolymerization, *rac*-lactide with 5-methyl-5-allyloxycarbonyl-1,3-dioxan-2-one, 234–242
- Crack resistance, bisphenol-A and 4,4'-dihydroxydiphenyl copolycarbonate, 99, 103
- Craze growth and breakdown in polymers, 123–128
- Crazing in BPA-PC sample compared to bisphenol A and 4,4'-dihydroxydiphenyl copolycarbonate, 113, 116*f*
- Cryofractured extracted strands, polyethylene blended with polycarbonate composite with multiwalled carbon nanotubes, 169–170
- Crystallization rate, BPA polycarbonate, effect on synthesis by solid state polymerization, 17
- Cyanobiphenyl carbonate end groups
¹H NMR spectrum, 64
 probe for end group functionalization, 61–62
- Cyanobiphenyl-terminated oligomers, characterization by mass spectrometry techniques, 73–83
- Cyclic carbonate transesterification process, DPC preparation, 24*f*, 26–27
- Cyclic oligomers in polycarbonate synthesis, 15–16
- Cylindrical melt reactor, TMCBD polycarbonates, synthesis, 220
- D**
- Deactivation, cation exchange resins, in BPA production, 31–32
- Deformation mechanism, 4,4'-dihydroxydiphenyl and bisphenol A copolycarbonate, 117–118*f*
- Density effect on degree of polymerization, simulations, 205, 207–208, 209*f*
- Density functional/Monte Carlo simulations, ring-opening and branching, 200–215
- 4-Dialkylaminopyridines, catalysts in polycarbonates of hindered bisphenols, preparation, 12
- 1,1-Dichloro-2,2-bis[4-(4'-hydroxyphenyl)phenyl]ethene in synthesis and polycarbonate incorporation, 138, 139–141, 143, 144
- 1,1-Dichloro-2,2-bis(4-hydroxyphenyl)ethene in bisphenol C polycarbonate development, 134
- Diethylmethylamine catalyst in polycarbonates of hindered bisphenols, preparation, 12
- Differential scanning calorimetry (DSC) bisphenol-A and 4,4'-dihydroxydiphenyl copolycarbonate, 104*f*–105
 end-functionalized polycarbonate oligomers, characterization, 67–68
 polycarbonate composites with multiwalled carbon nanotubes, 152
- Diffusion coefficient, phenol, dependence on sweep fluid, 91
- 4,4'-Dihydroxydiphenyl and BPA, copolycarbonates
 mechanics and morphology, 112–121
 structure with BPA polycarbonate structure, 97*f*
 technical properties, 96–111
- Dimethyl carbonate (DMC)
 commercial and industrial uses, 25

- key intermediate in processes to prepare diphenyl carbonate, 23–25
 - patents for industrial processes, 25–26*t*
 - syntheses, industrial processes, 13, 25–27
 - Dimethyl oxalate decarbonylation process to prepare DPC, 24*f*, 26
 - Dimethylbutyl amine catalyst in hindered bisphenol polycarbonates, preparation, 11–12
 - Diphenyl carbonate (DPC)
 - co-monomer for BPA polycarbonate, 23
 - large scale polymerizations, TMCBD polycarbonates, 222–226*t*
 - production, patents for industrial processes, 25*t*
 - syntheses, industrial processes, 23–27
 - See also* Melt phase synthesis
 - Diphenyl oxalate, decarbonylation process to prepare DPC, 24*f*, 26
 - Diphosgene, laboratory alternative to phosgene, 13
 - Direct oxidative carbonylation, phenol, DPC preparation, 24*f*, 27
 - Dispersion, multiwalled carbon nanotubes in polycarbonate composites, 155–156
 - DMC. *See* Dimethyl carbonate
 - Double percolation phenomena, 165
 - DPC. *See* Diphenyl carbonate
 - Dreiding Force Field for radial distribution function, 105, 106*f*
 - DSC. *See* Differential scanning calorimetry
 - Ductile-brittle transition in polymers, temperature, definition, 124
 - Ductile polycarbonates with bisaryl units, 122–132
 - Dynamic mechanical analysis
 - polycarbonate composites with multiwalled carbon nanotubes, 151–152
 - polyethylene blended with polycarbonate composite with multiwalled carbon nanotubes, 167
 - Dynamic mechanical results, TABPA-BPA polycarbonate, copolymer compared to BPA-PC polymer, 129, 131*f*
- ## E
- Electrical conductivity measurements
 - polycarbonate composites with multiwalled carbon nanotubes, 150
 - polyethylene blended with polycarbonate composites with multiwalled carbon nanotubes, 166, 172–173
 - Electrical properties, multiwalled carbon nanotubes in polycarbonate composites, 152–155
 - Electrospray-ionization mass spectrometry
 - comparison to other analytical tools, 83–84*t*
 - cyanobiphenyl-terminated oligomers, 73–74
 - End-functionalized BPA
 - polycarbonate oligomers
 - characterization by average property methods, 58–69
 - characterization by individual species methods, 70–85
 - examples, 43–55
 - synthesis, 40–43
 - End group discrimination from intensities of HPLC traces at varying wavelengths, 71–72
 - End group functionalization by gel permeation chromatography, 61–62

End group ratio in prepolymer, determination, 89
 Entanglements, role in craze growth and breakdown, 127–128
 Epoxidation scheme, MAC-copolymers, 239–241
 Eugenol. *See* Polycarbonate/Eugenol-siloxane copolymer

F

^{19}F NMR, trifluoroacetic acid and trifluoroacetic anhydride mechanism determination, 65
 Flame resistance, BPA and 4,4'-dihydroxydiphenyl, copolycarbonate, 102, 119
 Flexural and tensile properties, BPA and 4,4'-dihydroxydiphenyl copolycarbonate, 119
 Flory, most probable molecular weight distribution, 182
 Fluorenone polycarbonate, T_g and γ transition data, 135*f*
 Forward reaction rate constants, solid state polymerization rate, Arrhenius relationship, 89, 90
 Fourier-transformed infrared (FTIR) spectroscopy, characterization, end-functionalized poly(bisphenol A) carbonate oligomers, 60
 Fractionated polycarbonate-siloxane copolymers, characterization, 193–196
 Fractionation, preparative, polycarbonate, experimental, 184–187
 FTIR. *See* Fourier-transformed infrared spectroscopy

G

G' . *See* Shear storage modulus

G'' . *See* Shear loss modulus
 Gel permeation chromatography (GPC)
 BPA and 4,4'-dihydroxydiphenyl copolycarbonate, 108, 109*f*
 characterization, end-functionalized poly(bisphenol A) carbonate oligomers, 60–63
 comparison to other analytical tools, 83–84*t*
 multiwalled carbon nanotubes in polycarbonate composites, 160–161
 Gel transition and polymerization, polycarbonates, in 2D and 3D simulations, 208–211
 Gelular cation exchange resin used in BPA production, 31
 Glass transition temperatures (T_g) multiwalled carbon nanotubes in polycarbonate composites, 158–160, 162
 polycarbonate oligomers, determination by differential scanning calorimetry, versus molecular weights, 67–68
 polyethylene blended with polycarbonate composite with multiwalled carbon nanotubes, 174–176
rac-lactide -MAC copolymers, 239, 240*f*
 TMCBD incorporation into polyesters, 221
 Glycolysis products, 245
 GPC. *See* Gel permeation chromatography

H

^1H NMR comparison to other analytical tools, 83–84*t*
 ^1H NMR for cis/trans TMCBD polycarbonate, 222–223*f*

- ¹H NMR for cyanobiphenyl end groups, 64
- ¹H NMR hydroxyl end group ratio determination, 89
- ¹H NMR in average molecular weight determination, end-functionalized poly BPA carbonate oligomers, 63–65
- ¹H NMR siloxane content and block lengths, fractionated polycarbonate-siloxane copolymers, 194–195*f*
- Heat aging, bisphenol-A and 4,4'-dihydroxydiphenyl, copolycarbonate, 101–102*t*
- Heterogeneous acid catalysts in acid catalyzed condensation, phenol with acetone, BPA synthesis, 29
- 4,4'-
(Hexafluoroisopropylidene)diphenol, co-monomer in copolycarbonates, 144
- High performance liquid chromatography (HPLC)
characterization, end-functionalized polycarbonate oligomers, 71–72
comparison to other analytical tools, 83–84*t*
separation with APCI mass spectrometry, cyanobiphenyl terminated oligomers, 77–79
- Hindered bisphenol polycarbonates, preparation, 11–12
- Homopolycarbonate synthesis, 143–144
- HPLC. *See* High performance liquid chromatography
- Hydrochloric acid, catalyst in acid catalyzed condensation, phenol with acetone, BPA synthesis, 29
- Hydrolysis and ammonolysis, poly(ethylene terephthalate), 245
- Hydrolysis and reference fuel resistance, BPA and 4,4'-dihydroxydiphenyl copolycarbonate, 119, 120*f*
- Hydroxy-based end-groups, determination by NMR spectroscopy, 65
- 2-(4'-Hydroxyphenyl)-2-[4'-(4-hydroxyphenyl)-phenyl]-propane, synthesis by Suzuki reaction, 138
- ## I
- I-DDT synthesis, *See* 2,2-Bis(4-iodophenyl)-1,1,1-trichloroethane
- Impact resistance, BPA polycarbonate, 3
- In-situ* bending measurements, 4,4'-dihydroxydiphenyl and bisphenol A copolycarbonate, 113–116*f*
- Increase methods for average molecular cross-sectional area (MCSA), 136–137
- Individual species methods in characterization, end-functionalized polycarbonate oligomers, 70–85
- Indole acrylic acid matrix, 79
- Interfacial phase transfer catalyst, BPA polycarbonate synthesis, 10–12, 19
- Interfacial processes
amine-catalyzed synthesis, commercial polycarbonate production, 9–13, 22
bischloroformates in BPA polycarbonates, 12–13, 19–20
BPA polycarbonate, industrial production, 181–182
thermal redistribution mixed BPA polycarbonate products, 192
- Intrinsic reaction kinetics, solid state polymerization rate, 89–93
- Isolation and purification, BPA from phenol-acetone condensation, 32, 33

Isomer effect, unzipping TMCBD polycarbonate at trans isomer sites, 224–225

Isomerization, BPA in phenol under strongly acidic conditions, 33–34

Isophorone polycarbonate, structure and properties, 130*t*, 135*f*

K

Kolbe-Schmitt reaction, thermal rearrangements, polycarbonates in melt, 182–183*f*

L

Laboratory alternatives to phosgene in BPA polycarbonate synthesis, 13

Lennard-Jones particles, 204

Lexan SLX, block polycarbonate-resorcinol polyarylate, structure, 3

Lithium hydroxide, catalyst in prepolymer synthesis, 88

Lithium phenoxide in ring-opening polymerization, cyclic BPA-PC oligomers, 201–203

M

MAC. *See* 5-Methyl-5-allyloxycarbonyl-1,3-dioxan-2-one

Macroreticular cation exchange resin in BPA production, 31

MALDI-TOF and MS

characterizations

comparison to other analytical tools, 83–84*t*

cyanobiphenyl-terminated oligomers, 73–83

end-functionalized oligomers, 79–83

oligomers from BPA and 4,4'-dihydroxydiphenyl copolycarbonates, 108, 109–110*t*

Matrix-assisted laser desorption/ionization. *See* MALDI-TOF

MCSA. *See* Average molecular cross-sectional area

Mechanical and morphological properties, BPA and 4,4'-dihydroxydiphenyl copolycarbonates, 112–121

Mechanical and physical properties, BPA and 4,4'-dihydroxydiphenyl, copolycarbonates, 98, 100–102*f*

Mechanical failure in polymers, modes, 123

Mechanical reinforcement, multiwalled carbon nanotubes in polycarbonate composites, 158–161

Mechanism, acid catalyzed condensation, phenol with acetone, BPA synthesis, 28

Melt-mixed blends, carbon nanotubes filled polycarbonate with polyethylene, 164–177

Melt-mixed produced multiwalled carbon nanotubes, polycarbonate composites, 148–163

Melt phase synthesis

BPA polycarbonate compared to solved based synthesis, 15*t*, 17–18

BPA polycarbonate in laboratory, 18–19

commercial polycarbonate production, 13–15, 23–35

See also DPC synthesis

Melt polymerization with DMC and TFEC, TMCBD polycarbonate, synthesis, 219–220

Melt-polymerized polycarbonate, branching distribution determination, 189–191

Melt-transesterification process

- BPA polycarbonate, industrial production, 182
- end-functionalized polycarbonate oligomers synthesis, 41
- thermal redistribution mixed bisphenol A polycarbonate products, 192–192
- Metal phenoxides, catalytic effect on ring-opening polymerizations, 204–205
- 5-Methyl-5-allyloxycarbonyl-1,3-dioxan-2-one (MAC) copolymerization with *rac*-lactide, 234–242
- synthesis, 232–233, 234–235
- Methyl nitrite process to prepare DPC, 24*f*, 25–26
- Methylene chloride, solvent for interfacial, amine-catalyzed commercial polycarbonate synthesis, 10, 22
- Metropolis algorithm in constant volume Monte Carlo simulations, 204
- Microscopic techniques, polyethylene blended with polycarbonate composite with multiwalled carbon nanotubes, 166–167
- Mixing time effect on morphology, 171–172*f*
- Model simulations, polycarbonate polymerization, 203–207
- Molecular weight determination after solid state polymerization by GPC, 88
- Molecular weight determination by gel permeation chromatography compared to molecular weight determination by NMR spectroscopy, 66
- Molecular weight determination by technique atmospheric pressure chemical ionization-mass spectroscopy, 76
- electrospray-ionization-mass spectrometry, 74
- gel permeation chromatography, 60–63
- LC/atmospheric pressure chemical ionization-mass spectroscopy, 77–79
- matrix-assisted laser desorption/ionization-MS, 79–83
- NMR spectroscopy, 63–64
- Molecular weight distribution (MWD) BPA and 4,4'-dihydroxydiphenyl copolycarbonate, 108–110
- BPA polycarbonate, ammonolysis, 249–250*f*
- solution characterization of polycarbonate materials, 180–199
- Molecular weight product by solid state polymerization, dependence on monomer ratio, 91–94
- Molecular weights compared to glass transition temperatures determined by DSC, 67–68
- end-functionalized polycarbonate oligomers, by different analytical tools, 83–84*t*
- poly(1,6-hexanediyl carbonate) extracts, 254–259
- Monomer geometries and polymer toughness, 123–128
- Monomer ratio (diphenyl carbonate/bisphenol A), effect on polymer molecular weight produced via solid state polymerization, 91–94
- Monomeric tetraarylbisphenols, synthesis by Suzuki reaction, 137
- Monomers for polycarbonate manufacture, 22–38
- Monte Carlo simulations branching distribution melt-polymerized polycarbonate, 190–191

- constant volume, polycarbonate polymerization, 204–207
- density functional studies, ring-opening and branching, 200–215
- redistribution processes, 192–194*f*
- Morphological and mechanical properties, 4,4'-dihydroxydiphenyl and bisphenol A copolycarbonate, 112–121
- Morphology, conductive polycarbonate composite with polyethylene blends, 167–172
- Multiwalled carbon nanotubes in polycarbonate composites (MWNT), 148–163
- MWD. *See* Molecular weight distribution
- MWNT. *See* Multiwalled carbon nanotubes

N

- N,N-dimethylbutylamine, in 3,5,3',5'-tetramethyl-BPA polycarbonate synthesis, 20
- Network like structure, multiwalled carbon nanotubes in polycarbonate composites, 154
- NMR characterization, end-functionalized poly(bisphenol A) carbonate oligomers, 63–66
- NMR studies. *See* ¹³C NMR, ¹⁹F NMR, ¹H NMR
- Notched Izod impact
 - BPA and 4,4'-dihydroxydiphenyl, copolycarbonate, 100*t*, 101*t*, 119, 120*f*
 - TMCBD-polycarbonate, 219
- Nuclear Magnetic Resonance Spectroscopy. *See* NMR
- Nucleophilic amine catalysts in preparation, polycarbonates of hindered bisphenol, 11–12

O

- Oligomer, definition, 39–40
- One step process for diphenyl carbonate preparation, 24*f*, 27
- Optical properties, BPA and 4,4'-dihydroxydiphenyl, copolycarbonate, 97–98*f*, 117, 119
- Orientation, multiwalled carbon nanotubes in polycarbonate composites, 156–158*f*
- Oscillatory rheometry, 153
- Oxidative carbonylation, end-functionalized polycarbonate oligomer synthesis, 43, 54–55

P

- P-TADDT synthesis. *See* 1,1,1-Trichloro-2,2-bis[4'-(4-methoxyphenyl)-phenyl]ethane
- Packing length, 124–130*t*
- Pendent olefin and epoxide functional groups in aliphatic poly(ester carbonates), synthesis, 229–243
- Percolation concentration, 149
- Percolation in multiwalled carbon nanotubes in polycarbonate composites, 152–155
- Phase transfer catalysts in solvent-based polycarbonate synthesis, 10–12, 19
- Phenol-acetone condensation with thiol promoter, BPA production, 29–30
- Phenol diffusivity in solid state polymerization, N₂ and scCO₂ as sweep fluids, 91
- Phenol oxidative carbonylation, one step DPC preparation, 24*f*, 27
- Phenol recovery by base catalyzed cracking in phenol-acetone condensation BPA synthesis, 34–35*f*

- Phenolphthalein polycarbonate
chemical structure and properties,
130*t*
T_g and γ transition data, 135*f*
- Phenoxide catalytic effect on ring-
opening polymerizations, 204–205
- Phenoxide reactions in ring-opening
polymerization, cyclic BPA-PC
tetramer, 201–203
- Phosgene-free synthesis,
polycarbonate, 13–15
- Phosgene gas, safety note, 18
- Phosgene in interfacial, amine-
catalyzed synthesis, commercial
polycarbonate production, 9
- Phosgene process for DPC
preparation, 24*f*, 27
- Physical and mechanical properties
BPA and 4,4'-dihydroxydiphenyl,
copolycarbonate, 98, 100–102*f*
TMCBD polycarbonates, 227
- Polarizing light microscopy, BPA
copolycarbonate, 113, 115*f*
- Poly(bisphenol A), solid state
polymerization, supercritical carbon
dioxide facilitation, 86–94
- Polycarbonate composites with
multiwalled carbon nanotubes, 148–
163
- Polycarbonate/Eugenol-siloxane
copolymer, 183–186, 189
- Polycarbonate homopolymers,
continuous polymer fractionation,
187, 188
- Polycarbonate materials, solution
characterization, 180–199
- Polycarbonate polymerization, model
simulations, 203–207
- Polycarbonate process technologies,
evolution, 8–21
- Polycarbonate-siloxane copolymers,
continuous polymer fractionation
for characterization, 185, 187–188*t*,
193–196
- Polycarbonate synthesis from cyclic
oligomers, 15–16
- Polycarbonates
advances, overview, 1–5
ammonolysis with supercritical
ammonia, 244–261
branching and polymerization
simulations, 207–211
continuous polymer fractionation
procedures, 185–187
- Polycarbonates filled with carbon
nanotubes, melt-mixed blends with
polyethylene, 164–177
- Polyethylene and polycarbonate,
carbon nanotube filled, melt mixed
blends, 164–177
- Poly(ethylene terephthalate),
hydrolysis and ammonolysis, 245
- Poly(1,6-hexanediyl carbonate), 254–
260
- Polymer analogous reactions,
synthesis, end-functionalized
polycarbonate oligomers, 43
- Polymer toughness and monomer
geometries, 123–128
- Polymerization simulations,
polycarbonates, 203–212
- Positional isomers, synthesis, TABPA
and TABPC analogues, 140
- Preparative fractionation,
polycarbonate, experimental, 184–
187
- Prepolymer particle size, effect on
molecular weight evolution, 89
- Prepolymer synthesis, melt
polymerization, BPA and diphenyl
carbonate, 88
- R**
- Radial distribution function, BPA and
4,4'-dihydroxydiphenyl
copolycarbonate, 105, 106*f*

- Re-synthesis from recycled bisphenol-A, BPA polycarbonate, 253
- Reaction kinetics, solid state polymerization, BPA with supercritical carbon dioxide, sweep fluid, 86–94
- Reaction rate constant, dependence on sweep fluids in solid state polymerization, BPA, 89–91
- Recovery/purge process in phenol-acetone condensation, BPA synthesis, 34–35
- Recycled BPA in BPA polycarbonate re-synthesis, 253
- Recycling, BPA polycarbonate-based composites, 251–253
- Refractive index, end-functionalized poly(BPA) carbonate oligomers, 62
- Rheological measurements
 polycarbonate composites with multiwalled carbon nanotubes, 150–151
 polyethylene blended with polycarbonate composite with multiwalled carbon nanotubes, 166, 173–174*f*
- Rheological threshold composition, polycarbonate composites with multiwalled carbon nanotubes, 154
- Ring flip process, phenyl, 135, 137
- Ring-opening and branching, density functional/Monte Carlo studies, 200–215
- Ring-opening polymerization
 cyclic BPA-PC oligomers, phenoxide reactions, 201–203
 cyclic oligomers, polycarbonate synthesis, 15–16
 oligomeric cyclic BPA carbonates, synthesis, end-functionalized polycarbonates, 42–4
 transesterification with arylcarbonates in end-functionalized polycarbonate synthesis, 42*f*
- S**
- Safety note, phosgene, 18
- Salicylic acid-based end-groups, determination by NMR spectroscopy, 65
- Scanning electron microscopy (SEM)
 multiwalled carbon nanotubes in polycarbonate composites, 155
 polycarbonate composites with multiwalled carbon nanotubes, 151
 polyethylene blended with polycarbonate composite with multiwalled carbon nanotubes, 166–167, 168, 169–172*f*
- Scratch application for TMCBD-polycarbonate, 218–219
- Scratch resistance, TMCBD polycarbonates, 227
- SEC-IR, BPA-polycarbonate-siloxane analysis, 194, 195*f*
- Selective extraction, polycarbonate, 167
- SEM. *See* Scanning electron microscopy
- Shear loss modulus (G''), polyethylene blended with polycarbonate composite with nanotubes, 175*f*
- Shear storage modulus (G')
 multiwalled carbon nanotubes in polycarbonate composites, 158–159*f*
 polyethylene blended with polycarbonate composite with nanotubes, 173–176
- Shear yielding compared to craze formation and breakdown in polymers, 123–124
- Siloxane-polycarbonate copolymers, continuous polymer fractionation for characterization, 185, 187–188*t*, 193–196

- Size exclusion chromatography. *See* SEC
- Solid state polymerization
 BPA polycarbonate synthesis, 17, 20
 high molecular weight BPA synthesis, 86–94
 TMCBD polycarbonates, 220–221, 225–226*t*
- Solubility, polymers and ammonolysis products, 247, 248*t*
- Solution characterization across molecular weight distribution, polycarbonate materials, 180–199
- Solution synthetic processes, end-functionalized polycarbonate oligomers, 41, 43–45*t*
- Solvent based synthesis
 commercial BPA polycarbonate production, 9–13
 comparison to melt phase synthesis for BPA polycarbonate, 15*t*, 17–18
 laboratory BPA polycarbonates, 19–20
- Spirobiindane polycarbonate chemical structure and properties, 130*t*
T_g and γ transition data, 135*f*
- SSF. *See* Successive Solution Fractionation
- Stannous ethoxide, copolymerization catalyst, 5-methyl-5-allyloxycarbonyl-1,3-dioxan-2-one, 231, 236–238
See also Tin
- Stoichiometry and side reactions, phenol-acetone condensation in BPA synthesis, 32, 33*f*
- Stress-strain-behavior, polycarbonate composites, multiwalled carbon nanotubes, 152
- Structure-property comparisons, polycarbonates, 137
- Styrene-divinylbenzene copolymers, cation exchange resins in BPA synthesis, 30–31
- Successive Solution Fractionation (SSF), 181
- 4,4'-Sulfonylbiphenol, co-monomer in copolycarbonates, 144
- Supercritical ammonia in polycarbonate ammonolysis, 244–261
- Supercritical carbon dioxide comparison to N₂, sweep fluids, 91
- Supercritical carbon dioxide facilitation, poly(bisphenol A), solid state polymerization 86–94
- Supercritical fluid extractor for solid state polymerization with supercritical carbon dioxide, 88
- Suzuki reaction in asymmetric bisphenol A analogue synthesis, 138
- Suzuki reaction in tetraarylbiisphenols syntheses, 137–140
- Sweep fluids, supercritical carbon dioxide comparison to N₂, 91
- Synthetic biodegradable polymers, applications, 230

T

T_g. *See* Glass transition temperature

Telechelic, definition, 39–40

TEM. *See* Transmission electron microscopy

Temperature effects on polycarbonate polymerization, 206–207, 212

Temperature Rising Elution Fractionation (TREF), 181

Tensile and flexural properties, BPA and 4,4'-dihydroxydiphenyl copolycarbonate, 119, 120*f*

Tertiary amines, catalysts for solvent-based polycarbonate synthesis, 10

- Tertiary*-butylphenol based end-groups, determination by NMR spectroscopy, 65
- Tetraaryl polycarbonates
 average molecular cross-sectional area, 129–130*t*
 chemical structure, 129*f*
 dynamic mechanical data, 131*f*
 packing length, 129–130*t*
- Tetraarylbisphenol A-BPA polycarbonate, copolymer, dynamic mechanical results compared to BPA-PC polymer, 129, 131*f*
- Tetraarylbisphenol A polycarbonate, chemical structure and properties, 130*t*
- Tetraarylbisphenol A synthesis by ligandless Suzuki coupling, 139
- Tetraarylbisphenol C synthesis, 139–141
- Tetrabromobisphenol polycarbonate, preparation, 11–12
- 3,5,3',5'-Tetramethyl polycarbonates, preparation, 11–12, 20
- 1,1,3,3-Tetramethylcyclobutane-2,4-diol (TMCBD) monomer, synthesis, 217
- 1,1,3,3-Tetramethylcyclobutane-2,4-diol (TMCBD) polycarbonates
 physical properties, 227
 structure and synthesis, 217–218*f*
- Thermal properties, BPA and 4,4'-dihydroxydiphenyl, copolycarbonate, 98, 119
- Thermal rearrangement, polycarbonate in melt, branching product structures, 182, 183*f*
- Thermally induced redistribution, fractionated polycarbonate, 192–194*f*
- Thermodynamically controlled molecular weight distribution, 14
- Thiol promoted phenol-acetone condensation, BPA production, 29–30
- Tin macroinitiator adducts, 233, 238*t*, 239, 240
See also Stannous ethoxide
- TMCBD. *See* Tetramethylcyclobutanediol
- Transesterification synthetic processes, end-functionalized polycarbonate oligomers, 41–43, 46–54
- Transmission electron microscopy (TEM)
 multiwalled carbon nanotubes in polycarbonate composites, 155–156
 polycarbonate composites with multiwalled carbon nanotubes, 151
- Transparency, BPA and 4,4'-dihydroxydiphenyl copolycarbonate, 120*f*
- TREF. *See* Temperature Rising Elution Fractionation
- Tributylammonium-6-(N,N-diethyl)hexane bromide, bifunctional catalyst, 11
- 1,1,1-Trichloro-2,2-bis[4'-(4-methoxyphenyl)-phenyl]ethane, (p-TADDT), synthesis, 142–143
- Triethylamine, catalyst for solvent-based polycarbonate synthesis, 10
- Triphosgene, laboratory alternative to phosgene, 13
- Triphosgene method in polycarbonate synthesis, 140–141
- ## U
- Ultraviolet-visible (UV-vis) spectroscopy, characterization, end-functionalized poly(bisphenol A) carbonate oligomers, 59, 61–63
- Unhindered amine in 3,5,3',5'-tetramethyl-BPA polycarbonate synthesis, 20

United States production capacity,
BPA, 28
Unsymmetrical triaryl systems,
synthesis by Suzuki reaction, 138
Unzipping TMCBD polycarbonate at
trans isomer sites, 224–225
UV-vis. *See* Ultraviolet-visible
spectroscopy

V

Vicat softening temperature, 4,4'-
dihydroxydiphenyl and bisphenol A
copolycarbonate, 120*f*
Vincent's characterization, ductile-
brittle transition for polymers, 123–
124, 125*f*
Viscosity, TMCBD polycarbonates,
227

W

Weatherable polycarbonate
compositions, 3

Weathering properties, polymers,
216–217
Window glass replacement material,
BPA polycarbonate, 3

X

X-Ray diffraction spectra, BPA and
4,4'-dihydroxydiphenyl
copolycarbonate, 105, 106*f*

Y

Yield stress compared to brittle
strength in polymers, temperature
dependence, 124

Z

Zimm-Schultz distribution, 205

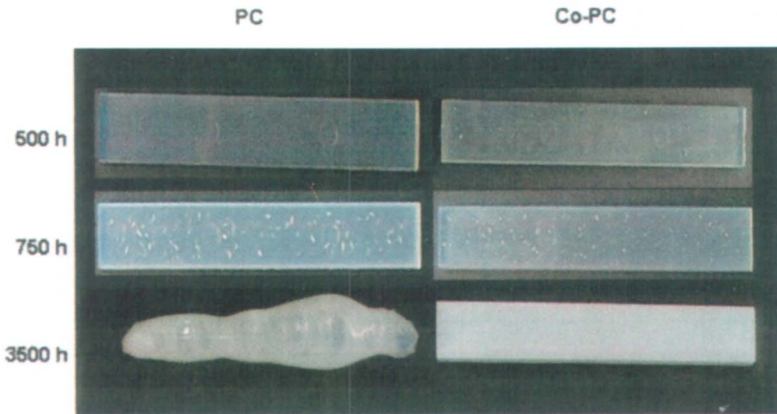
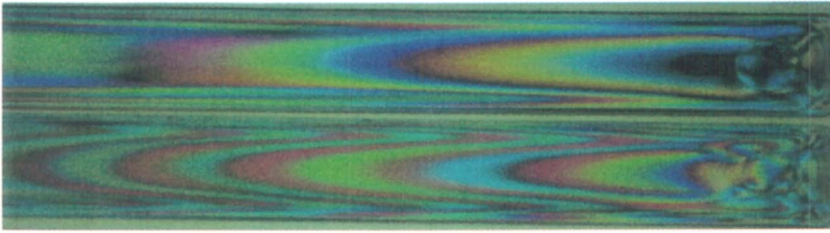


Figure 8.2. a) Injection molded samples of BPA-PC (top) and DOD-co-PC (bottom) shown under polarized light. b) Effect of boiling-water immersion on BPA-PC and DOD-co-PC.

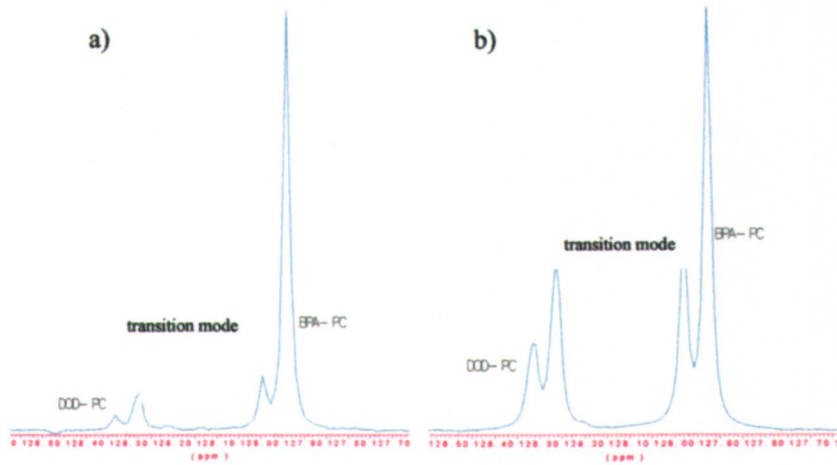


Figure 8.3. ^{13}C -NMR of Aromatic CH Groups of DOD-BPA-copolycarbonates with 12.6 and 30 mole % of DOD (a and b, respectively)

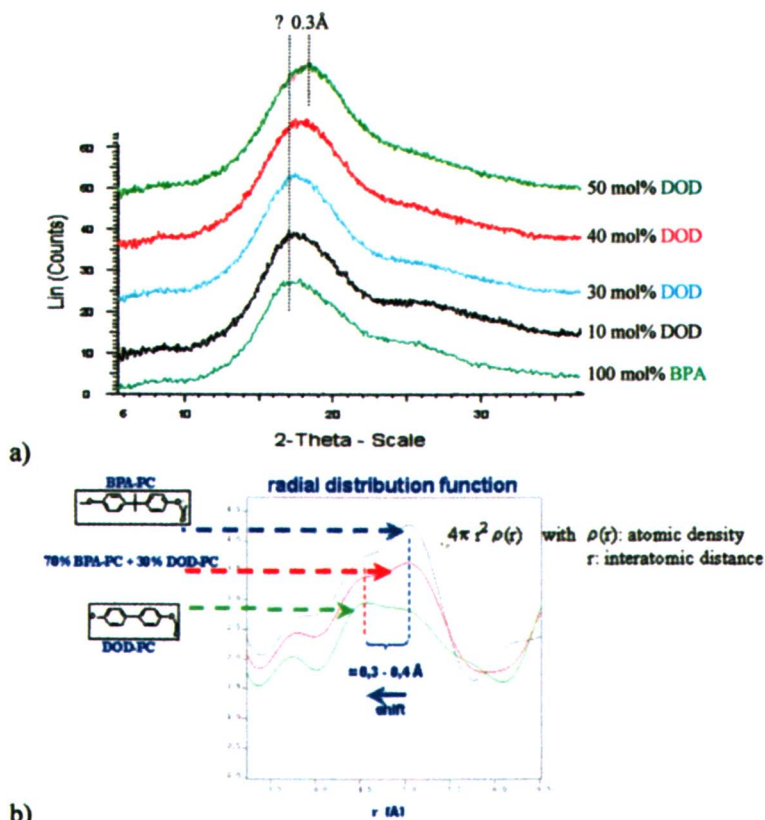


Figure 8.5. a) XRD Spectra measurements of DOD-BPA-copolycarbonates, b) Radial Distribution Function of DOD-co-PC.

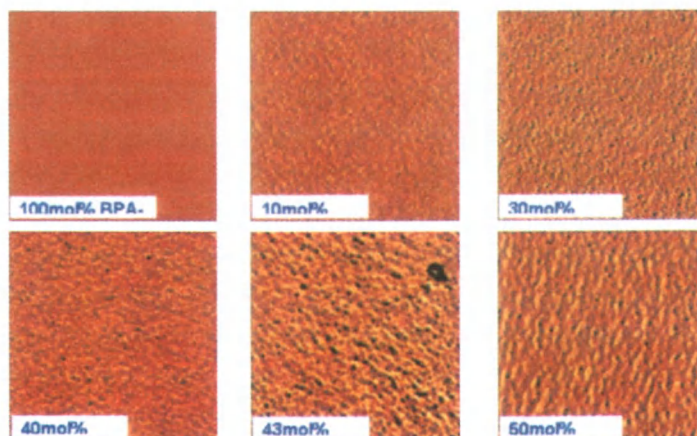


Figure 8.6. AFM phase contrast images of different compounds. Scan size: 1 μm².

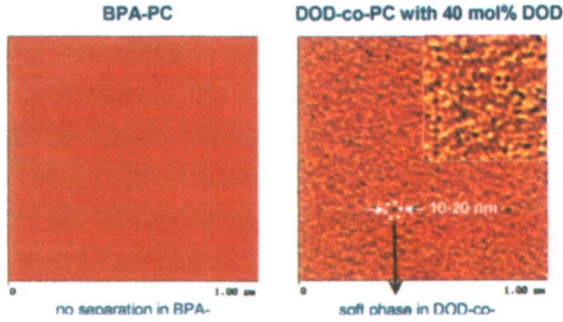


Figure 8.7. a) AFM phase contrast images of the BPA-PC and the 40 mol% DOD-co-PC.

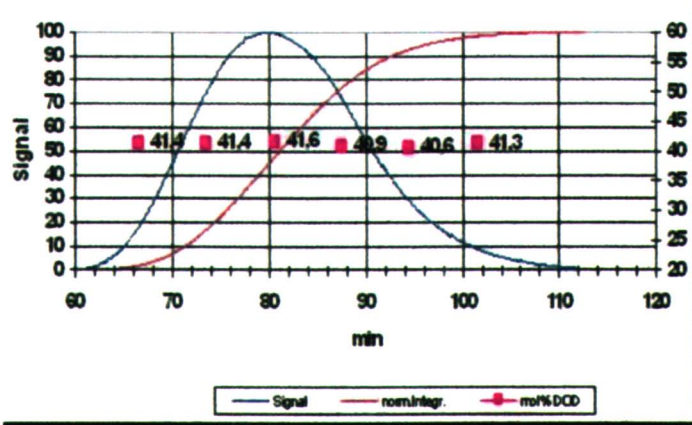
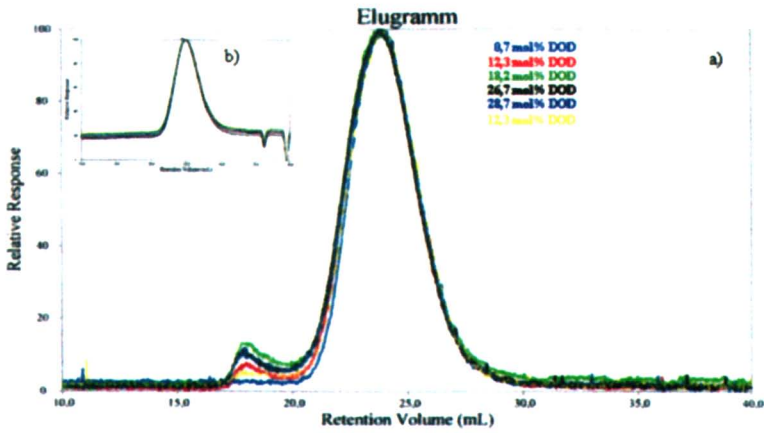


Figure 8.8. GPC chromatogram of DOD-BPA copolycarbonates a) RI-detection b) LS-detection. c) GPC chromatogram, chemical composition (NMR) as a function of molecular weight.

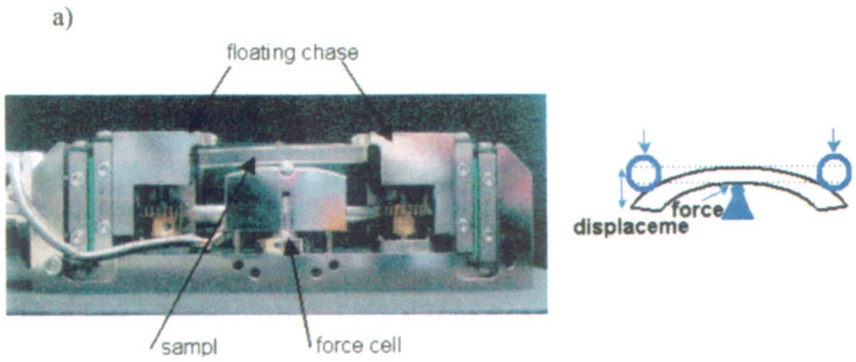


Figure 9.1. a) 3-Point-Bending-Module

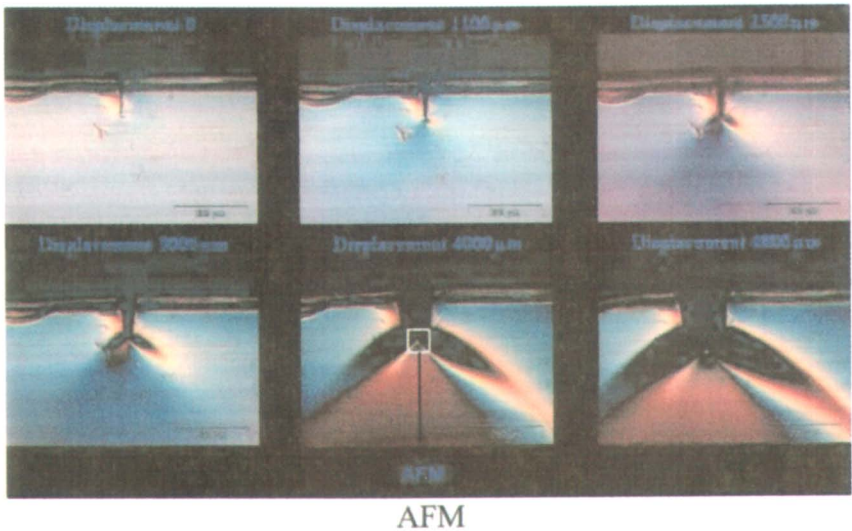


Figure 9.2. Light microscopy of BPA-PC in 3-point-bending-test.

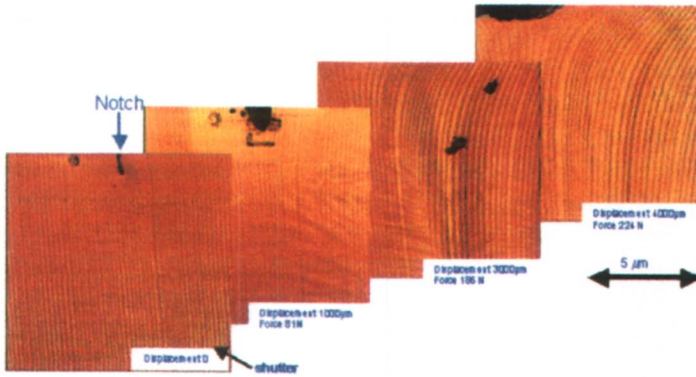


Figure 9.3. AFM of BPA-PC in 3-point-bending-test.

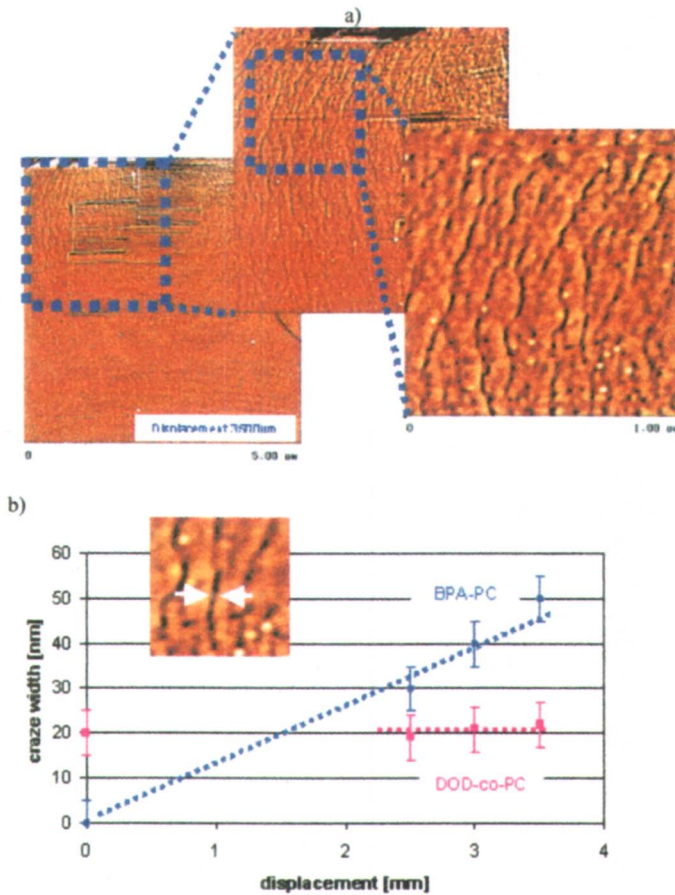


Figure 9.4. a) AFM phase contrast of 30 mol% DOD-co-PC in 3-point-bending-test. b) 3-Point-bending, crazing in BPA-PC compared to DOD-co-PC.

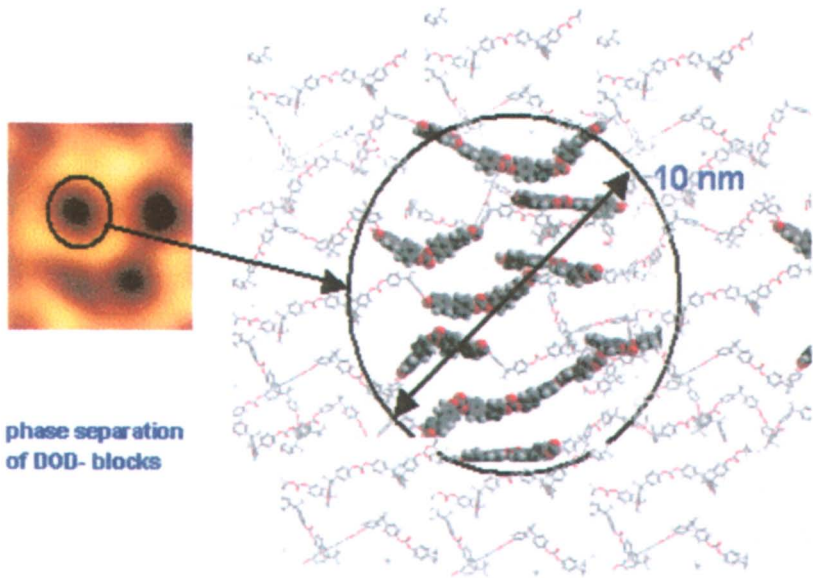


Figure 9.5. Proposed morphological structure of the DOD-co-PC (DOD-blocks: balls, BPA-units: sticks).

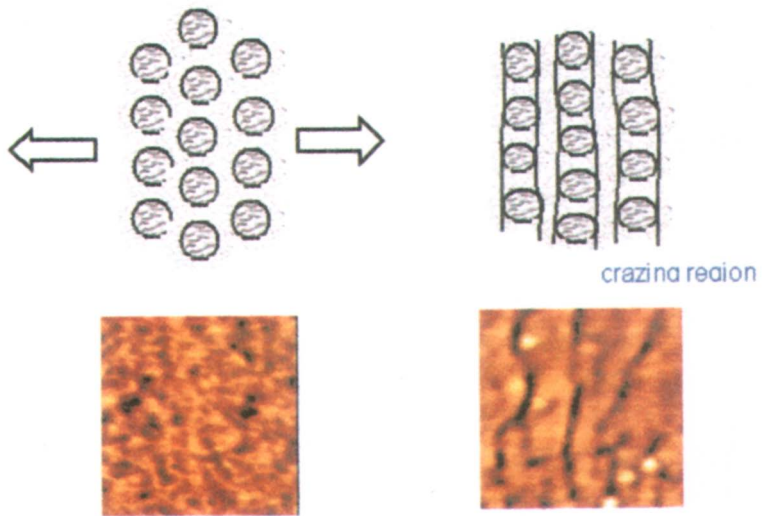


Figure 9.6. Model of deformation mechanism of DOD-co-PC.

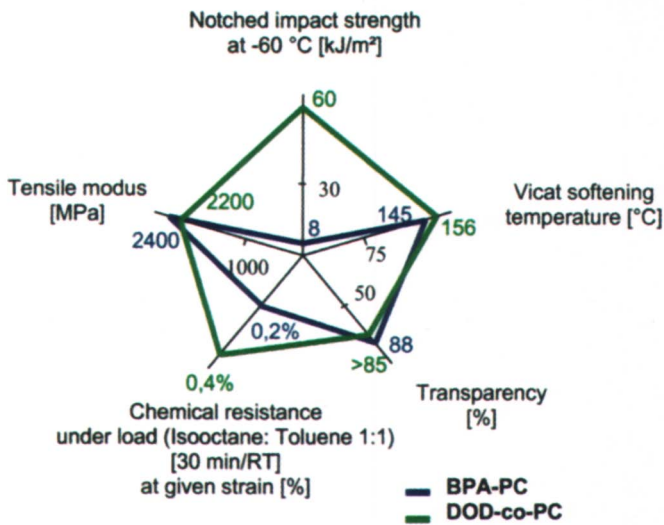


Figure 9.7. Comparison of properties of the DOD-co-PC with BPA-PC.